PLATE ANCHORS IN SAND UNDER STATIC AND CYCLIC LOADS

by

William McCallum Stewart

A thesis submitted for the degree of Doctor of Philosophy

University of Glasgow
Department of Civil Engineering
August 1988.

Dedicated to my Mum

CONTENTS

ACKNOWLEDGEMENTS

I wish to express my sincere thanks to two people in particular: my Head of Department, Dr. David Green, for giving me the impetus and opportunity to complete the task of writing up my research, and for his advice and encouragement throughout the past year; my wife Gladys, for her forbearance, good-humour and support during the preparation of this thesis.

I also acknowledge the help and assistance provided by Professor Hugh B. Sutherland and Mr Tom Finlay throughout the research project.

During the experimental part of the research, I received invaluable technical assistance from Mr. Willie Henderson, Mr. Ian Todd and the late Mr. Hugh McIvor. Thanks are also due to Dr. David Ponniah, now of Edinburgh University, for many useful discussions on experimental problems and techniques.

Dr. David Naylor of Swansea University helped considerably with the finite element study, and the assistance of my colleague, Dr. Trevor Davies, with this part of the research is also acknowledged.

The typing was undertaken by Mrs. June Lawn, whose friendly disposition and skill helped considerably in the production of this thesis.

The research was supported in part by a grant from the Marine Technology Directorate of SERC. This support is gratefully acknowledged.

SUMMARY

This thesis reports on an investigation into the behaviour of circular plate anchors embedded in dry cohesionless soil and subjected to vertical static or cyclic uplift loading. The experimental part of the investigation used model testing techniques, and details of the test rigs, sand, sand placement method and test procedures are given in Chapter 3.

A total of thirty static tests were completed in dense (D_r=93.0%) and medium-dense (D_r=59.4%) Leighton-Buzzard sand, using anchor embedment ratios ranging from 2.0 to 15.0. The anchor embedment ratio is the anchor depth (D) divided by the anchor diameter (B). Usually at least two tests were performed at each embedment ratio. The anchors consisted of 6mm thick brass discs, with diameters ranging from 25mm to 100mm. The anchor shaft was a length of smooth brass rod, 6mm in diameter.

The static test results established a data base of anchor failure loads for use in setting the load levels in the cyclic tests. The results for dense sand ($D/B<8$) and medium dense sand ($D/B<4$) compared well with those of previous investigations which used Leighton-Buzzard sand. In dense sand at $D/B>8$, the results were seriously affected by boundary and scale effects, leading to substantial differences in the dimensionless uplift resistance factor, N_u, for the same embedment ratio. The static test results were also used for comparison with the results of a finite element analysis of the anchor uplift problem. The analysis confirmed two characteristics of shallow anchor behaviour : the presence of an elastic wedge of sand above the anchor and the inverted frustum shape of the failure surface in the sand. With respect to ultimate uplift resistance, the finite element analysis predicted failure loads of up to three times the experimental values.

The cyclic tests were undertaken principally to investigate cyclic creep, the mechanism whereby the anchor sustains a continuing upward displacement during cyclic loading. An anchor embedment ratio of 4.5 was used in all fourteen cyclic tests. Sinusoidal loading with a frequency of approximately 0.1Hz was applied to the anchor. The load parameters varied were mean load and amplitude of load, both expressed as a percentage of the static failure load (sfl). Various combinations of mean and amplitude were applied to the anchors during the test series, with some anchors subjected to over 1 million cycles of loading.

The cyclic test results show that, with respect to cyclic displacement, the load amplitude is the controlling parameter : the greater the load amplitude, the greater the cyclic displacement, in tests loaded to the same maximum load. In tests with different mean loads but the same load amplitude, the anchor cyclic displacements were similar. A reduction in sand density leads to an increase in cyclic displacement, for anchors subjected to the same relative loading levels. The test results also indicate that the cyclic creep mechanism is affected by attrition of the sand grains in the vicinity of the anchor. For the anchors which failed during cycling, the failure mechanism can be described in terms of the behaviour of simple shear samples of sand subjected to cyclic loading.

Design considerations regarding the offshore deployment of plate anchors are discussed.

NOTATION

The symbols in general use throughout the thesis are listed below. Symbols peculiar to a particular theory or part of the thesis are defined in the text when they occur.

B – anchor diameter

B_c – container diameter

c – cohesion

D – anchor depth

D_r – relative density

E – Young's modulus

e – void ratio

G – shear modulus

m_c – anchor movement per cycle.

N – number of cycles

N_u – uplift resistence factor

P – anchor load

P_u – ultimate anchor load

p – uplift pressure $= 4P/\pi B^2$

p_u – ultimate uplift pressure $= 4P_u/\pi B^2$

sfl – static failure load

γ – shear strain

Δ – anchor displacement

Δ_c – anchor cyclic displacement

Δ_{pc} – anchor displacement per cycle

ϵ – normal strain

ν – Poisson's ratio

ρ – bulk density

σ – normal stress

τ – shear stress

φ – friction angle

CHAPTER ONE – INTRODUCTION

1.1 GENERAL

This thesis reports on an investigation into the behaviour of circular plate anchors embedded in dry cohesionless soil and subjected to vertical static or cyclic uplift loading. The investigation was undertaken using model tests, and was principally concerned with the displacement behaviour of plate anchors during cyclic loading. The investigation forms part of a continuing programmme of research at Glasgow University into the fundamental behaviour of plate anchors under uplift loads. Other aspects of plate anchor behaviour in sand reported in recent years are the effect of ground disturbance during placing (Zakaria, 1986) ; group effects (Wang, 1986) ; plate anchors under static loading (Fadl, 1981). Ponniah (1984) reported on the behaviour of plate anchors in cohesive soil under static and cyclic loading.

The present investigation is associated with the development of oil and gas production platforms for deep water sites. Most of the design concepts for these platforms incorporate foundation elements which would be subjected to cyclic uplift forces caused by environmental loading conditions. The behaviour of these elements under cyclic loading is of paramount importance to the safety and integrity of the platforms. Bea, et al (1982) discussed the foundation design of deep water structures and suggested that plate type embedment anchors could be used, provided they were proven to be reliable under cyclic loading. The model study described herein will help to identify some important parameters in this respect.

Chapter 1 continues with a section describing the more common types and uses of anchors, and this is followed by a brief discussion on the use of models in soil mechanics and the applicability of the present model study. Chapter 2 reviews the previous theoretical and experimental work done on plate anchors, with particular emphasis on plate anchors in cohesionless soil. Experimental studies involving static loading and cyclic loading are reviewed, and a section on the cyclic loading behaviour of cohesionless soil in triaxial tests and simple shear tests is also included. Boundary and scale effects in model tests are discussed in the final section of Chapter 2. Chapter 3 contains details of the experimental procedure, including descriptions of the loading system, the type of sand and the instrumentation and data acquisition set–up used in the tests. Discussion on the formation of uniform sand beds and sand density measurement is also included.

The test results are presented in Chapter 4, for both static and cyclic loading, and Chapter 5 contains details and discussion of a finite element study undertaken on the static load–displacement behaviour of the model anchors. Discussion of the experimental results from this and previous investigations is contained in Chapter 6, and Chapter 7 presents the conclusions from this investigation and suggestions for further study.

1.2 TYPES AND APPLICATIONS OF ANCHORS

Plate–type anchors are only one of many types of ground anchors designed primarily to resist uplift (tensile) forces. Others include grouted anchors, tension piles, suction anchors, gravity anchors and drag anchors. For marine applications, details of the properties and performance of many types of anchors are given in McCormick (1979) and Karal (1982).

a) Grouted anchors

Figure 1.1 shows the general arrangement of a grouted anchor and the terminology associated with its description. Ostermayer (1974), Littlejohn and Bruce (1977) and Hanna (1980) gave detailed advice on the design and construction of grouted anchors for use in soil or rock. Applications include tying–back retaining walls, stabilising slopes and providing the reaction in pile loading tests.

b) Tension piles

Tension piles have been the subject of much research in recent years, principally because of their potential use as anchorages for tethered buoyant structures offshore. In fact, the anchorage system of the Hutton tension leg platform deployed in the northern North Sea uses groups of tension piles to resist the uplift forces generated by wind, waves and buoyancy (Tetlow, et al, 1983). Figure 1.2 illustrates the basic concept and components of a tension leg platform.

c) Suction anchors

Another concept developed for offshore use is the suction anchor. These can be deployed either on the seabed, as in Figure 1.3 (a) (Wang, et al, 1978), or, by using high pressure water jets, buried in the seabed, as in Figure 1.3 (b)

(Wilson and Sahota, 1980). A major drawback to their use is the need for a pump to maintain the pressure differential essential for their succesful operation. One possible application for suction anchors is in the mooring of wave energy converters (Karal, 1982).

d) Gravity anchors

A gravity (deadweight) anchor is basically a large mass which resists uplift forces by virtue of its weight. Gravity anchors have been used for many years, particularly in the marine environment, where they are used to provide the restraint for ships' moorings. A typical gravity anchor is shown in Figure 1.4. The skirts on the base of the anchor increase the resistance to lateral loads by mobilising the shear strength of the seabed soil.

e) Drag anchors

Drag anchors are the anchors used routinely by ships and most large semi– submersibles. They may also be used to help restrain compliant offshore structures, such as a guyed tower (Maus, et al, 1985). Dropped to the seabed, the drag anchor is buried by pulling on the mooring line. The mooring line angle at the seabed must be very small ($< 5^0$) in order to ensure proper embedment.(See Figure 1.5). When deployed, drag anchors resist load in one general direction only, and so a multiple anchor system is required to resist omni– directional loading.

f) Plate anchors

Plate– type anchors include the single or multiple helix (Mitsch and Clemence, 1984 ; Mooney, et al, 1984) ; propellant embedment anchors (True and Link, 1979) and the "Hydropin" anchor (Kerr, 1976). These examples are illustrated in Figure 1.6. Applications include general mooring problems, foundations of pylons and transmission masts, and anchorages for tension roof structures.

Plate anchors can be sub– divided into shallow or deep anchors by their mode of failure at ultimate load. Shallow anchors exhibit a general failure mode, in which the failure surface extends from the edge of the anchor to the ground surface, and the entire soil mass contained within these boundaries is deformed (See Figure 1.7 (a)). By contrast, deep anchors exhibit a local failure mode, in which only the soil adjacent to the anchor is deformed (See Figure

1.7 (b)). The greater overburden pressure constrains the development of the failure surface, and the anchor fails by punching into the overlying soil. The deep anchor failure mode is very similar to that of a deep foundation subjected to compressive load.

The failure mode of plate anchors can be characterised by the ratio of anchor embedment depth, D, to anchor diameter (or equivalent), B. This ratio is called the embedment ratio, D/B (See Figure 1.7). The embedment ratio at which the transition from shallow to deep failure mode begins depends primarily on the type of soil. For medium–dense sand, the transition begins at an embedment ratio of approximately 6. This limiting embedment ratio increases with sand density.

1.3 MODEL STUDIES

Model studies have been used extensively in soil mechanics, principally because the complex nature of soil stress–strain behaviour makes analytical solutions difficult to obtain and extremely limited in application. Numerous papers have been written on the role of model tests in soil mechanics (e.g. Rocha, 1957 ; Roscoe, 1968 ; Bolton et al 1973), and the 7th European Conference on Soil Mechanics and Foundation Engineering in Brighton devoted an entire session to "The use of physical models in design". (BGS, 1980).

James (1971) made a useful contribution to the discussion on model tests by identifying three basic categories of test, as follows:

Category 1 model tests are concerned only with predicting the behaviour of a specific prototype structure from that of the model. In this type of test the principles of similarity as applied to soils must be satisfied as closely as possible (Rocha, 1957 ; Roscoe, 1968). One method of improving the similitude between prototype and model is to use a centrifuge model, in which the specific weight of the soil is increased by subjecting the model to a centrifugal acceleration through rotational motion. When subjected to an Nxg acceleration field, a 1/Nth scale model experiences the same stress as the prototype. Centrifuge testing has been used to investigate the uplift capacity of plate anchors (Ovesen, 1981). This investigation and its implications for the present study are discussed in the next chapter.

In category 2 model tests, the model is considered to be a small prototype, and its behaviour under various controlled conditions is compared with

that predicted by some method of analysis. For these models it is imperative that the model conforms with any assumptions inherent in the method of analysis adopted, e.g. homogeneous, isotropic soil with no boundary effects present. In certain circumstances, the results of category 2 model tests can be applied to a prototype situation (Sutherland, 1965).

Category 3 model tests are designed specifically to reveal stress and deformation information about a problem. It is not necessary that a full scale version of the problem exists, as the prime objective of this type of test is to investigate the soil–structure interaction, such that new methods of analysis may be developed.

These basic categories of model test are interrelated to a greater or lesser extent. The model tests undertaken in the present study are predominately category 2, but also have attributes associated with category 3 model tests. Practical considerations such as anchor shape or the effects of anchor placement methods were not included in the model study. Despite this, the qualitative aspects of the cyclic displacement characteristics identified by this investigation can be applied in general to shallow, plate–type anchors embedded in medium–dense or dense sand.

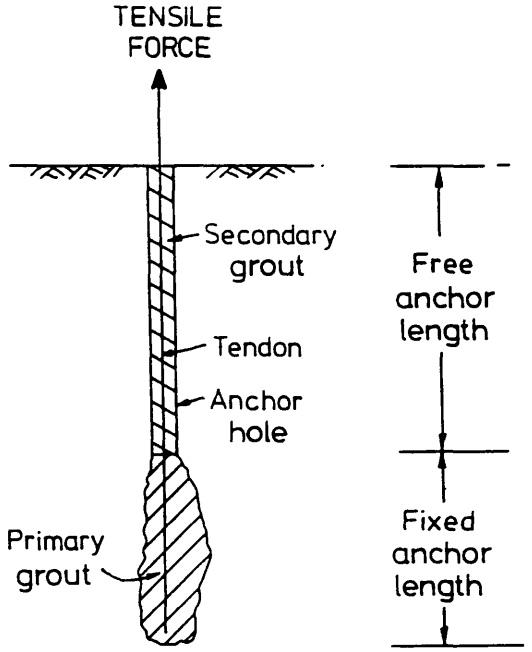

FIGURE 1.1 - Grouted Anchor (After Hanna, 1980)

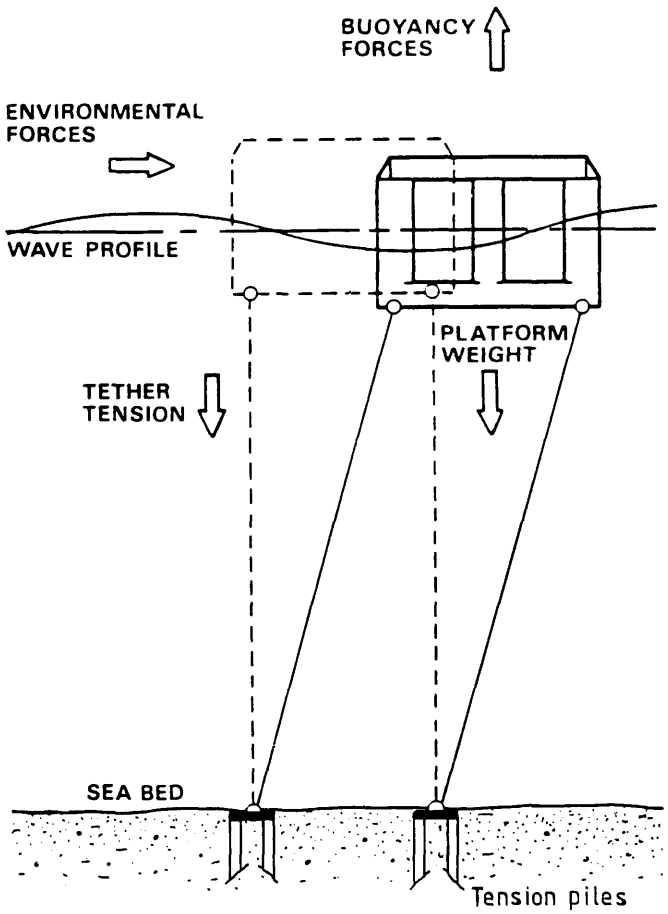

FIGURE 1.2 - Tension Leg Platform (After Tetlow, et al, 1983)

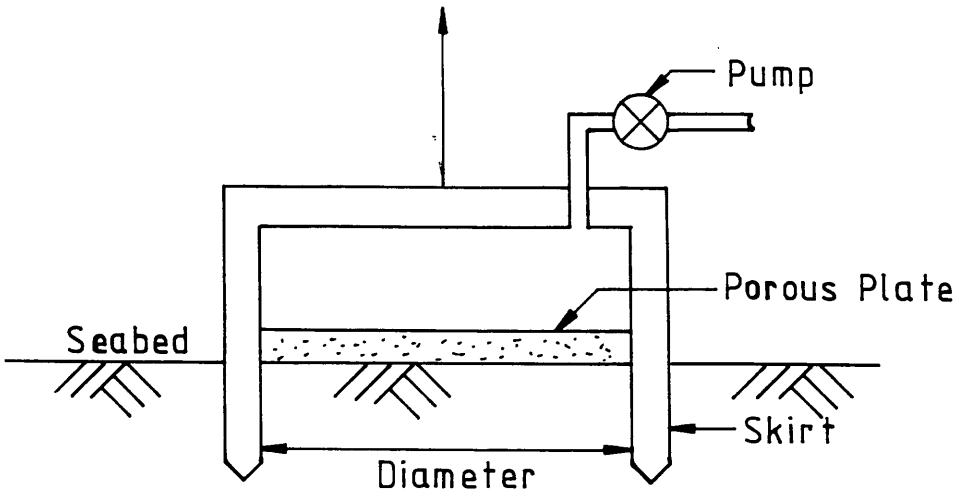

FIGURE 1.3(a) - Suction Anchor (After Wang, et al, 1978)

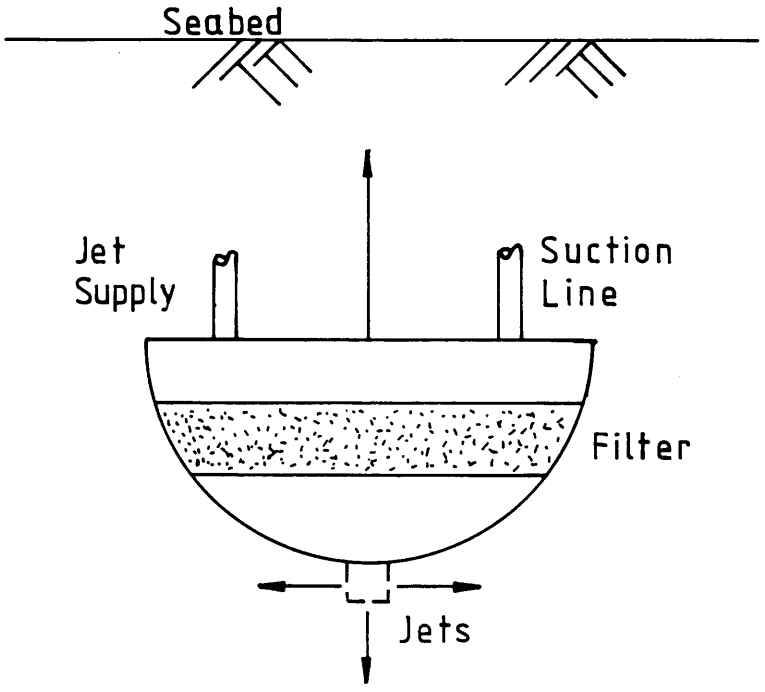

FIGURE 1.3 (b) - Suction Anchor (After Wilson and Sahota, 1980)

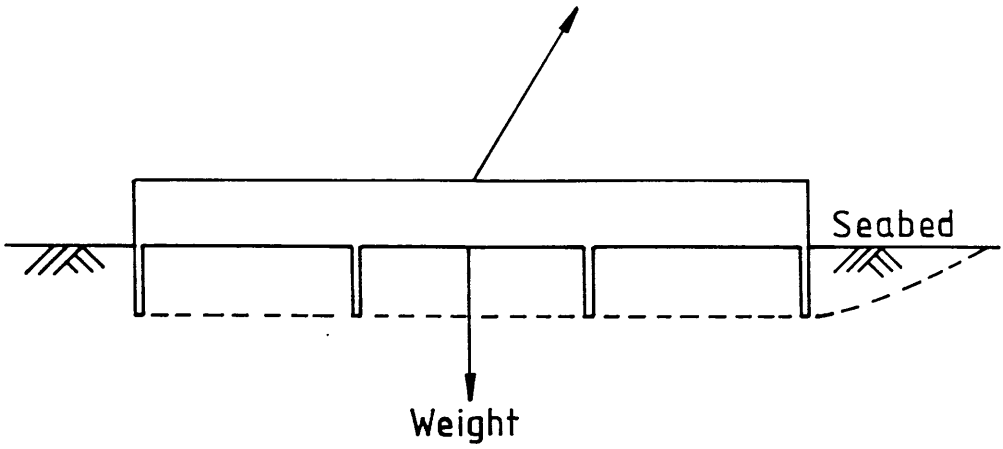

FIGURE 1.4 - Gravity Anchor

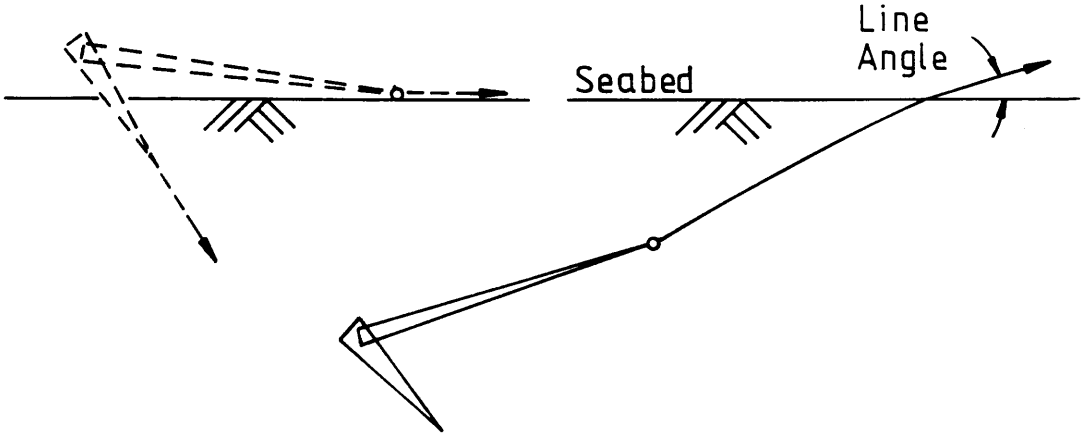

FIGURE 1.5 - Drag Anchor

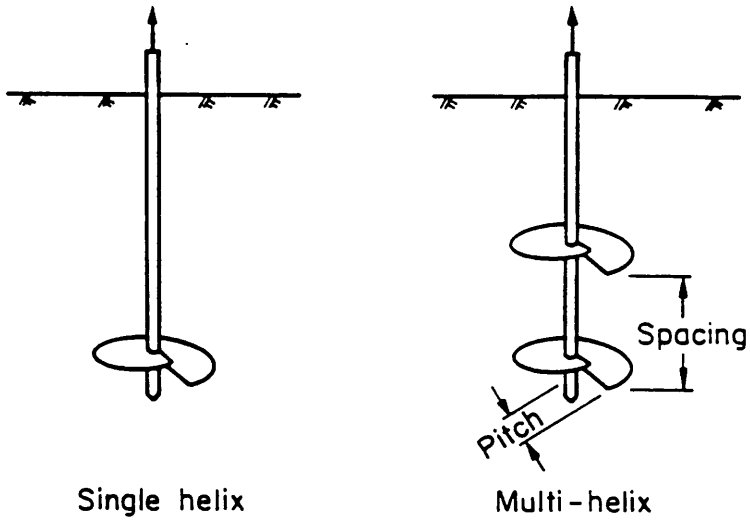

(After Mitsch and Clemence, 1984)

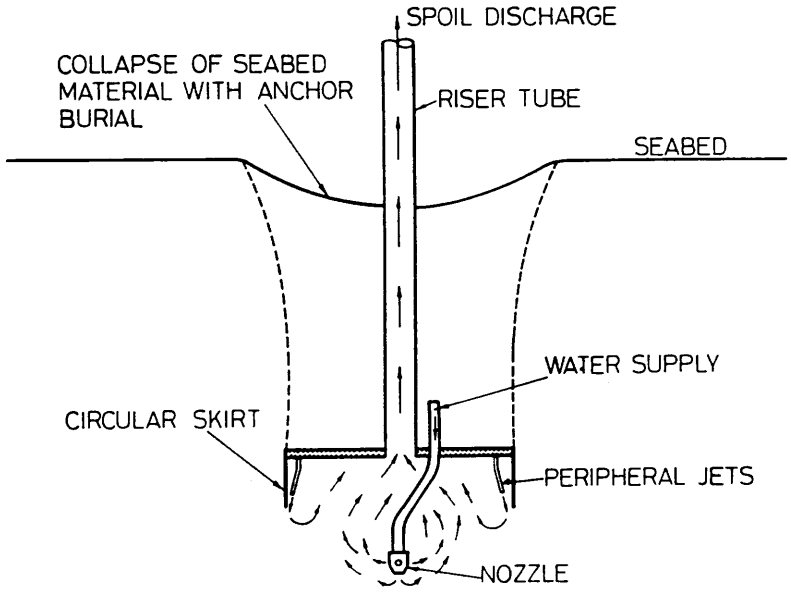

"Hydropin" anchor (After Kerr, 1976)

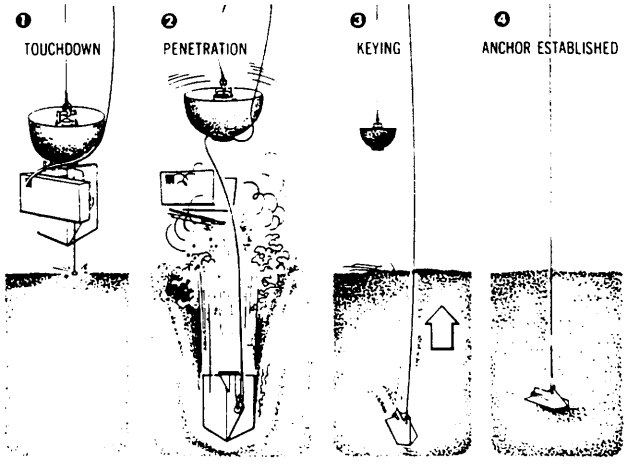

Propellant embedment anchor (After True and Link 1979)

FIGURE 1.6 - Plate Anchors

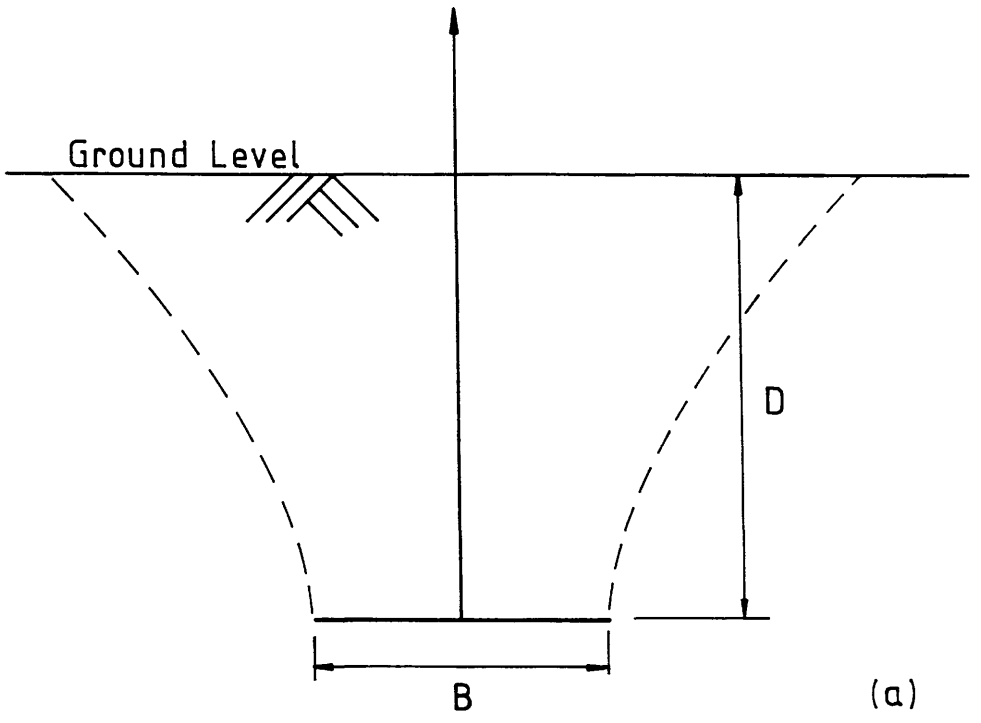

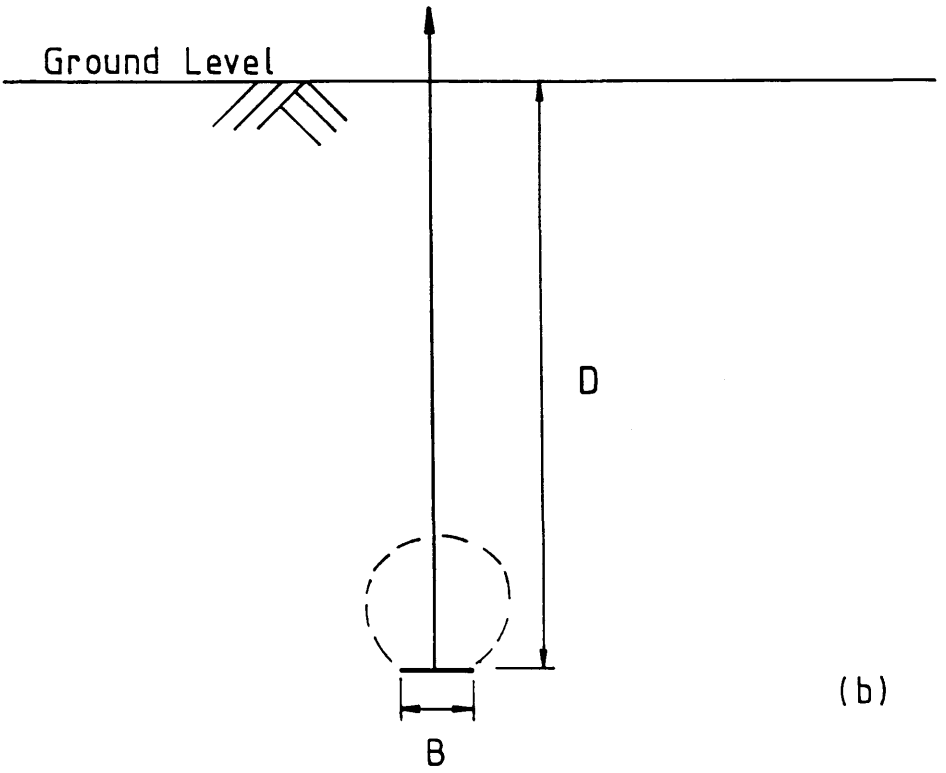

FIGURE 1.7 - Failure modes for plate anchors. (a)shallow anchor, (b) deep anchor.

CHAPTER 2 – REVIEW OF PREVIOUS WORK

2.1 INTRODUCTION

Research work on plate anchors in soil has been undertaken by a number of investigators over the years, covering a wide range of parameters associated with plate anchor behaviour. Most of the work has involved theoretical and/or experimental studies of the static pullout resistance of plate anchors, and comprehensive reviews of this work are given by Maddocks (1978), Andreadis (1979), Fadl (1981), Ponniah (1984) and, for shallow anchors only, Kulhawy (1985). Only the major theoretical contributions are repeated in this review, with particular reference to anchor pullout resistance in cohesionless soil. These are presented in sub–section 2.2.1 for both shallow and deep anchor failure, together with material not covered previously. The most recent experimental studies involving static loading are reviewed in sub–section 2.2.3.

A short, general review of the behaviour of cohesionless soil subjected to cyclic loading is given in sub–section 2.3.1. This is followed by a detailed review of the work done on the specific problem of plate anchors subjected to cyclic loading. In section 2.4 the boundary and scale effects associated with modelling plate anchor behaviour are discussed. The numerical work done on anchor uplift resistance is reviewed in Chapter 5.

2.2 STATIC LOADING

2.2.1 Theoretical Methods

Theoretical methods for calculating the ultimate pullout resistance of plate anchors buried in cohesive or cohesionless soil are based on either the limit equilibrium concept or the method of characteristics (usually with empirical corrections). The methods incorporate assumptions regarding the slope of the failure surface and the proximity of the soil surface above the anchor.

The expressions derived for the ultimate resistance are presented initially in the notation used by the original author(s). Where possible, these are revised to obtain an expression in the following form:

$$p_u = N_u \gamma' D,$$

where

p_u = ultimate uplift pressure on anchor

$\gamma'D$ = effective overburden pressure on anchor

N_u = uplift resistance factor.

This will allow comparison between methods on the basis of the dimensionless parameters N_u and D/B, the embedment ratio.

Matsuo (1967) derived an equation for the ultimate uplift resistance of a footing by considering the frictional and cohesive forces acting on the failure surface shown in Figure 2.1. The curved portion is parabolic, extending from the edge of the footing to meet a tangential straight line which intersects the horizontal ground surface at an angle of $(45 - \varphi/2)^o$. The method is similar to that proposed by Balla (1961), in which the form of the failure surface is assumed to be circular and extends from the edge of the footing to the soil surface.

For Matsuo, the ultimate uplift resistance, R, of a shallow footing is given by:

$$R = G + \gamma' (B_2^3 K_1 - V_3) + cB_2^2 K_2,$$

where

G = weight of footing,

V_3 = volume of footing shaft,

γ' = effective unit weight of soil

c = soil cohesion

$B_2^3 K_1$, $B_2^2 K_2$ = functions of λ and φ

λ = depth/radius = D/B_1

φ = angle of internal friction.

For cohesionless soil,

$$R = (G - \gamma' V_3) + \gamma' B_2^3 K_1$$

The ultimate uplift pressure p_u = R/anchor area and so

$$p_u = \frac{(G - \gamma' V_3)}{\pi B_1^2} + \frac{B_2^3 K_1}{\pi B_1^2} \gamma'$$

Neglecting the first term as small with respect to the second term, then

$$p_u = \frac{B_2^3 K_1}{\pi D B_1^2} \gamma' D$$

and $$N_u = \frac{B_2^3 K_1}{\pi D B_1^2} \qquad (2.1)$$

Originally, values of $B_2^3 K_1$ (and $B_2^2 K_2$) were obtained by a tedious procedure explained in Matsuo (1967). A subsequent paper (Matsuo 1968), presented expressions which gave approximate values for $B_2^3 K_1$ (and $B_2^2 K_2$). Those for $B_2^3 K_1$, are given below:

$$B_2^3 K_1 = (0.056\varphi + 4.0) B_1^3 \lambda^{(0.007\varphi + 1.0)}, \text{ for } 0.5 < \lambda < 1.0$$

$$B_2^3 K_1 = (0.056\varphi + 4.0) B_1^3 \lambda^{(0.016\varphi + 1.1)}, \text{ for } 1.0 < \lambda < 3.0$$

$$B_2^3 K_1 = (0.597\varphi + 10.4) B_1^3 (\lambda/3)^{(0.023\varphi + 1.3)}, \text{ for } 3.0 < \lambda < 10.0$$

The error in $B_2^3 K_1$ when using these expressions was quoted as less than 3% (φ in degrees).

Meyerhof and Adams (1968) proposed equations for shallow and deep anchor pullout which were based on the frictional (F) and cohesive (C_F) forces acting on a curved failure surface, as shown in Figure 2.2. Due to computational difficulties associated with using a curved failure surface, Meyerhof and Adams simplified the problem by assuming a vertical cylindrical surface passing through the edge of the anchor. This surface was acted on by the passive earth pressure, P_P, at an average angle of δ, and the soil cohesion, c (see Figure 2.2).

The ultimate uplift resistance for shallow anchors was expressed as :

$$R = \pi BDc + \pi BD \frac{\gamma' D}{2} S K_u \tan\varphi + W \qquad (2.2)$$

where K_u = a nominal coefficient of earth pressure on a vertical plane through the anchor edge.

S = shape factor = $1 + m (D/B)$

S has a maximum value of $1 + m (H/D)$

m = coefficient dependent on friction angle φ

H/B = embedment ratio at which the failure mode changes from shallow to deep.

W = weight of soil cylinder above anchor.

The values of m, S_{max}, H/B and K_u are all dependent on the friction angle and typical values are given in Table 2.1.

Table 2.1 – Typical values for parameters in Meyerhof and Adams' theory

Friction angle, φ	0	20	25	30	35	40	45
Coefficient, m	-	0.05	0.10	0.15	0.25	0.35	0.50
Maximum shape factor, S_{max}	-	1.12	1.30	1.60	2.25	3.45	5.50
Limit for shallow anchors, H/B	2.34	2.50	3.00	4.00	5.00	7.00	9.00
Earth pressure coefficient, K_u	-	0.85	0.89	0.92	0.94	0.95	0.95

For cohesionless soil and considering the ultimate uplift pressure, equation 2.2 becomes

$$p_u = [2D/B\ SK_u\tan\varphi + 1]\gamma'D$$

and

$$N_u = [2D/B\ SK_u\tan\varphi + 1] \qquad (2.3)$$

For deep anchors (D> H), the failure surface does not extend to the ground surface and the soil above the top of the failure surface was considered to act as a surcharge. In this case, the ultimate uplift resistance was expressed as:

$$R = \pi BHc + \pi BH\gamma'/2\ (2D - H)\ SK_u\tan\varphi + W$$

Re–writing this equation for cohesionless soil and uplift pressure gives:

$$p_u = \left[\frac{2H}{B} SK_u\tan\varphi \left[2 - \frac{H}{D}\right] + 1\right] \gamma'D$$

and

$$N_u = \left[\frac{2H}{B} SK_u\tan\varphi \left[2 - \frac{H}{D}\right] + 1\right] \qquad (2.4)$$

Vesic (1971, 1972) developed expressions for the ultimate internal pressure required to expand spherical and cylindrical cavities in an elasto–plastic soil. The expressions were modified to incorporate the problem of anchor uplift resistance for both shallow and deep anchors. In the former case, a spherical cavity expands under pressure until, at a limiting pressure, a circular failure surface forms above the cavity (see Figure 2.3(a)). The ultimate radial pressure, q_u, at which this occurs is given by:

$$q_u = cF_c + \gamma' D F_q$$

where F_c and F_q are cavity breakout factors. Applied to anchor uplift resistance, this equation becomes:

$$p_u = c\bar{F}_c + \gamma' D \bar{F}_q \ ,$$

where $\bar{F}_c$ and $\bar{F}_q$ are (plate) anchor breakout factors and $\bar{F}_c = F_c$; $\bar{F}_q = F_q + {}^1/_3({}^B/_D)$

For cohesionless soil,

$$p_u = \left[F_q + \frac{1}{3} \frac{B}{D} \right] \gamma' D$$

and

$$N_u = \left[F_q + \frac{1}{3} \frac{B}{D} \right] \qquad (2.5)$$

Values of F_c, F_q and $\bar{F}_q$ are tabulated in Vesic (1971) against φ and embedment ratio ($^D/_B \leqslant 5.0$).

Deep anchor failure was considered to be analagous to a spherical cavity expanded to a radius R_u by a pressure q_u, with a plastic zone extending to a radius R_p, as shown in Figure 2.3(b). The soil within the plastic zone was assumed to behave as a compressible plastic solid, defined by the Mohr–Coulomb strength parameters c and φ, and an average volumetric strain, Δ. The soil outside the plastic zone was assumed to behave in a linear elastic manner, with Young's modulus, E and Poisson's ratio, ν.

By considering the equilibrium of elements in the two zones (elastic and plastic), Vesic obtained the ultimate cavity pressure as :

$$q_u = cF_c + \gamma' D F_q \qquad (2.6)$$

where

$$F_c = (F_q - 1)\cot\varphi$$

and $$F_q = \frac{3(1+\sin\varphi)}{(3-\sin\varphi)}\left[I_{rr}\right]\exp\left[\frac{4\sin\varphi}{3(1+\sin\varphi)}\right]$$

F_c and F_q are spherical cavity expansion factors and

$$I_{rr} = \text{reduced rigidity index} = \frac{I_r}{1+I_r\Delta}$$

$$I_r = \text{rigidity index} = \frac{E}{2(1+\nu)(c+\gamma' D\tan\varphi)}$$

Δ = average volumetric strain in plastic zone.

For an incompressible material, $\Delta = 0$ and $I_{rr} = I_r$. Equation 2.6 is directly applicable to the uplift resistance of deep anchors. Hence for cohesionless soil,

$$p_u = \gamma' D F_q$$

and $$N_u = F_q = \frac{3(1+\sin\varphi)}{(3-\sin\varphi)}\left[I_{rr}\right]\exp\left[\frac{4\sin\varphi}{3(1+\sin\varphi)}\right] \qquad (2.7)$$

With respect to deep anchor failure, Vesic also considered the expansion of a cylindrical cavity. This was related to work done by Mariupolskii (1965) and resulted in the following expression for anchor uplift resistance:

$$p_u = \frac{2c}{(2-\tan\varphi)}F_c' + \frac{2\gamma' D}{(2-\tan\varphi)}F_q'$$

where

$$F_c' = (F_q' - 1)\cot\varphi$$

$$F_q' = (1+\sin\varphi)\,[I'_{rr}\sec\varphi]\exp\left[\frac{\sin\varphi}{1+\sin\varphi}\right]$$

F_c' and F_q' are cylindrical cavity expansion factors and

$$I'_{rr} = \frac{I_r}{1+I_r\Delta\sec\varphi}$$

Hence, for cohesionless soil, the anchor uplift factor is given by

$$N_u = \frac{2(1+\sin\varphi)}{(2-\tan\varphi)}\,[I'_{rr}\sec\varphi]\exp\left[\frac{\sin\varphi}{1+\sin\varphi}\right] \qquad (2.8)$$

Values of F_c, F_q, F_c' and F_q' as functions of I_{rr}, I'_{rr} and φ are given in tabular form by Vesic (1972).

Kwasnieski, Sulikowska and Walter (1975) derived equations for shallow and deep anchor pullout resistance in sand which were based on an inverted frustum failure surface. Solving Kotter's equation for the distribution of shear stress on the failure surface, the pullout resistance for shallow anchors is given by:

$$Q_1 = \frac{\pi B^2}{4} \gamma' D \left[1 + K_1 \frac{2D}{B} + K_2 \frac{4D^2}{B^2} \right]$$

where

$$K_1 = - \frac{\cos(2\alpha+\varphi)\sin\varphi}{\sin^2\alpha}$$

$$K_2 = \frac{K_1}{3\tan\alpha}$$

α = angle from horizontal to sloping side of frustum.

In terms of uplift pressure,

$$p_u = \left[1 + \frac{2D}{B} K_1 + \frac{4D}{B} K_2 \right] \gamma' D$$

and

$$N_u = \left[1 + \frac{2D}{B} K_1 + \frac{4D^2}{B^2} K_2 \right] \qquad (2.9)$$

For $\alpha = 90 - \varphi$, the equation reduces to the wedge theory equation of Matsuo (1967), where the pullout resistance is simply the weight of the soil frustum.

The deep anchor equation was derived by considering the situation shown in Figure (2.4). The frustum above the anchor extends upwards a distance 7B, making an angle φ with the vertical. The pressure 'p' on the upper face of the frustum increases with depth, but reaches a limiting value due to arching.

The deep anchor pullout resistance is then defined as

$$Q_2 = \frac{\pi B^2}{4m}\gamma' B\left[1+2\left[\frac{D}{B}\right]_{cr}\tan\varphi\right]^2\left[1-\exp\left[-m\left[\frac{D}{B}-\left[\frac{D}{B}\right]_{cr}\right]\right]\right] + Q_1$$

where $m = 4(1-\sin\varphi)\tan\varphi$ for fully mobilised friction.

Q_1 is calculated with $\alpha = 90-\varphi$ and $D/B = (D/B)_{cr}$, which is taken as 7.

Using these values for α and D/B, the uplift resistance pressure is given by:

$$p_u = \gamma' D\frac{B}{Dm}\left[1+14\tan\varphi\right]^2\left[1-\exp\left[-m\left[\frac{D}{B}-7\right]\right]\right] + \gamma' D\left[1+14\tan\varphi+\frac{196}{3}\tan^2\varphi\right]$$

and

$$N_u = \frac{B}{Dm}\left[1+14\tan\varphi\right]^2\left[1-\exp\left[-m\left[\frac{D}{B}-7\right]\right]\right]+1+14\tan\varphi+\frac{196}{3}\tan^2\varphi \qquad (2.10)$$

Saeedy (1975) assumed a logarithmic spiral failure surface and calculated the distribution of shear stress on the surface using Kotter's equation. The surface had a vertical tangent at the edge of the anchor and extended up to the ground surface, intersecting at an angle of $(45-\varphi/2)^o$ to the horizontal. Utilizing a computer program to solve Kotter's equation, Saeedy produced non-dimensional curves for the determination of the ultimate pullout resistance of shallow plate anchors in sand. The curves are reproduced in Figure (2.5).

Clemence and Veesaert (1977) used the results from semi-spatial tests to define the failure surface for shallow anchors in dense sand ($D/B \leqslant 5$). This surface was mapped as the familiar wedge shape and is shown in Figure 2.6. The equation for the ultimate resistance was then derived as follows:

$$Q_s = \gamma' V_s + \gamma' K_o \tan\varphi \cos^2(\varphi/2)\pi\left[\frac{BD^2}{2}+\frac{D^3\tan(\varphi/2)}{3}\right]$$

where V_s = volume of sand in truncated cone

K_o = coefficient of lateral earth pressure.

The first term in the equation is simply the weight of sand in the truncated cone. The second term is an expression for the shear resistance, derived by integrating the shear stress over the failure surface and assuming that the normal stress (σ_n in Figure 2.6) on the surface is a linear function of depth. The value of K_o is assumed to be constant with depth.

Expressing V_s in terms of B, D and φ and dividing by $\pi B^2/4$, the uplift factor, N_u, is given by the following:

$$N_u = 1 + \frac{2D}{B}\tan\varphi/2 + \frac{4D^2}{3B^2}\tan^2\varphi/2 + K_o\tan\varphi\cos^2\varphi/2\left[\frac{2D}{B} + \frac{4D^2}{3B^2}\tan\varphi/2\right] \quad (2.11)$$

Fadl (1981) proposed a method which took account of the relative density of the soil as well as the angle of internal friction. The method was based on the earth cone and earth pressure methods of Matsuo (1967) and assumed a failure surface as shown in Figures 2.7(a) and (b) for shallow and deep anchors respectively.

The ultimate uplift resistance is given by

$$R = \frac{\pi B^2}{4}\frac{\gamma' D}{3}\left[8Z^2 + 12Z + 3\right]$$

for shallow anchors, and

$$R = \frac{\pi B^2}{4}\frac{\gamma' B}{3}\left[3 + 24Z_H(1+Z_H) - \frac{4Z_H}{Z}(3+4Z_H) + \frac{6K_o\tan(\bar{c}\varphi)}{\tan\alpha}(1+2Z_H)\left[Z + \frac{Z_H}{Z}(Z_H-2)\right]\right]$$

for deep anchors, where

$Z = (D/B)\tan\alpha$

$Z_H = (H/B)\tan\alpha$

H/B = embedment ratio at which failure mode changes from shallow to deep. Value dependent on φ.

$K_o = (1-\sin\varphi)$.

α = half apex angle of (truncated) cone = $M\varphi$

$M = 0.25\,[D_r(1+\cos^2\varphi) + (1+\sin^2\varphi)]$

D_r = relative density of sand

$\bar{c} = D_r\cos\varphi$.

The expressions for the constants M and $\bar{c}$ were obtained from an examination of the results of Fadl's pullout tests and those of other investigators. A total of 25 tests were examined. The relationship between H/B, D_r and φ for the Leighton Buzzard sand used by Fadl is reproduced in Figure 2.8.

Re-arranging Fadl's equations gives:

$$N_u = \left[\frac{8Z^2}{3} + 4Z + 1 \right] \qquad (2.12)$$

for shallow anchors, and

$$N_u = \left[1 + 8Z_H\left[1 + Z_H\right] - \frac{4Z_H}{Z}\left[1 + \frac{4Z_H}{3}\right] + \right.$$

$$\left. + \frac{2K_0}{\tan\alpha}\tan(\bar{c}\varphi)(1+2Z_H)\left[Z + \frac{Z_H}{Z}\right](Z_H - 2)\right] \qquad (2.13)$$

for deep anchors.

Ovesen (1981) presented the results of centrifuge model tests on shallow anchors buried in sand. Using curve fitting techniques and statistical analysis, Ovesen produced the following equations for ultimate uplift resistance :

For vertical pullout,

$$N_u = \frac{p}{\gamma' D} = 1 + (4.32\tan\varphi - 1.58)\left[\frac{D}{B_e}\right]^{3/2} \qquad (2.14)$$

where B_e= equivalent side length of square anchor. For example, if B (the diameter) is 50mm, anchor area= 1963mm^2 and $B_e = (1963)^{\frac{1}{2}} = 44.3$mm.

For inclined pullout,

$$N_u{}^{\theta} = N_u\left[1 - 0.33\left[\frac{2\theta}{\pi}\right] + 1.27\left[\frac{2\theta}{\pi}\right]^2 \tan\varphi\right] \qquad (2.15)$$

where θ = angle of inclination from vertical (in radians)

The equations were valid for $D/B \leqslant 3.5$, $29^0 \leqslant \varphi \leqslant 42^0$ and $\theta \leqslant 45^0$.

Ponniah (1984) was primarily concerned with cohesive soils, and he characterised previous pullout theories in terms of two basic parameters, N_{ce} and N_{qe}. These were used in the following equation:

$$p_u = N_{ce}c + N_{qe}\gamma'D \qquad (2.16)$$

where P_u = ultimate pressure on the anchor face

c = cohesion of the soil

$\gamma'D$ = effective overburden pressure on the anchor

N_{ce} = equivalent bearing capacity factor for soil cohesion

N_{qe} = equivalent bearing capacity factor for soil overburden.

Expressions for N_{ce} and N_{qe} were derived for the theories of Matsuo (1967), Mariupolskii (1965), Meyerhof and Adam (1968) and Vesic (1971, 1972) for shallow and deep anchor failure.

Ponniah concluded that the cylindrical Vesic method (Vesic, 1971) provided the most satisfactory estimates of pullout resistance in cohesive soil. To improve the correlation between different field and/or model tests for undrained conditions, Ponniah suggested that the undrained shear strength of the soil should be taken into account, in addition to D/B and N_{ce}.

Finally, Vermeer and Sutjiadi (1985) derived an expression for the uplift resistance of shallow rectangular anchors in sand. The expression was based on the assumption that straight rupture lines are formed from the anchor plate to the soil surface. The inclination of the rupture lines from the vertical was taken as the angle of dilatancy of the sand. This angle varies with relative density, typically in the range 0^0 to 20^0 for loose to dense sand. The expression was not modified to suit circular anchors.

2.2.2 Comments on Theoretical Methods

The expressions for uplift resistance factor, N_u, derived in the previous sub– section take many different forms. This is not surprising, because each method is based on specific, but differing assumptions regarding the form of the failure surface and the distribution of forces acting on the failure surface (e.g. plane strain conditions are assumed for an axisymmetric problem). The exception to this is the equation reported by Ovesen (1981), which was derived from model test results.

Dealing initially with the theories relevant to shallow anchor failure, Figures 2.9 and 2.10 illustrate the range of N_u values obtained for loose and dense sand, respectively. In Figure 2.9, all the curves are drawn for $\varphi = 30^0$. The relative density (D_r) is assumed to be 20%, which defines the sloping angle of failure used by Fadl (1981) ($\alpha = 12^0$ from vertical). The same slope was used by Kwasnieski et al (1975), although the angle is defined from the horizontal (i.e. $\alpha = 78^0$ from horizontal) The curves of Saeedy (1975) and Kwasnieski et al (1975) provide upper and lower bounds, respectively, to the values of uplift resistance factor, with the upper values almost exactly twice the lower values.

The dense sand curves shown in Figure 2.10 are drawn for $\varphi = 40^0$ and $D_r = 80\%$. In this case, the Fadl failure angle is 27^0 (63^0 for Kwasnieski et al). The curves of Fadl (1981) and Ovesen (1981) are very similar and mark the upper bound of the results for dense sand. Although Ovesen's equation was presented for $D/B \leqslant 3.5$, at greater embedment ratios the results are still in very good agreement with those obtained by Fadl. The lower bound curve of Vesic (1971) has uplift factors approximately half those of the upper bound.

The deep anchor curves are presented in Figures 2.11 and 2.12 for loose and dense sand, respectively, and for the same values of φ and D_r used in the shallow anchor case. In addition, the Vesic theory requires two other parameters to be specified, viz. the rigidity index (I_r) and the volumetric strain (Δ). Vesic (1972) suggests $70 \leqslant I_r \leqslant 150$ for loose to dense sand, and these upper and lower bound values were used, together with $\Delta = 0$ (i.e. no volumetric strain). The effect on N_u of varying the rigidity index and the volumetric strain is shown in Figures 2.13 and 2.14, respectively. In Figure 2.13, N_u increases with increasing stiffness for zero volume change, but for large volume changes, the stiffness of the soil does not significantly affect N_u for $I_r > 100$. [Note: Vesic quotes $100 \leqslant I_r \leqslant 500$ for rock, $I_r \simeq 300$ for stiff clay]. Figure 2.14 shows that increasing the volumetric strain leads to a decrease in N_u. An increase in volume change is equivalent to a decrease in stiffness, and the consequent drop in N_u is consistent with the stiffness effect described above.

Figures 2.11 and 2.12 show a large variation in N_u values obtained from the deep anchor equations, especially in the dense sand. The variation is greater than that obtained for shallow anchor failure such that, at embedment ratios > 20 in dense sand, Fadl's curve gives N_u values over three times as large as the next highest value.

The curves for Kwasnieski et al (1975) are rather peculiar, showing a maximum N_u value at D/B≃9 and reducing asymptotically to the maximum shallow anchor value of N_u, calculated for D/B= 7.0 and $\alpha = 90 - \varphi$. This peak is a function of the equation derived for N_u and is not reproduced by any test results known to the author. The expressions for the deep anchor uplift factors of Kwasnieski et al (1975) and Fadl (1981) are particularly elaborate and it is difficult to grasp the significance of the various terms in the equations. Fadl claims that his method is more generally applicable than others because it takes account of the relative density of the sand. The Vesic deep anchor theory is independent of embedment ratio, but the lower limiting value is not specified. It was taken as D/B= 10.0, to allow for the transition from shallow (max. D/B= 5.0) to deep anchor behaviour. This independence of embedment ratio is not consistent with experimental results. Vesic's theory is considered more relevant to deep anchor failure in cohesive soil (Ponniah, 1984).

For both shallow and deep anchors, the relative position of some of the curves is markedly changed by a change in density, mirroring the relative importance of a change in the angle of friction in the respective equations. This highlights the basic problem with the theories and the derived equations : they do not yield consistent results, except for the conditions under which they were established, and therefore must be used with extreme caution. It is unlikely that a general theory for anchor uplift resistance will be established, and further work in this direction is considered to be of low priority.

Table 2.2 presents the N_u values used to draw the curves of N_u versus D/B (shallow and deep anchors in loose and dense sand). The values of φ and D_r were chosen as representative of loose and dense sand and used for comparative purposes only.

2.2.3 Experimental Studies

Previous reviews by Maddocks (1978), Andreadis (1979) and Fadl (1981) have covered many of the experimental studies into the uplift resistance of plate anchors in sand. The current review is written to augment the work done by these authors and is not intended to be a comprehensive survey of all previous work.

Colp and Herbich (1975) carried out model anchor uplift tests using vertical and inclined loading. The 75mm diameter anchors were buried in dense Ottawa sand at a dry density of 1730kg/m^3. Uplift tests were also carried out using samples of marine sediments from the Gulf of Mexico. Using regression analysis techniques, Colp and Herbich developed a dimensionless relationship between the maximum pullout force, its angle of inclination, the soil shear strength and the embedment ratio, which was valid for their test results. They reported that the anchor uplift resistance increased with increasing inclination from the vertical (up to 45^0), for both the dense sand and the marine sediments.

Kwasnieski, Sulikowska and Walter (1975) investigated the uplift resistance of single anchors and anchor groups buried in dry beach sand at two densities, 1790kg/m^3 and 1660kg/m^3. The anchor tests were carried out in a large tank lm x 2m x 2m deep, which was filled with layers of sand, each layer being compacted by vibration. The steel model anchor plates had diameters of 75mm and 150mm. Semi–spatial tests were also undertaken and, using information obtained from all these tests, together with some simplifying assumptions, the authors presented equations for calculating the uplift resistance of shallow or deep anchors buried in sand. These equations were reviewed in sub–section 2.2.1 of this thesis. Kwasnieski, et al also presented equations for the calculation of the uplift resistance of anchor groups in sand.

Das and Seeley (1975a and b, 1976) reported on laboratory tests carried out on rectangular, square and circular model anchors subjected to vertical, inclined, and eccentric loading, respectively. The rectangular anchors were 5lmm wide with aspect ratios of 1,2,3 and 5. The square anchors were 64mm x 64mm and the circular anchors had diameters of 64mm and 76mm. All the anchors were made from 3mm thick aluminium plate. The silica sand used in the tests was compacted in 25mm thick layers to a density of 1510kg/m^3. At this density the angle of friction and the relative density were 31^0 and 21% respectively. For vertical pullout of shallow rectangular plate anchors, Das and Seeley (1975b) concluded that the theory of Meyerhof and Adams (1968) could be used to predict the uplift capacity, up to an embedment ratio of about 0.75 x the critical embedment ratio. The critical embedment ratio marks the change from shallow anchor behaviour to deep anchor behaviour and is usually defined as $(D/B)_{cr}$. They also noted that the critical embedment ratio increased with increasing aspect ratio.

Maddocks (1978) used a stereo–photogrammetric technique to study the soil–anchor interaction in plane strain model tests. Using photographs of the edge plane of the model taken during a test, a stereo–comparator measured the displacements of sand grains which were then processed by a computer. This produced contour diagrams of the displacement and strain fields around an anchor for each increment of load, thus providing a continuous record of the interaction between the sand and the model anchors throughout a test. Plane strain equivalents of plate and cylindrical anchors were tested up to embedment ratios of 40, in beds of dense, dry, Leighton–Buzzard sand. The cylindrical anchors had either a rough or smooth surface finish.

Maddocks reported that the plane strain model of a deep plate anchor resisted the applied loading by end bearing only. The sand above the plate was compacted as it resisted the initial loading and the displacement of the plate was accompanied by a punching shear failure around its perimeter. As the loading increased, the punching shear developed into a local shear failure immediately above the plate, allowing the plate and a wedge of sand above it to penetrate the overlying sand. Sand grain movements were observed within a zone which extended ten times the anchor diameter on either side of the anchor and at least twenty diameters above the anchor. He concluded that the behaviour of the soil–anchor interaction was far too complex to be analysed on the basis of assumptions regarding the soil stress–strain relationship or the form of a potential failure surface, and suggested that the problem should be tackled using the finite element technique.

Tsangarides (1978) investigated, inter alia, the effects of varying the pullout rate, the anchor shaft diameter and the anchor thickness on the ultimate pullout resistance of circular model anchors buried in sand. The sand used was Halls No.1, a uniform, medium sand. The density of the dry sand was controlled by vibration (both vertical and horizontal) and a maximum density of 1701kg/m^3 was achieved (relative density= 93%, φ= 43.2^0 from shear box test). The use of vibration resulted in some inhomogeneity in the sand bed (denser at the top, reducing towards the bottom). Tsangarides found that varying the pullout rate within the range 0.5mm/min to 29mm/min did not effect the load–displacement behaviour of the anchors. A rate of 28mm/min was used during testing.

If the ratio of anchor diameter (B) to shaft diameter (B_s) was greater than four then the effect of the shaft diameter could be ignored. For ratios less than four and for the same anchor diameter, the ultimate uplift resistance

was reduced. Shaft diameters and anchor diameters ranged from 3mm to 25mm and from 13mm to 51mm, respectively.

If the ratio of anchor thickness (t) to anchor diameter (B) was less than three, then the effect of anchor thickness could be ignored. The ultimate load and the displacement at which it occurred both increased for increasing values of t/B above 3. The maximum anchor thickness used in the tests was 102mm.

Tsangarides also measured the horizontal stresses at locations throughout the depth of his tank (1800mm x 1800mm x 1200mm deep) in order to obtain K_o values for initial stress calculations and to investigate the effect of the proximity of the lateral boundaries on the distribution of horizontal stress in the sand bed. This part of the work is discussed in more detail in Section 2.4.

Andreadis (1979) and Andreadis, et al (1981) reported the results of static pullout tests conducted on cylindrical, conical, plate and fluke–type anchors buried in a uniform medium sand (Borough Green sand). The test tank was 2.44m in diameter by 1.22m deep and the anchors were placed in a fluidised column at the centre of the tank. The saturated sand beds were then densified by vibration to a relative density of 66% (ρ_d= 1560 kg/m^3, φ= 37^0). After vibration, induced horizontal stresses in the sand bed were reported. Some of the fluke anchors were embedded by impact loading.

Load–controlled and displacement–controlled tests were carried out and there was good agreement between the load–displacement graphs obtained. Most of the tests were displacement–controlled at a rate of 0.5mm/min. This pullout rate ensured that any changes in porewater pressure were negligible.

Andreadis (1979) concluded that the mode of failure of an anchor embedded in dense, cohesionless soil was primarily controlled by the embedment ratio, the relative density of the soil and the shape of the anchor. The ultimate resistance of cylindrical and plate anchors was approximately equal (the former being slightly larger), but that of conical shaped anchors was about 15% less. This difference increased with increasing embedment ratio and was attributed to the ease with which sand grains could flow around the anchor as it moved upwards. Compared to cylindrical anchors, fluke anchors experienced a local shear failure at shallower depths.

On the effects of anchor installation procedures, Andreadis concluded that systems which involved considerable loosening of adjacent sand, e.g. fluidisation,

resulted in the anchor failing by punching into the overlying disturbed sand without a full transfer of load to the surrounding dense sand. This behaviour was confirmed by Zakaria (1986) in a study specifically designed to investigate the effects of soil disturbance on anchor uplift resistance. Zakaria reported reductions in uplift resistance of up to 60%, depending on the lateral extent of the zone of disturbance.

Fadl (1981) carried out a large number of pullout tests in dry Leighton–Buzzard sand. Anchor diameters varied from 27mm to 75mm, and the embedment ratio varied from 1 to 25. The anchors, subjected to vertical and inclined loading, were embedded in dense, medium–dense and loose sand beds with relative densities of 85%, 50% and 25%, respectively. Measurements of anchor load, anchor displacement and surface deformations were recorded. Some tests incorporated thin (both laterally and vertically) horizontal strips of cement powder within the sand bed. After loading, the sand and cement layers were moistened and the cement allowed to harden. One half of the bed was then carefully removed to reveal the pattern of internal deformation. Fadl concluded that the uplift resistance of shallow and deep anchors in sand was significantly affected by the density (in terms of φ) and the relative density (D_r) of the sand, and incorporated these parameters into equations for shallow and deep anchor pullout (see sub–section 2.2.1).

Ovesen (1981) reported on shallow anchor pullout tests in dry sand performed in a centrifuge at the Danish Engineering Academy. Both vertical and inclined pullout tests were performed. Ovesen also considered scaling effects with respect to model anchor pullout tests. This part of the study is covered in more detail in section 2.4.

The centrifuge used by Ovesen had an effective radius of 0.72m, with a small swing–bucket container of 140mm internal diameter x 110mm deep. The sand used for most of the tests was a uniform diluvial sand called Dansk Normalsand No.1. Dense and loose sand beds were used, with relative densities of 95% and 36%, respectively. An acceleration of 500g could be achieved with this centrifuge. Ovesen presented equations for the uplift resistance of square and circular anchors subjected to vertical or inclined pullout. (see sub–section 2.2.1).

2.2.4 Summary

From the foregoing review of experimental work done on anchor uplift resistance, it is clear that the principal characteristics of plate–type anchors buried in cohesionless soil and subjected to static loading are well–established. These can be summarised as follows:

i) The mode of failure and the ultimate uplift resistance are primarily dependent on the anchor embedment ratio, the anchor shape and the relative density of the sand.

ii) The uplift resistance factor (N_u) increases sharply with increasing embedment ratio in the shallow range. For loose sands, the increase in Nu slows rapidly as the anchor embedment ratio moves into the deep range. For deep anchors in dense sand, the rate of increase of Nu reduces more slowly. Typical curves of Nu versus D/B are shown in Figure 2.15.

iii) The method of installation can substantially reduce the anchor uplift resistance.

In the present study, the static tests were performed to provide the necessary information on ultimate uplift resistance for use in setting the load levels in the cyclic loading tests. Parameters varied were the anchor embedment ratio and the sand relative density. Circular anchors were used throughout and the effects of disturbance were not investigated. The static test results were also used for comparison with some of the previous model test results mentioned in this review and with the numerical analysis described in Chapter 5.

2.3 CYCLIC LOADING

2.3.1 General

A great number of studies have been undertaken on the behaviour of soils subjected to cyclic loading. Cyclic loading can take many forms and it is important to distinguish between two fundamental types : dynamic loading, in which inertial effects are significant, and repeated loading, in which inertial effects can be ignored. The rate of loading at which a problem becomes

dynamic depends very much upon the mass and stiffness of the soil involved. For typical specimens used in laboratory tests, inertial forces generally do not become significant until the frequency of loading exceeds 25Hz (Lambe and Whitman, 1979). The cyclic testing described in Chapter 3 was undertaken at a frequency of approximately 0.1Hz, i.e. it was repeated loading with no inertial effects.

This brief review will concentrate on the repeated loading behaviour of sand, although many of the characteristics described are also relevant to dynamic loading conditions. The behaviour as determined from triaxial testing and simple shear box testing is considered separately.

a) Cyclic triaxial tests

Trollope et al (1962), Morgan (1966), Timmerman and Wu (1969), Tanimoto and Nishi (1970), Marr and Christian (1981) and others have reported on the cyclic loading behaviour of sand in triaxial tests. The results of Morgan (1966) are used to illustrate the principal conclusions of this work. His tests were carried out on samples of dry sand and the parameters investigated were the magnitude of the repeated load (deviator stress), the magnitude of the confining pressure and the number of cycles of loading. The samples, 100mm in diameter and 200mm high, were subjected to 1 million cycles of square wave loading at a frequency of 0.83Hz. A few samples were loaded for 2 million cycles. The level of repeated load applied to the samples ranged from 17% to 83% of the equivalent static failure load. The deformation along the vertical axis and the deformation of the diameter were monitored continuously.

The effect of deviator stress and confining pressure on the variation of permanent axial strain with number of cycles is illustrated in Figure 2.16. For tests at constant confining pressure, the permanent axial strain increases with increase in deviator stress (Figure 2.16 (a)). At constant deviator stress, the permanent axial strain decreases with increase in confining pressure (Figure 2.16 (b)).

Morgan found that the permanent axial deformation of all the samples tested continued to increase, even after 2 million cycles of loading. After an initial loading of up to 200,000 cycles, the rate of increase of the axial deformation reduced to a very small, constant value. Even when the applied load was 83% of the equivalent static failure load, the rate of axial deformation still decreased to a very small value. Morgan suggested that at this stage the

sand could be considered to be effectively in a stable condition : the deformations during each cycle of load were almost fully recoverable, and the sand was behaving elastically with a constant resilient modulus(ratio of the change in axial stress in a cycle of load to the axial strain recoverable in that cycle). However, Morgan also observed that small permanent deformations were accumulating, and that the resilient deformation of the sand gradually decreased as the number of load applications increased. This implied that the sand was becoming stiffer and was continuing to deform very slowly. Morgan suggested that these phenomena might be due to movement of the sand grains, causing very small plastic deformations, or attrition of the sand grains themselves. These phenomena would accompany the elastic deformations of the skeletal structure of the sand.

The variation of resilient modulus (E_r) with confining pressure and deviator stress is shown in Figure 2.17. At a given confining pressure, the modulus decreases slightly with increasing deviator stress (Figure 2.17 (a)), whilst for a constant deviator stress, the modulus increases with confining pressure (Figure 2.17 (b)). In most cases, there is a general trend of increasing resilient modulus with number of cycles, up to an approximately constant value in the range 10^5 to 10^6 cycles.

Timmerman and Wu (1969) separated the axial strain into two components : volumetric strain and shear strain. In general, these strains increased with the number of cycles, but at a rapidly decreasing rate. After approximately 2000 cycles the axial strain rate was very small indeed.

Under repeated loading, specimens with densities ranging from loose to dense exhibited progressive volumetric compression. Timmerman and Wu noted that the volumetric component was a relatively small part of the total axial strain and concluded that, within the stress range used, shear strain rather than volumetric strain was the major cause of densification.

In an earlier study, Ko and Scott (1967) investigated the effect of repeated cycles of hydrostatic compression on cubic samples of sand. This loading produced only volumetric strain on the sample as a whole, and Ko and Scott reported that a small amount of irreversible volumetric compression, or density increase, occurred during the first few cycles of loading. After this initial permanent compression of the sample, deformations during additional cycles were found to be non– linear but completely elastic.

Marr and Christian (1981) carried out cyclic triaxial tests in connection with the Oosterschelde barrier in the Netherlands. The tests were conducted under isotropic and anisotropic conditions, as defined in Figure 2.18. With respect to axial strain, the results are similar in form to those reported by Morgan (1966). It is clear from the results that the initial shear stress has an important effect on the strains developed during cyclic loading.

Summarising the conclusions with respect to the cyclic loading of sand in triaxial tests leads to the following:

i) Samples subjected to repeated loading continue to deform throughout the test due to volume change and shear distortion. The amount of deformation caused by each is dependent on the initial shear stress.

ii) The axial deformation of samples increases with increasing repeated load level (deviator stress) and decreasing confining pressure.

iii) The rate of axial deformation decreases rapidly at the beginning of a test and, after a large number of cycles, the rate is reduced to a very small value. This also applies to volumetric deformation.

At this stage, the behaviour of a sample during a single cycle of load is almost elastic, but over a large number of cycles the sample suffers further small permanent deformations and becomes more stiff. An explanation for this behaviour is that, while the sand grains and the skeleton formed by the sand grains behave in a predominantly elastic manner, small permanent deformations continue to accumulate due to movement of the sand grains and/or attrition of the sand grains.

iv) For non–inertial frequencies ($\leqslant$25Hz), varying the frequency has little effect on the behaviour of the sand samples

v) No significant behavioural differences exist between samples tested dry and similar samples tested in a saturated, but fully drained, condition.

b) Cyclic shear tests

Youd (1970, 1971, 1972), Silver and Seed (1971a, 1971b), Moussa (1975), Wood and Budhu (1980) and others have reported on the cyclic loading

behaviour of sand in simple shear. The results of Youd (1972) and Silver and Seed (1971a) are used to illustrate the main conclusions of this work.

Youd (1972) tested a standard gradation of Ottawa sand C−109 in a simple shear apparatus based on the NGI design. Up to 150,000 cycles of shear were applied to samples at shear strain amplitudes ranging from ±0.05% to ±4.50% (approximately), under normal (vertical) stresses ranging from 4.8kPa to 192kPa. Shear displacement and volume changes were continuously monitored, and the effects of frequency and saturation were also investigated.

Figure 2.19 shows the void ratio versus strain history of a sample cyclically strained in simple shear. During each cycle, the sample contracts and dilates, but the net result is a reduction in void ratio (increase in density). A minimum void ratio is established after a few thousand cycles. The effect of shear strain amplitude on the minimum void ratio per cycle is shown in Figure 2.20. Although the reduction in void ratio increases markedly with shear strain amplitude, all the curves asymptotically approach the same minimum void ratio. The number of cycles to achieve this minimum void ratio increases with decreasing amplitude.

In Figure 2.21, the change in void ratio occurring in a given number of cycles is plotted against shear strain amplitude for tests carried out at different values of vertical stress (σ_v). Within the range of parameters used, changing σ_v has virtually no effect on the void ratio for a given strain amplitude and number of cycles, whilst the influence of shear strain amplitude is obvious. Similar observations were reported by Silver and Seed (1971b), who also reported that for the same shear strain amplitude, the lower the relative density of the sample, the greater the reduction in void ratio after the same number of cycles.

The form of the volume changes within cycles shown in Figure 2.19 was confirmed by Wood and Budhu (1980). They carried out cyclic shear tests on samples of Leighton Buzzard sand in the Cambridge simple shear apparatus and obtained volume change cycles as shown in Figure 2.22. The amount of contraction or dilation during each cycle increases with shear strain amplitude. The void ratio at the end of each cycle is plotted in Figure 2.23 for loose and dense sand. The graph for dense sand gives results contrary to the shear strain amplitude effect shown in Figure 2.20. As the strain amplitude increases, the reduction in void ratio decreases. In fact, for the strain amplitude of ±10%, there is a net increase in void ratio during cyclic straining. At this large strain amplitude in a dense sand, dilation effects predominate during the first few

cycles of shear and the void ratio increases. Subsequent cycling at the same large strain amplitude is unable to reduce the void ratio significantly.
The initially dense sand becomes denser when cycled at the smaller shear strain amplitudes of ±2.5% and ±1.0%.

Silver and Seed (1971a) investigated the shear stress– strain behaviour of sand subjected to cyclic loading. They used a modified NGI simple shear apparatus and samples of a uniform, angular quartz sand (Crystal Silica No.20). Small shear strain amplitudes ranging from ±0.01% to ±0.5% were applied to the samples, which had relative densities of 45%, 60% or 80%. The vertical stress varied from 24kPa to 192kPa.

Silver and Seed plotted values of shear stress versus strain for discrete cycles, yielding the hysteresis loops shown in Figure 2.24. The testing was stopped after 300 cycles, by which time the hysteresis had reduced significantly and the shear modulus had increased. The shear modulus (G_{eq}) was defined as the slope of the line passing through the origin and the top and bottom of the hysteresis loop (see Figure 2.24).

The increase in shear modulus with cycles is apparent from Figure 2.25, which also shows that the shear modulus increases with vertical stress and decreases with increasing strain amplitude. The relationship between shear modulus, shear strain amplitude, vertical stress and relative density as reported by Silver and Seed for cycle 10 of their tests is shown in Figure 2.26.

Summarising the conclusions with respect to the cyclic loading of sand in simple shear leads to the following:

i) Both compression and expansion occur in samples during each cycle of shear strain.

ii) All other parameters being equal, the lower the relative density of the sample, the greater the reduction in void ratio.

iii) In general, the reduction in void ratio (increase in density) which takes place during cycling increases with shear strain amplitude. Exceptionally for very large shear strain amplitudes in dense sand, the void ratio may increase due to dilation effects.

iv) The number of cycles to achieve the minimum void ratio increases with decreasing shear strain amplitude.

v) The volume change behaviour is not significantly affected by changes in vertical stress, frequency or whether the sample is dry or saturated(but fully drained).

vi) The cyclic shear modulus increases with number of cycles, vertical stress and relative density of the sample, and decreases with increasing shear strain amplitude.

2.3.2 Plate Anchors

The experimental investigation of cyclic loading effects could involve most of the parameters used in static loading tests plus those relevant to cyclic loading, e.g. frequency, number of cycles, cyclic load level and form of cyclic loading. This range of parameters leads to difficulties when comparing the results of different investigations, as the combined effects of the various parameters used means that each investigation is unique in itself. Accordingly, this review groups together, whenever possible, work which has used a reasonably consistent set of parameter values. General conclusions from the work presented will be made at the end of the review.

In almost every study, the testing was undertaken at frequencies which ensured that inertial effects were minimal. Figure 2.27 illustrates the forms of cyclic loading used. These are (a) repeated loading, (b) sustained–repeated loading and (c) alternating loading. Repeated loading cycles from zero to a predetermined tensile load, usually expressed as a percentage of the static failure load (sfl). Sustained–repeated loading cycles between two tensile load levels, whereas alternating loading cycles from a tensile load to a compressive load. In testing, repeated loading has been used most often, usually with a sinusoidal or square waveform. A further point to note regarding cyclic loading is that anchor failure is not well defined. Any definitions used are usually related to anchor displacement, either total displacement or rate of displacement, with limiting values being placed on these quantities.

Trofimenkov and Mariupolskii (1965) were the first to report on the effects of cyclic loading on anchor uplift resistance. They tested large screw

piles (0.25m to 1.0m in diameter) in moist and saturated sand under repeated and alterating load. The effect of the cyclic loading was to considerably reduce the anchor uplift resistance. With respect to the static uplift resistance in saturated or dry sand, Trofimenkov and Mariupolskii recommended reduction factors of 0.5 and 0.3 for repeated and alternating load, respectively. For moist sand, the reduction factor was 0.7 for both types of loading. Trofimenkov and Manupolskii also observed a reduction in uplift resistance if stepwise loading was used instead of continuous pullout, and suggested a general reduction factor of 0.8 in this case.

Matsuo (1967) reported on short term cyclic loading tests on circular anchors (240mm diameter) buried in sand. Fifty cycles of loading were applied, at a frequency of 2 cycles per minute. Repeated and sustained–repeated loading were used, with the former having a more detrimental effect on anchor displacement. From the results of static tests, Matsuo defined an upper yield point, based on anchor displacement rates, which was approximately 80% of the ultimate uplift resistance. If the maximum load per cycle in repeated load tests was kept below this limit, then the anchor displacement did not differ greatly from that obtained in an equivalent static test. Repeated loading above this limit resulted in substantial anchor displacements and rapid failure.

Work carried out in the early seventies at the University of Massachusetts (Amherst) was concerned with the static and cyclic uplift resistance of marine anchor flukes in sand and clay. Kalajian (1971), Bemben, Kalajian and Kupferman (1973), Kupferman (1974) and Bemben and Kupferman (1975) reported at various stages on the results of the research. The sand used was a medium to fine sand, known as Sutherland sand, and anchor fluke tests were undertaken in loose sand ($D_r \simeq 25\%$) and dense sand ($D_r \simeq 90\%$). The fully saturated sand had corresponding friction angles of 38^0 and 46^0. The cyclic loading, applied via a hydraulic piston, had a sinusoidal waveform and a period of approximately 8 seconds (frequency = 0.13Hz). Repeated loading was used in all the tests. Fluke anchors of 76mm diameter and 152mm diameter were used, having horizontal projected areas of $3948mm^2$ and $15787mm^2$, respectively.

A typical set of test results is presented in Figure 2.28, in terms of relative anchor displacement, Δ/B, and peak cyclic load, P_c, expressed as a percentage of the static failure load. These results show that, over the period of testing, there was a continuing vertical displacement of the fluke, and the rate of displacement increased with increasing P_c. Visual observations of sand grain movements around the anchor fluke, made during semi–spatial tests,

showed that sand grains flowed under the bottom edges of the fluke as it moved upwards. On unloading, the fluke was prevented from returning to its original position by the presence of these sand grains. This characteristic was described as cyclic creep and was considered to be responsible for the continuing anchor displacement during repeated loading. In order to quantify the cyclic creep, Kupferman (1974) defined a parameter called the cyclic creep factor, c_λ, as follows:

$$c_\lambda = \frac{\Delta/B}{(1 + \log t_1)}$$

where t_1 = duration of repeated loading in days.

Figure 2.29 shows the results for dense and loose Sutherland sand in terms of cyclic creep factor and peak cyclic load. From these results it is clear that the cyclic creep factor is dependent on the anchor embedment ratio, the relative density of the sand and the peak cyclic load.

Taylor and Lee (1973) and Taylor, Jones and Beard (1975), working at the Naval Civil Engineering Laboratory, Port Hueneme, California, presented design recommendations for the long term repeated loading capacity of full-scale embedment anchor systems. For anchors in cohesionless soil, two important parameters were identified: the grain size distribution and the embedment ratio. If the median grain size (d_{50}) is greater than 0.2mm then, for shallow anchors, the design repeated load capacity is taken as half of the equivalent static capacity. For deep anchors, it is taken as half the static capacity calculated at the critical depth, i.e. the depth which defines the change from shallow to deep behaviour. The critical depth was defined after Meyerhof and Adams (1968) (see sub-section 2.2.1).

If the median grain size is in the range 0.02mm to 0.2mm then the authors suggest the use of a different mooring technique or high factors of safety (>10). No explanation was given for the distinction made in respect of d_{50}, but it was probably connected with the cyclic creep effect experienced by the anchors.

A number of investigations into the behaviour of plate anchors buried in sand and subjected to cyclic loading have been undertaken at the University of Sheffield. Some preliminary results were reported by Carr (1970) and Abu-Taleb (1974). The former, working on shallow anchors in loose sand, observed that repeated loading increased the anchor displacement, but when

subsequently loaded to failure, the anchor static failure load was unchanged. Carr also reported that complete unloading during a cycle resulted in greater anchor displacement than unloading to 50% of the static failure load.

Abu–Taleb carried out a limited number of tests on prestressed anchors, and noted that repeated loading gradually reduced the initial prestress load in the system. Prolonged repeated loading could eventually eliminate the entire prestress load, the number of cycles to achieve this depending on the magnitude of the load change per cycle. Abu–Taleb also noted that the anchor displacement per cycle reduced with increasing initial prestress.

Extensive studies of anchor behaviour under cyclic loading were carried out by Sivapalan (1976) and Senturk (1977), and these were concisely reported in Hanna, Sivapalan and Senturk (1978). A major objective of the research was to establish relationships between the number of load cycles and the anchor displacement, for different cyclic loads at different overconsolidation ratios in the sand. The consolidation–type pressure cells developed by Carr (1970) were used to test the anchors, in which overconsolidation ratios of up to 8 could be achieved. The cyclic loading, applied through a lever arrangement attached to a reciprocating mechanism, had a square waveform and a period of 60 seconds. The uniform, medium, dry sand was placed at a relative density of approximately 77% ($\rho_d \simeq 1720 kg/m^3$). The friction angle was 39.5^0.

In all, a total of 44 tests were performed : four static tests to establish the static failure load, 19 repeated load tests, 3 sustained–repeated load tests and 18 alternating load tests. Based on the repeated load test results, the following observations were made:

i) The effect of overconsolidation ratio (OCR) was relatively small and inconsistent. This is illustrated in Figure 2.30, in which the anchor displacement is plotted against the logarithm of number of cycles. Figure 2.30 also shows that anchor failure is not well defined.

ii) The anchors sustained non–recoverable displacements, with the displacement per cycle decreasing as the number of cycles increased, as shown in Figure 2.31.

iii) The hysteresis loop of load versus displacement reduced in area until, after a few thousand cycles, the loops reached a near stable state. At this stage the anchor displacement per cycle was almost completely recovered and the sand exhibited a stiffer response to the loading (c.f. Morgan, 1966 ; Silver and Seed, 1971a).

iv) The stiffer sand response resulted in greater post–cyclic uplift resistance. This is illustrated in Figure 2.32.

The use of alternating load had a much more detrimental effect on anchor behaviour. As shown in Figure 2.33, the anchor displacement per cycle did not continue to reduce, as it did with repeated loading (Figure 2.31), but instead turned upwards, leading to instability and failure.

Hanna and Al–Mosawe (1981) reported on a subsequent study of prestressed anchors subjected to cyclic loading. This confirmed the findings of Abu–Taleb (1974) and concluded that the prestress of an anchor, whilst increasing its "life" with respect to repeated or alternating load, did not prevent deterioration in the anchor behaviour. Essentially, the life span of the anchor was increased, but the same general trends found for non–prestressed anchors applied. Evidence of a change in gradation of the sand near the anchor was presented by Hanna and Al–Mosawe. Attrition of the sand grains during cyclic loading was considered to be the most likely cause.

Dynamic loading of circular plate anchors buried in a dense, dry, uniform sand was investigated by Clemence and Veesaert (1977). The sand, placed at an average relative density of 96% (ρ_d= 1700kg/m^3), had a friction angle of 41°. Semi–spatial tests were also carried out in order to observe, using still and movie photography, the formation and shape of any failure surfaces created during static and dynamic loading. The time to peak dynamic load was less than 1/3rd second in all the tests, and measurements of anchor acceleration gave an average value of approximately 0.2g. Embedment ratios up to seven were investigated, using 76mm and 127mm diameter anchors.

Clemence and Veesaert concluded that the dynamic resistance of shallow anchors in dense sand was greater than the equivalent static resistance. The dynamic resistance could be estimated by modifying their equation for static resistance (Equation 2.11) to take account of inertia forces and increased shear resistance due to rapid strain rates. Clemence and Veesaert also reported no

discernible difference in the shape of failure surfaces formed during static and dynamic loading.

The study by Maddocks (1978) described in sub–section 2.2.3 included dynamic tests on rough, cylindrical anchors. The tests were carried out at frequencies of 1,5 and 10Hz, using a sine wave signal varying in amplitude between 0 and 25% of the equivalent static failure load. A full description of the movement of the sand grains around the anchor was given by Maddocks, and this included an account of the cyclic creep effect. Maddocks reported that, for the deep anchors tested, the rate of displacement reduced throughout the test but the total displacement of the anchor continued to increase. During a test, the sand above the anchor stiffened and developed a greater resistance to the applied loading and any subsequent re–loading. However, the post–cyclic failure load was less than the equivalent static failure load. For the range considered, the behaviour of the anchor model was independent of the frequency of loading.

A large research project into the behaviour of anchors under cyclic loading was carried out at Queen Mary College, London. The research group has published numerous papers on their work, but the two principal references are Andreadis (1979) and Andreadis, Harvey and Burley (1981). These references have already been reviewed with respect to static loading behaviour (see sub–section 2.2.3).

The repeated and sustained–repeated tests used sinusoidal loading at a frequency of 0.5Hz, which was judged to produce a non–dynamic response. Pore–pressure measurements at anchor level indicated that drained conditions prevailed. The effects of varying, inter alia, the embedment ratio, the sand density and the peak cyclic load value were investigated.

Andreadis et al reported a number of conclusions from their work, the most important of which were as follows:

i) The repeated loading behaviour of a particular anchor could be represented by a family of hyperbolic curves, as shown in Figure 2.34, in which the relative anchor displacement, Δ_c/B, is plotted against the logarithm of number of cycles, log N.

   Similar curves could be drawn for different anchor embedment ratios and sand densities and for sustained–repeated loading. In all cases,

an increasing anchor displacement developed due to the cyclic creep effect (c.f. Hanna, et al, 1978).

ii) Failure of the anchor could be defined using a graph of relative anchor displacement against relative anchor displacement per cycle, Δ_{pc}/B. An example is reproduced in Figure 2.35. The anchor was considered to have failed when Δ_{pc}/B began to increase and the value of Δ_c/B at this point was defined as the critical cyclic relative displacement, $(\Delta_c/B)_{cr}$. The value of $(\Delta_c/B)_{cr}$ increased with increasing embedment ratio, but a mean value of 0.1 was suggested for design purposes.

iii) With respect to the distribution of horizontal stresses in the sand, the effects of repeated loading were confined to a relatively small zone around the anchor body, in which the stresses were considerably smaller than the static values obtained at the same load level as the peak repeated load. Figure 2.36 illustrates this effect for an anchor loaded to $40\%P_u$.

iv) The post–cyclic response to static loading was characterised by a steeper load–displacement curve than the equivalent static test, indicating that the sand had become stiffer. This was associated with soil density changes around the anchor and supported by evidence of a progressive reduction in area of the load–displacement hysteresis loops during the first few thousand cycles of loading (c.f. Hanna, et al, 1978). This stiffening effect is shown in Figure 2.37, for a cylindrical anchor at an embedment ratio of 8. Note that the value of the ultimate uplift resistance was not affected by the stiffer response. This was characteristic of most of the post cyclic tests.

v) Anchors subjected to repeated loading increased their resistance to displacement at a decreasing rate, as the total displacement accumulated. The anchors therefore attained an ultimate stiffness and further repeated loading did not increase that stiffness.

Clemence and Smithling (1983) performed cyclic loading tests on quarter–scale helix anchors in dry sand. The uniform, fine sand had a relative density of 67.5% (ρ_d= 1562kg/m^3) and a friction angle of 35°. The anchors, 38mm in diameter, were buried at a constant embedment ratio of eight. A sinusoidal cyclic displacement was applied at a frequency of 6Hz and the effect

of varying the displacement amplitude was investigated. Repeated and sustained–repeated tests were carried out, and in some tests the horizontal stresses in the vicinity of the anchor were measured.

From the results of their tests, Clemence and Smithling concluded that an increase in displacement amplitude leads to more rapid failure. Figure 2.38 shows this clearly for displacement amplitudes of ±1.78mm and ±0.68mm. Surprisingly, the latter test was quoted as having the larger peak cyclic load. This does not seem reasonable.

Near the anchor, the effect of helical anchor installation caused an increase in horizontal stresses and densified the sand. During cyclic loading, the horizontal stresses reduced in magnitude (c.f. Andreadis, et al, 1981). Cyclic creep occurred in both repeated and sustained–repeated tests.

The post–cyclic uplift resistance of anchors in sustained–repeated tests was lower than the equivalent ultimate static resistance. Clemence and Smithling claimed that the reduction was caused by loosening of the sand during cyclic loading. This is contrary to the findings of all other investigators, who reported a densification of the sand around the anchor during cyclic loading.

2.3.3 Summary

From the foregoing review of previous investigations into the behaviour of plate–type anchors in cohesionless soil subjected to cyclic loading, the following conclusions can be made:

i) The anchors sustain non–recoverable displacement which continues to accumulate throughout the loading period. This displacement is caused by individual grains of sand flowing under the anchor as it moves upwards during every cycle of load, thus preventing the anchor from returning to its pre–cycle position. This mechanism is called the cyclic creep effect and is of paramount importance in this context.

ii) The displacement characteristics of an anchor are profoundly affected by the amplitude of the loading : the larger the amplitude, the greater the anchor displacement at any particular time.

iii) The anchor displacement per cycle (or rate of displacement) initially decreases with time (or number of cycles). However, as the test progresses, the rate of displacement may begin to increase. This reversal in displacement rate can be used as a failure criterion for the anchor.

iv) The sand around the anchor becomes stiffer and more dense. This is associated with movement of the sand grains and/or attrition of the sand grains during repeated loading. There is some evidence to suggest that the sand in this zone attains an ultimate stiffness, and further repeated loading does not increase the stiffness.

v) Reflecting the change in sand stiffness, the post–cyclic static response of an anchor has a steeper load–displacement curve than the equivalent static test, but there is disagreement about the magnitude of the post–cyclic failure load vis–a–vis the static failure load.

vi) The effects of applying alternating load are much more detrimental to anchor behaviour. In particular, the anchor displacement increases at a much faster rate, leading to instability and failure in a relatively short time.

Further conclusions regarding, for example, the effects of sand over–consolidation ratio, anchor prestress and installation procedures can be made, but they are not relevant to the present series of cyclic loading tests. These were undertaken to investigate the cyclic creep effect, and the overall displacement response of an anchor when subjected to different cyclic loading levels.

2.4 MODELLING CONSIDERATIONS

2.4.1 Introduction

The basic types of model studies used in soil mechanics were defined in the introduction to the thesis. Irrespective of the type of model study undertaken, there are two important aspects of modelling that should be considered, viz. boundary effects and scale effects. Therefore, before moving on to Chapter 3, these aspects of modelling are discussed in the following two sub–sections, with particular reference to anchor model tests.

2.4.2 Boundary Effects

It is not possible to model a semi-infinite mass of soil and therefore, in laboratory testing, the soil is enclosed within a rigid boundary. The possible effects of this boundary on the subsequent test results must at least be acknowledged, though the exact nature of the interference may be difficult to identify, let alone quantify. Previous investigations of anchor uplift resistance have used the ratio of container diameter (or equivalent), B_c, to anchor diameter, B, as a marker for possible boundary effects. Minimum ratios ranging from 3 (Wang, et al, 1977) to 32 (Tsangarides, 1978) have been quoted, with the majority in the range $10 \leqslant B_c/B \leqslant 20$.

Attempts have been made to assess the zone of disturbance associated with anchor uplift in sand. Carr (1970) and Yilmaz (1971) used specially designed sand movement gauges to measure sand movement around an anchor. They reported no movement in the zone outside $B_c/B > 8$, i.e. greater than 4 anchor diameters from the anchor. The stereo-photogrammetric technique used by Maddocks (1978) to study sand grain movements around a plane strain anchor revealed grain movements up to 10 anchor diameters from the anchor (i.e. $B_c/B = 20$). This was for deep anchors in dense sand (D/B up to 40).

Measurements of horizontal stresses at the boundary were made by Tsangarides (1978) and Andreadis, Harvey and Burley (1981) using electronic soil pressure gauges. The gauges were placed at locations throughout the depth of the sand bed in order to monitor the soil stresses during anchor testing. Figure 2.39 shows the distribution of horizontal stresses at the tank wall caused by the pullout of a 125mm diameter cylindrical anchor. The ratio of B_c/B was 20. Presumably the stress distribution of Figure 2.39 is in addition to the initial in-situ horizontal stresses, although this is not made clear. The initial vertical stress at 500mm depth was 7.65kPa.

Andreadis et al noted that the magnitude of the horizontal stresses increased with increasing anchor diameter (D/B constant), and suggested that a much larger mass of sand was affected by anchor testing than had been considered previously.

In order to assess the effect of the proximity of rigid boundaries on the ultimate uplift resistance of an anchor (P_u), Tsangarides carried out a series of pullout tests in tanks of various sizes. Using a 50mm diameter anchor (102mm thick) in dense sand, Tsangarides found that, for $D/B < 10$, the value of P_u was

constant for tests in tanks 600mm x 600mm ($B_c/B = 12$), 900mm x 900mm ($B_c/B = 18$), 1200mm x 1200mm ($B_c/B = 24$) and 1800mm x 1800mm ($B_c/B = 36$). Tests in a tank 300mm x 300mm ($B_c/B = 6$) resulted in a marked increase in P_u.

Apart from the need to minimise boundary effects, considerations of soil handling procedures and apparatus design affect the final choice of container size. For the author's model tests, a 500mm diameter container was used, which resulted in B_c/B varying between 5 and 20. Most tests used a 50mm diameter anchor, giving $B_c/B = 10$.

The range of B_c/B was considered sufficient to avoid significant boundary effects, especially if the embedment ratio was limited to less than 10. In fact, for $D/B > 8$ in dense sand, P_u was affected by the proximity of the rigid boundary, and this is highlighted in the discussion presented in Chapter 6.

2.4.3 Scale Effects

In Chapter 1 it was stated that the present model tests would be considered to be small prototypes, and therefore problems of similitude should not arise. Nevertheless, it is instructive to review the paper by Ovesen (1981), which discussed in some detail the scaling laws relating to anchor uplift tests in sand when modelling prototype situations. Ten parameters were identified by Ovesen as potentially important in determining the anchor uplift resistance.

B, anchor diameter
D, anchor depth
θ, angle of pullout from vertical
γ, unit weight of sand
e, void ratio of sand
φ_μ, angle of interparticle friction
σ_c, interparticle cohesion
σ_g, crushing strength of grains
E_g, modulus of elasticity of grains
d_{50}, average grain size

Ovesen stated that these parameters were independent, but clearly this is not the case for all of them : at least γ and e are dependent on each other. The uplift resistance factor, N_u, was then expressed as a function of eight

"independent" dimensionless products, as follows:

$$N_u = p_u/\gamma_D = f[\theta,\ e,\ \varphi_\mu,\ D/B,\ d_{50}/B,\ \sigma_c/\gamma_D,\ \sigma_g/\gamma_D,\ E_g/\gamma_D] \quad (2.17)$$

In order to ensure complete similarity, the prototype and model values of the respective dimensionless products must be equal. Ovesen tabulated the similarity requirements for conventional model tests and centrifugal model tests with respect to a prototype, and these are reproduced in Table 2.3. In the author's opinion, the last three dimensionless products in equation 2.17 are of secondary importance in determining the uplift resistance of an anchor in sand and could be ignored without loss of accuracy. Also, the friction angle, φ, is considered a more appropriate parameter than φ_μ, the angle of interparticle friction (Ovesen also switched to using φ). For any particular sand, there is a relationship between void ratio and φ, and therefore only one of these parameters need be considered. For vertical pullout, the angle of pullout, θ, is not required. Hence the uplift resistance factor reduces to a function of D/B, φ and d_{50}/B.

From Table 2.3, the embedment ratio and the friction angle are dimensionally similar between prototype and model, for both conventional and centrifugal tests. The average grain size ratio is not similar, again for both conventional and centrifugal tests. Therefore, assuming that the anchor uplift factor can be accurately expressed as a function of D/B, φ and d_{50}/B, there is no benefit in using centrifugal modelling of anchor uplift tests.

The validity of this statement is certainly borne out in some circumstances, for example the conventional model tests undertaken by Sutherland (1965) in connection with shaft–raising operations. These tests provided realistic upper and lower bounds to the prototype uplift resistance encountered in the field (See Figure 2.40). Further evidence is presented in Ovesen's paper itself, and is reproduced in Figure 2.41. For shallow anchors in loose sand ($D/B \leqslant 3.5$), there is indeed little difference between the uplift factors from conventional and centrifugal tests. In dense sand, the uplift factors from conventional tests are approximately 25% higher than those obtained using centrifugal testing. However, these characteristics of Figure 2.41 are not supported by the theoretical work discussed in sub–section 2.2.2. Referring back to Figure 2.10 (shallow anchors, dense sand), the curves of Fadl and of Ovesen are almost coincident, but Fadl's curve was derived from conventional test results whereas Ovesen's was derived from centrifugal test results. The corresponding curves for shallow anchors in loose sand (Figure 2.9) have the

uplift factors from centrifugal tests greater than those from conventional tests. Why these anomalies should arise is not clear, but a possible explanation may lie in the effect of the third parameter, d_{50}/B, which is not modelled properly in either test situation. This may result in scale effects being present in either or both types of test. A very similar parameter was identified by Steenfelt (1982) in an investigation of scale effects in model tests of footings in cohesionless soil.

Consider the results from Ovesen's centrifugal tests, presented in Figure 2.42, in which the uplift resistance factor, N_u, is plotted against anchor diameter, B. These results show no scale effect for D/B= 1.85. Similar results from conventional model tests by Hutchison (1982) are shown in Figure 2.43. For embedment ratios of 6 and 8, there is clear evidence of a scale effect on the value of uplift resistance factor. However, for D/B= 2.0, there is negligible scale effect for the relatively large anchor diameters used (66mm and 104mm). The figure adjacent to each point in Figure 2.43 is the value of B_c/B for that test. Note that if boundary effects were present, the N_u values would increase with decreasing B_c/B.

The grain size ratios from these tests are listed in Table 2.4 for comparison. Note that the comparison is made for circular anchors in dense sand. The reciprocal of d_{50}/B is used purely for convenience. Over the range 50 to 144 for B/d_{50} from centrifugal tests, no scale effects are evident. Similarly, over the range 83 to 130, no scale effects are present in the conventional tests reported by Hutchison. Referring to the test results compared in Figure 2.41, they all have the same value of B/d_{50}, viz. 65. This should ensure that scale effects are not present in the centrifugal tests. However, this may not be true for the conventional tests because, as the ratio B/d_{50} reduces, there is a greater likelihood of scale error. This would result in larger values for N_u, thus contributing to the difference between the dense sand curves in Figure 2.41.

To the author's knowledge, centrifugal tests in the deep anchor range have not been reported, and therefore it is not possible to compare results for this case. Based on Figure 2.43, conventional tests in the deep anchor range are likely to suffer substantial scale error.

Finally, with respect to cyclic loading, inertia effects could be a further complication in model tests. However, when there is no requirement to model the dissipation of porewater pressure (as in dry sand), inertia effects can be

eliminated by using a low frequency of loading. Therefore, compared to static tests, no additional scale effects are likely to be present. Further discussion of scale effects and boundary effects is presented in Chapter 6.

TABLE 2.2 - Theoretical Values of N_u

(a) Shallow anchors, loose sand (ϕ = 30°)

D/B	Matsuo	Meyerhof and Adams	Vesic[1]	Kwasnieski et al	Fadl[4]	Ovesen[5]	Saeedy[6]	Clemence[7] and Vessaert
1	2.7	2.2	2.1	1.7[2](2.6)[3]	2.0	2.1	2.8	2.8
2	4.0	3.8	-	2.6 (5.1)	3.2	4.1	4.9	5.1
2.5	-	-	4.4	- -	-	-	-	-
3	6.0	5.6	-	3.9 (8.5)	4.6	6.7	7.8	8.0
4	7.9	7.8	-	5.4 (12.7)	-	9.8	11.1	11.5
5	9.9	-	9.9	7.3 (17.9)	-	13.2	15.0	15.5
6	-	-	-	9.4 (23.9)	-	17.1	19.1	-
7	-	-	-	11.8 (30.8)	-	21.3	-	-

Footnotes:
(1) Calculated using breakout factors from Table 2 of Vesic (1971).
(2) Calculated using 'α' after Fadl (1981), i.e. α = 90 - 12 = 78°.
(3) Calculated using α = 90 - ϕ = 60°.
(4) Calculated using Dr = 20%, H/B = 3.0, α = 12°.
(5) Strictly valid for D/B < 3.5 only.
(6) Values taken from graph. (See Figure 2.5).
(7) Strictly valid for dense sand only.

(b) Shallow anchors, dense sand (ϕ = 40°)

D/B	Matsuo	Meyerhof and Adams	Vesic[1]	Kwasnieski et al	Fadl[4]	Ovesen[5]	Saeedy[6]	Clemence and Vessaert
1	3.3	3.2	2.4	2.3[2] (3.6)[3]	3.7	3.5	3.1	3.7
2	5.2	6.4	-	4.7 (8.1)	7.8	7.9	6.0	7.3
2.5	-	-	5.5	- -	-	-	-	-
3	8.5	10.8	-	8.2 (14.5)	13.3	13.7	9.9	12.1
4	12.0	16.3	-	12.7 (22.7)	20.2	20.6	14.7	17.8
5	15.8	22.9	13.0	18.3 (32.9)	28.5	28.4	20.0	24.6
6	-	30.6	-	24.9 (44.9)	38.1	37.0	26.7	-
7	-	39.5	-	32.7 (58.8)	49.2	46.4	-	-

Footnotes:
(1) Calculated using breakout factors from Table 2 of Vesic (1971).
(2) Calculated using 'α' after Fadl (1981), i.e. $\alpha = 90 - 27 = 63°$.
(3) Calculated using $\alpha = 90 - \phi = 50°$.
(4) Calculated using Dr = 80%, $H/B = 10.0$, $\alpha = 27°$.
(5) Strictly valid for $D/B < 3.5$ only.
(6) Values taken from graph. (See Figure 2.5).

(c) Deep anchors, loose sand (ϕ = 30°)

D/B	Meyerhof and Adams	Vesic	Kwasnieski[3] et al	Fadl[4]
5	9.2	-	-	6.7
10	11.9	11.7[1](9.1)[2]	37.8	9.0
15	12.8	" "	35.6	10.4
20	13.2	" "	34.4	11.6
25	13.5	" "	33.7	12.8
30	13.7	" "	33.2	13.9

Footnotes: (1) Calculated using spherical cavity expansion equation with Δ = 0 and I_{rr} = 70.
(2) Calculated using cylindrical cavity expansion equation with Δ = 0 and I_{rr} = 70.
(3) Calculated using $\alpha = 90 - \phi = 60°$.
(4) Calculated using Dr = 20%, H/B = 3.0, α = 12°.

(d) Deep anchors, dense sand (ϕ = 40°)

D/B	Meyerhof and Adams	Vesic	Kwasnieski[3] et al	Fadl[4]
10	51.0	28.9[1](22.3)[2]	71.9	89.3
15	60.0	" "	67.8	147.4
20	64.5	" "	65.5	185.4
25	67.2	" "	64.2	215.5
30	69.0	" "	63.3	241.5

Footnotes: (1) Calculated using spherical cavity expansion equation with Δ = 0 and I_{rr} = 150.
(2) Calculated using cylindrical cavity expansion equation with Δ = 0 and I_{rr} = 150.
(3) Calculated using $\alpha = 90 - \phi = 50°$.
(4) Calculated using Dr = 80%, H/B = 10.0, α = 27°.

TABLE 2.3 - Similarity Requirements for a Conventional Model and a Centrifugal Model (after Ovesen, 1981).

PROTOTYPE	CONVENTIONAL MODEL		CENTRIFUGAL MODEL	
Scale - 1:1	Scale - 1:n		Scale - 1:n	
Gravity - g	Gravity - g		Gravity - ng	
$\frac{D}{B}$	$\frac{D/n}{B/n}$	similar	$\frac{D/n}{B/n}$	similar
θ	θ	similar	θ	similar
e	e	similar	e	similar
ϕ_μ	ϕ_μ	similar	ϕ_μ	similar
$\frac{\sigma_c}{\gamma_D}$	$\frac{\sigma c}{\gamma D/_n}$	not similar	$\frac{\sigma c}{\gamma nD/n}$	similar
$\frac{\sigma_g}{\gamma D}$	$\frac{\sigma_g}{\gamma D/n}$	not similar	$\frac{\sigma_g}{\gamma nD/_n}$	similar
$\frac{E_g}{\gamma D}$	$\frac{E_g}{\gamma D/n}$	not similar	$\frac{E_g}{\gamma nD/_n}$	similar
$\frac{d_{50}}{B}$	$\frac{d_{50}}{B/n}$	not similar	$\frac{d_{50}}{B/n}$	not similar

TABLE 2.4 - Comparison of Grain Size Ratios used in Conventional Tests and Centrifugal Tests.

CENTRIFUGAL TESTS (after Ovesen, 1981)			CONVENTIONAL TESTS (after Hutchison, 1982)		
Dense sand (Dr = 95%), D/B = 1.85, d_{50} = 0.25 mm.			Dense sand (Dr = 91%), D/B = 2.0, d_{50} = 0.8 mm.		
B (mm)	B/d_{50}	N_u	B (mm)	B/d_{50}	N_u*
12.5	50	4.2	66	83	8.3
20.0	80	4.5	66	83	8.1
36.0	144	4.3	104	130	8.1

* Estimated from test results reported for $D/B = 2.27$ (66 mm ϕ anchor) and $D/B = 2.16$ (104 mm ϕ anchor).

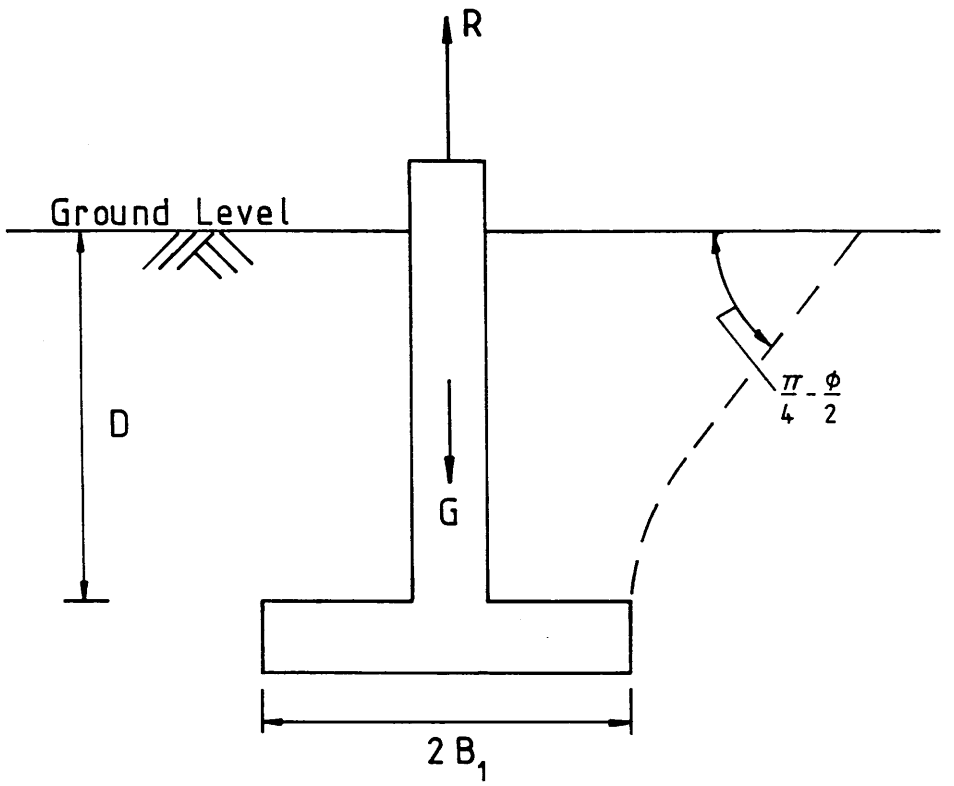

FIGURE 2.1 - Shallow anchor failure surface after Matsuo (1967).

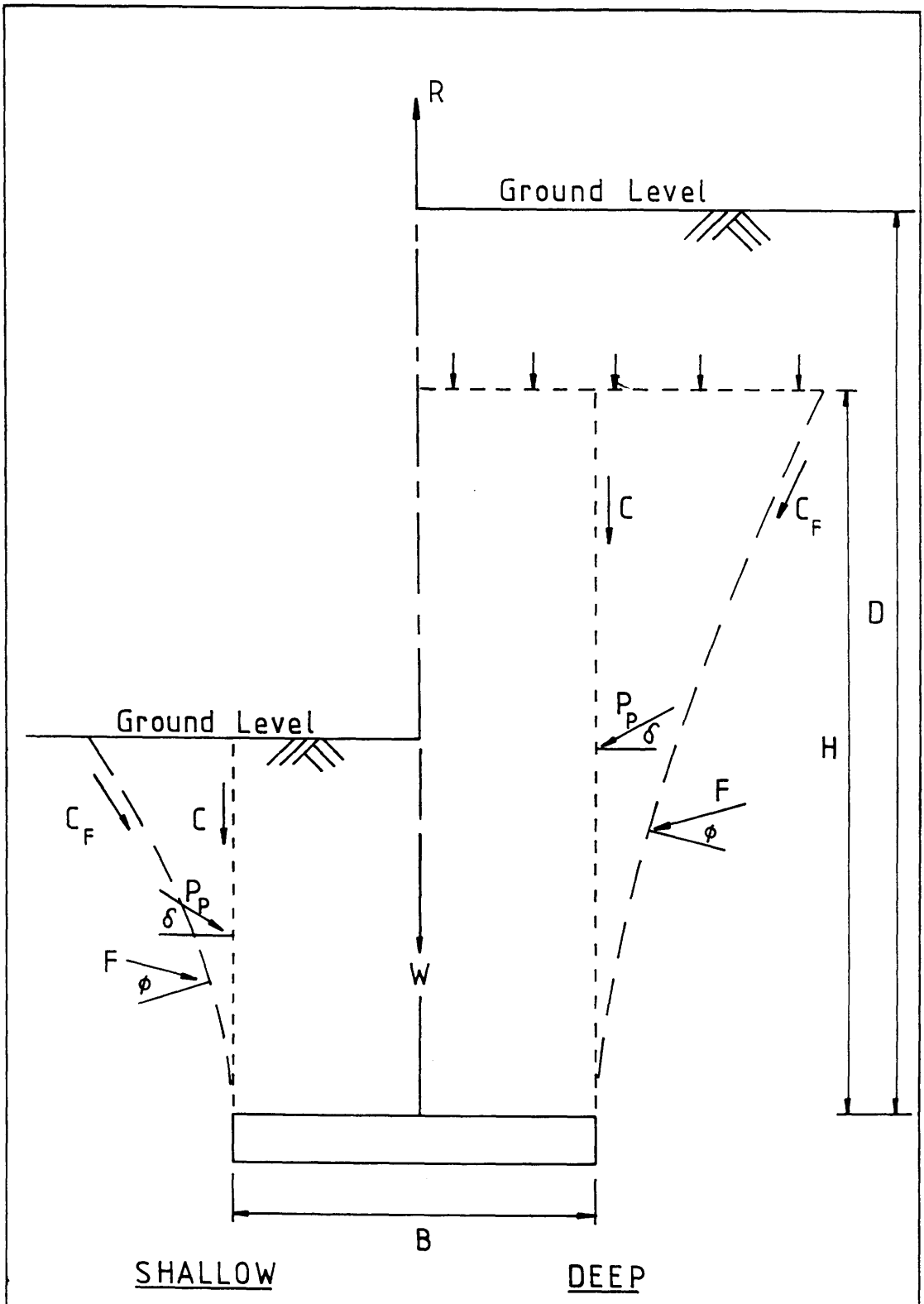

FIGURE 2.2 - Failure surfaces after Meyerhof and Adams (1968).

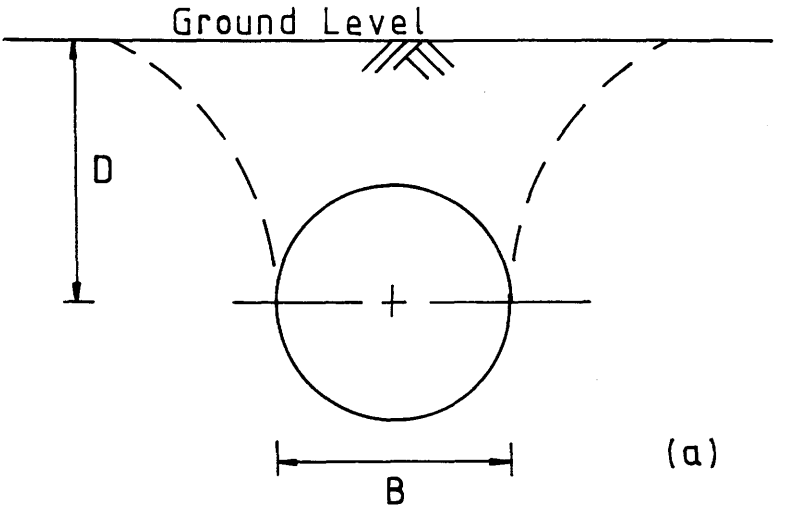

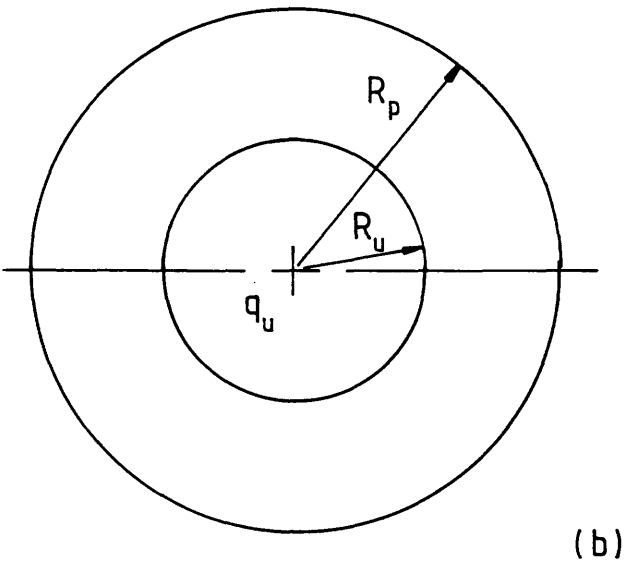

FIGURE 2.3 - Failure surfaces after Vesic (1971, 1972)
(a) shallow anchor, (b) deep anchor.

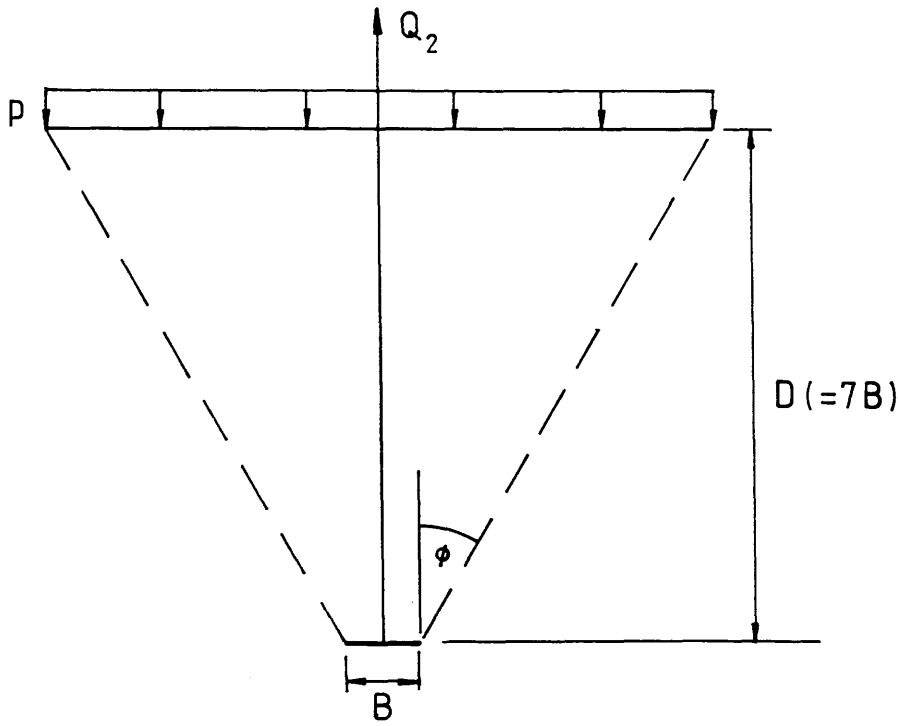

FIGURE 2.4 - Deep anchor failure surface after Kwasnieski, et al (1975).

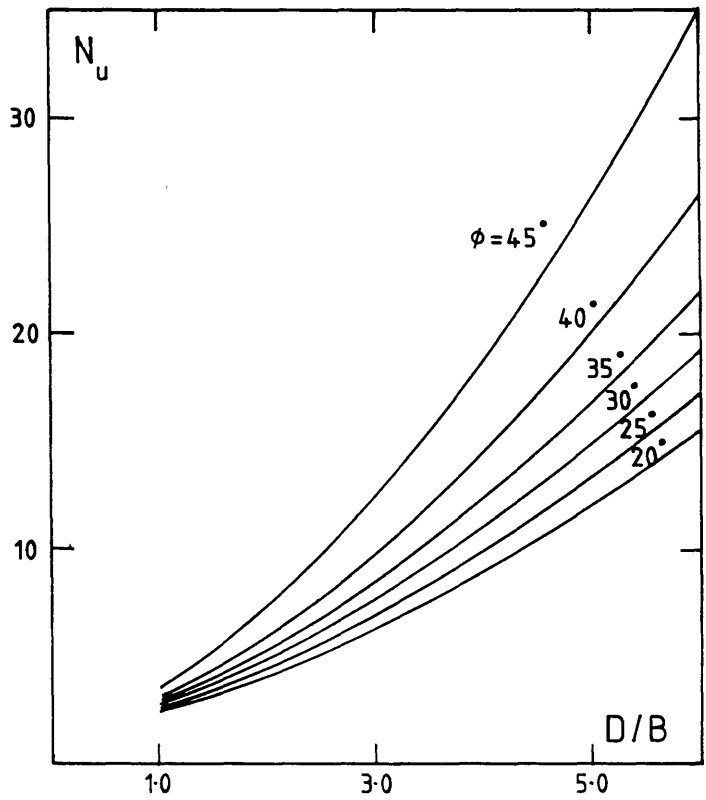

FIGURE 2.5 - Pullout resistance curves after Saeedy (1975).

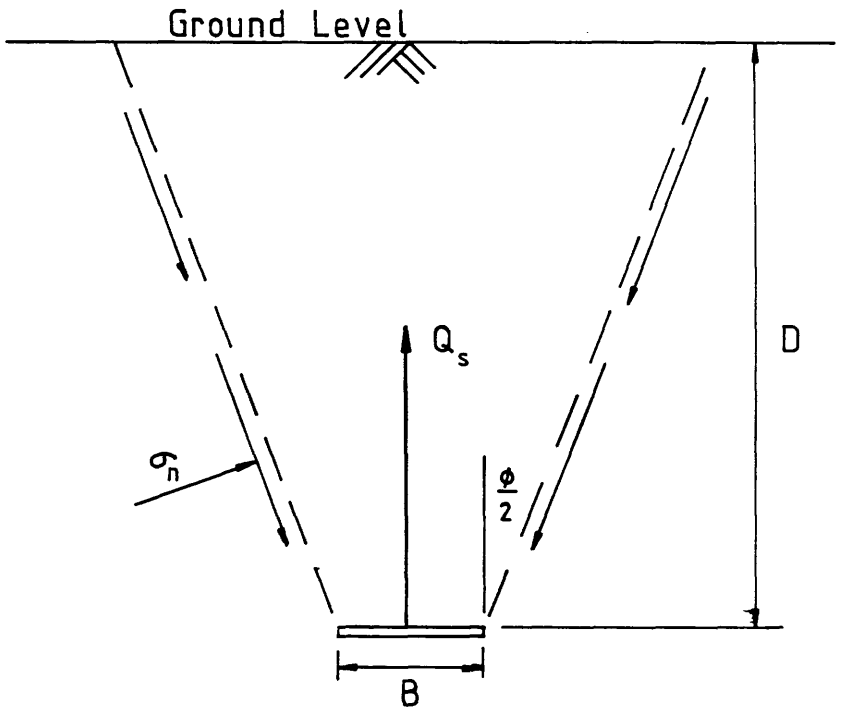

FIGURE 2.6 - Shallow anchor failure surface after Clemence and Veesaert (1977).

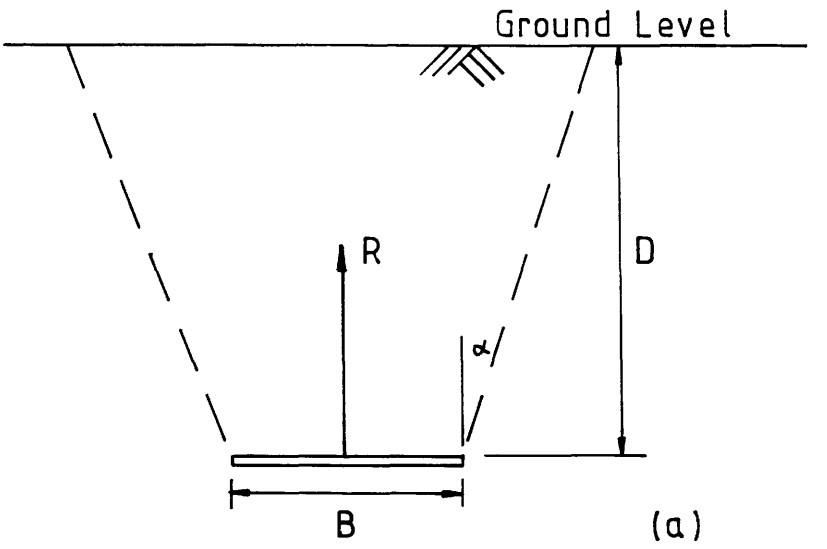

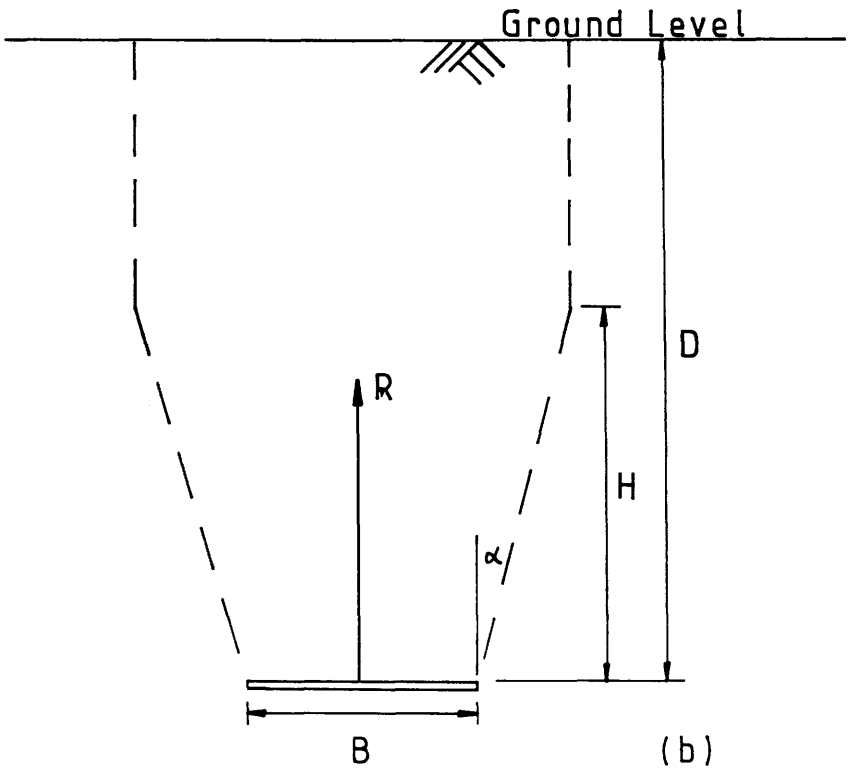

FIGURE 2.7 Failure surfaces after Fadl (1981).
(a) shallow anchor, (b) deep anchor.

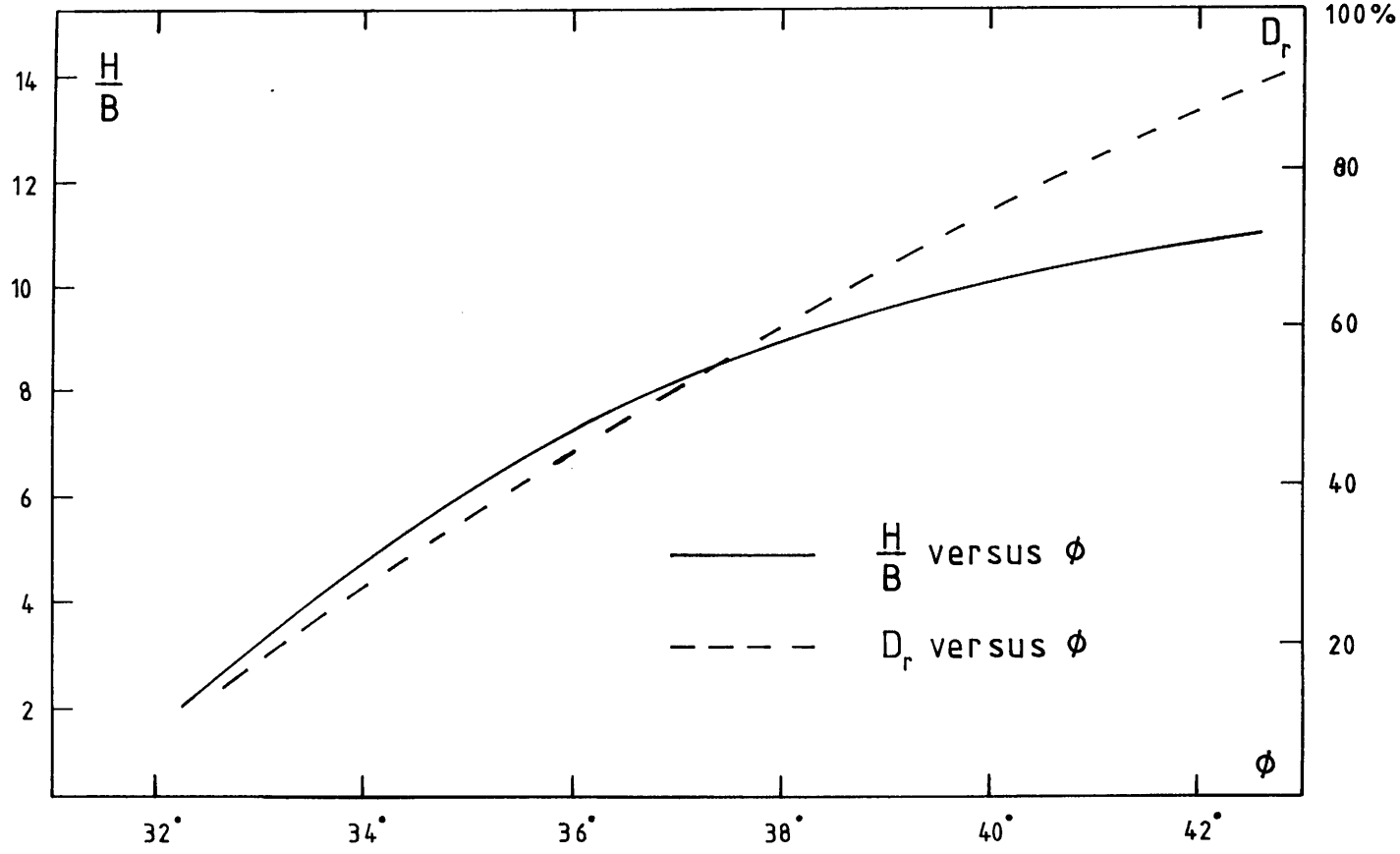

FIGURE 2.8 - Relationship between critical embedment ratio ($^{H}/B$), relative density (D_r) and friction angle (ϕ) after Fadl (1981)

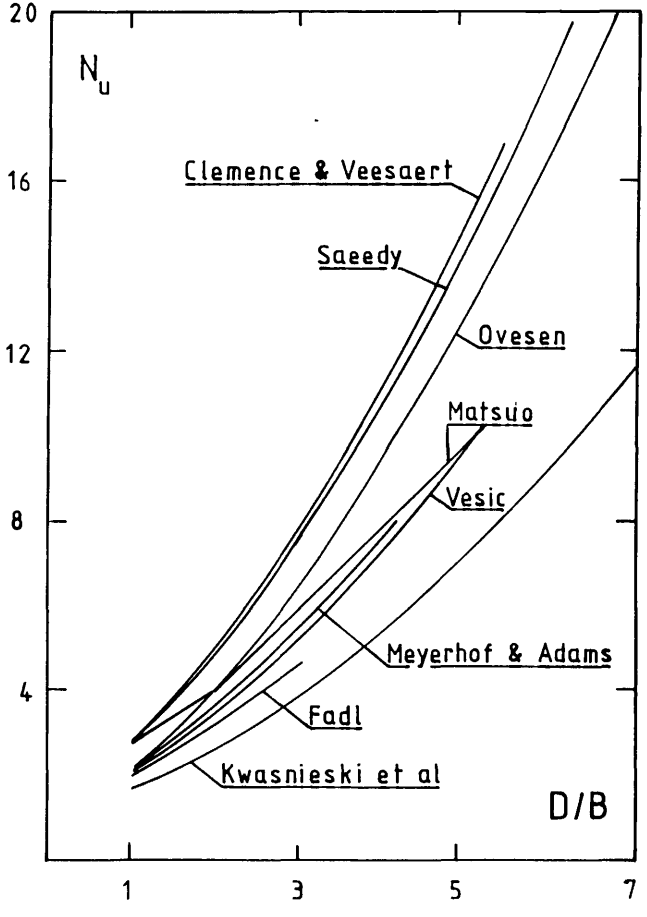

FIGURE 2.9 - Shallow Anchors: Theoretical curves for loose sand (ϕ = 30°)

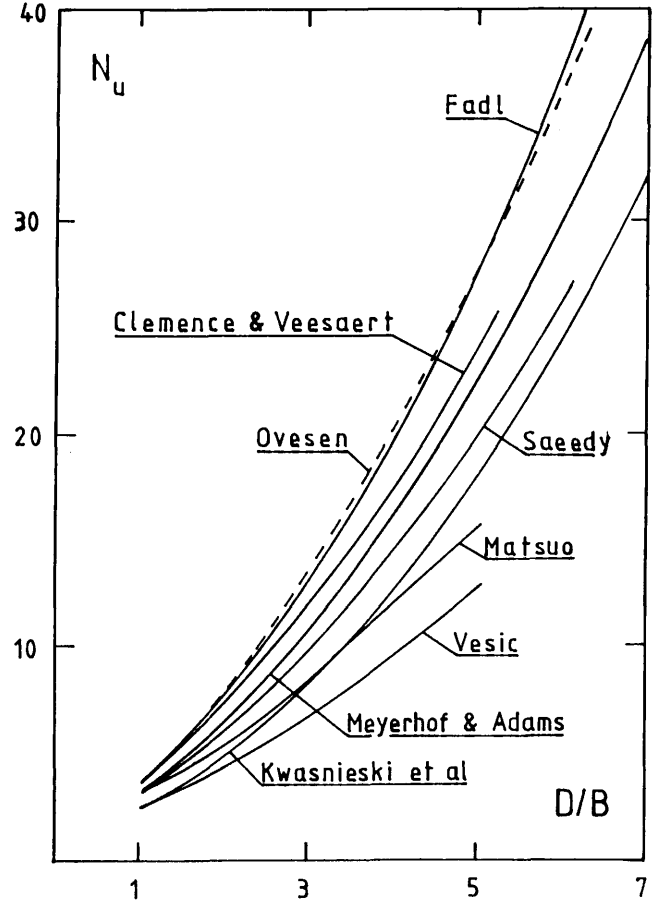

FIGURE 2.10 - Shallow Anchors: Theoretical curves for dense sand (ϕ = 40°)

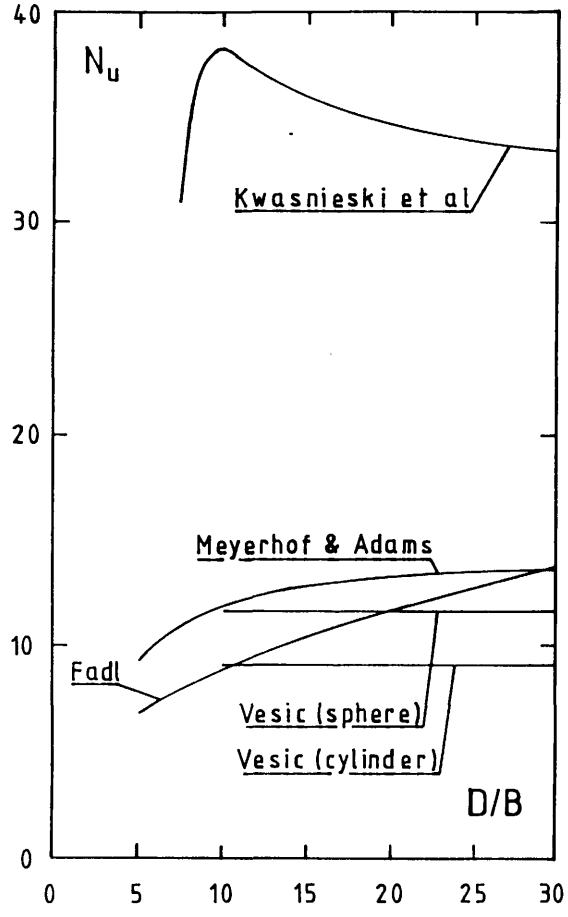

FIGURE 2.11 - Deep Anchors: Theoretical curves for loose sand(ϕ = 30°)

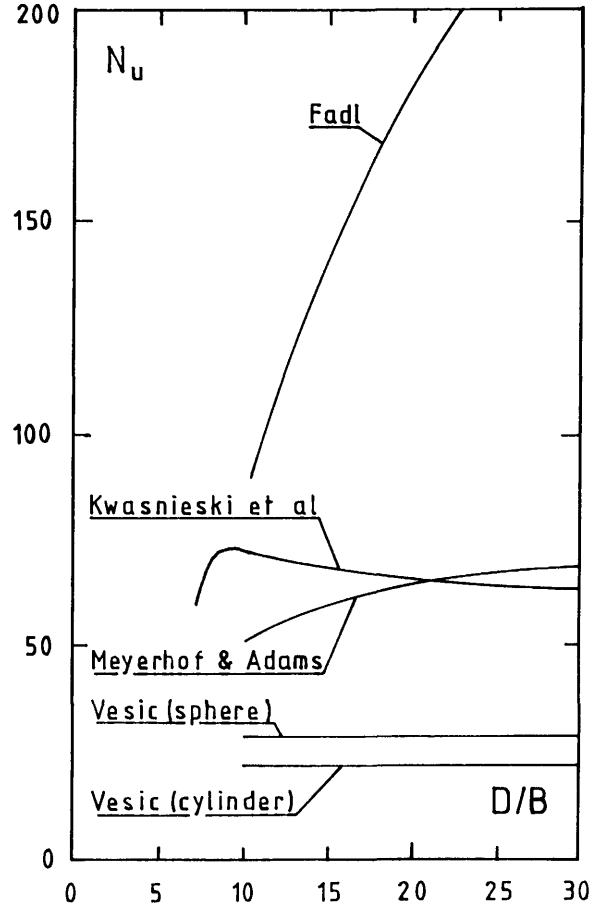

FIGURE 2.12 - Deep Anchors: Theoretical curves for dense sand (ϕ = 40°)

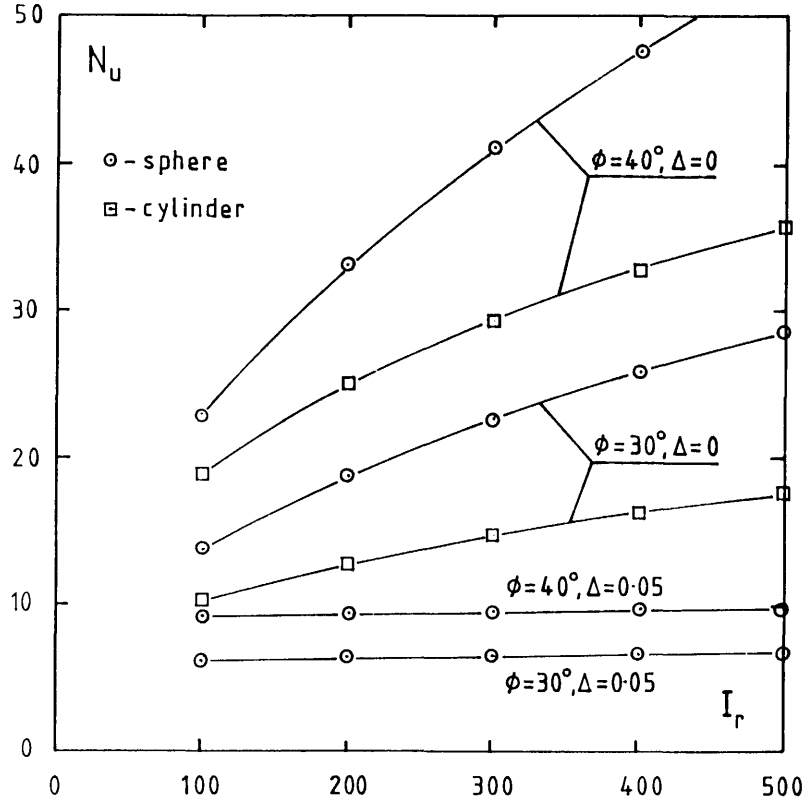

FIGURE 2.13 - Deep Anchors: Effect of varying rigidity index (I_r) on uplift resistance factor (N_u) (Vesic theory).

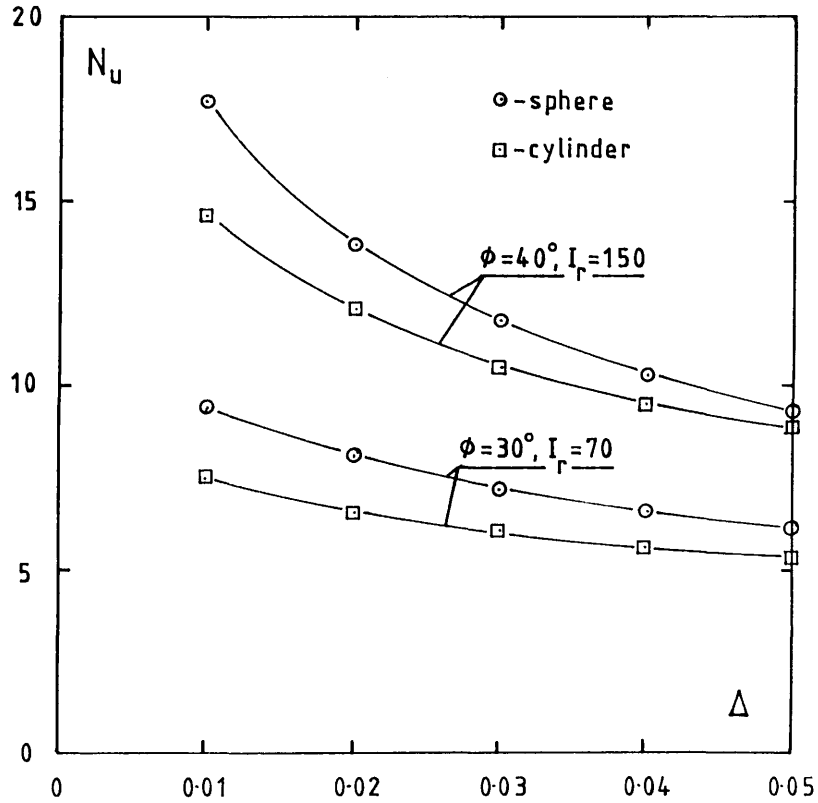

FIGURE 2.14 - Deep Anchors: Effect of varying volumetric strain (Δ) on uplift resistance factor (N_u) (Vesic theory).

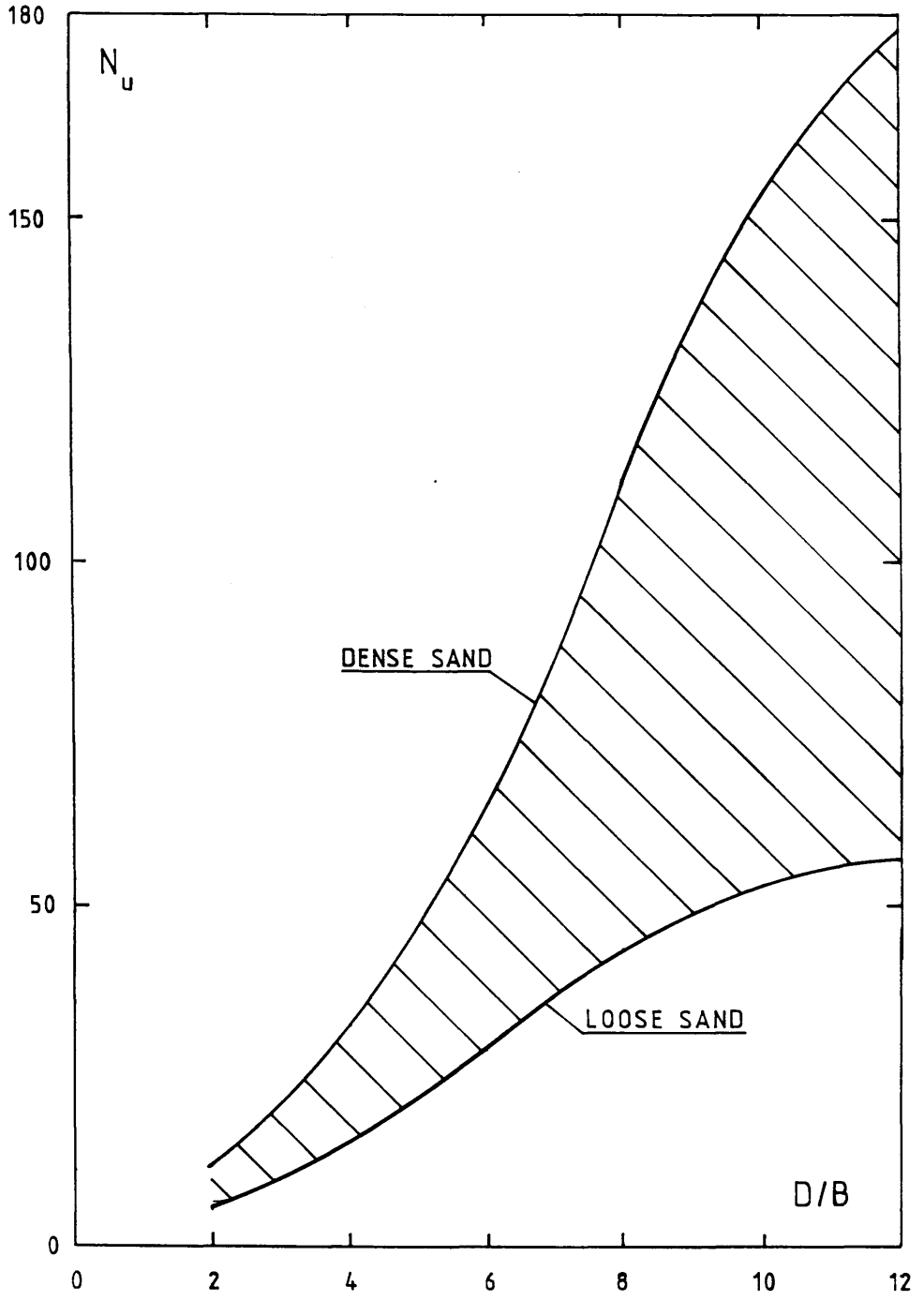

FIGURE 2.15 - Range of N_u-values from previous experimental investigations (After Andreadis, 1979).

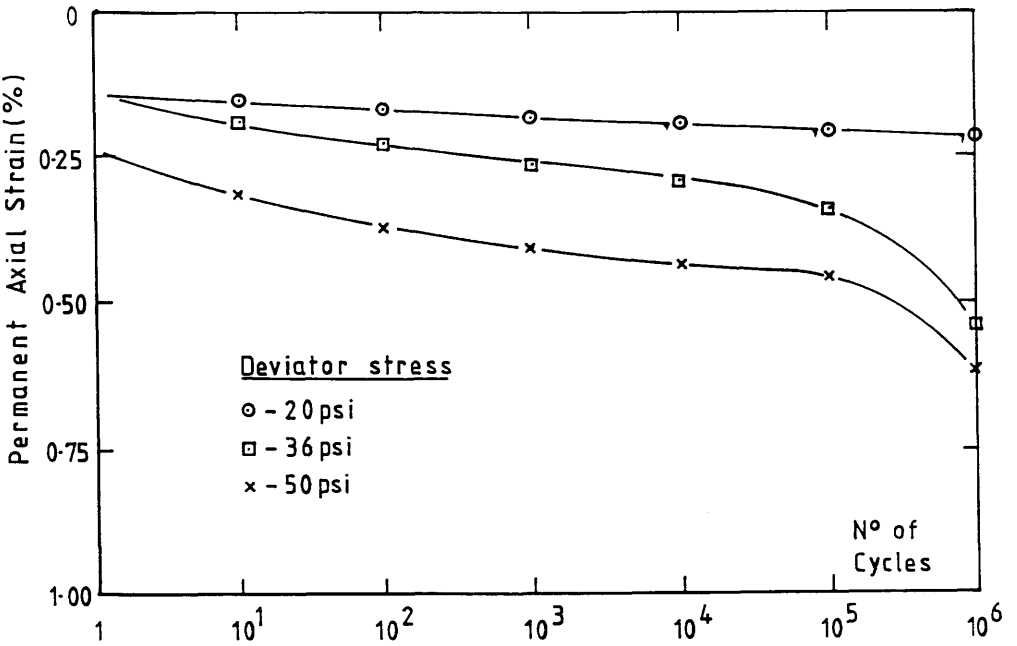

FIGURE 2.16(a) - Triaxial Tests: Variation of permanent axial strain with number of cycles. Confining pressure 30 psi (After Morgan, 1966).

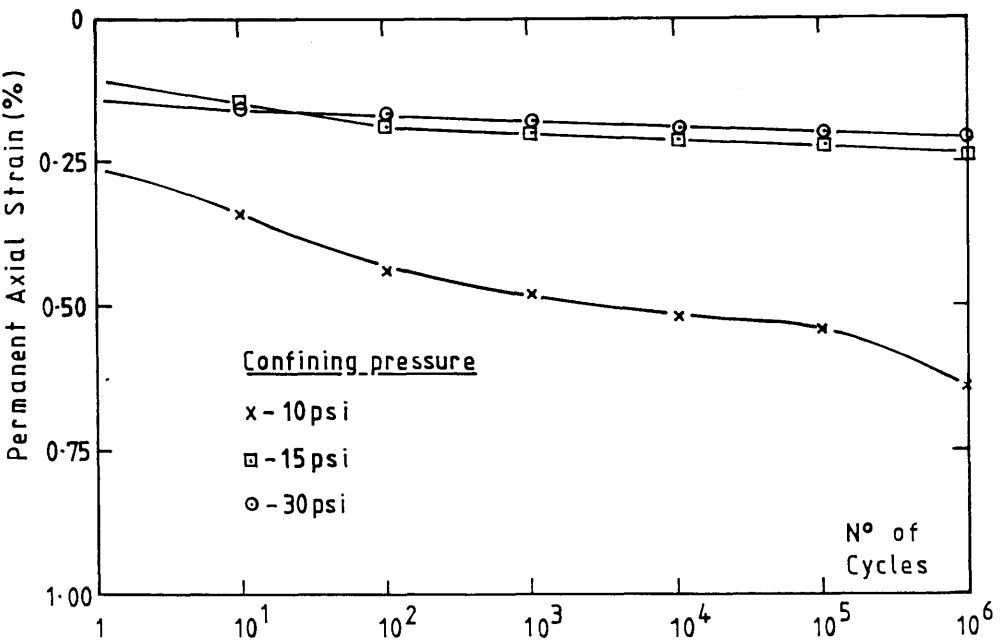

FIGURE 2.16(b) - Triaxial Tests: Variation of permanent axial strain with number of cycles. Deviator stress 20 psi (After Morgan, 1966).

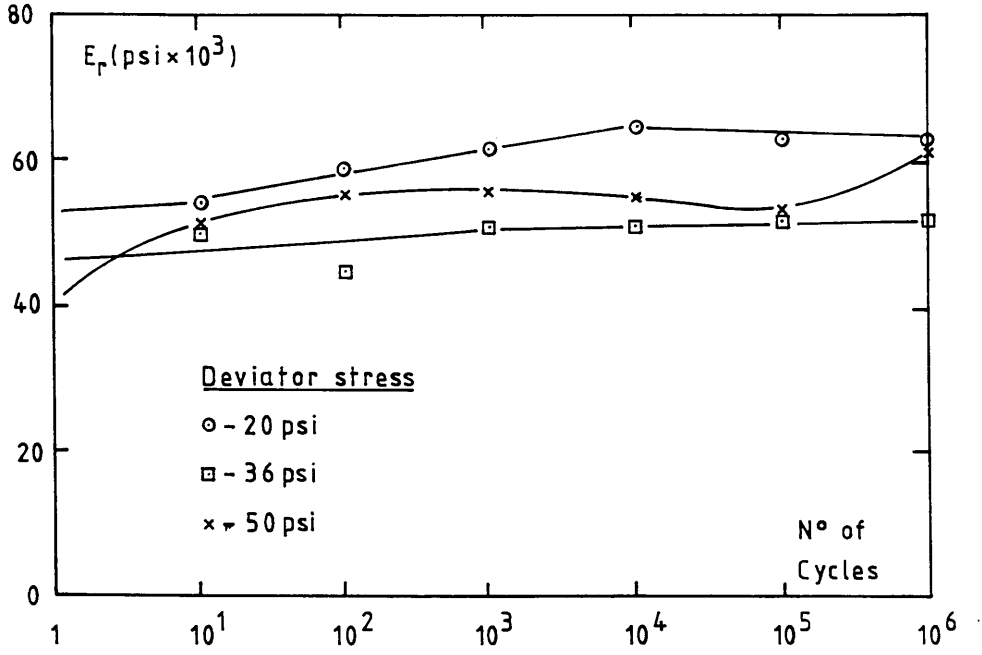

FIGURE 2.17(a) - Triaxial Tests: Variation of resilient modulus (E_r) with number of cycles. Confining pressure 30 psi (After Morgan, 1966).

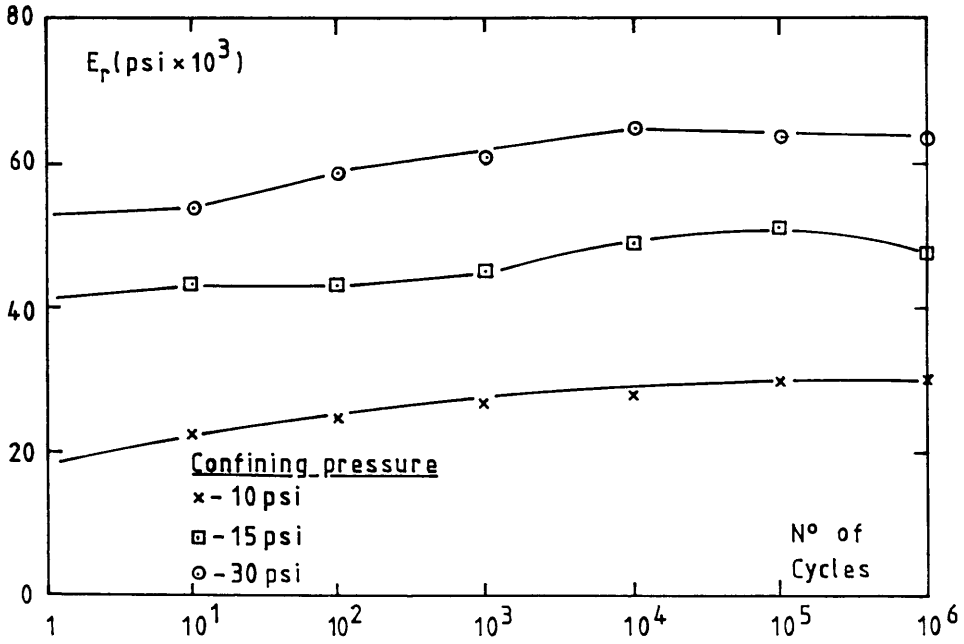

FIGURE 2.17(b) - Triaxial Tests: Variation of resilient modulus (E_r) with number of cycles. Deviator stress 20 psi (After Morgan, 1966).

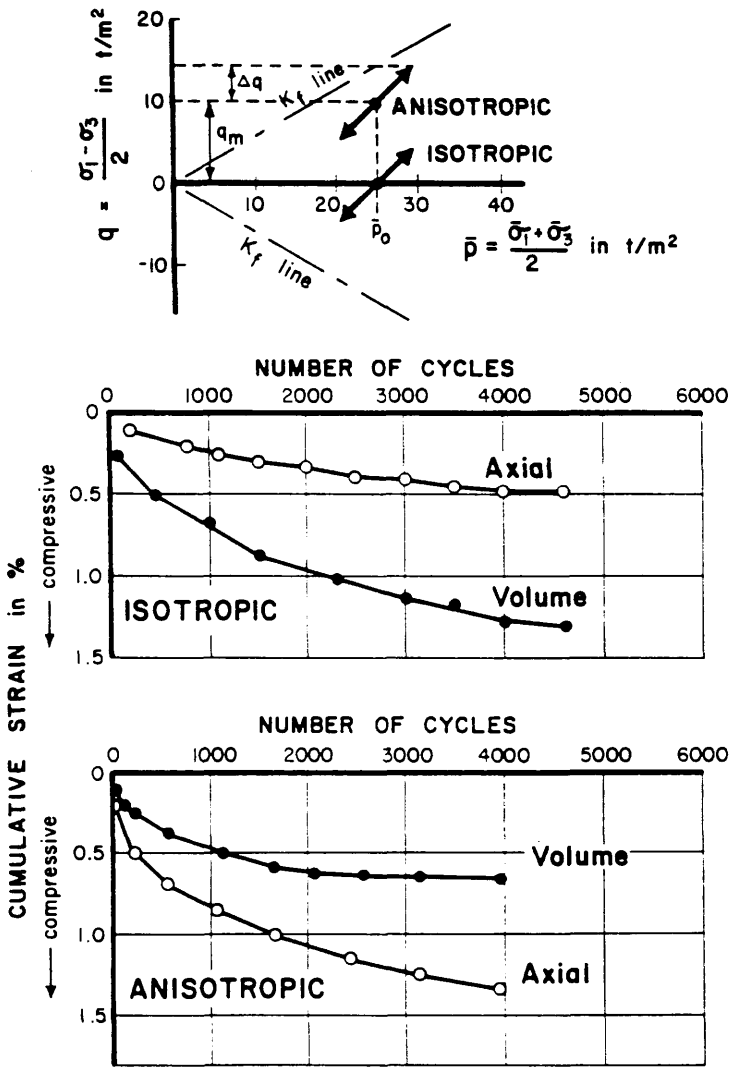

FIGURE 2.18 - Drained cyclic triaxial test results. (After Marr and Christian, 1981).

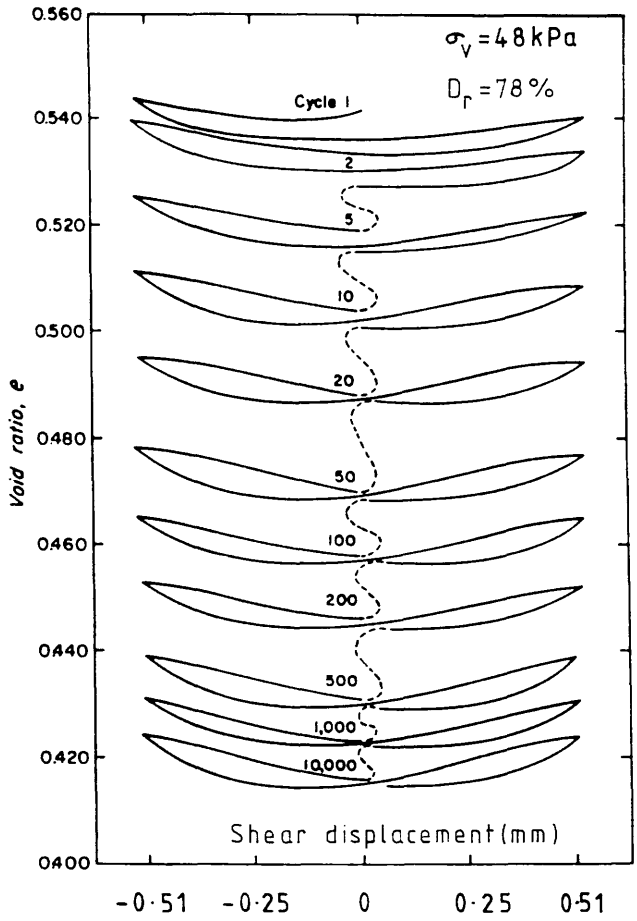

FIGURE 2.19 - Simple Shear Tests: Void ratio versus strain history (After Youd, 1972).

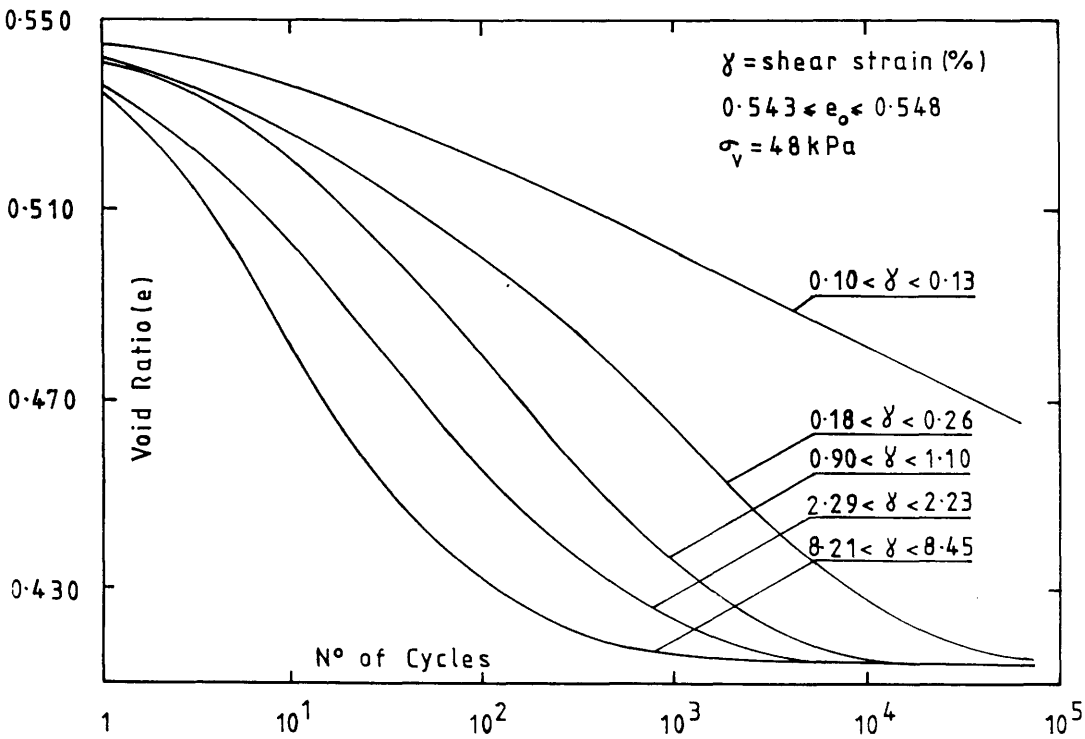

FIGURE 2.20 - Simple Shear Tests: Effect of shear strain amplitude and number of cycles on void ratio (After Youd, 1972).

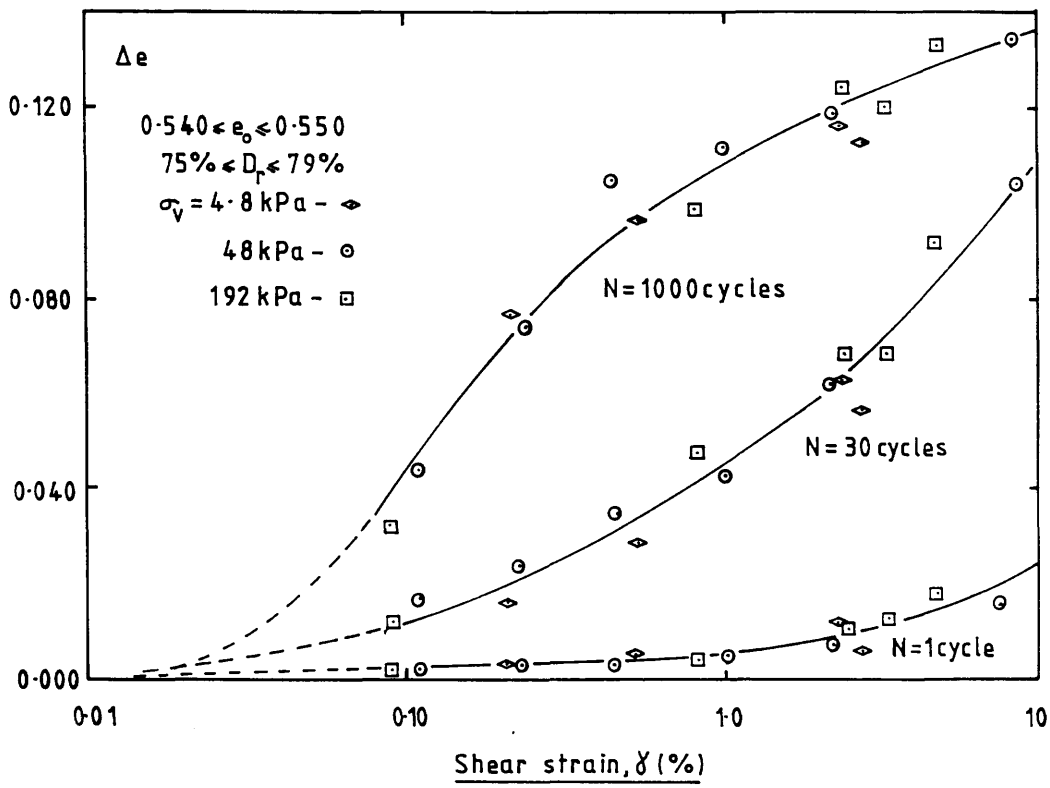

FIGURE 2.21 - Simple Shear Tests: Change in void ratio as a function of number of cycles, shear strain amplitude and vertical stress (After Youd, 1972)

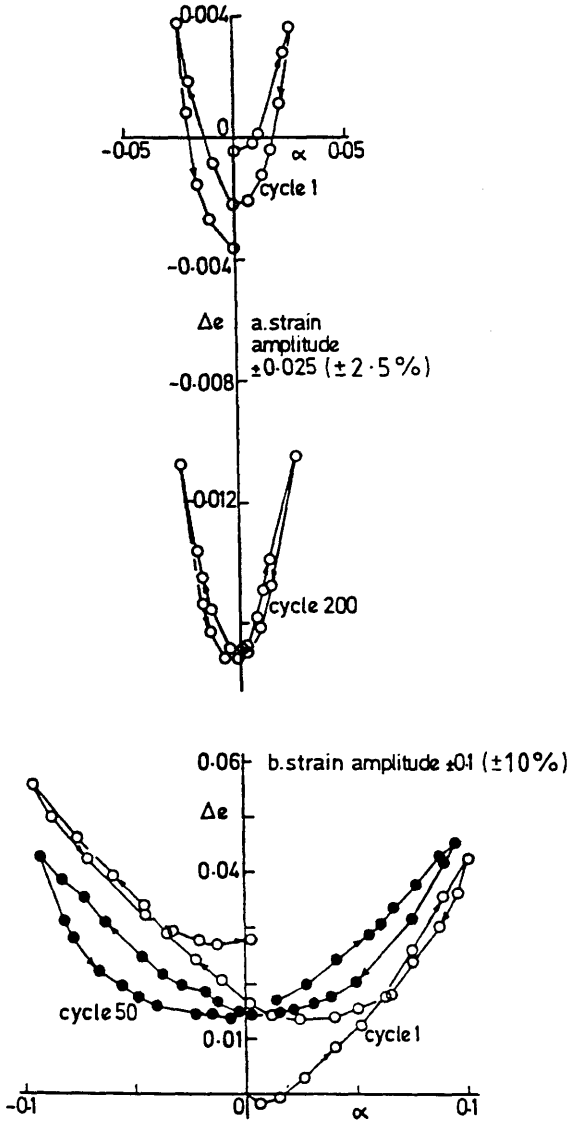

FIGURE 2.22 - Simple Shear Tests: Volume changes within cycles for dense sand (After Wood and Budhu, 1980).

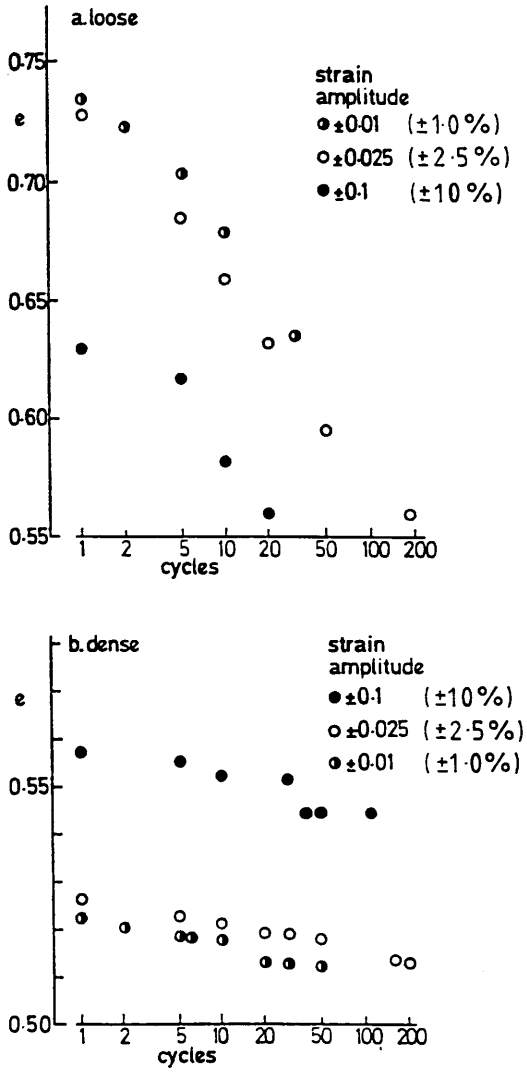

FIGURE 2.23 - Simple Shear Tests: Void ratio at end of each cycle for (a) loose and (b) dense sand. (After Wood and Budhu, 1980).

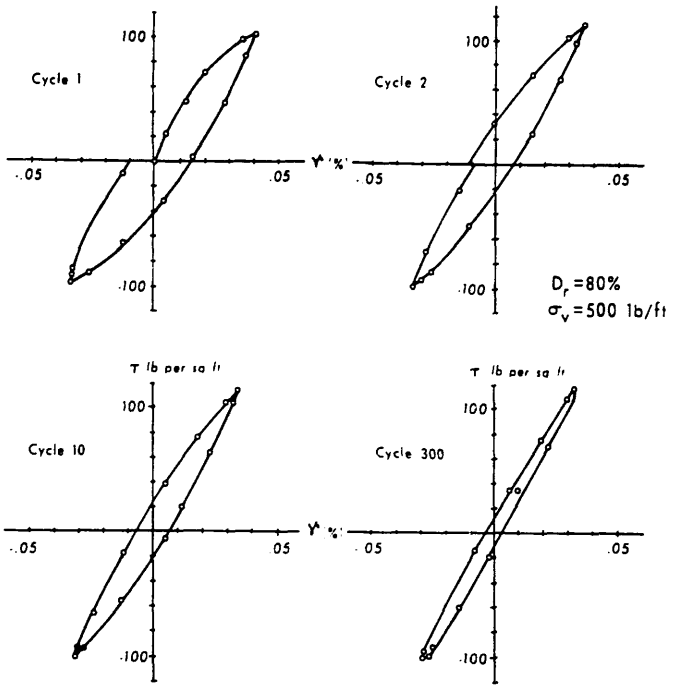

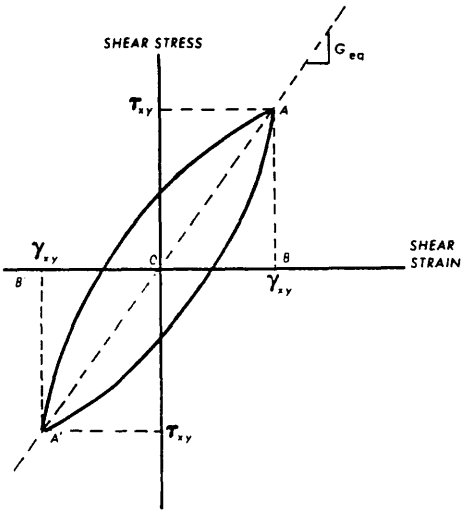

FIGURE 2.24 - Simple Shear Tests: Graphs of shear stress versus shear strain showing hysteresis loops (After Silver and Seed, 1971a).

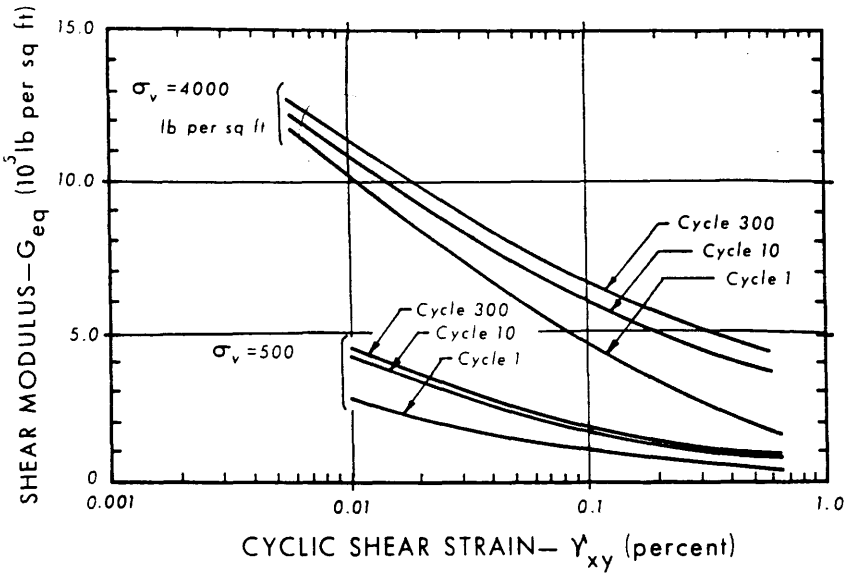

FIGURE 2.25 - Simple Shear Tests: Shear modulus as a function of cyclic shear strain, number of cycles and vertical stress. (After Silver and Seed, 1971 (a)).

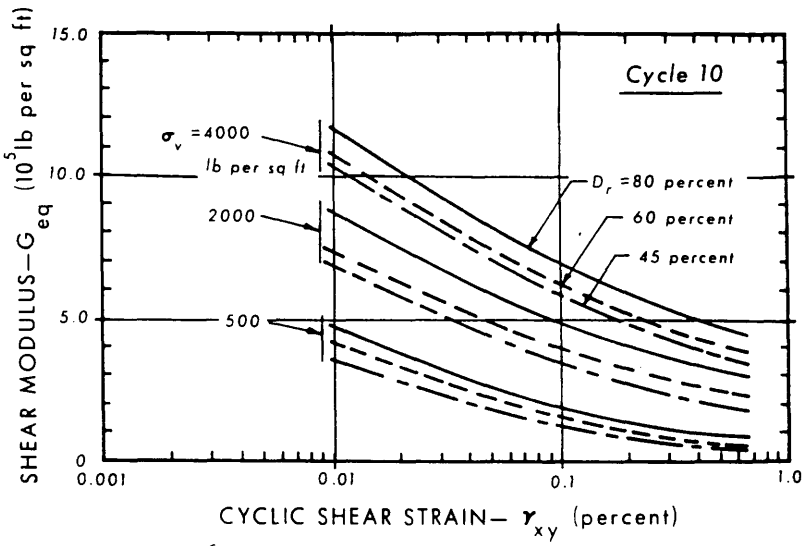

FIGURE 2.26 - Simple Shear Test: Shear modulus as a function of cyclic shear strain, vertical stress and relative density for cycle 10 (After Silver and Seed, 1971(a)).

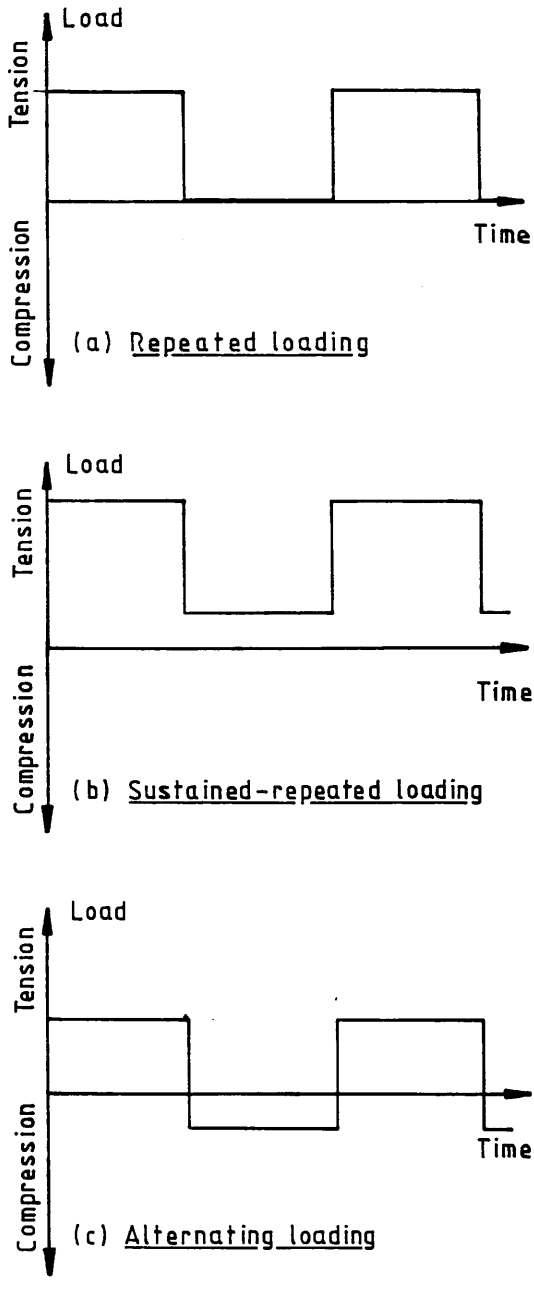

FIGURE 2.27 - Types of Cyclic Loading (Ilustrated using square wave form.

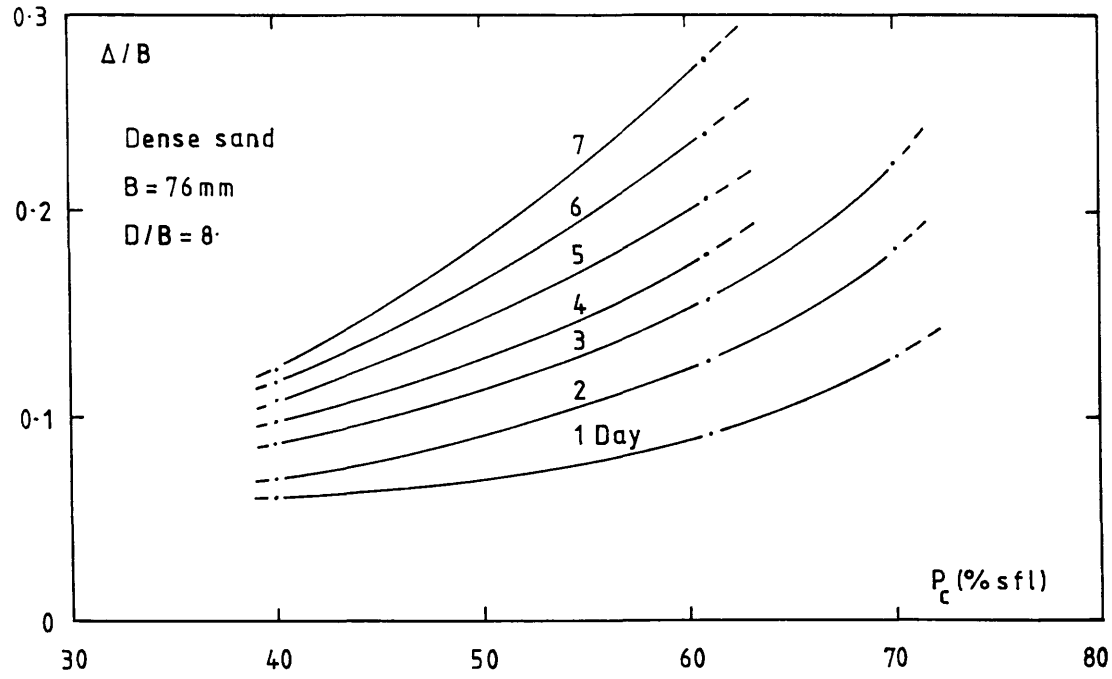

FIGURE 2.28 - Plate Anchor Tests: Variation in relative anchor displacement (Δ/B) with peak cyclic load (P_c) (After Bemben and Kupferman, 1975)

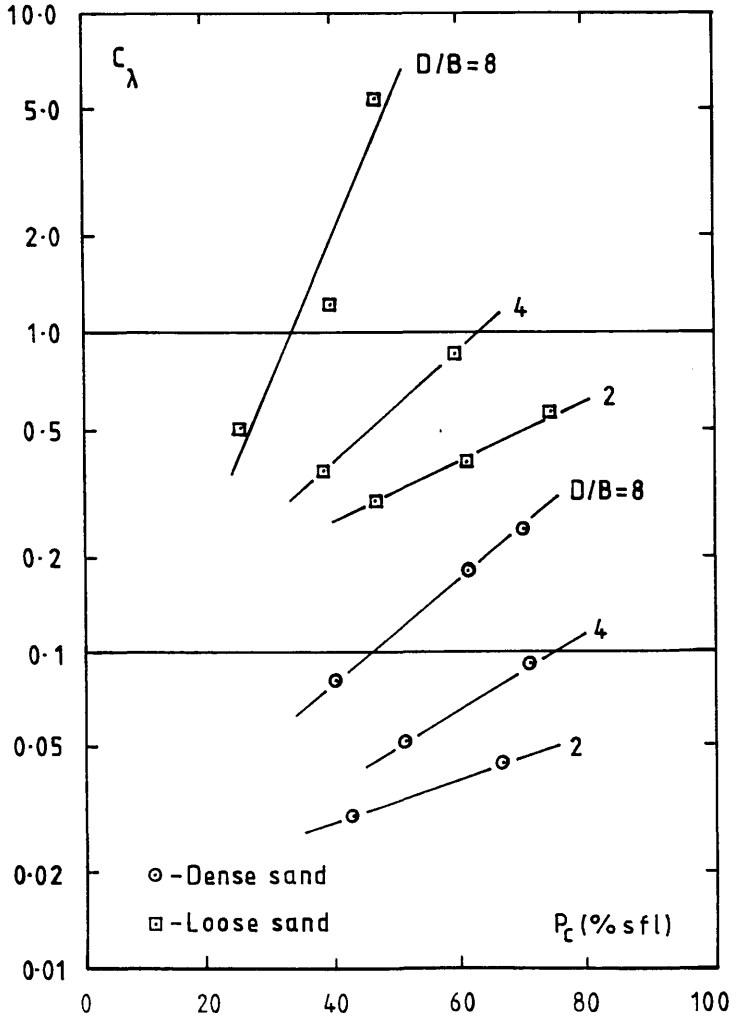

FIGURE 2.29 - Plate Anchor Tests: Cyclic creep factor (c_λ) as a function of peak cyclic load, embedment ratio and sand density (After Bemben and Kupferman, 1975).

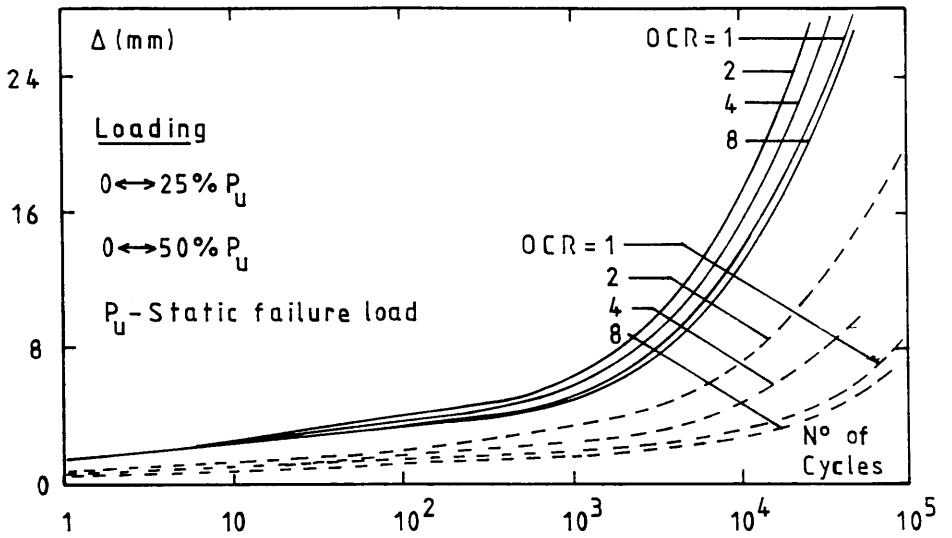

FIGURE 2.30 - Plate Anchor Tests: Effect of overconsolidation ratio (OCR) on anchor displacement (After Hanna, et al, 1978).

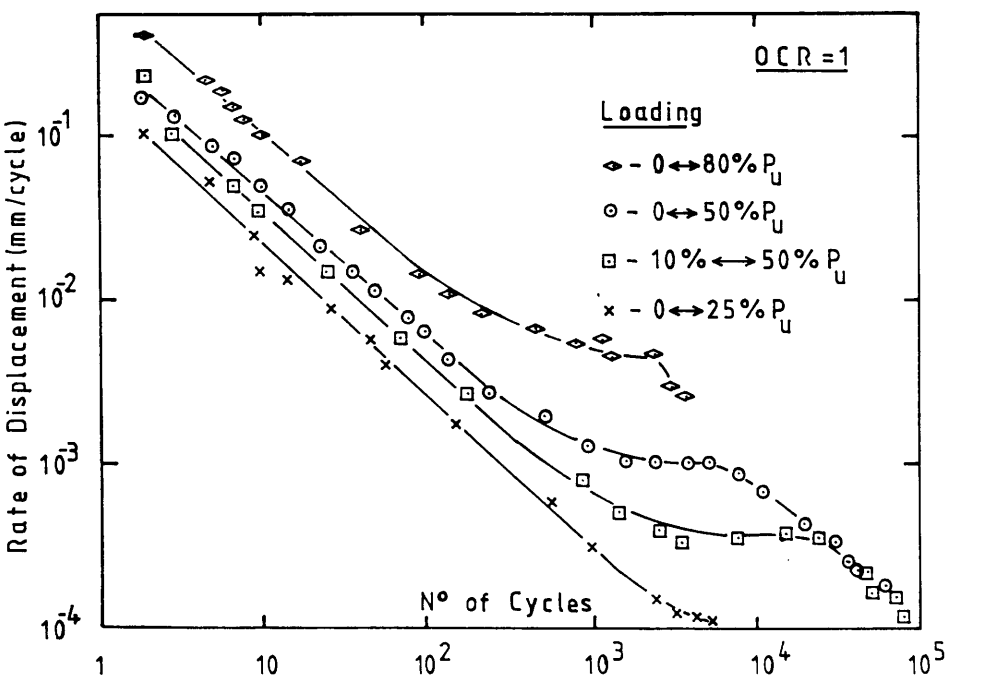

FIGURE 2.31 - Plate Anchor Tests: Effect of load level and number of cycles on anchor displacement rate (After Hanna, et al, 1978).

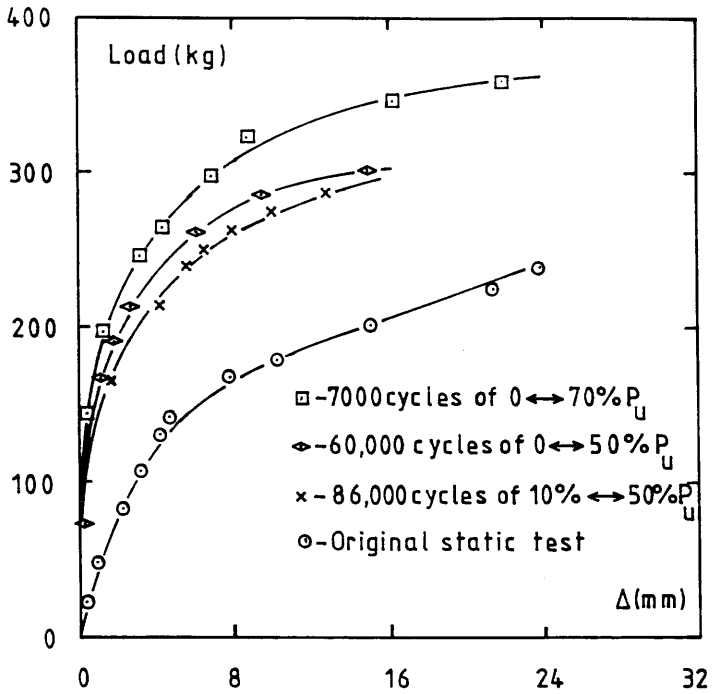

FIGURE 2.32 - Plate Anchor Tests: Post-cyclic static loading response (after Hanna, et al, 1978)

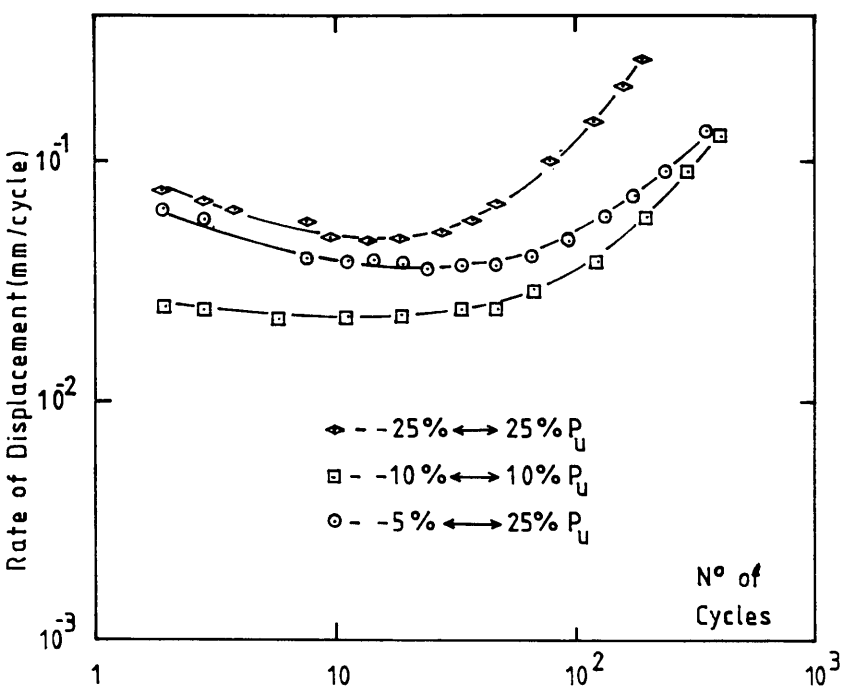

FIGURE 2.33 - Plate Anchor Tests: Effect of alternating load on anchor displacement rate (after Hanna, et al, 1978)

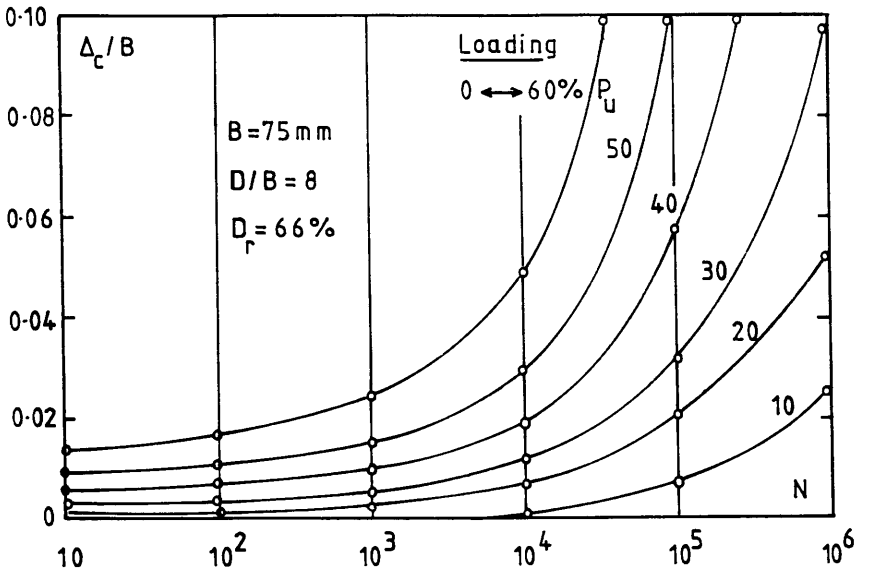

FIGURE 2.34 - Plate Anchor Tests: Family of hyperbolic curves showing effect of load level on anchor cyclic displacement (after Andreadis, et al, 1981).

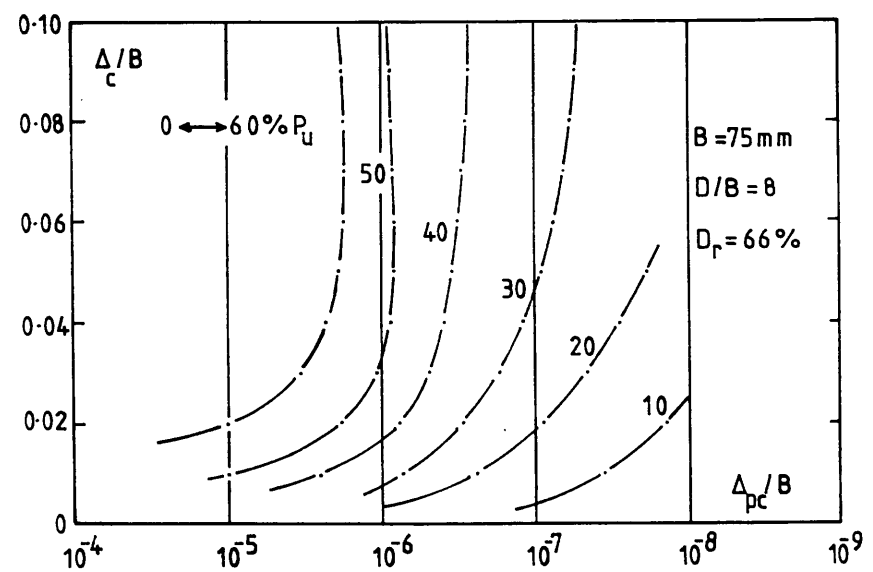

FIGURE 2.35 - Plate Anchor Tests: Effect of cyclic load level on anchor displacement per cycle (after Andreadis, et al, 1981).

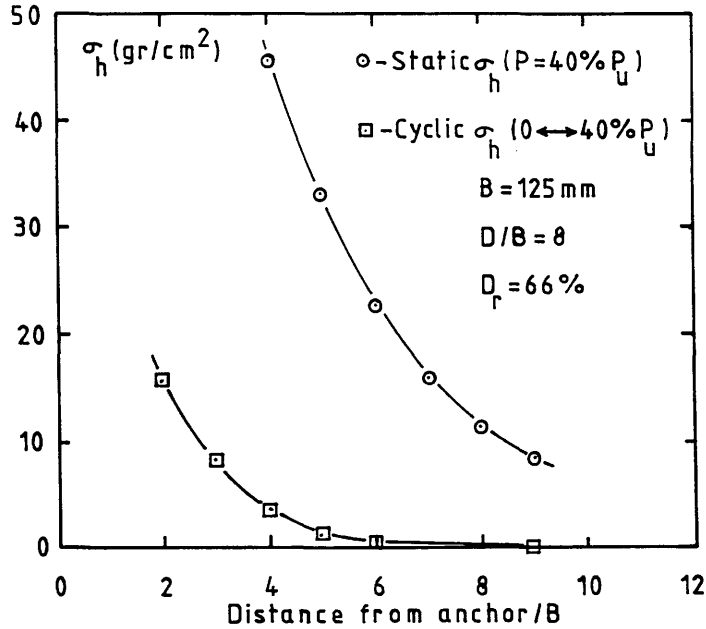

FIGURE 2.36 - Plate Anchor Tests: Conparison of static and cyclic horizontal stresses (after Andreadis, et al, 1981).

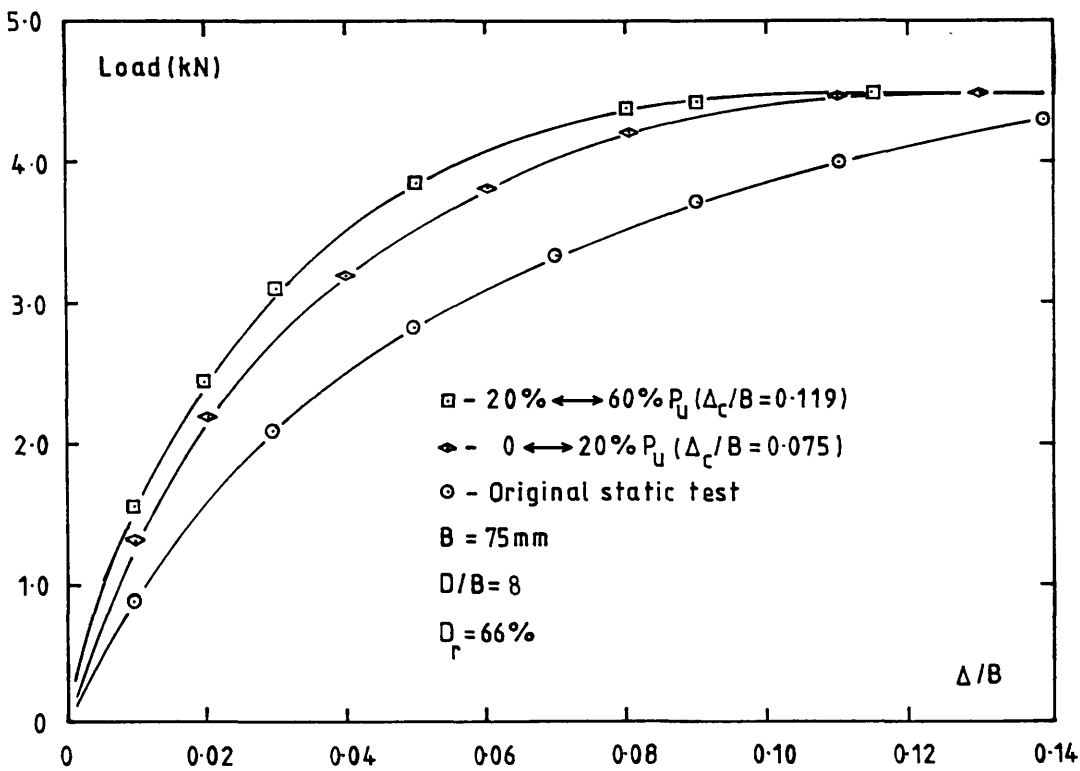

FIGURE 2.37 - Post-cyclic static loading response (after Andreadis, 1979).

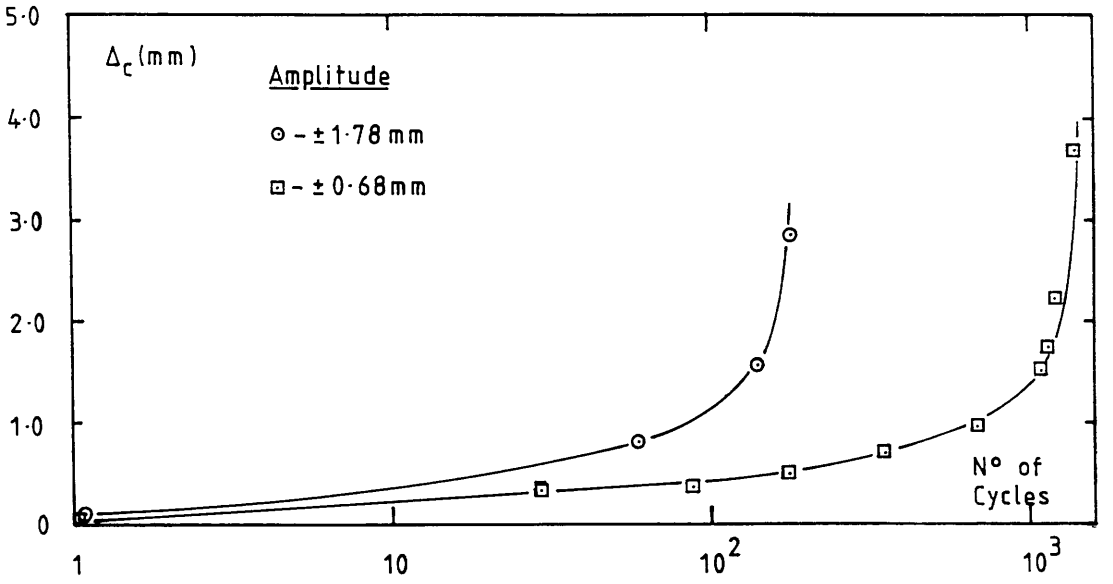

FIGURE 2.38 - Plate Anchor Tests: Effect of displacement amplitude and number of cycles on anchor displacement (after Clemence and Smithling, 1983).

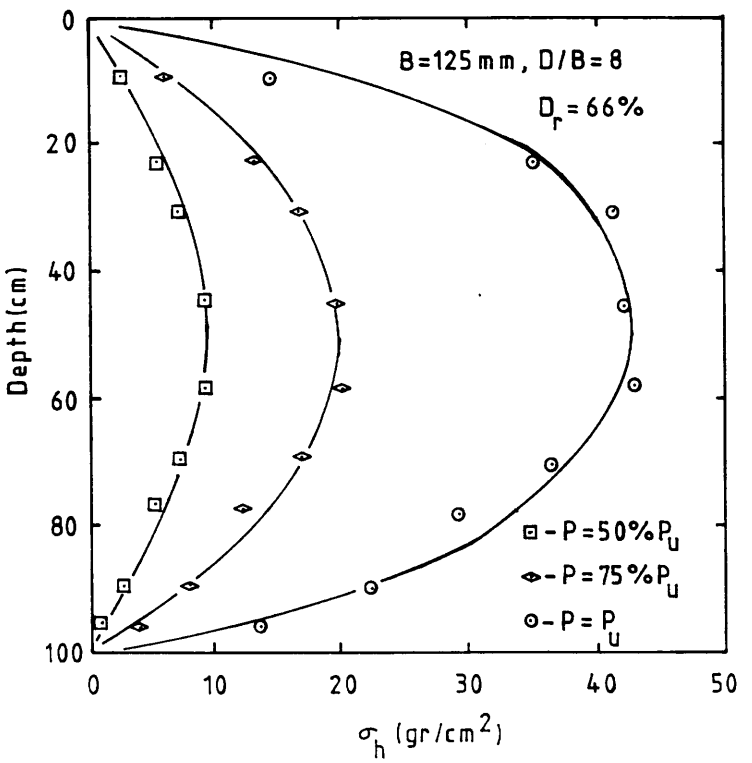

FIGURE 2.39 - Distribution of horizontal stress at tank wall (after Andreadis, et al, 1981).

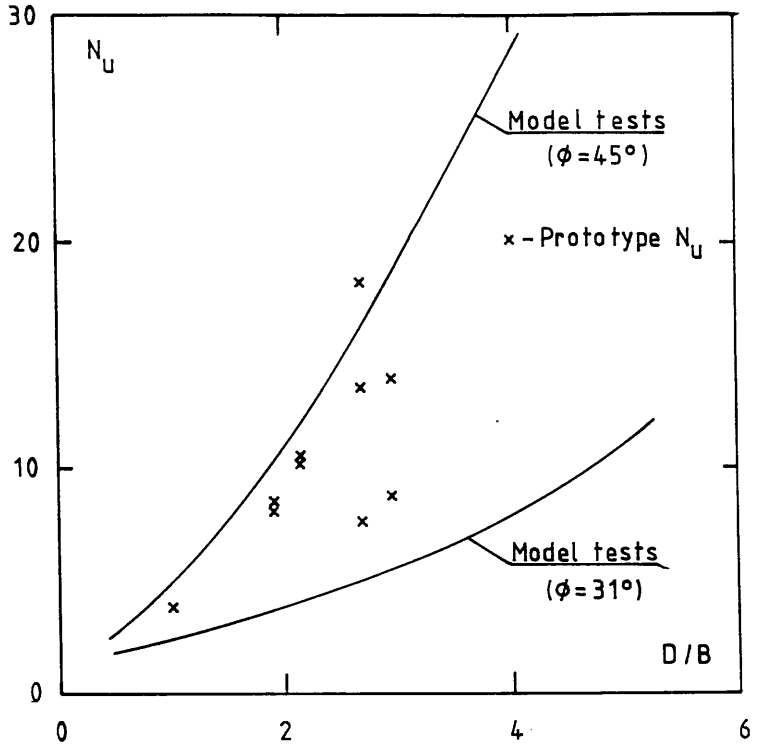

FIGURE 2.40 - Comparison of model test and prototype uplift resistance factors (after Sutherland, 1965).

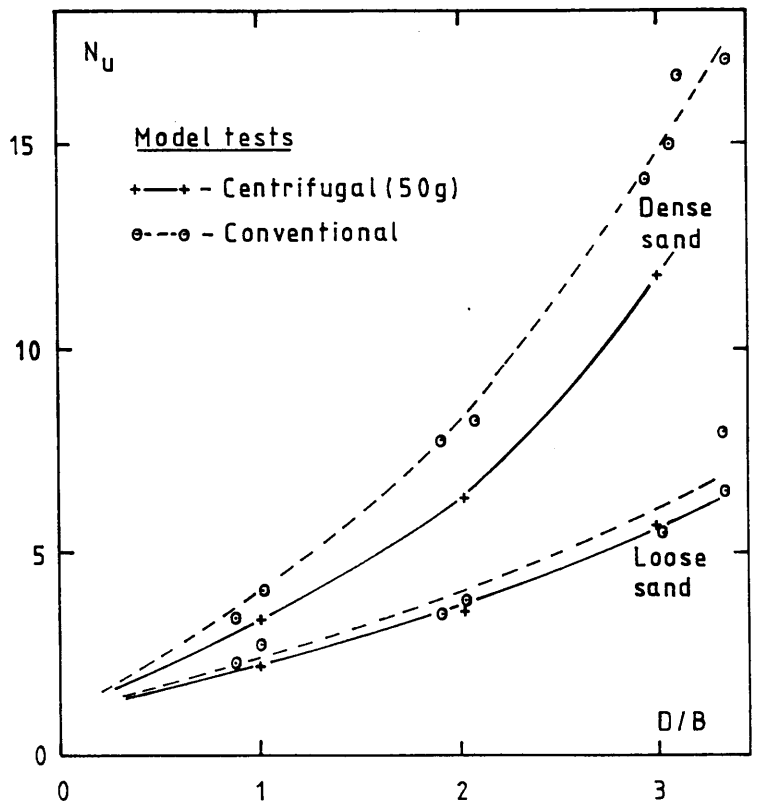

FIGURE 2.41 - Comparison between conventional and centrifugal model tests (after Ovesen, 1981).

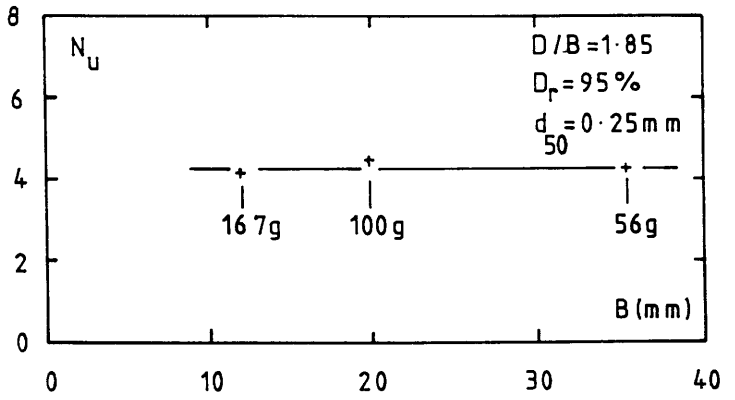

FIGURE 2.42 - Centrifugal Test Results: Effect of varying anchor diameter on uplift resistance factor (after Ovesen, 1981).

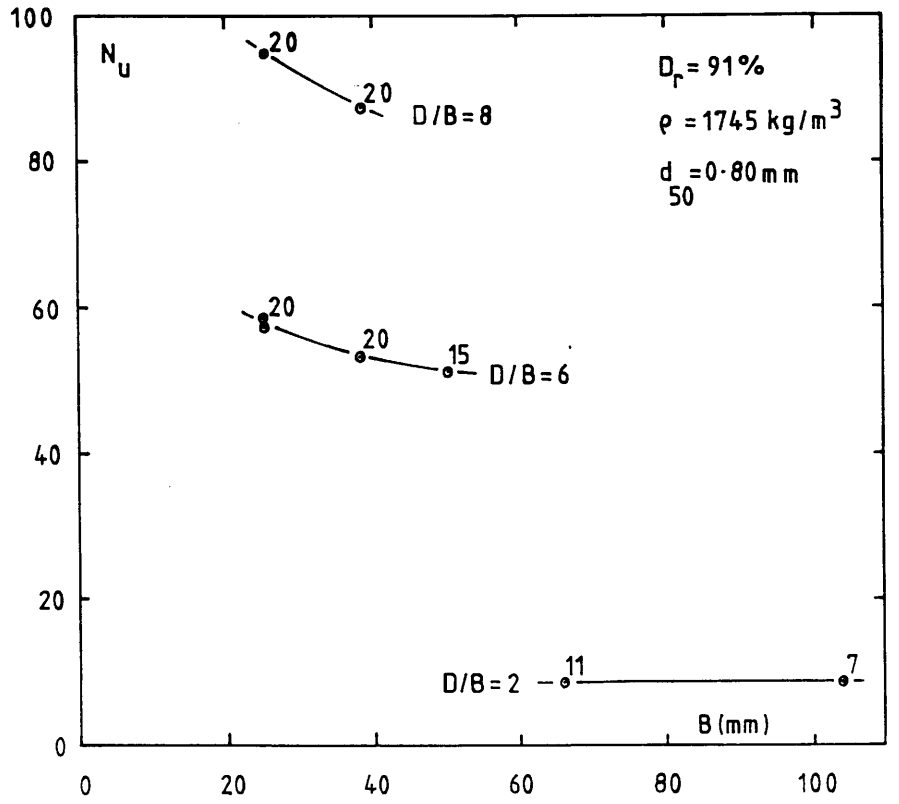

FIGURE 2.43 - Conventional Test Results: Effect of varying anchor diameter on uplift resistance factor (after Hutchison, 1982).

CHAPTER 3 : EXPERIMENTAL PROCEDURE

3.1 INTRODUCTION

The experimental investigation was divided into two basic parts : static loading tests and cyclic loading tests. The static tests were performed to provide the necessary information on ultimate uplift capacity for use in setting the load levels in the cyclic loading tests. The static test results were also used for comparison with previous model test results and with the numerical analysis described in Chapter 5.

The cyclic tests were undertaken principally to investigate cyclic creep, a characteristic described in the previous chapter and one which was considered by the author to be of paramount importance . Both types of tests were carried out in dense and medium dense Leighton Buzzard sand.

Details of the test rigs, sand, sand placement method and test procedures are presented in the following sections, together with details of supplementary tests carried out to assess the relevant parameters of the sand used in the anchor tests.

3.2 TYPE OF SOIL

The soil used in the model tests was Leighton Buzzard sand, grade 1630. This type of sand has been used extensively in laboratory and model testing throughout the U.K. and this particular grade has been used at Glasgow University over several years in a number of investigations associated with anchor pullout (Fadl, 1981 ; Zakaria, 1986 ; Wang, 1986). Grade 1630 Leighton Buzzard sand is a uniform, medium–grained sand with predominantly sub–rounded particles ranging from 0.2mm to 2.0mm. The mineral composition is mainly quartzite.

The particle size distribution curve was obtained using the standard wet sieving method in BS 1377 (1975) and is shown in Figure 3.1. The uniformity coefficient, Cu, was 1.69 and the mean particle diameter, d_{50}, was 0.8mm. Maximum and minimum void ratio values were established using the methods proposed by Kolbuszewski (1948). In the loosest and densest states, the void ratio values were 0.812 and 0.490, respectively. The specific gravity of the soil grains was 2.65.

3.3 SHEAR STRENGTH PARAMETERS

The shear resistance of dry cohesionless sand is influenced by many factors, but by far the most important are void ratio and confining pressure. In model testing, confining pressures are usually very low, and this can affect the shear strength and deformation characteristics of the sand. Ponce and Bell (1971) carried out a series of drained triaxial compression tests on a uniform, quartz sand at extremely low cell pressures. The cell pressure varied from 240kPa to 1.4kPa, and samples with relative densities ranging from 5% to 94% were tested.

Ponce and Bell identified a limiting cell pressure of approximately 35kPa, below which the sand displayed an increased dilatancy during shear, leading to an increase in the principal stress ratio at failure. However, the angle of shearing resistance obtained from the slope of the Mohr envelope for cell pressures above and below 35kPa differed by less than 0.5^{0}.

El– Rayes (1965) used a vacuum pump to obtain comparatively low confining pressures in a triaxial cell, and the same method was used by the author. By using a vacuum pressure, the physical dimensions of the sample could be measured and used to determine the initial density and void ratio. All the samples were nominally 100mm in diameter x 200mm in length. Lateral pressures of 10, 20 and 40kPa were applied to the samples and the densities corresponded to 1752kg/m^3 and 1635kg/m^3, approximately (D_r values of 93% and 59%). The samples were prepared for testing using the general procedures described by Bishop and Henkel (1962). Volume change measurements were not taken.

The variation in peak angle of internal friction with void ratio, for grade 1630 Leighton Buzzard sand, is shown in Figure 3.2. The figure incorporates results from triaxial tests carried out on the same sand by other researchers, and there is good agreement between the results obtained. Appendix I contains details of the author's triaxial tests, including Mohr envelopes and deviator stress versus axial strain graphs.

The triaxial tests were carried out principally to obtain information on the stiffness of the sand for use in the numerical analysis described in Chapter 5. The effect of cyclic loading on the strength and deformation characteristics of sand, as measured in the triaxial test, was not investigated. (see sub– section 2.3.1).

3.4 FORMATION OF UNIFORM SAND BEDS

There are a number of ways of forming uniform beds of dry sand for use in model tests. Butterfield and Andrawes (1970) divided the methods into two distinct categories:

i) methods where the density is adjusted after deposition (usually to densify the sand).

ii) methods where the density is controlled during deposition.

The former category consists of methods involving vibration, tamping, stirring or fluidization using air. When the sand is placed in layers, tamping or stirring is usually employed to give a uniform density, whereas vibration or fluidization can be applied to entire sand beds.

In the second category, the methods used are based on the work of Kolbuszewski (1948), who found that the density of a sand bed formed by vertical deposition was dependent primarily on two parameters:

i) Height of fall of particles from hopper to surface of sand bed and

ii) Intensity of deposition of sand, i.e. weight deposited per unit area per unit time.

In general, the greater the height of fall, the denser the sand bed ; the greater the intensity, the looser the sand bed. Therefore for a dense sand, the intensity should be a minimum and the height of fall a maximum, and vice versa for a loose sand.

There are two methods of deposition associated with this category. In the first, the sand is deposited in layers over the total surface area of the test bed by using a controlled intensity sand raining technique. This technique was used by Kolbuszewski and Jones (1961), who constructed a hopper in which the intensity of deposition was controlled by varying the overlap of holes drilled in two plates at the base of the hopper. The height of fall was controlled by raising or lowering the hopper itself. According to Kolbuszewski and Jones, this technique produced sand beds with very little variation in density between layers. For large test bed areas, the frictional resistance between the two plates could

be considerable, and the weight of the sand made vertical adjustment of the hopper a difficult operation.

The second method of deposition uses a controlled intensity curtain of sand traversing the test bed area to produce a uniform bed of sand. Basically, a sand–filled hopper with a slot near its base travels to and fro across the plan area of the test bed, gradually building up the thickness of sand. Various types of apparatus have been constructed based on this method, differing mainly in the technique used to control the intensity of deposition (James 1967 ; Walker and Whitaker, 1967, Butterfield and Andrawes, 1970). An inherent problem with this method is that it produces distinctly layered sand beds, especially in the case of medium dense and loose deposits. This layering can be reduced by placing a diffuser mesh between the sand curtain and the bed (James, 1967).

In the present study, the controlled intensity sand raining technique was adopted for the following reasons:

i) The area of the test bed was relatively small (500mm diameter) and therefore handling problems would be minimised,

ii) The method could produce a uniform sand bed over a range of densities. This was in contrast to the methods involving vibration, tamping or stirring which were generally limited to producing dense sand beds. The use of vibration techniques could lead to problems of non–homogeneity (Tsangarides, 1978) and induced horizontal stresses (Andreadis, 1979) in the sand bed. Finally, the particular sand curtain setup used by Fadl (1981), which was available for use in the present study, was unable to provide high intensity deposition, and therefore was also limited to producing dense sand beds.

3.4.1 Apparatus

The final form of the sand raining apparatus used in the model tests is shown diagrammatically in Figure 3.3. It consisted of a circular hopper the same diameter as the test container (500mm) with interchangeable base plates drilled to form a grid of holes. The base plate covers were hinged at opposite sides of the hopper and held closed by metal pins pushed through the supporting frame and underneath the cover plates. A range of sand densities was achieved by varying both the hole diameter in the plates and the height of fall. Calibration curves showing the variation in dry density against fall height

for hole diameters ranging from 3.5mm to 8.0mm are shown in Figure 3.4. These curves indicate that, for the hole diameters used, the dry density reaches a maximum value and any further increase in fall height is not effective in increasing the value of dry density. Clearance for the cover plates constrained the minimum height of fall to 950mm.

When forming a bed of sand, the intensity of deposition and the height of fall were kept constant ; the former by simply choosing a suitable base plate and the latter by placing the sand in approximately 75mm layers and lifting the entire hopper assembly after each layer was deposited. To place a bed of sand, the hopper was filled to a depth of approximately 75mm with the base plate covers closed. The pins were then removed, and the cover plates swung away to start sand raining down into the container. A photograph of the apparatus in operation is presented as Figure 3.5.

For a dense sand bed, the intensity of deposition was low and there were no problems associated with air displacement from the tank. However, for a medium–dense sand bed, because of the high intensity of deposition, air was displaced upwards from the tank around its circumference. This updraught of air resulted in sand layers shaped as shown in Figure 3.6. Sand density measurements established that the formation of sand layers shaped in this way did not adversely affect the homogeneity of the resulting sand bed. The measurement of sand density is discussed in the following section.

3.4.2 Measurement of Sand Density

Various methods of measuring the density of dry sand beds placed under controlled laboratory conditions have been reported. These include the spoon penetration test (Gibbs and Holtz, 1957) ; vacuum sampling apparatus (Ovesen, 1962) ; density pots (Butterfield and Andrawes, 1970).

Whilst it is important to establish values for the density and relative density of a particular sand bed, it is equally important to be aware of the potential measurement errors involved. The accuracy of density and relative density measurements was discussed in some detail in a paper by Tavenas and La Rochelle (1972). Using classical error theory, they calculated that the error in relative density measurement, even under the most favourable laboratory conditions, was of the order of ±6%. This error increased to around ±18% if results from different experimenters were compared . Tavenas and La Rochelle concluded that the relative density should not be used as a quantitative

parameter but rather as a qualitative indication of the state of compactness of a cohesionless soil deposit.

With respect to the present study, it was not considered necessary that the relative density be measured with great accuracy, simply that the method used should provide consistent results in the dense and medium dense sand ranges. As all the methods made similar claims of good reproducibility, the choice therefore became one of convenience, and based on the experience of Fadl (1981) and others, it was decided to use density pots.

The density pots were 75mm in diameter and 50mm deep, with a knife edge upper rim. The volume of the pots was measured by weighing them filled with water. To obtain the calibration curves presented in Figure 3.4, three density pots were placed within the test container for each height of fall. The calibration tests were repeated twice. From the maximum and minimum void ratio values previously measured, the maximum and minimum dry densities were 1778kg/m^3 and 1463kg/m^3 respectively. A dense sand was defined as having $D_r \geqslant 90\%$, which corresponded to a dry density of $\geqslant$1741kg/m^3. Using a combination of 3.5mm diameter holes and 950mm fall height, a dry density greater than the required value could be achieved. In practice, a dry density of 1752±2kg/m^3 was achieved, which represented an error of ±0.6% on the range of dry density (assuming this range to be constant), and ±0.5% on the relative density value of 93.0%. For medium dense sand, a combination of 8mm diameter hole and 950mm fall height gave a dry density of 1635±7kg/m^3. The error in this case was ±2.2% on both the dry density range and relative density value of 59.4%.

On a number of occasions, the dry density, as obtained using density pots, was checked by estimating the overall density of the sand bed. This was achieved by weighing the total amount of sand placed and estimating the volume of sand by measuring down to the sand surface from a rigid (but moveable) horizontal datum placed across the top of the tank. The average of seventeen distance measurements multiplied by the cross-sectional area of the tank established the unfilled volume. From this the filled volume was calculated and hence the overall density of the sand bed. Figure 3.7 shows a graph of sand bed density as measured by density pots against overall sand bed density. The results cluster around a line drawn at 45^0, illustrating good agreement between the two values of density.

3.5 TEST RIGS

The test rigs were designed using information obtained from various sources, but particularly Kupferman (1974) and Motherwell and Wright (1978). The final design was a compromise between a sophisticated (and expensive), loading and data–recording system with full feed–back control of cyclic loading, and a simple mechanical set–up of multiple rigs which lacked versatility, especially in the type of cyclic loading that could be applied to the anchor.

In the present study, three test rigs were constructed, and each one consisted of three basic components: the structural items (e.g. sand container, loading frame, yoke assembly); the loading system (for static and cyclic loading); instrumentation and data acquisition. Although not identical, corresponding components of each test rig performed the same function. These components are described in the following sections.

3.5.1 Structural Items

Figure 3.8 illustrates the main structural items. The test container was fabricated from 6mm mild steel plate into a right cylinder 500mm in diameter and 650mm in length, with a circular base plate welded to one end to form the bottom. The container was placed on an un–reinforced concrete pedestal measuring 600mm x 600mm x 500mm, in an effort to dampen any vibrations from the laboratory floor.

The loading frame was constructed of 100mm x 100mm x 6mm R.H.S. as a simple portal frame with internal dimensions of 1400mm horizontally and 1750mm vertically. The top member was removed during sand placing operations.

A pneumatic piston centred on the top portal member provided the uplift load to the anchor through an adjustable yoke assembly. The top cross–member of the yoke had a spherical centre point which located in the dished end of the piston rod. A photograph of these items is presented as Figure 3.9.

3.5.2 Loading System

The loading system consisted of a filtered, regulated air supply ; an electro–pneumatic (e–p) converter ; an electrical signal generator designed and built in–house ; air lubricator ; pressure gauge ; pneumatic piston. A schematic of the loading system is shown in Figure 3.10.

The electrical signal generator could supply four different signals : a ramp signal for constantly increasing load, and sine, square and triangular wave signals for cyclic loading. The mean, amplitude and period of the waves were adjusted using variable resistances. A digital counter monitored the number of cycles of loading. The output signal from the generator controlled the e–p converter, which in turn supplied an air pressure change to the piston in proportion to the input current change. Figure 3.11 shows a photograph of the loading system attached to an upright of the loading frame.

In order to reduce the amount of calibration work, the individual components of each loading system were not interchanged during the test series. Figure 3.12 shows typical calibration curves for the combination of e–p converter, signal generator and piston. The straight line relationships were easily reproduced and very stable. The ramp speeds shown in Figure 3.12 could be varied by adjusting the output from the signal generator (see Figure 3.18).

3.5.3 Instrumentation and Data Acquisition

The principal measurements taken during testing were anchor load and anchor displacement. In some tests, the deformation of the sand surface was also measured. The anchor loads were measured using Sangamo Type D91 load cells, with load ranges of 0–445N and 0–2225N (Sensitivity of 1.0N/division at DVM). The anchor displacements were measured at the top of the anchor shaft, using two Sensonic Type SR displacement transducers calibrated to ±25mm (Sensitivity of 0.02mm/division at DVM). The arrangement of load cell and displacement transducers is shown in Figure 3.13.

Surface deformation was measured by placing a row of displacement transducers across a diameter of the test tank. The transducers, calibrated to ±10mm (Sensitivity of 0.01mm/division at DVM), were located in a small length of square hollow section which was suspended from the tank walls, as shown in Figure 3.14

The electrical signals from the load and displacement transducers were collected by a signal conditioning unit which consisted of a digital voltmeter and conditioning/calibration cards for each transducer. A Solartron data logger linked to a Commodore Pet micro-computer monitored the signal data at convenient time intervals, depending on the type and stage of the test. Some of the cyclic loading tests lasted for more than three months, and during this time signal data was obtained every two hours. Each set of data for a cyclic test was made up of 40 scans of each data channel in use, which ensured that four complete cycles of loading had taken place. The computer calculated the average values of the maximum and minimum readings for that data set and printed out the results, together with the channel numbers used and the date, day and time the readings were taken. A schematic layout of the data acquisition system showing the interaction of the components is shown in Figure 3.15.

During static loading tests the channels were scanned more frequently at the beginning and end of each test. This was accomplished by setting the changes in frequency of scanning to correspond with some pre-set load values between zero and the estimated failure load.

All load cells and displacement transducers were calibrated against the DVM readout on the signal conditioning unit. The load cells were calibrated using dead weights, and Figure 3.16 shows a typical load cell calibration curve. To calibrate the displacement transducers, a small rig was used which incorporated a micrometer. A typical calibration curve for the displacement transducers is shown in Figure 3.17. During the period of testing, the calibrations were checked from time to time and found to be extremely consistent.

Details of the load cells, displacement transducers and other items of equipment for each of the test rigs used in this investigation are given in Appendix II.

3.6 ANCHOR TESTS

Static and cyclic anchor tests in air-dried sand could be carried out on each of the three test rigs. All the tests were load controlled rather than displacement controlled. Andreadis (1979) showed that the load-displacement characteristics of an anchor were not affected by this choice.

3.6.1 Static Tests

The static tests were carried out using a ramp signal which resulted in a loading rate of approximately 50N/min. Calibration curves for the ramp signal to a 150mm diameter piston are shown in Figure 3.18. The effect of rate of loading on the ultimate resistance was not investigated. For displacement controlled tests, Tsangarides (1978) reported that varying the pullout rate from 0.5mm/min to 29mm/min resulted in only a 4% range difference in ultimate resistance.

The tests covered embedment ratios ranging from 2 to 15 in dense and medium–dense Leighton Buzzard sand. Usually at least two tests were performed at each embedment ratio. The anchors were 6mm thick brass discs with diameters of 25mm, 37.5mm, 50mm, 75mm and 100mm. A length of smooth brass rod, 6mm in diameter, served as the anchor shaft.

3.6.2 Procedure for Static Loading Tests

Using the sand raining apparatus described in section 3.4.1, a bottom layer of sand 75mm thick was placed in the container. The anchor and anchor shaft were then carefully placed in the centre of the container, resting on top of the sand layer. A three–legged guide ensured that the anchor shaft remained vertical during subsequent sand raining operations. Although the presence of the guide did interrupt the sand raining curtain, the effect on density measurements was imperceptible. This stage in the preparation of the sand bed for an anchor test is illustrated in Figure 3.19. When the appropriate depth of sand above the anchor had been placed, the sand raining apparatus was removed.

The top frame member was positioned across the test container and the piston centred approximately above the anchor shaft. The yoke was suspended from the piston and the load cell connected to the bottom cross–member of the yoke. In order to ensure that the pull from the yoke was applied axially along the anchor shaft, a small universal joint was incorporated in the connection between the top of the load cell and the yoke, as shown in Figure 3.13. Also shown is the adapter used to facilitate connection between the anchor shaft and the bottom of the load cell. Using the adjustment available on the threaded rods of the yoke, vertical alignment of adapter and load cell could be achieved, and the 6mm diameter shear pin located with ease. The anchor was now ready for testing.

With the air supply to the e–p converter turned on, the ramp option on the signal generator was selected and the loading commenced.

3.6.3 Cyclic Tests

For the cyclic tests, the loading frequency was largely governed by the response time of the loading system and pneumatic piston. Using a sinusoidal wave signal with a period of approximately 10 seconds, the load response of the anchor was found to be slightly distorted. This distortion is evident in Figure 3.20 and is thought to be associated with friction in the piston, compression of air in the system and the response characteristics of the yoke assembly. The distortion increased with increasing frequency and at values greater than 0.2Hz the applied load response was unacceptably asymmetrical. Taking this value as an upper limit on the frequency, and bearing in mind the potential offshore application of anchor research mentioned in the introduction, it was decided to use a loading frequency of around 0.1Hz. This placed the loading conveniently within the range of periods usually associated with wave forces, typically 5 to 20 seconds (Standing, 1981). At this low frequency, inertia effects could be ignored.

In deciding upon the embedment ratio to use in the cyclic tests, consideration was given to boundary and scale effects in the experimental set–up. Boundary and scale effects were highlighted in Chapter 2, and their influence on the static test results reported in this thesis is discussed in Chapter 6. On the basis of these results, and noting that the cyclic behaviour of plate anchors is essentially independent of embedment ratio (see Chapter 2), a value of D/B= 4.5 was used in all the cyclic tests.

The load parameters varied in the cyclic tests were mean load and amplitude of load, both expressed as a percentage of the static failure load (sfl). Numerous combinations of mean and amplitude were applied to the anchors during the test series, with some anchors subjected to over 1 million cycles of loading. Replicate tests were carried out in order to assess the repeatability of the results. The test results are presented in detail in the next chapter.

3.6.4 Procedure for Cyclic Loading Tests

For the formation of the sand bed and the positioning of the anchor and top frame member, the procedure was identical to that used in the static loading tests. When ready for testing, it was necessary to pre–set the mean

and amplitude load values, at least approximately, before connecting the load cell to the anchor shaft. In order to do this, a rigid cross–member was suspended from the main loading frame between the load cell and the adapter on top of the anchor shaft, as shown in Figure 3.21. With the base of the load cell connected by a shear pin, the cross–member acted as a reaction against the force developed in the piston and through the yoke to the load cell. Using this arrangement, the appropriate mean and amplitude load values were pre–set by adjusting the controls on the signal generator, noting the maximum and minimum values of the electrical signal as well as those of the load.

When satisfied that the equipment was operating properly and the maximum and minimum load values were correct, the sine wave was switched off and the load reduced to zero. The cross–member was then removed and the connection made between the adapter and the load cell. Note that for the cyclic tests in which the load reduced to zero, or nearly so, the shear pin was located in a vertical slot in the adapter, in order to ensure that no compressive load was applied to the anchor shaft during testing.

With the air supply to the piston turned off, the previously noted electrical signal was reproduced by the signal generator and hence also the same air pressure from the e–p converter. The air valve to the piston was then opened, the cycle counter activated and cyclic loading commenced. During the first 50 or so cycles the maximum and minimum load values usually required some adjustment, but because the mean and amplitude of the loading had been pre–set, these adjustments were small and easily accomplished.

The loading system had no feed–back facility, so regular monitoring of the load read–out was essential, with adjustments being made as necessary. During proving tests on the loading system, minor adjustments were required 2 or 3 times per week.

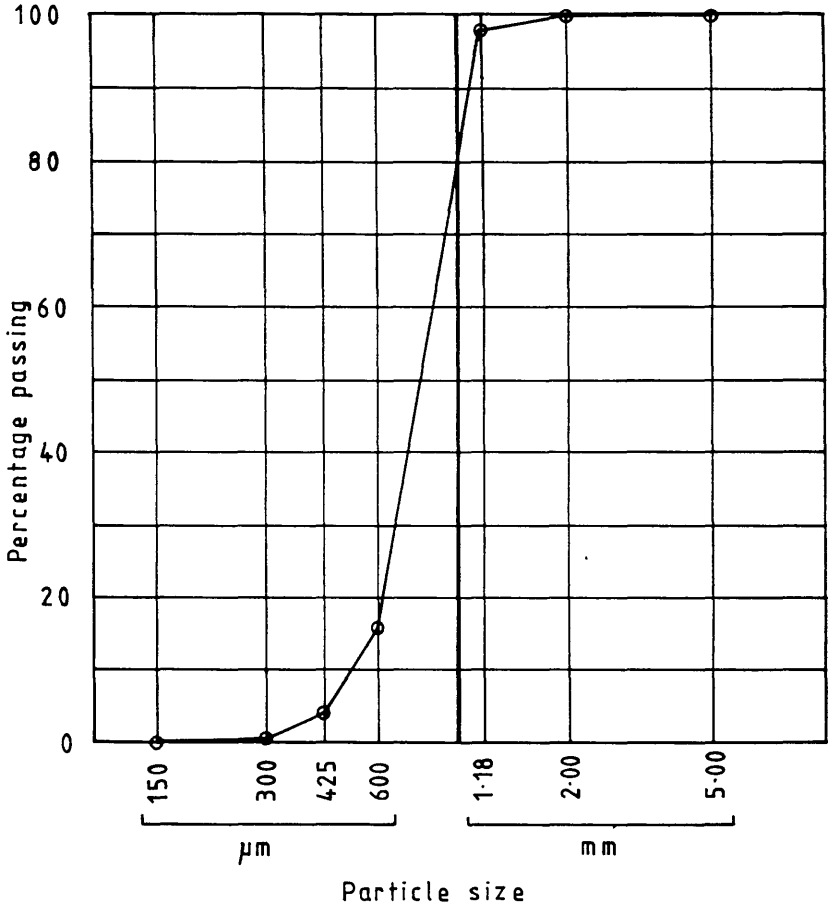

FIGURE 3.1 - Particle size distribution for grade 1630 Leighton Buzzard sand.

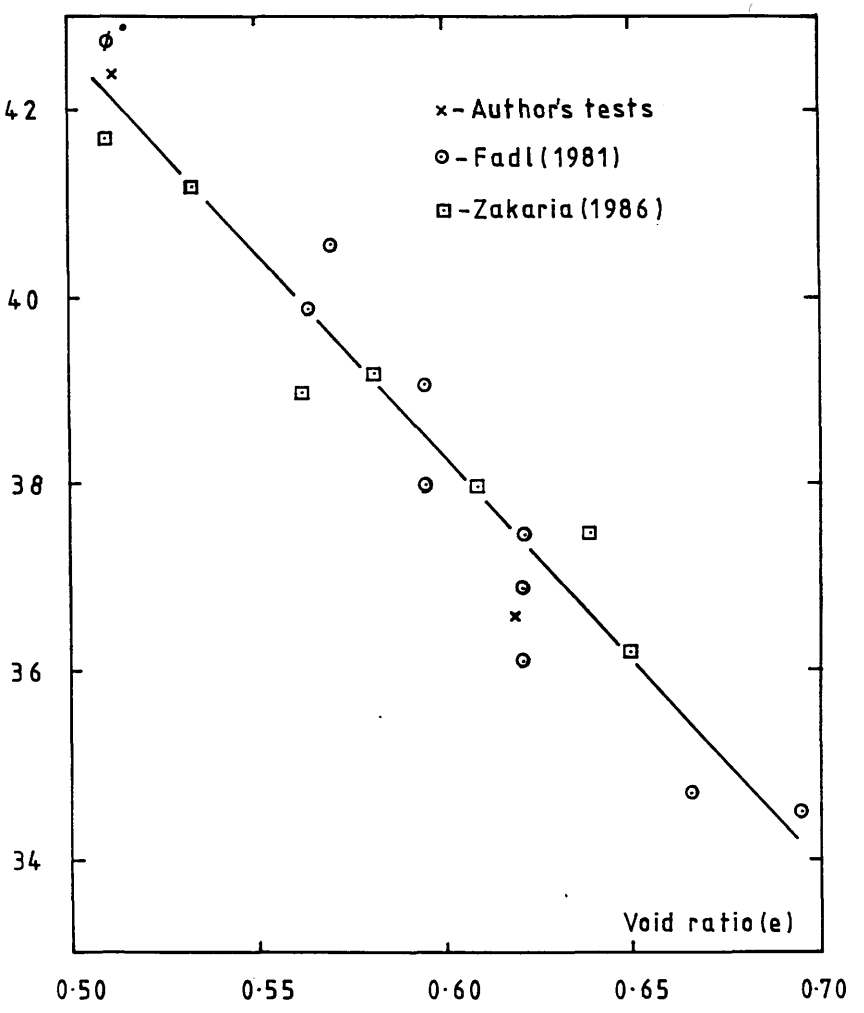

FIGURE 3.2 - Variation in peak angle of friction with void ratio for grade 1630 Leighton Buzzard sand.

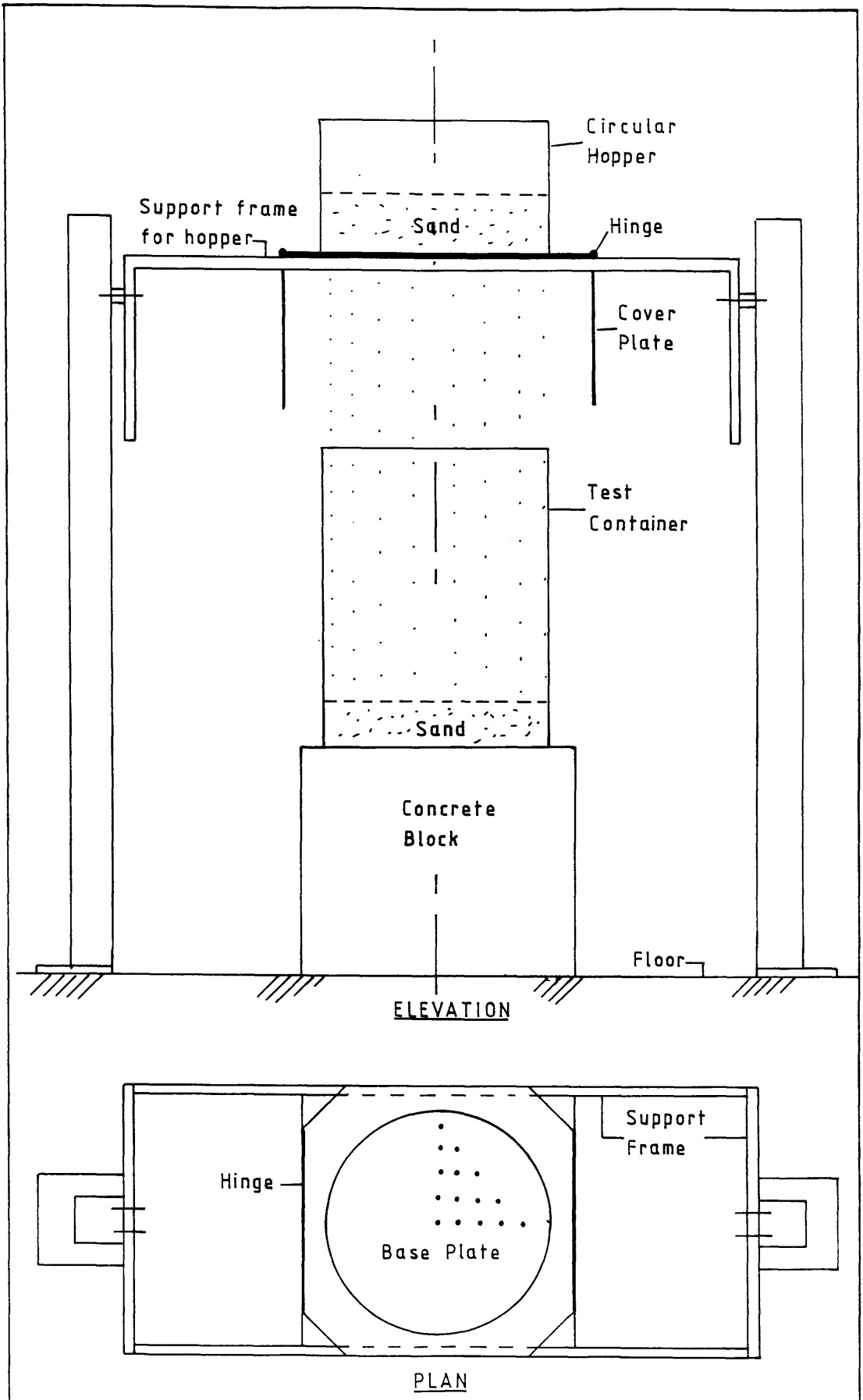

FIGURE 3.3 - Sand Raining Apparatus.

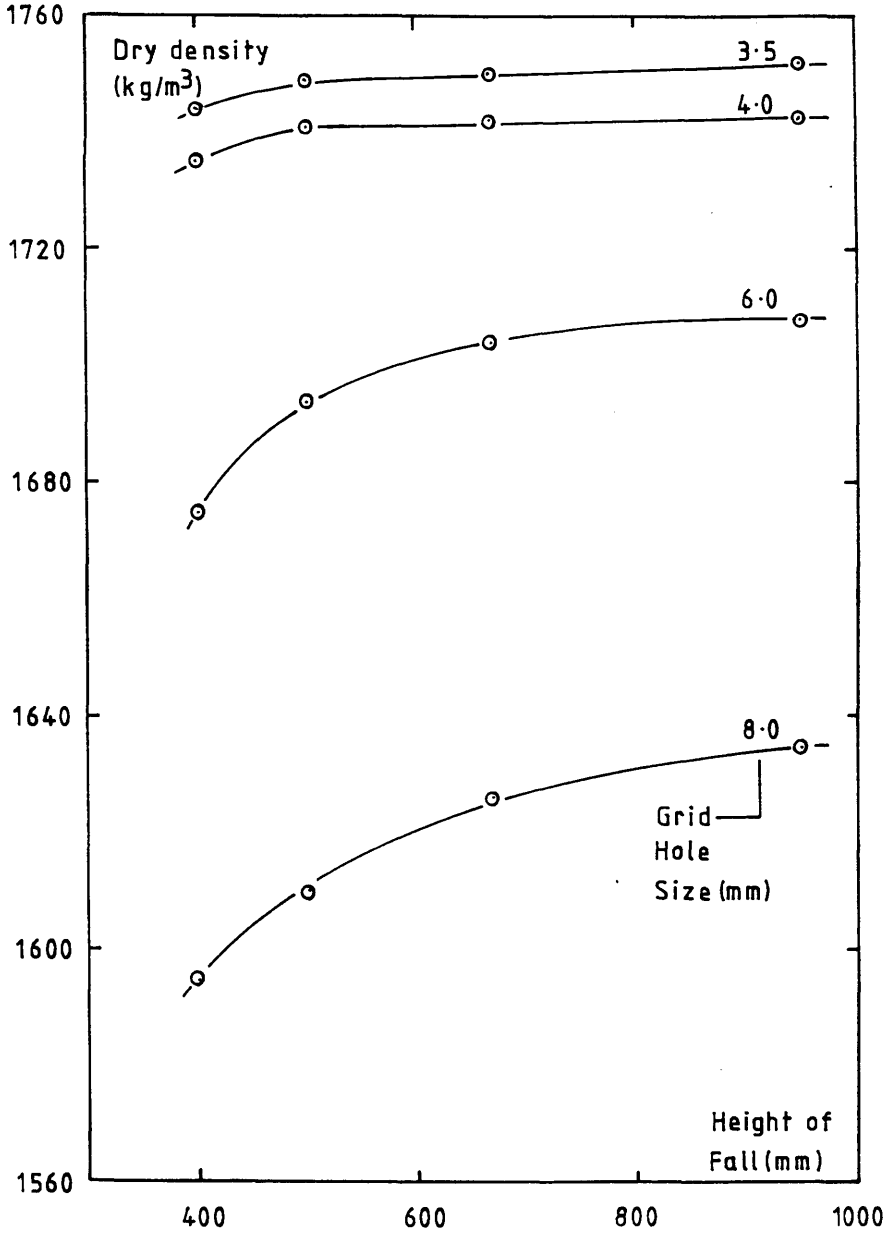

FIGURE 3.4 - Calibration curves for sand raining apparatus.

FIGURE 3.5 - Photograph of sand raining apparatus in operation.

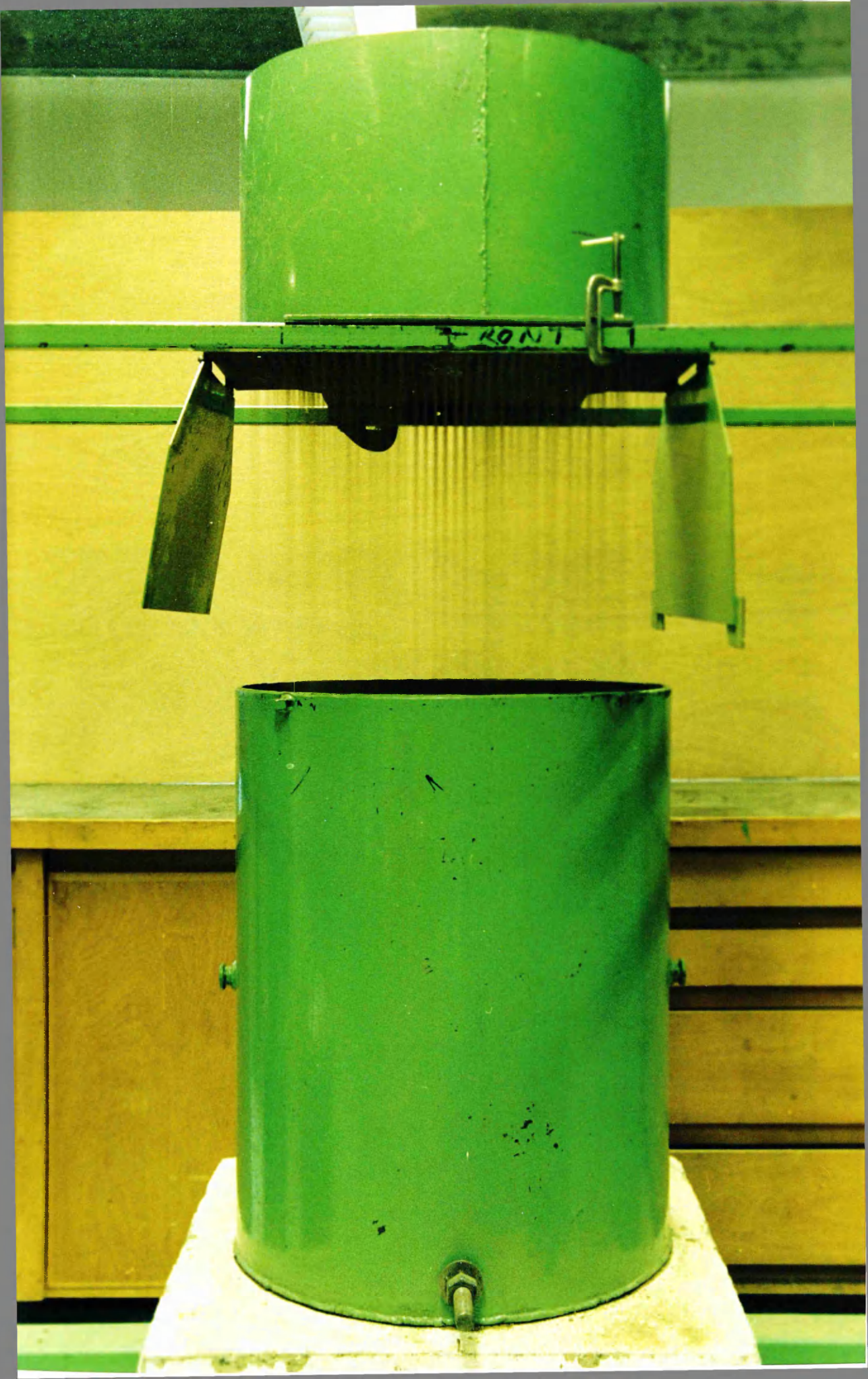
FRONT

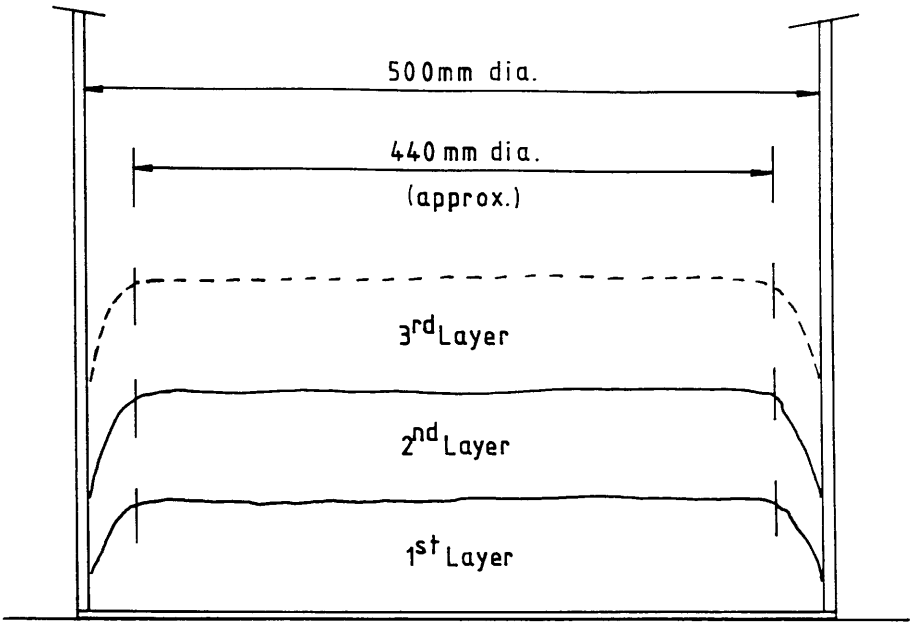

FIGURE 3.6 - Shape of sand layers in medium-dense sand beds.

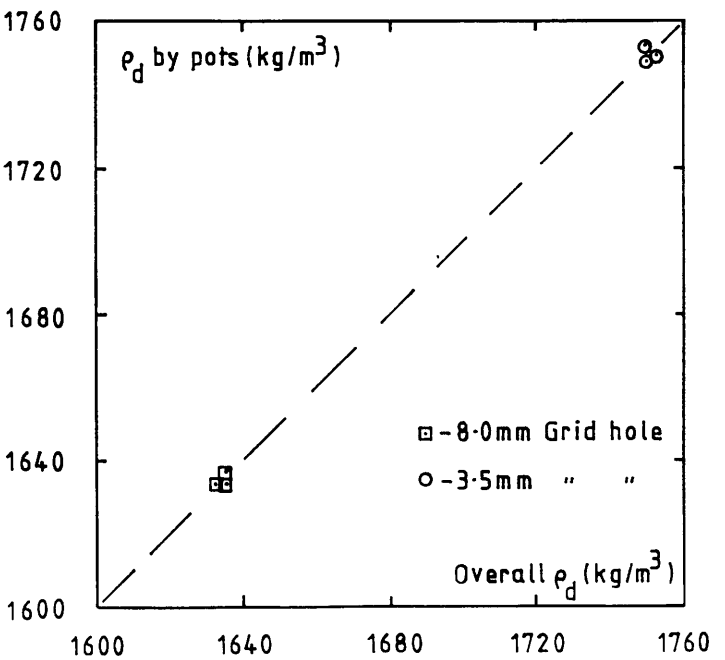

FIGURE 3.7 - Comparison between methods of sand density measurement.

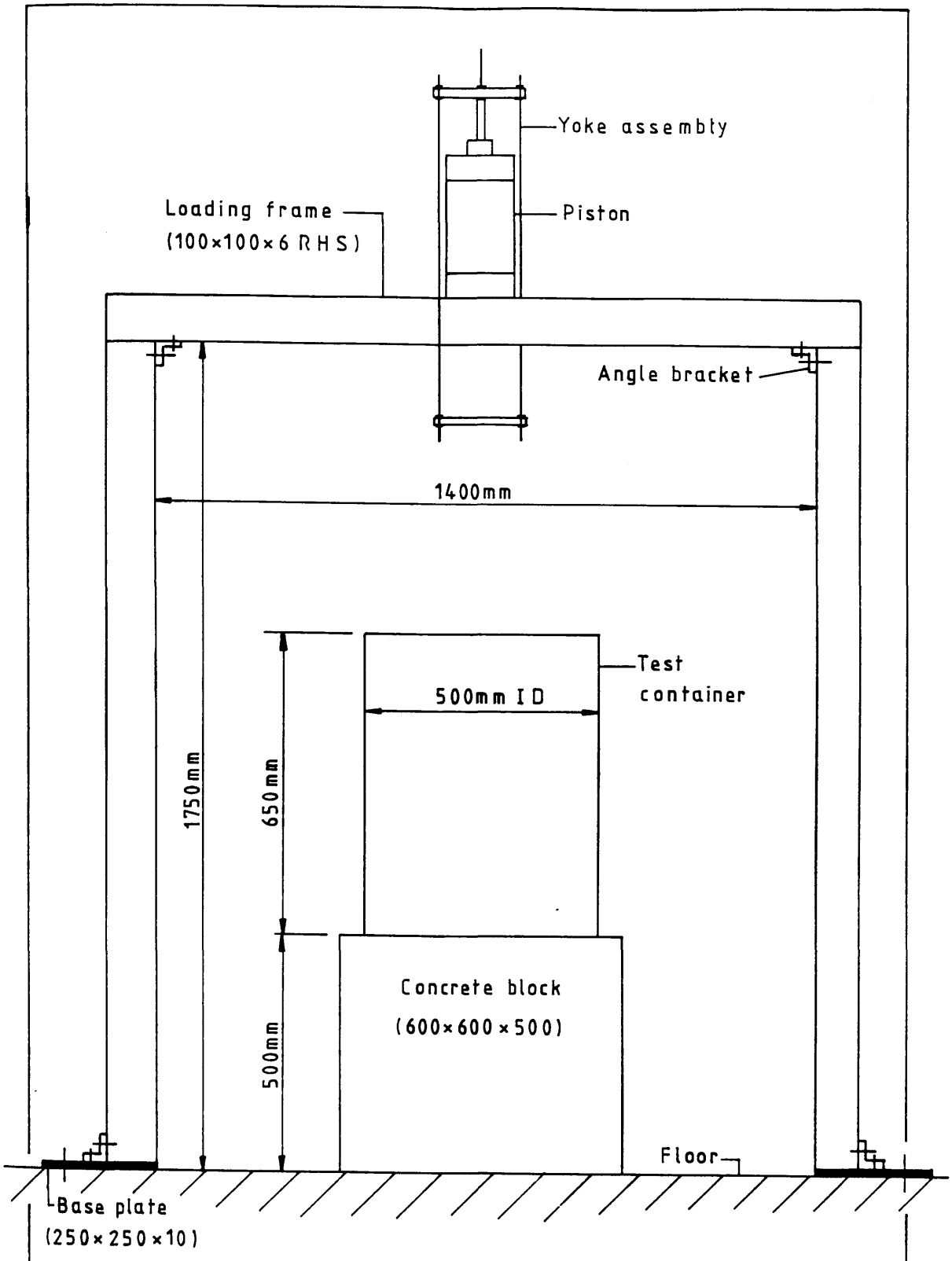

FIGURE 3.8 - Structural items of test rigs.

FIGURE 3.9 - Photograph of structural items of test rigs.

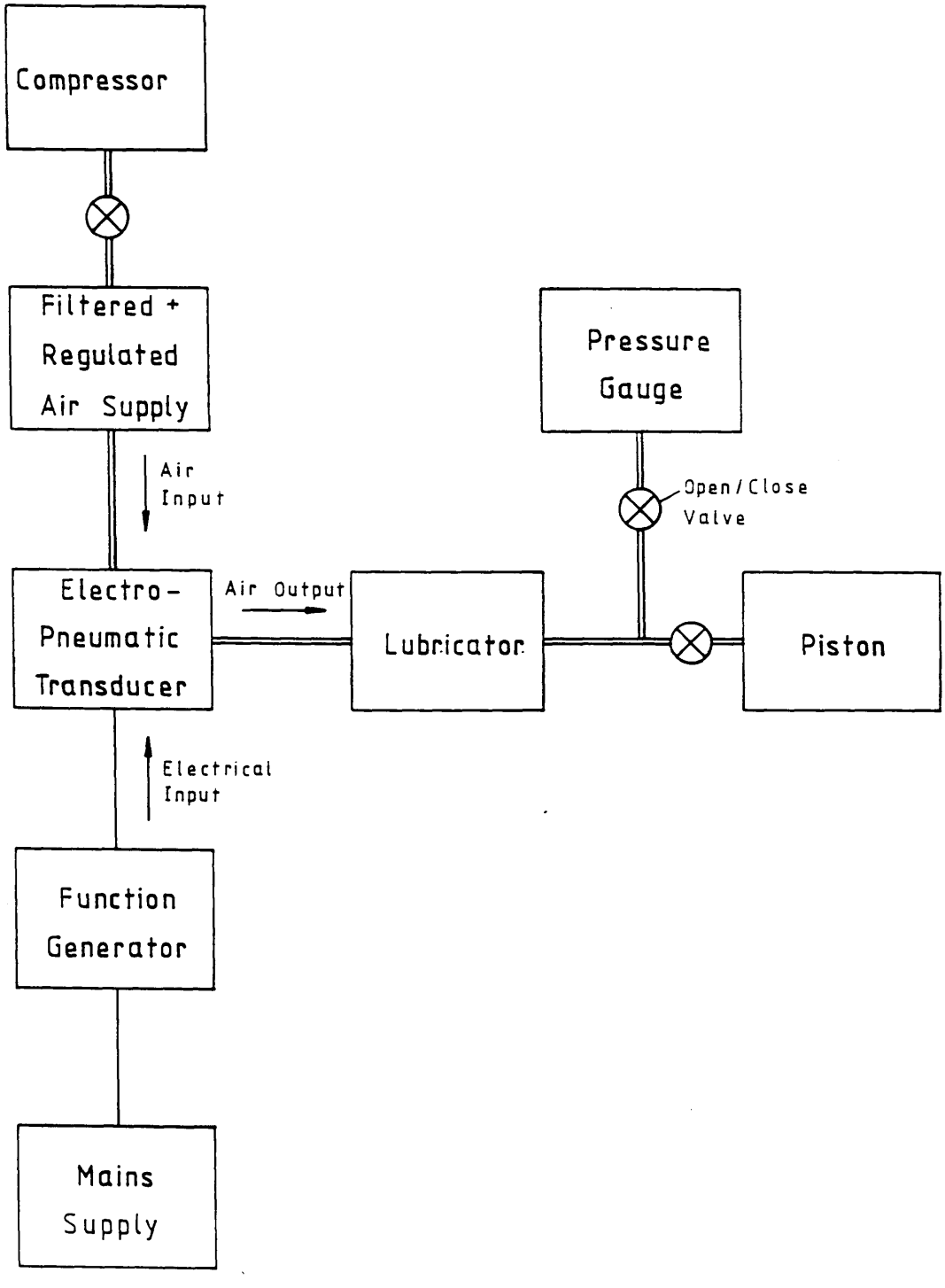

FIGURE 3.10 - Schematic of loading system.

FIGURE 3.11 - Photograph of loading system.

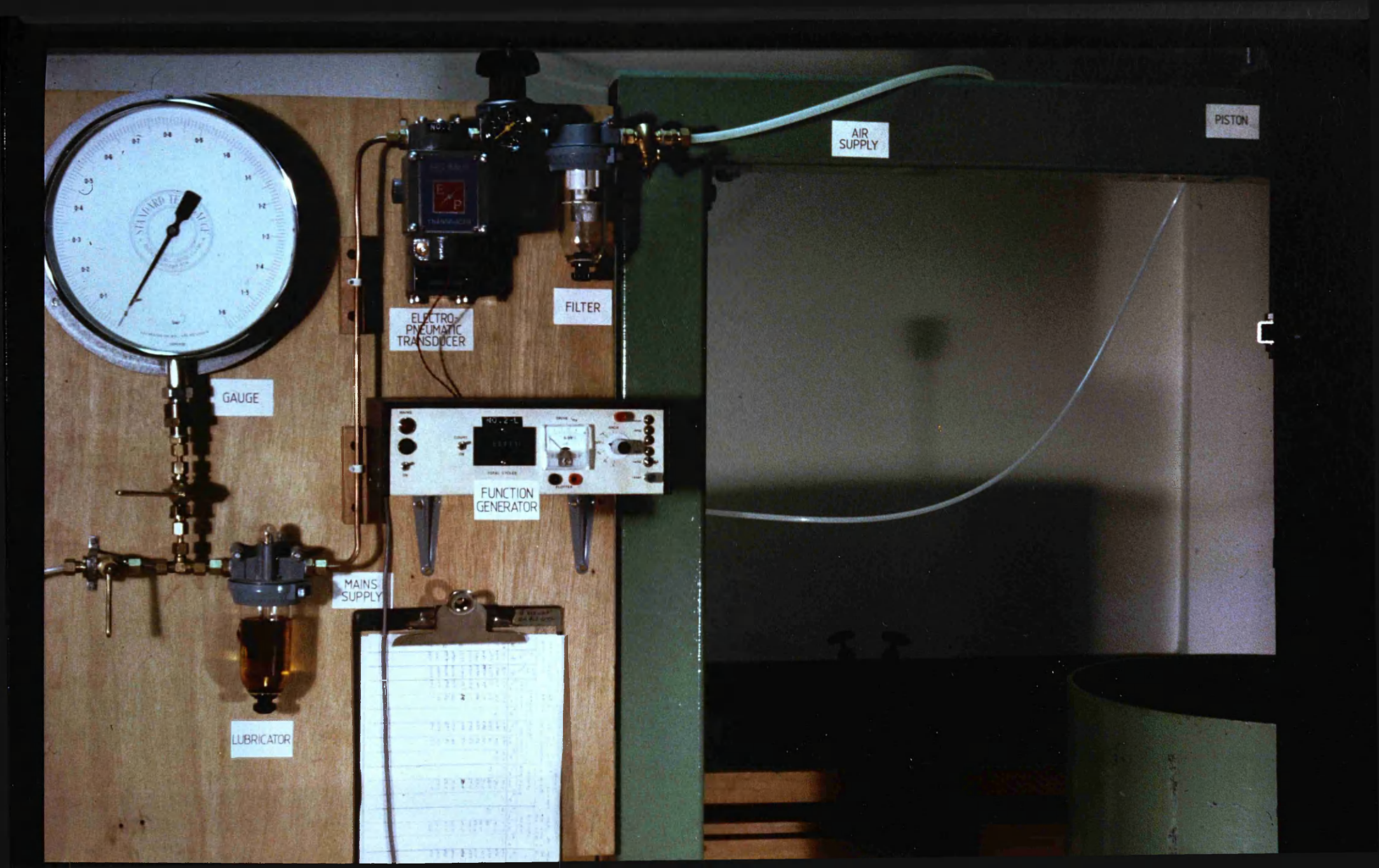
GAUGE
ELECTRO-PNEUMATIC TRANSDUCER
FILTER
AIR SUPPLY
PISTON
FUNCTION GENERATOR
MAINS SUPPLY
LUBRICATOR

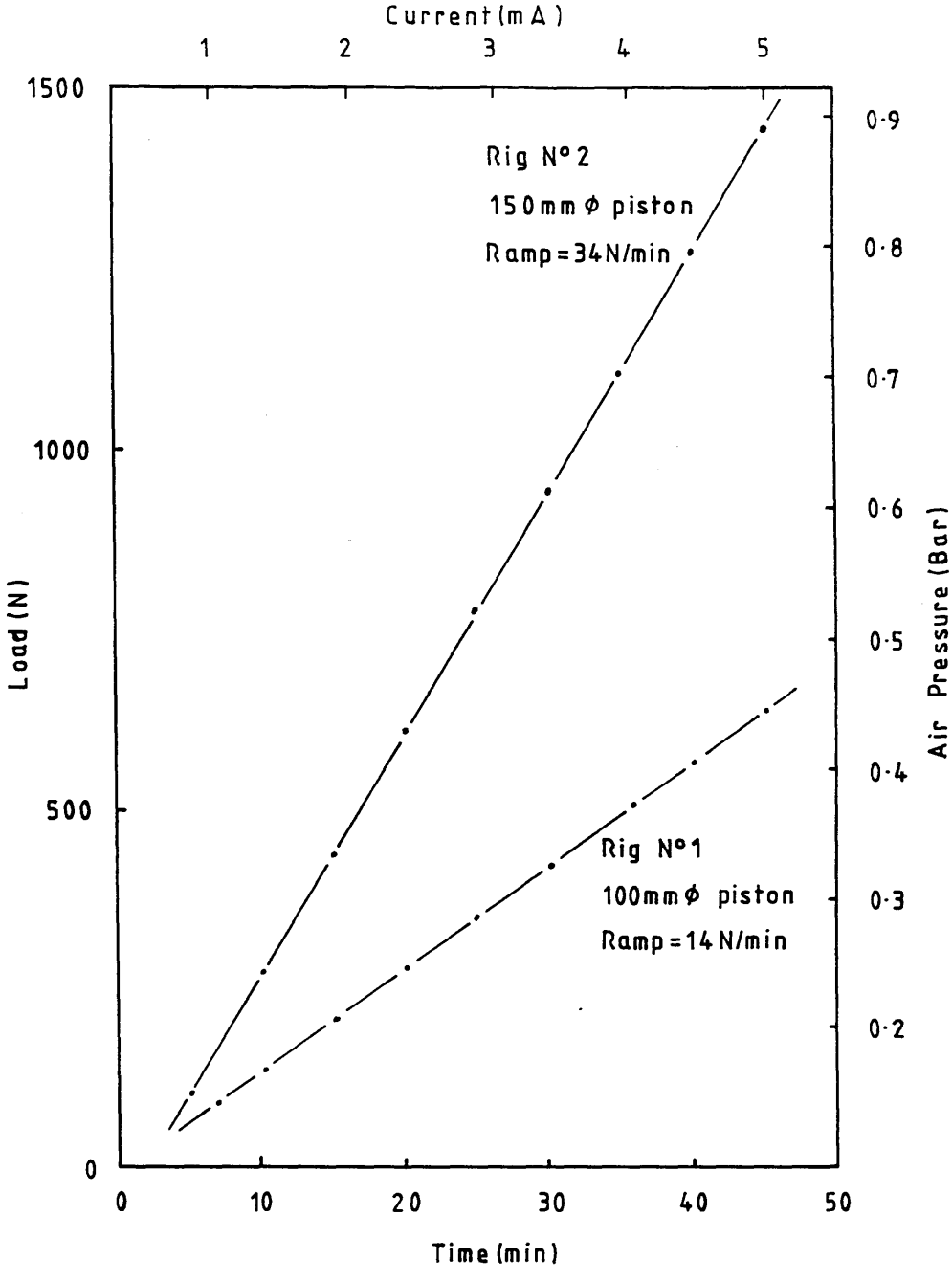

FIGURE 3.12 - Typical calibration curves for loading system.

FIGURE 3.13 - Photograph showing arrangement of load cell and displacement transducers.

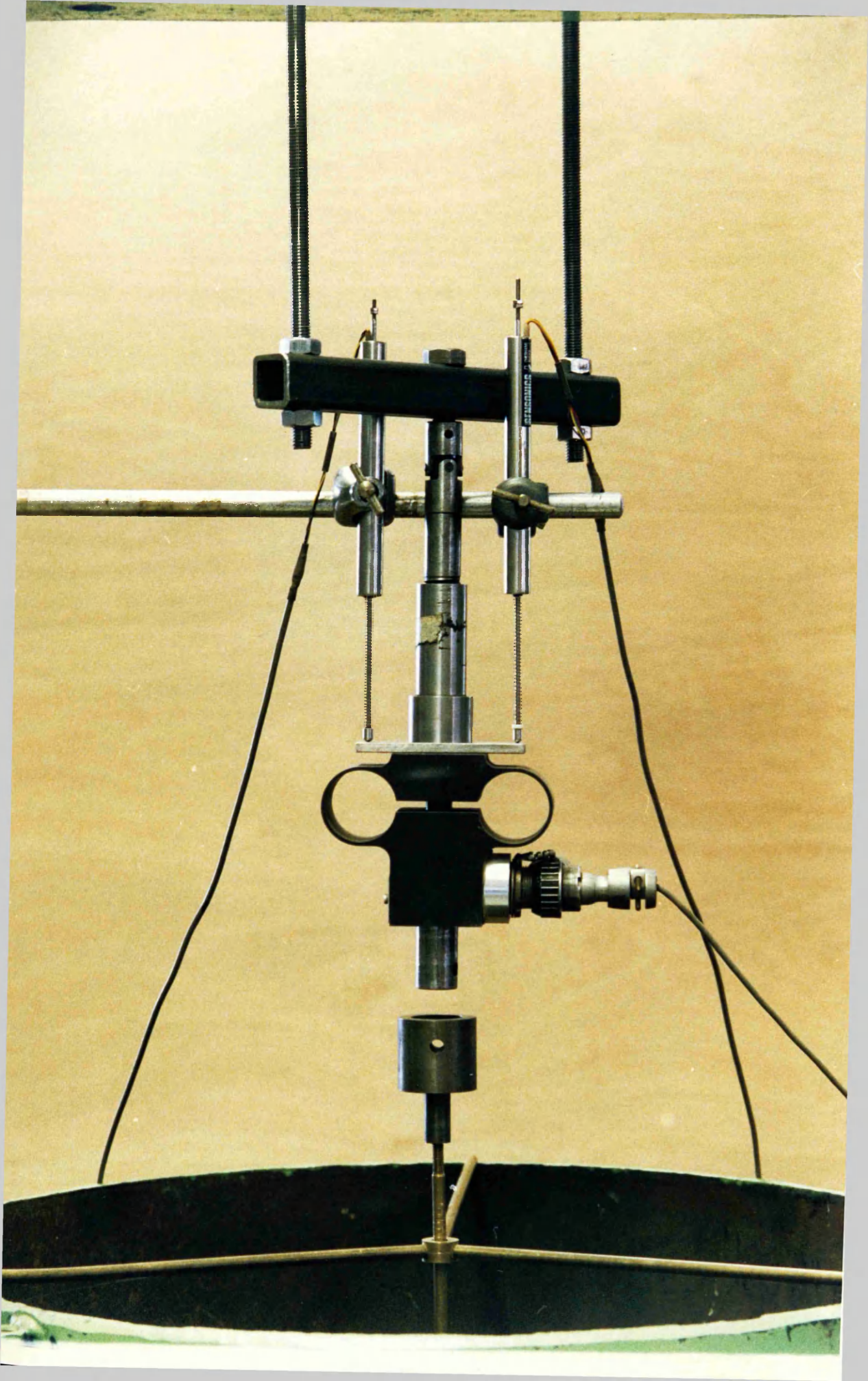

FIGURE 3.14 - Photograph showing arrangement of displacement transducers to measure surface displacement.

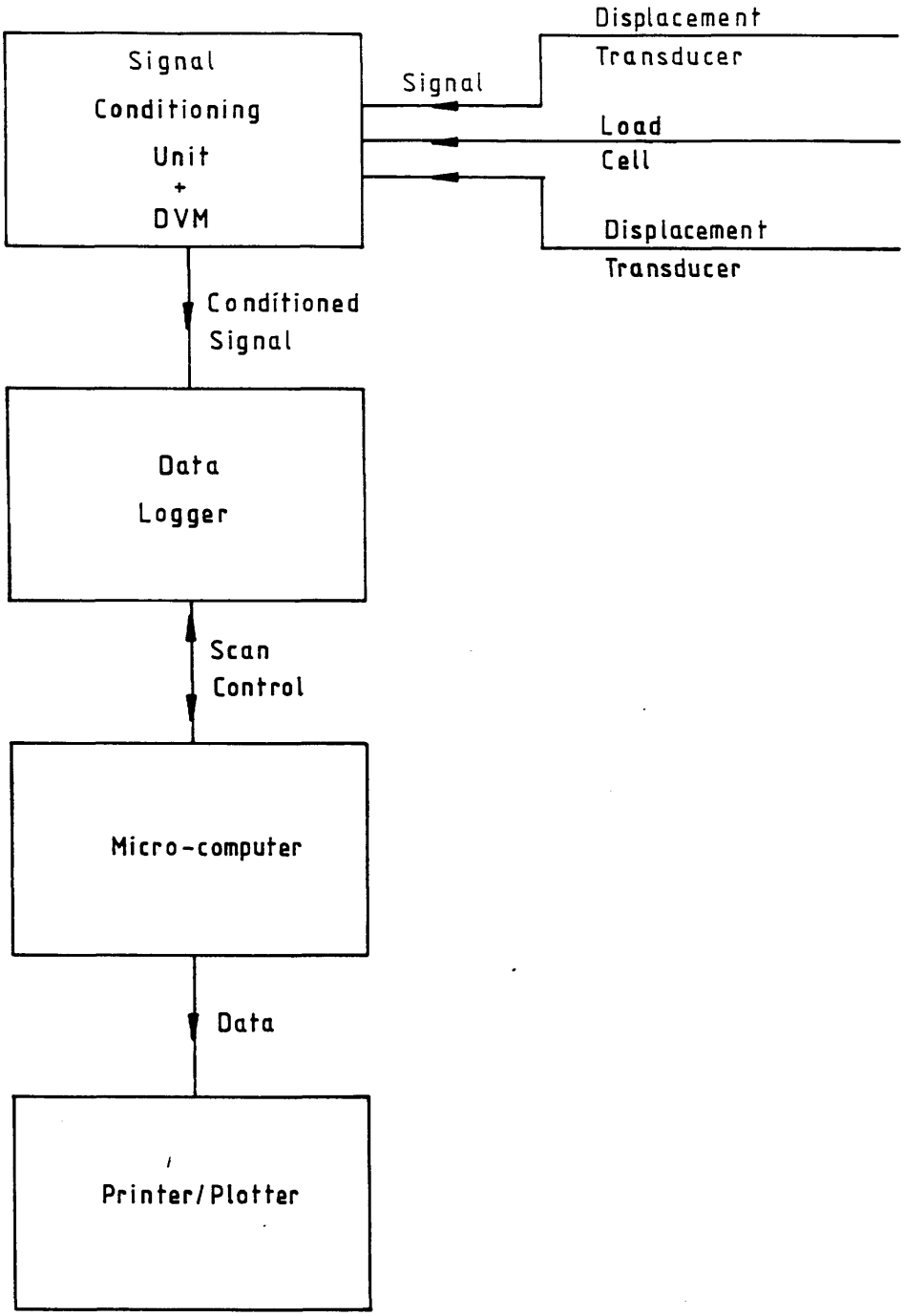

FIGURE 3.15 - Schematic of data acquisition system.

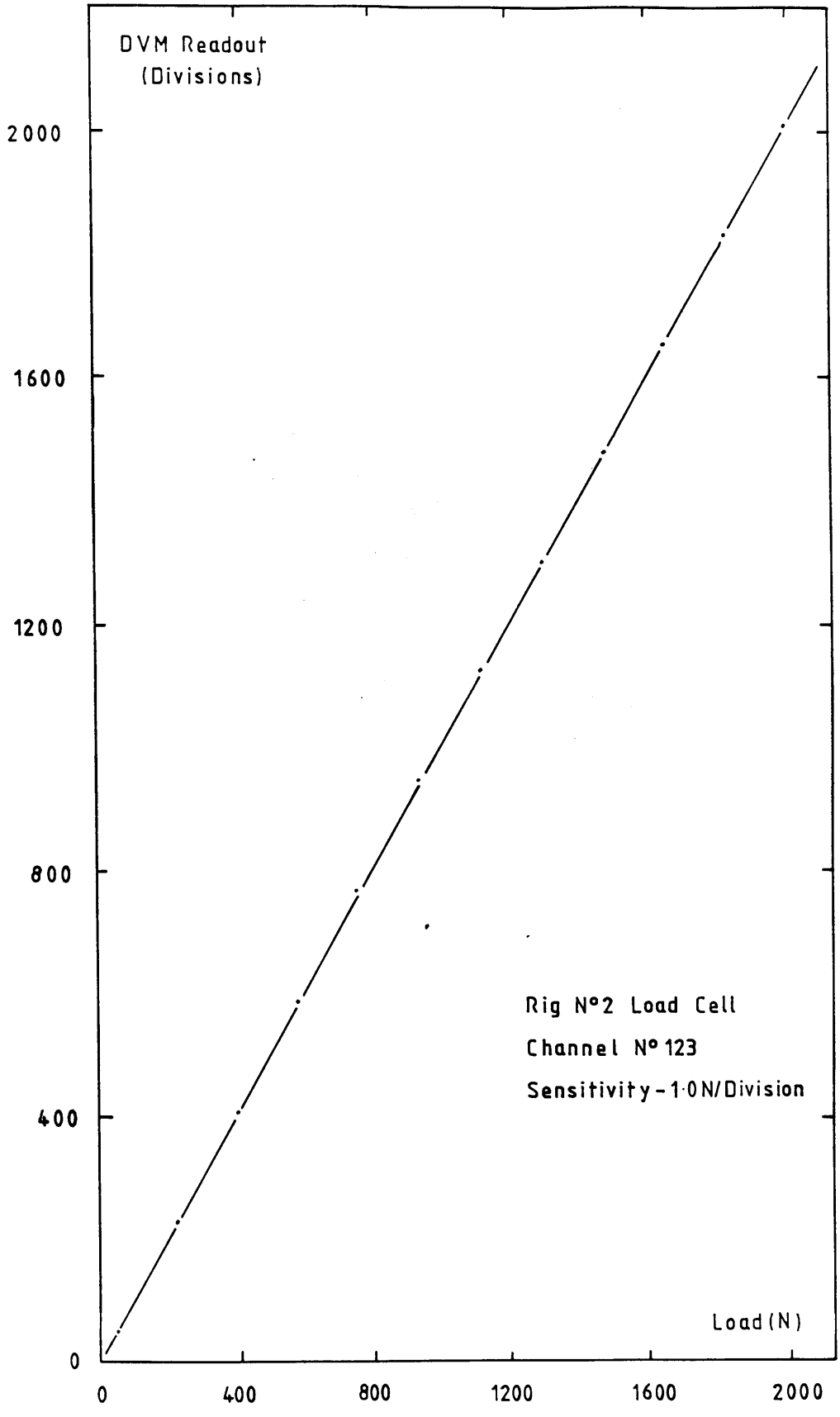

FIGURE 3.16 - Typical calibration curve for load cells.

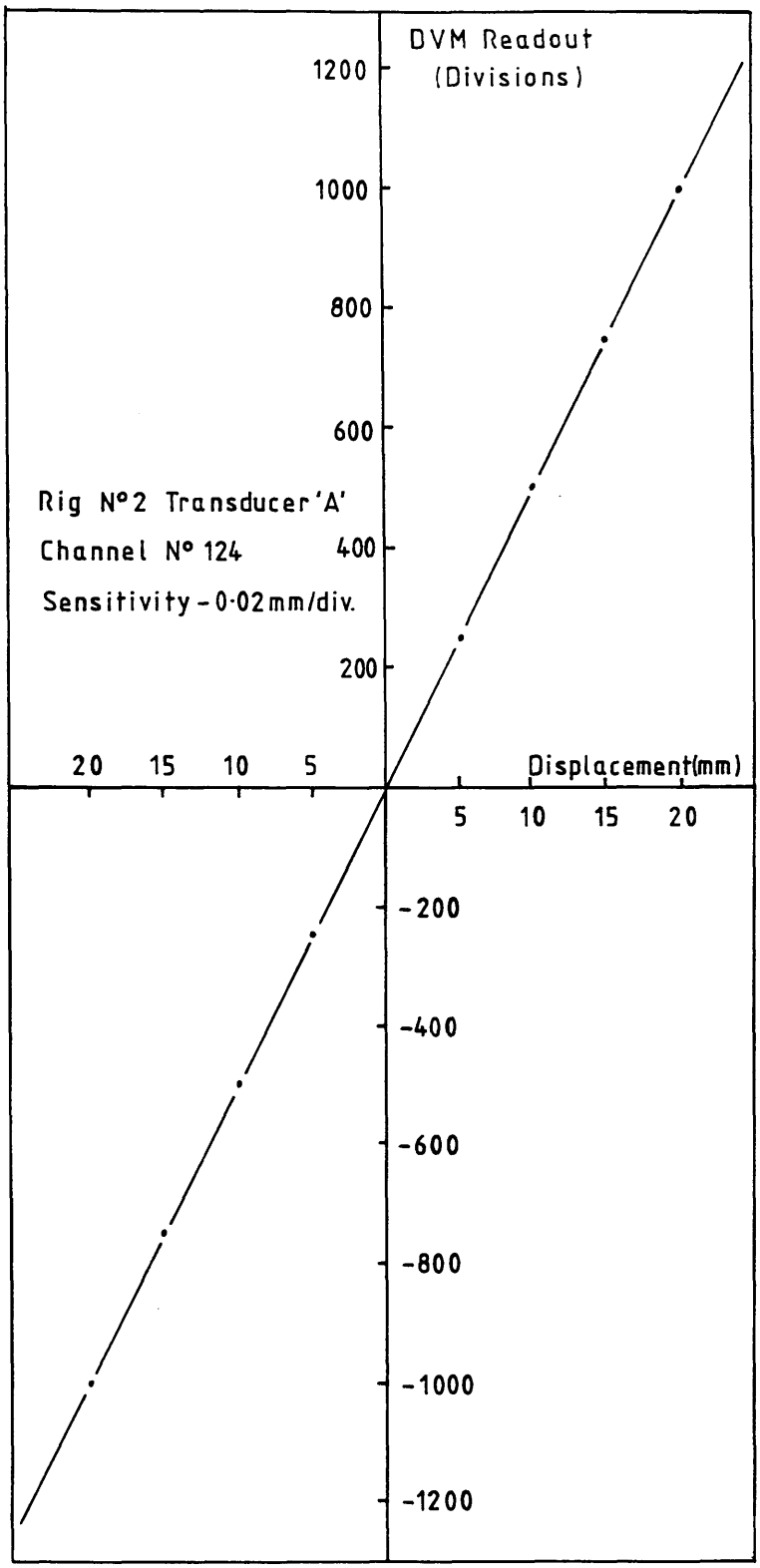

FIGURE 3.17 - Typical calibration curve for displacement transducers.

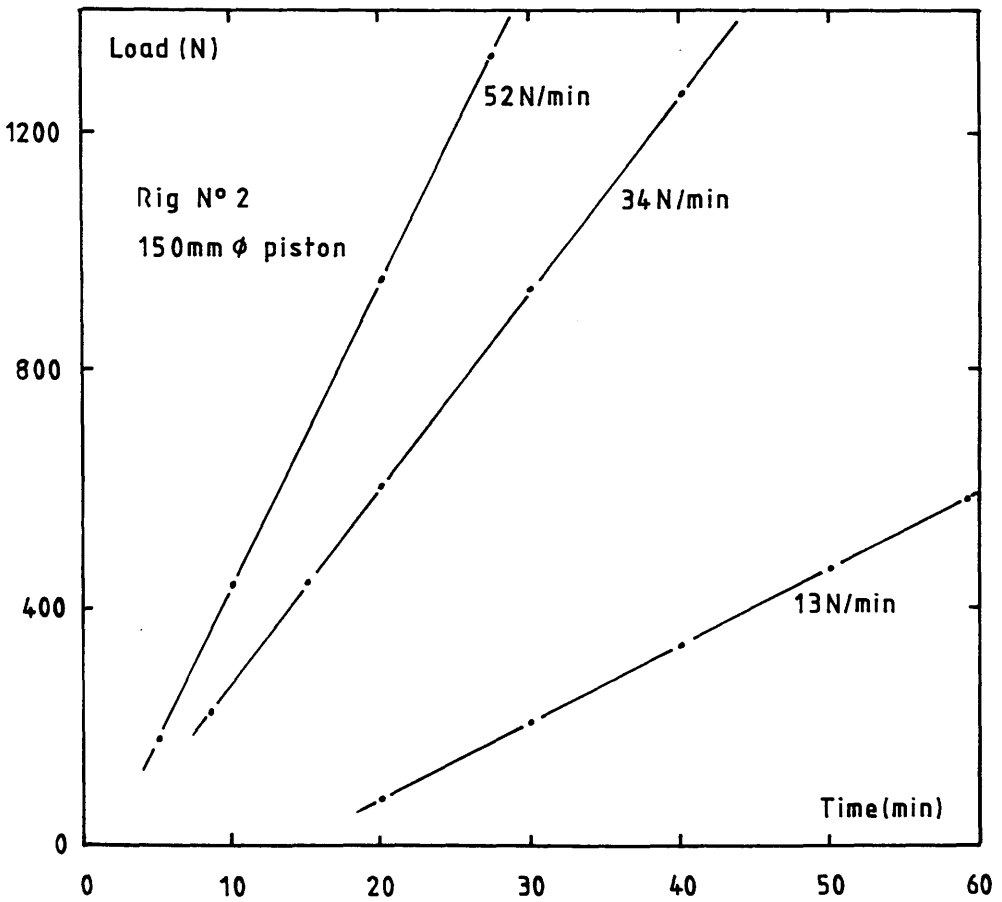

FIGURE 3.18 - Static Tests: Typical loading rate calibration curves.

FIGURE 3.19 - Photograph showing anchor and guide before deposition of overburden.

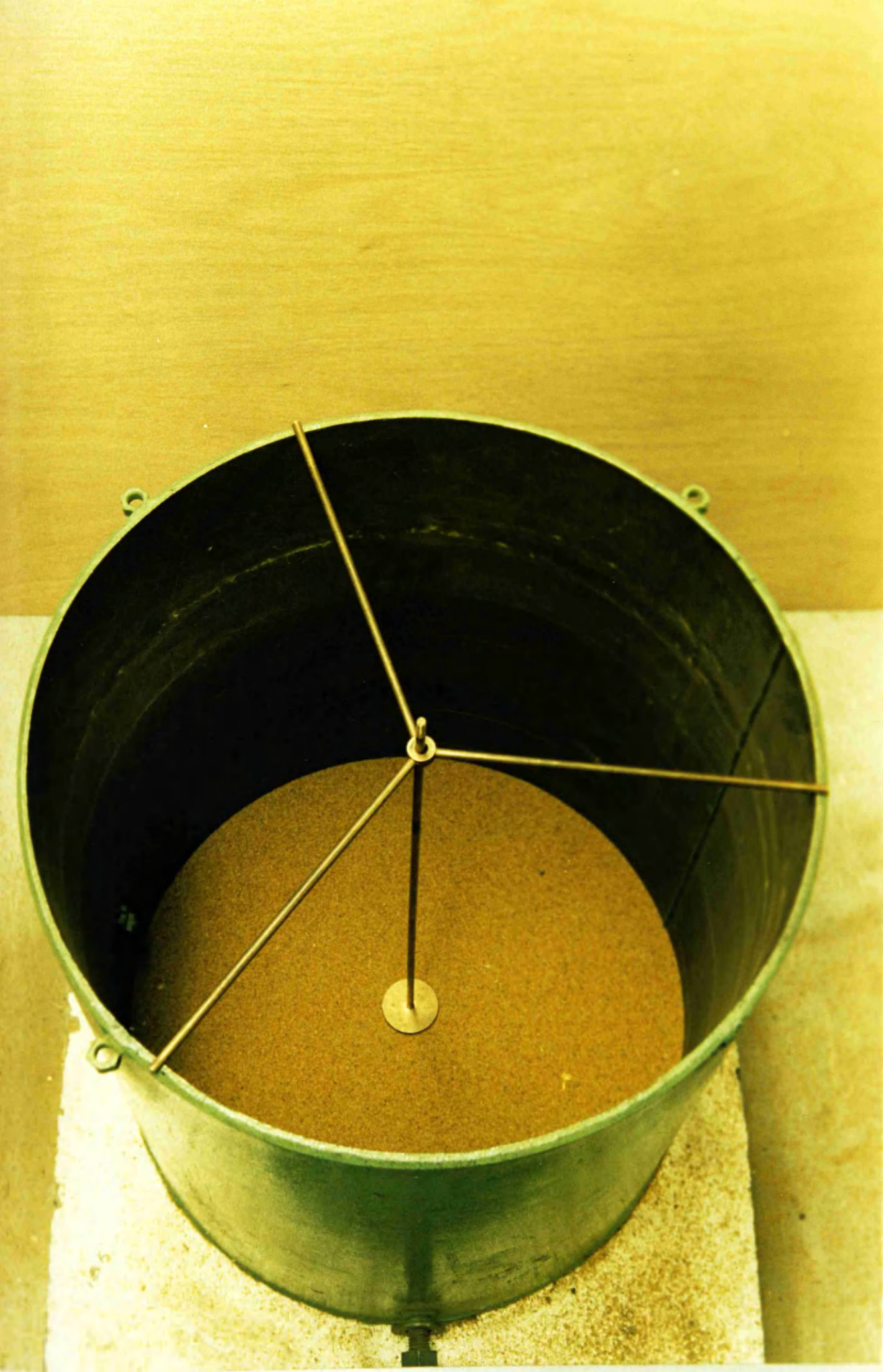

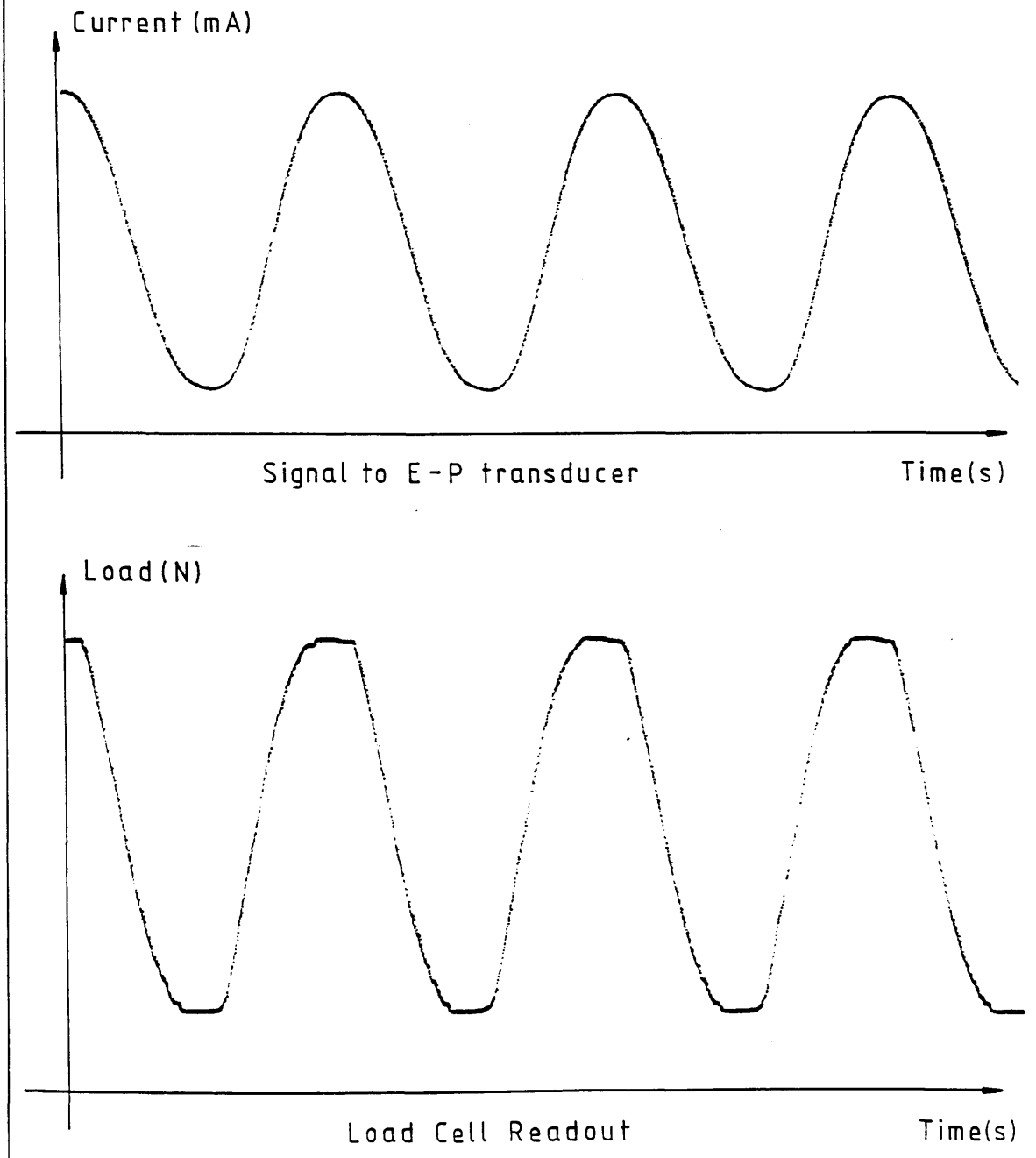

FIGURE 3.20 - Cyclic Tests: Comparison between input signal and load response.

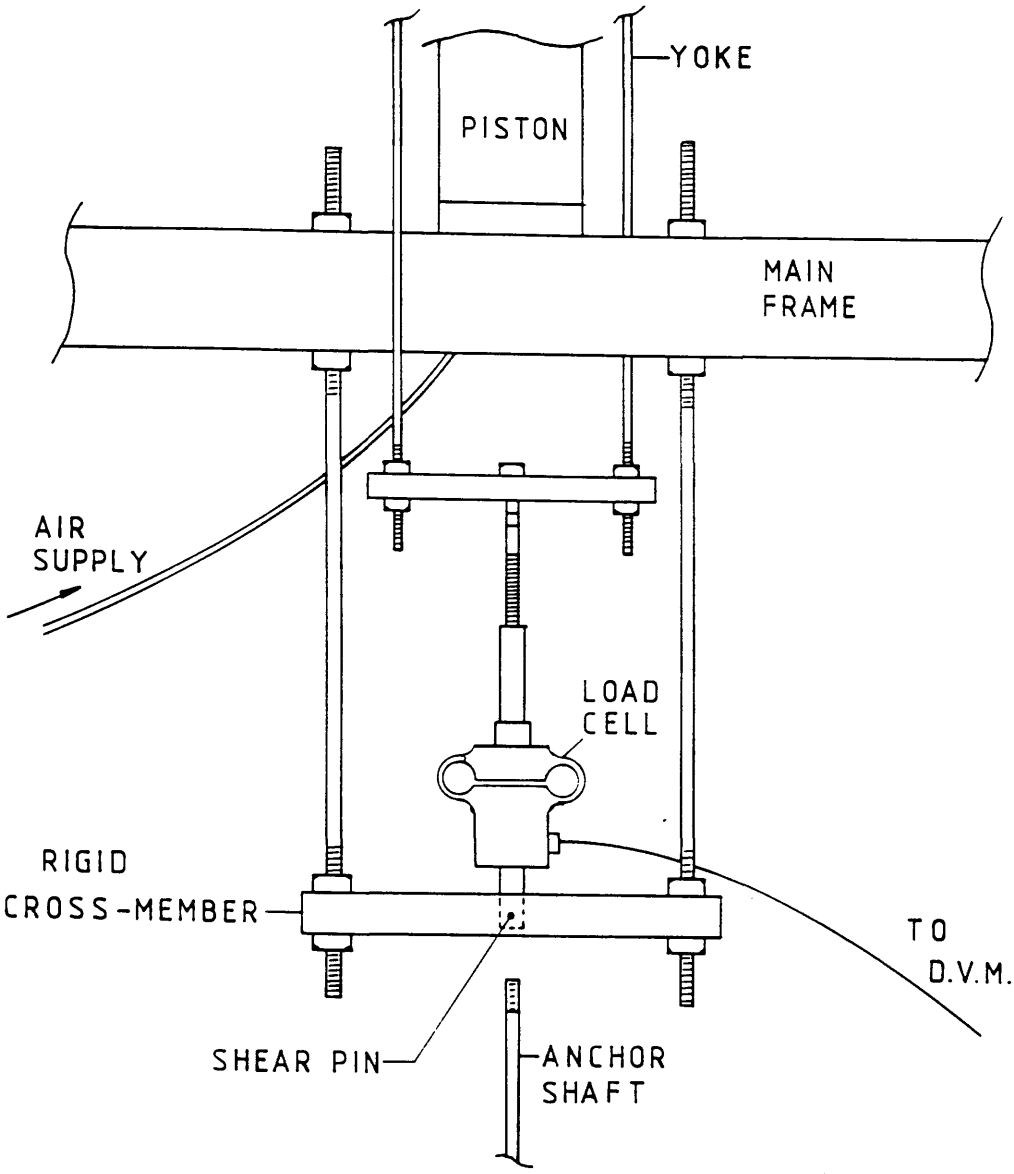

FIGURE 3.21 - Cyclic Tests: Arrangement for pre-setting cyclic load levels.

4.1 INTRODUCTION

The results of the static and cyclic tests are presented in this chapter. Brief comments on the results are made at this stage, but the detailed discussion is presented in Chapter 6.

The static test results are straightforward, and are presented in terms of the two dimensionless parameters N_u and D/B, the anchor uplift resistance factor and the anchor embedment ratio, respectively. Load–displacement graphs for all the static tests are contained in Appendix III.

The cyclic test results refer to anchors loaded in the form (M±A), where M is the mean load and A is the load amplitude, both expressed as a percentage of the static failure load (sfl). Thus, for example, a loading of (20±20) has a mean load of 20%sfl and a load amplitude of 20%sfl, giving an overall variation of load from zero to 40%sfl. The results are presented in a number of different graphical forms in order to illustrate particular aspects of the anchor behaviour. For ease of comparison, the scales used in sets of the same graph have been standardised. The parameters used in the graphs are defined in section 4.3.

Note that, in most of the cyclic tests, the total anchor displacements were very small (< 2mm). Consequently, there was no need to consider adjusting the load levels during a test to take account of the very small, gradual change in embedment ratio.

4.2 STATIC TEST RESULTS

The results of eighteen static pullout tests undertaken in dense Leighton–Buzzard sand are shown in Table 4.1. The results are presented graphically in Figure 4.1, with D/B and N_u as abscisse and ordinate, respectively. Average values of N_u from Table 4.1 are plotted for embedment ratios 2.0, 3.0,. 4.5 and 6.0.

Results for thirteen static pullout tests in medium–dense Leighton–Buzzard sand are shown in Table 4.2 and Figure 4.2. Results for D/B ⩽8.0 are shown in Figure 4.3 for dense and medium–dense sand.

The results confirm the expected rapid increase in uplift factor with embedment ratio. The effect of relative density is clearly illustrated in Figure 4.3, with the difference in N_u increasing with embedment ratio. Boundary and scale effects associated with these results are discussed in Chapter 6.

Typical load–displacement curves for dense and medium–dense sand are shown in Figure 4.4, for an anchor embedment ratio of six. In both cases, the relationship remains linear for a large proportion of the load, but the displacement increases rapidly as failure approaches. The slope of the linear portion of the curves is indicative of the relative stiffness of the sand. The load–displacement curves are somewhat similar to the stress/strain curves obtained from the triaxial tests on dense and medium–dense sand. (See Appendix I).

4.3 CYCLIC TEST RESULTS

Large amounts of data were collected during the cyclic test series, and these have been condensed into the form shown in Tables 4.3 and 4.4, which present the results of the cyclic tests carried out in dense and medium–dense Leighton Buzzard sand, respectively. All the anchors were 50mm in diameter and 6mm thick, buried to a depth of 225mm (D/B= 4.5). The results for tests in dense sand are presented first.

Figure 4.5 presents the results for the repeated loading tests CD1 to CD5, in which the relative cyclic displacement, Δ_c/B, is plotted against the number of cycles, N, on a logarithmic scale. The relative cyclic displacement is simply the cyclic displacement of the anchor, Δ_c, divided by the anchor diameter, B. The results show that, for the loadings applied, the cyclic displacement continues to increase throughout each test. However, the rate of increase is dependent on the applied loading : in test CD5 (45±45), the anchor failed very quickly (< 600 cycles), whereas in test CD1 (20±20), the anchor displacement after 835,000 cycles was only 0.49mm. The results for tests CD2, CD3 and CD4 are bunched together relatively closely, but maintain the relationship of increasing cyclic displacement with load, for any value of N.

Plotting the number of cycles (N) on a logarithmic scale results in visually misleading curves for the tests, as it appears that the cyclic displacement rate is increasing as the tests progress. By plotting the results to a linear scale for N, as shown in Figure 4.6, it is clear that the rate of displacement is reducing, approaching a constant value after approximately 250,000 cycles in tests CD1 to CD4.

The relative displacement per cycle, Δ_{pc}/B, is used in Figure 4.7 in an alternative presentation of the results for tests CD1 to CD5. The relative displacement per cycle is found by dividing the relative cyclic displacement, Δ_c/B, by the corresponding value of N. The curves of Figure 4.7 show a mirror image similarity to those plotted in Figure 4.5: both figures have the same values of Δ_c/B on the vertical axis. The effect of the applied loading is again apparent, as is the continuing increase in cyclic displacement, despite the continued decrease in Δ_{pc}/B. This type of plot has been used to identify anchor failure (Andreadis, 1979). When the slope of the curve becomes positive, this indicates that the relative displacement per cycle is increasing, and the anchor is considered to have failed. The criterion is certainly applicable to the results of test CD5.

The repeated loads in tests CD6 and CD7 were increased at intervals as the tests progressed. Dealing firstly with test CD6, the results are plotted in Figures 4.8 and 4.9, using the parameters defined above and assuming each change in loading to be the start of a "new" test. After 609,000 cycles of (20±20) loading, $\Delta_c/B = 0.0082$; after a further 919,000 cycles of (30±30) loading, $\Delta_c/B = 0.0343$. The anchor failed after a further 510,000 cycles of (35±35) loading. Imminent failure was indicated by the change to a positive slope shown in Figure 4.9 for the final loading stage (After Andreadis, 1979).

The results for test CD7 are presented in Figures 4.10 and 4.11 in a similar manner to the results of test CD6. The change from (30±30) loading to (40±40) loading took place after 795,000 cycles ($\Delta_c/B = 0.0296$). The anchor failed after a further 550,000 cycles, and the failure was again characterised by a positive slope in the graph of Δ_c/B versus Δ_{pc}/B. (See Figure 4.11, (40±40) loading).

Tests CD1 and CD2 had the same loading as the initial stages of tests CD6 and CD7 ((20±20) and (30±30), respectively), and when plotted on the same graph (Figure 4.12), the corresponding curves are in good agreement. The significance of the results from tests CD6 and CD7 will be discussed more fully in Chapter 6.

The results of the sustained–repeated tests, CD8 (40±20) and CD9 (60±20) are plotted in Figures 4.13 and 4.14. Despite the change in mean load, the results are very similar, and compare well with the results of other tests carried out using a load amplitude of ± 20%sfl (Tests CD1 and CD6 (first stage), see Figure 4.12). Taken together with the results of test CD2 (30±30) and test

CD4 (40±40), it is clear that the cyclic displacement of the anchor is dependent on the load amplitude rather than the maximum cyclic load applied to the anchor.

Figure 4.15 shows the variation in the anchor movement per cycle, m_c, throughout tests CD1 to CD5. The parameter m_c is defined as the amount of anchor movement in a half–cycle of loading, from minimum load to maximum load, or vice versa. It should not be confused with the parameter Δ_{pc}, the anchor displacement per cycle, i.e. the anchor displacement, Δ_c, divided by the number of cycles, N.

The results presented in Figure 4.15 show that the value of m_c is fairly consistent for any particular test, and the magnitude is generally dependent on the load level applied to the anchor. Values of m_c for tests CD2 (30±30), CD3 (35±35) and CD4 (40±40) are, however, similar, being in the range 0.20mm to 0.24mm.

The variation in m_c during tests CD6 and CD7 is shown in Figures 4.16 and 4.17, respectively. The results are again drawn assuming each change in loading to be the start of a "new" test. The variation in m_c throughout any particular loading period is small, and the first stage m_c plots for tests CD6 and CD7 compare well with those of tests CD1 (20±20) and CD2 (30±30), respectively. (See Figure 4.15).

In test CD6, the m_c values for the second and third stage loadings are slightly less than the "first time" tests at corresponding load levels (i.e. tests CD2 (30±30) and CD3 (35±35), see Figure 4.15). On the other hand, the second stage loading of test CD7 has m_c values which are slightly higher than the "first time" test at the same load level (i.e. test CD4 (40±40), see Figure 4.15).

Results for the sustained–repeated tests CD8 (40±20) and CD9 (60±20) are shown in Figure 4.18. The range of m_c for both these tests is small, and very similar to that obtained in tests CD1 (20±20) and CD6 (first stage). (See Figures 4.15 and 4.16, respectively). This again suggests that the load amplitude rather than the maximum cyclic load is the controlling parameter, this time with respect to anchor movement per cycle, m_c.

Medium–dense sand results for tests CM1 to CM4 are presented in Figures 4.19 to 4.24, using the parameters previously defined for the dense sand tests.

The results are similar in form to those presented for dense sand, but the cyclic displacement in corresponding tests is greater in the medium–dense sand. The effect of load amplitude is again apparent.

Finally, in order to assess any creep effect that may have taken place during the sustained–repeated tests, creep tests were carried out on anchors in dense and medium–dense sand for 14 days. The deadweight load was applied via two pulleys attached to the loading frame, and two dial gauges resting on a horizontal plate attached to the top of the anchor shaft measured any movement. The load levels applied were 40% sfl and 60% sfl in the dense sand and 40% sfl in the medium–dense sand. As shown in Figure 4.25, no discernible trend of creep movement was noted for either sand density.

Before moving on to a discussion of the results of this and previous experimental investigations, Chapter 5 describes a finite element analysis undertaken by the author on the anchor uplift problem. Results from the analysis are compared with those of the static tests presented in this chapter.

TABLE 4.1 - Results of Static Pullout Tests in Dense Leighton-Buzzard Sand
(ρ = 1752 kg/m^3 , D_r = 93.0%)

TEST No.[1]	D (mm)	B (mm)	D/B	Pu^2 (N)	Nu^3 ($=pu/\gamma D$)
SD 1	150	75.0	2.0	96.4	8.5
SD 2	150	75.0	2.0	92.0	8.1
SD 3	200	100.0	2.0	215.3	8.0
SD 4	200	100.0	2.0	214.4	7.9
SD 5	225	75.0	3.0	245.6	14.4
SD 6	225	75.0	3.0	241.7	14.1
SD 7	225	50.0	4.5	230.8	30.4
SD 8	225	50.0	4.5	226.4	29.8
SD 9	300	50.0	6.0	520.0	51.4
SD 10	300	50.0	6.0	511.1	50.5
SD 11	400	50.0	8.0	1125.0	83.4
SD 12	300	37.5	8.0	503.8	88.5
SD 13	375	37.5	10.0	1227.0	172.4
SD 14	375	37.5	10.0	1278.0	179.6
SD 15	450	37.5	12.0	1786.0	209.2
SD 16	300	25.0	12.0	495.2	195.7
SD 17	375	25.0	15.0	918.7	290.4
SD 18	300	SHAFT ONLY		3.7	-

1. SD = Static Dense.

2. Not including weight of anchor + shaft.

B (mm)	Wt (N)
25.0	4.2
37.5	4.5
50.0	4.9
75.0	5.9
100.0	7.1

3. p_u = Pu/area of anchor.

TABLE 4.2 - Results of Static Pullout Tests in Medium-Dense Leighton-Buzzard Sand (ρ = 1635 kg/m^3 , D_r = 59.4%)

TEST No.[1]	D (mm)	B (mm)	Δ/B	P_u[2] (N)	Nu[3] (= $pu/\gamma D$)
SM 1	200	100.0	2.0	148.6	5.9
SM 2	220	100.0	2.2	177.4	6.4
SM 3	220	75.0	2.9	141.9	9.1
SM 4	225	75.0	3.0	156.2	9.8
SM 5	255	75.0	3.4	207.8	11.5
SM 6	210	50.0	4.2	113.1	17.1
SM 7	225	50.0	4.5	132.5	18.7
SM 8	305	50.0	6.1	352.5	36.7
SM 9	315	50.0	6.3	390.0	39.3
SM 10	295	37.5	7.9	300.5	57.5
SM 11	290	37.5	7.7	286.7	55.8
SM 12	380	37.5	10.1	525.7	78.1
SM 13	390	37.5	10.4	562.4	81.4

1. SM = Static Medium - dense.

2,3. See Footnotes to Table 4.1.

TABLE 4.3 - Results of Cyclic Loading Tests in Dense Leighton-Buzzard Sand.
(ρ = 1752 kg/m^3, D_r = 93.0%, B = 50 mm, D/B = 4.5)

(a) TEST CD 1[1] Repeated loading: (20 ± 20)

N[2]	Δc[3] (mm)	$\Delta c/B$[4]	$\Delta pc/B$[5]	m_c[6] (mm)
10	0.909	0.0018	1.8×10^{-4}	0.104
100	0.146	0.0029	2.9×10^{-5}	0.104
1000	0.206	0.0041	4.1×10^{-6}	0.108
3000	0.220	0.0044	1.5×10^{-6}	0.106
12000	0.260	0.0052	4.3×10^{-7}	0.106
48000	0.286	0.0057	1.2×10^{-7}	0.110
110000	0.324	0.0065	5.9×10^{-8}	0.108
340000	0.396	0.0079	2.3×10^{-8}	0.112
670000	0.466	0.0093	1.4×10^{-8}	0.108
835000	0.492	0.0098	1.2×10^{-8}	0.110

1. CD = Cyclic Dense.

2. N = Number of cycles: after 10,000 cycles, N has been rounded to the nearest 1000 cycles.

3. Δc = Anchor cyclic displacement (mm).

4. $\Delta c/B$ = Relative cyclic displacement (B = anchor diameter = 50 mm)

5. $\Delta pc/B$ = Relative cyclic displacement per cycle (= $\Delta c/NB$)

6. m_c = Anchor movement per cycle (mm): from maximum load to minimum load (or vice versa).

(b) TEST CD 2 Repeated loading: (30 ± 30)

N	Δc (mm)	$\Delta c/B$	$\Delta pc/B$	m_c (mm)
10	0.126	0.0025	2.5×10^{-4}	0.212
100	0.212	0.0042	4.2×10^{-5}	0.212
1000	0.290	0.0058	5.8×10^{-6}	0.210
4800	0.394	0.0079	1.6×10^{-6}	0.208
14000	0.544	0.0109	7.8×10^{-7}	0.212
40000	0.684	0.0137	3.4×10^{-7}	0.210
138000	0.924	0.0185	1.3×10^{-7}	0.206
250000	1.058	0.0212	8.5×10^{-8}	0.204
430000	1.210	0.0242	5.6×10^{-8}	0.208
808000	1.420	0.0284	3.5×10^{-8}	0.210

(c) TEST CD 3 Repeated loading: (35 ± 35)

N	Δc (mm)	$\Delta c/B$	$\Delta pc/B$	m_c (mm)
10	0.184	0.0037	3.7×10^{-4}	0.230
50	0.264	0.0053	1.1×10^{-4}	0.218
100	0.324	0.0065	6.5×10^{-5}	0.220
860	0.420	0.0084	9.8×10^{-6}	0.202
3300	0.532	0.0106	3.2×10^{-6}	0.238
6500	0.604	0.0121	1.9×10^{-6}	0.218
17000	0.716	0.0143	8.4×10^{-7}	0.216
76000	0.954	0.0191	2.5×10^{-7}	0.200
210000	1.224	0.0245	1.2×10^{-7}	0.210
343000	1.424	0.0285	8.3×10^{-8}	0.210
595000	1.664	0.0333	5.6×10^{-8}	0.206
666000	1.724	0.0345	5.2×10^{-8}	0.210
780000	1.804	0.0361	4.6×10^{-8}	0.210

(d) TEST CD 4 Repeated loading: (40 ± 40)

N	Δc (mm)	$\Delta c/B$	$\Delta pc/B$	m_c (mm)
10	0.260	0.0052	5.2×10^{-4}	0.220
100	0.380	0.0076	7.6×10^{-5}	0.200
1460	0.500	0.0100	6.8×10^{-6}	0.220
8400	0.650	0.0130	1.5×10^{-6}	0.210
13000	0.716	0.0143	1.1×10^{-6}	0.200
17000	0.780	0.0156	9.1×10^{-7}	0.202
43000	0.960	0.0192	4.5×10^{-7}	0.206
103000	1.156	0.0231	2.2×10^{-7}	0.210
227000	1.440	0.0288	1.3×10^{-7}	0.214
375000	1.640	0.0328	8.7×10^{-8}	0.220
436000	1.720	0.0344	7.9×10^{-8}	0.230
592000	1.860	0.0372	6.3×10^{-8}	0.230

(e) TEST CD 5 Repeated loading: (45 ± 45)

N	Δc (mm)	$\Delta c/B$	$\Delta pc/B$	m_c (mm)
10	0.380	0.0076	7.6×10^{-4}	0.420
50	1.240	0.0248	5.0×10^{-4}	0.400
100	1.860	0.0372	3.7×10^{-4}	0.400
200	2.942	0.0588	2.9×10^{-4}	0.410
555	13.220	0.2644	4.8×10^{-4}	0.420
<600	ANCHOR FAILED		-	-

(f) TEST CD 6 Repeated loading: (20 ± 20); (30 ± 30); (35 ± 35)

N	Δc (mm)	$\Delta c/B$	$\Delta pc/B$	m_c (mm)
10	0.048	0.0010	1.0×10^{-4}	0.102
100	0.098	0.0020	2.0×10^{-5}	0.110
725	0.150	0.0030	4.1×10^{-6}	0.112
6500	0.216	0.0043	6.6×10^{-7}	0.106
68000	0.256	0.0051	7.6×10^{-8}	0.106
130000	0.288	0.0058	4.4×10^{-8}	0.094
214000	0.326	0.0065	3.0×10^{-8}	0.106
609000	0.410	0.0082	1.3×10^{-8}	0.110
	Repeated loading increased to (30 ± 30)			
35	0.006	0.0001	3.4×10^{-6}	0.170
740	0.026	0.0005	7.0×10^{-7}	0.162
2140	0.046	0.0009	4.3×10^{-7}	0.160
62000	0.254	0.0051	8.2×10^{-8}	0.164
118000	0.386	0.0077	6.5×10^{-8}	0.170
295000	0.618	0.0124	4.2×10^{-8}	0.148
430000	0.800	0.0160	3.7×10^{-8}	0.140
742000	1.120	0.0224	3.0×10^{-8}	0.146
801000	1.218	0.0244	3.0×10^{-8}	0.136
860000	1.258	0.0252	2.9×10^{-8}	0.130
919000	1.306	0.0261	2.8×10^{-8}	0.134
	Repeated loading increased to (35 ± 35)			
100	0.020	0.0004	4.0×10^{-6}	0.168
1200	0.120	0.0024	2.0×10^{-6}	0.168
27000	0.272	0.0054	2.1×10^{-7}	0.154
88000	0.418	0.0084	9.6×10^{-8}	0.152
149000	0.568	0.0114	7.6×10^{-8}	0.156
210000	0.702	0.0140	4.7×10^{-8}	0.156
271000	0.828	0.0166	6.1×10^{-8}	0.150
332000	0.928	0.0186	5.6×10^{-8}	0.162
393000	1.124	0.0225	5.7×10^{-8}	0.154
454000	1.296	0.0259	5.7×10^{-8}	0.172
488000	1.878	0.0376	7.7×10^{-8}	0.152
<510000	ANCHOR FAILED		-	-

(g) TEST CD 7 Repeated loading: (30 ± 30); (40 ± 40)

N	Δc (mm)	$\Delta c/B$	$\Delta pc/B$	m_c (mm)
10	0.168	0.0034	3.4×10^{-4}	0.212
100	0.220	0.0044	4.4×10^{-5}	0.218
1000	0.320	0.0064	6.4×10^{-6}	0.210
2500	0.418	0.0084	3.3×10^{-6}	0.214
10000	0.550	0.0110	1.1×10^{-6}	0.208
56000	0.800	0.0160	2.9×10^{-7}	0.202
111000	0.930	0.0186	1.7×10^{-7}	0.200
233000	1.126	0.0225	9.7×10^{-8}	0.202
342000	1.240	0.0248	7.3×10^{-8}	0.204
542000	1.360	0.0272	5.0×10^{-8}	0.202
795000	1.478	0.0296	3.7×10^{-8}	0.206
		Repeated loading increased to (40 ± 40)		
30	0.572	0.0014	3.8×10^{-4}	0.320
750	0.658	0.0132	1.8×10^{-5}	0.308
9350	0.726	0.0145	1.6×10^{-6}	0.306
27000	0.998	0.0200	7.3×10^{-7}	0.302
90000	1.392	0.0278	3.1×10^{-7}	0.320
153000	1.840	0.0368	2.4×10^{-7}	0.320
216000	2.228	0.0466	2.1×10^{-7}	0.318
279000	2.618	0.0524	1.9×10^{-7}	0.302
342000	3.012	0.0602	1.8×10^{-7}	0.308
405000	3.478	0.0696	1.7×10^{-7}	0.292
468000	3.738	0.0748	1.6×10^{-7}	0.302
504000	3.988	0.0798	1.6×10^{-7}	0.290
< 550000	ANCHOR FAILED		-	-

(h) TEST CD 8 Sustained-repeated loading: (40 ± 20)

N	Δc (mm)	$\Delta c/B$	$\Delta pc/B$	m_c (mm)
10	0.086	0.0017	1.7×10^{-4}	0.102
100	0.120	0.0024	2.4×10^{-5}	0.098
2300	0.172	0.0034	1.5×10^{-6}	0.100
17000	0.196	0.0039	2.3×10^{-7}	0.100
90000	0.278	0.0056	6.2×10^{-8}	0.104
250000	0.376	0.0075	3.0×10^{-8}	0.098
510000	0.462	0.0092	1.8×10^{-8}	0.098

(i) TEST CD 9 Sustained-repeated loading: (60 ± 20)

N	Δc (mm)	$\Delta c/B$	$\Delta pc/B$	m_c (mm)
10	0.084	0.0017	1.7×10^{-4}	0.104
100	0.112	0.0022	2.2×10^{-5}	0.104
1000	0.126	0.0025	2.5×10^{-6}	0.106
4000	0.156	0.0031	7.8×10^{-7}	0.108
14000	0.172	0.0034	2.4×10^{-7}	0.106
56000	0.202	0.0040	7.1×10^{-8}	0.110
170000	0.270	0.0054	3.2×10^{-8}	0.102
540000	0.386	0.0077	1.4×10^{-8}	0.104

TABLE 4.4 - Results of Cyclic Loading Tests in Medium-Dense Leighton Buzzard Sand (ρ = 1635 kg/m^3, D_r = 59.4%, B = 50 mm, D/B = 4.5)

(a) TEST CM 1[1] Repeated loading: (20 ± 20)

N[2]	Δc[3] (mm)	$\Delta c/B$[4]	$\Delta pc/B$[5]	m_c[6] (mm)
10	0.076	0.0015	1.5×10^{-4}	0.182
100	0.152	0.0030	3.0×10^{-5}	0.170
1000	0.242	0.0048	4.8×10^{-6}	0.152
4500	0.298	0.0060	1.3×10^{-6}	0.148
45000	0.524	0.0105	2.3×10^{-7}	0.152
211000	0.792	0.0158	7.5×10^{-8}	0.156
428000	0.926	0.0185	4.3×10^{-8}	0.152
664000	1.102	0.0220	3.3×10^{-8}	0.146
813000	1.150	0.0230	2.8×10^{-8}	0.148

1. CM = Cyclic Medium - dense.
2-6. See Footnotes to Table 4.3.

(b) TEST CM 2 Repeated loading: (30 ± 30)

N	Δc (mm)	$\Delta c/B$	$\Delta pc/B$	m_c (mm)
10	0.326	0.0065	6.5×10^{-4}	0.352
100	0.552	0.0110	1.1×10^{-4}	0.328
800	0.758	0.0152	1.9×10^{-5}	0.312
3000	0.970	0.0194	6.5×10^{-6}	0.304
15000	1.272	0.0254	1.7×10^{-6}	0.306
46000	1.580	0.0316	6.9×10^{-7}	0.310
85000	1.752	0.0350	4.1×10^{-7}	0.308
230000	2.046	0.0409	1.8×10^{-7}	0.308
354000	2.292	0.0458	1.3×10^{-7}	0.304
637000	2.584	0.0517	8.1×10^{-8}	0.304
875000	2.774	0.0555	6.3×10^{-8}	0.306

(c) TEST CM 3 Repeated loading: (40 ± 40)

N	Δc (mm)	$\Delta c/B$	$\Delta pc/B$	m_c (mm)
10	0.542	0.0108	1.1×10^{-3}	0.496
100	1.410	0.0282	2.8×10^{-4}	0.452
1000	2.398	0.0480	4.8×10^{-5}	0.428
5000	3.326	0.0665	1.3×10^{-5}	0.432
26000	4.622	0.0924	3.5×10^{-6}	0.438
58000	6.630	0.1326	2.3×10^{-6}	0.448
<60000	ANCHOR FAILED		-	-

(d) TEST CM 4 Sustained-repeated loading: (40 ± 20)

N	Δc (mm)	$\Delta c/B$	$\Delta pc/B$	m_c (mm)
10	0.092	0.0018	1.8×10^{-4}	0.172
100	0.170	0.0034	3.4×10^{-5}	0.158
1000	0.268	0.0054	5.4×10^{-6}	0.148
3500	0.336	0.0067	1.9×10^{-6}	0.146
19000	0.482	0.0096	5.1×10^{-7}	0.142
76000	0.650	0.0130	1.7×10^{-7}	0.144
263000	0.878	0.0176	6.7×10^{-8}	0.144
448000	1.034	0.0207	4.4×10^{-8}	0.142
724000	1.162	0.0232	3.2×10^{-8}	0.142

(e) TEST CM 5 Repeated loading: (30 ± 30)

N	Δc (mm)	$\Delta c/B$	$\Delta pc/B$	m_c (mm)
10	0.262	0.0052	5.2×10^{-4}	0.344
100	0.516	0.0103	1.0×10^{-4}	0.320
1000	0.786	0.0157	1.6×10^{-5}	0.308
10000	1.110	0.0222	2.2×10^{-6}	0.304

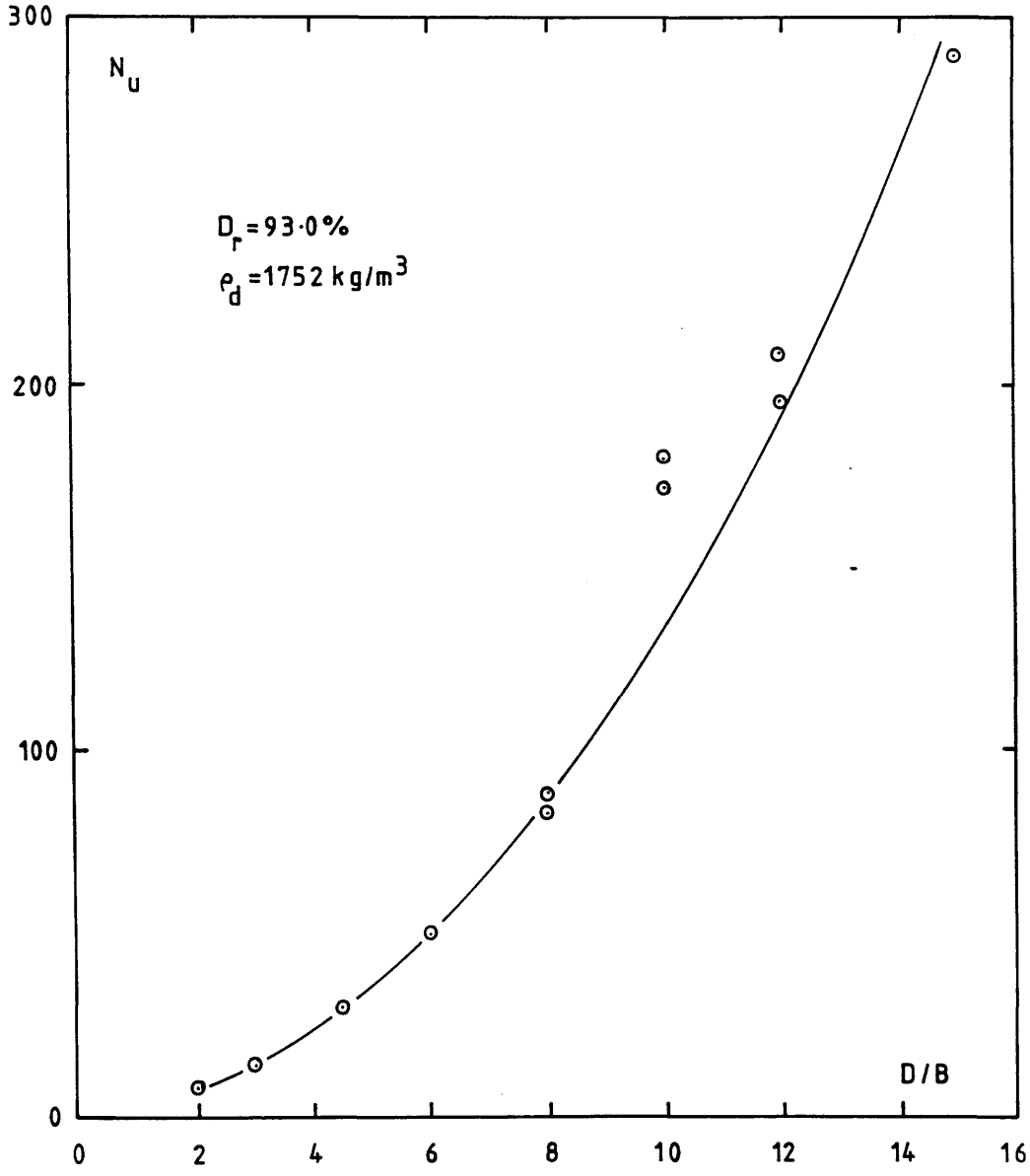

FIGURE 4.1 - Static Test Results : N_u versus D/B for dense sand.

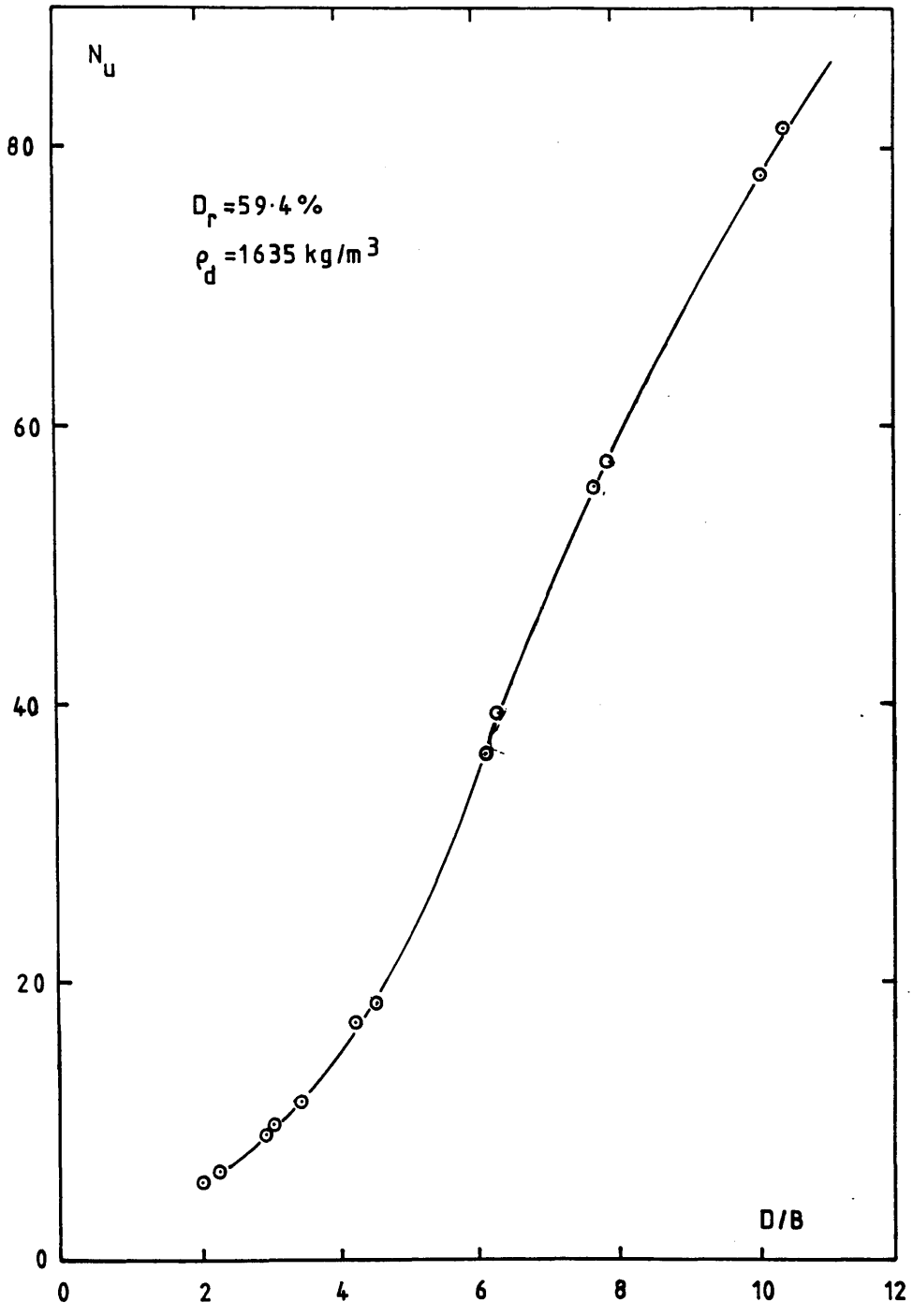

FIGURE 4.2 - Static Test Results: N_u versus D/B for medium-dense sand.

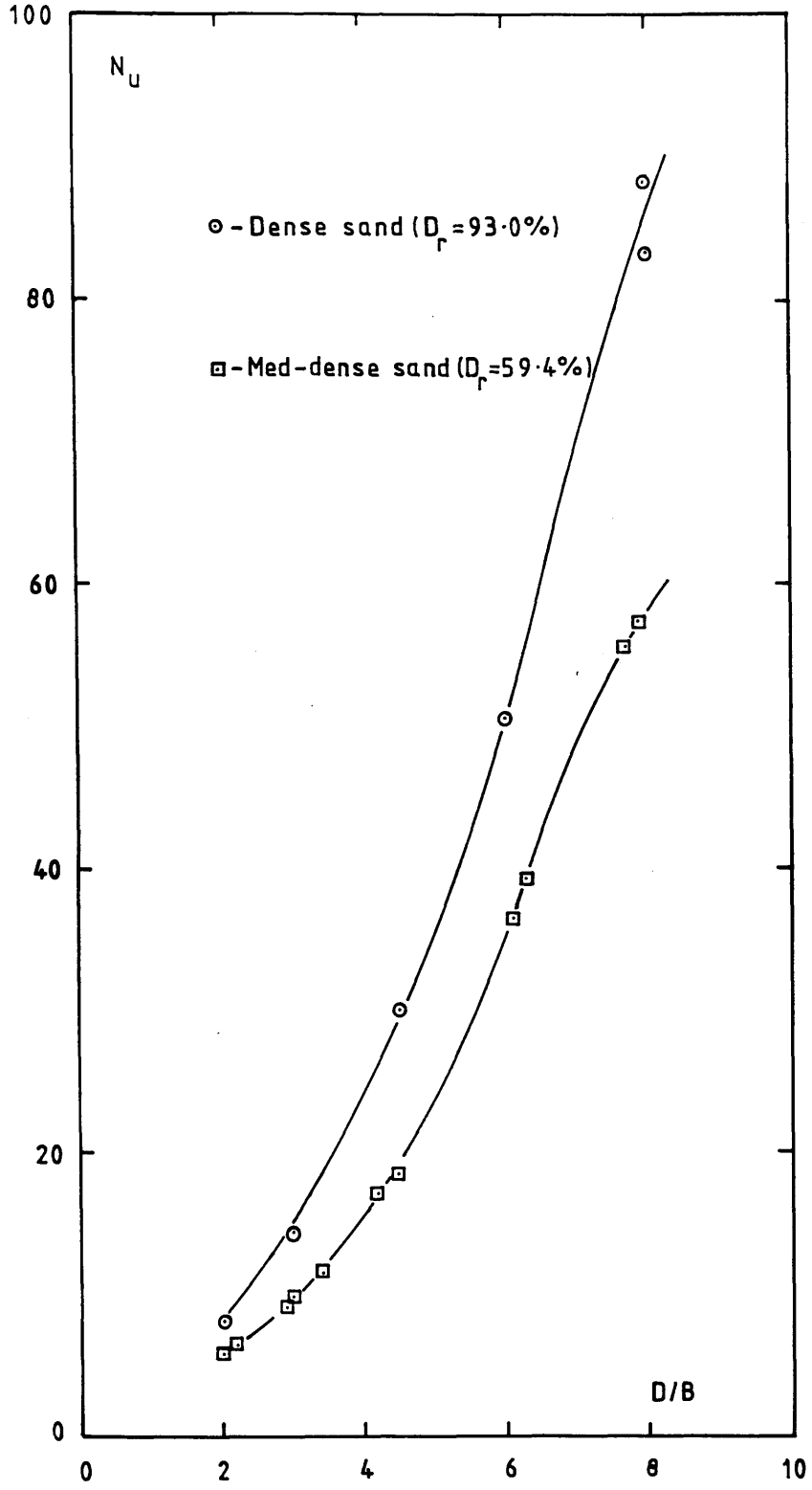

FIGURE 4.3 - Static Test Results: Comparision between dense and medium-dense sand results ($D/B \leqslant 8.0$).

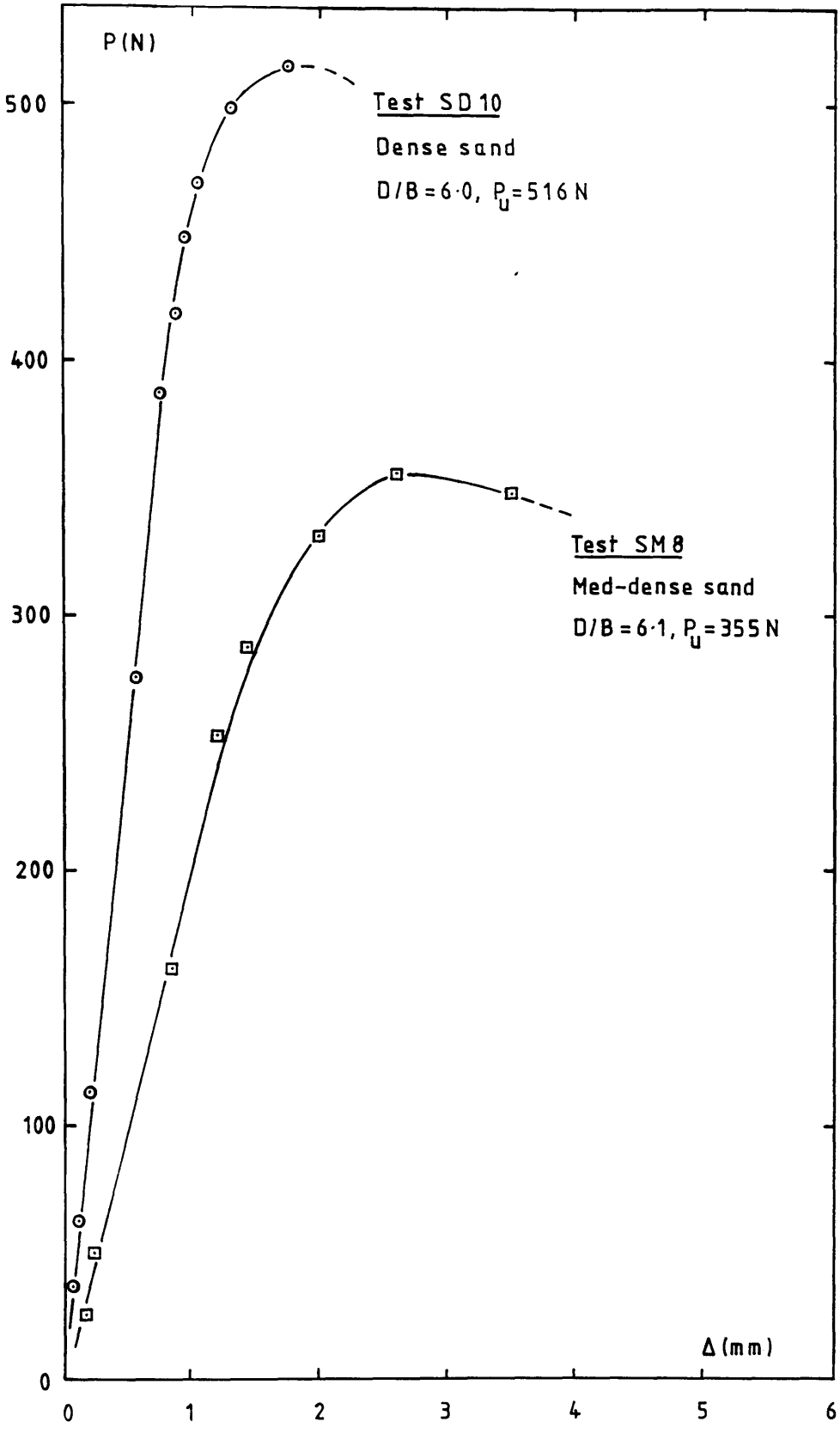

FIGURE 4.4 - Static Test Results: Load (P) versus displacement (Δ) for tests SD10 and SM8.

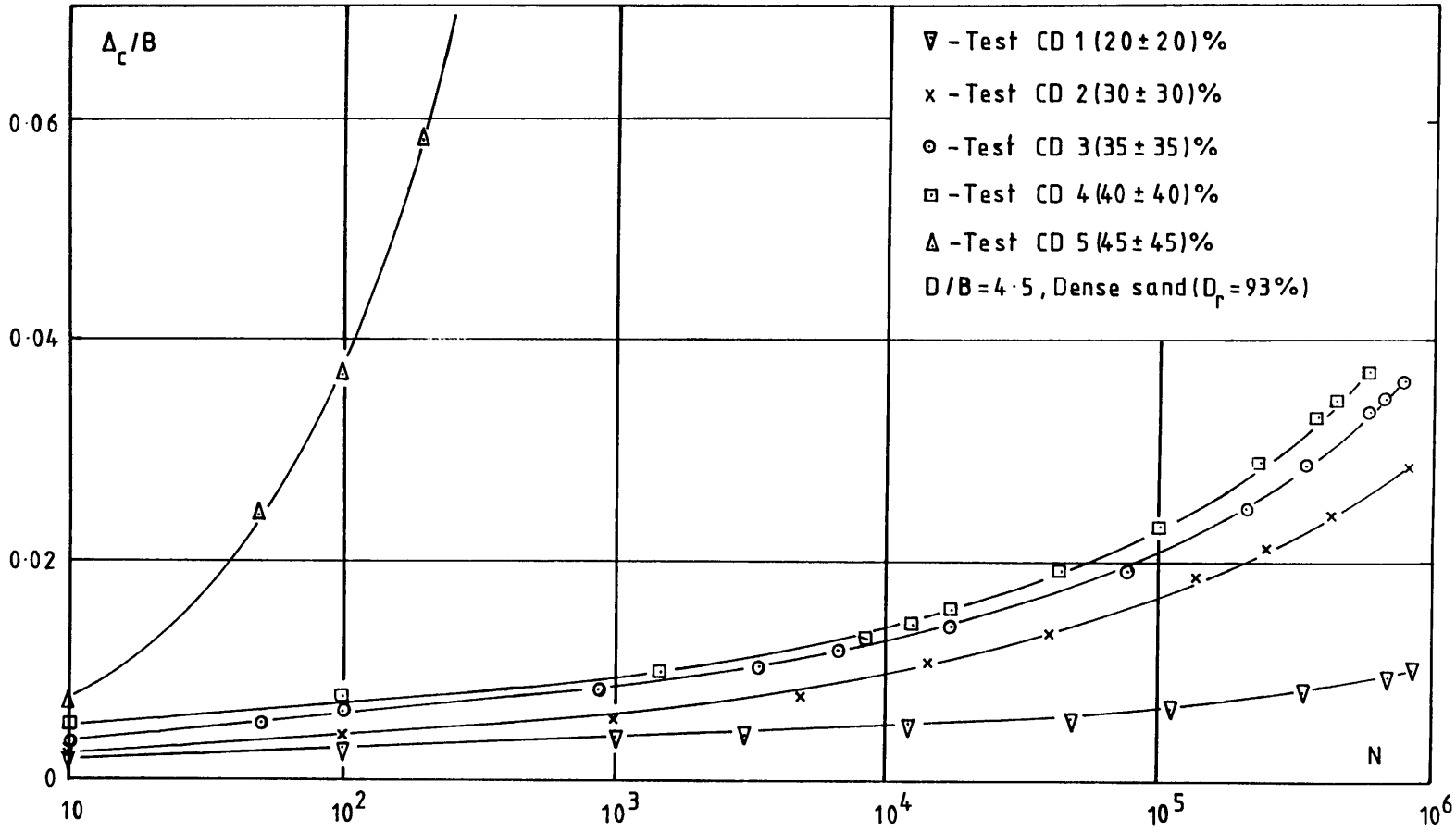

FIGURE 4.5 - Cyclic Test Results: Relative cyclic displacement (Δ_c/B) versus number of cycles (N) for tests CD1 to CD5.

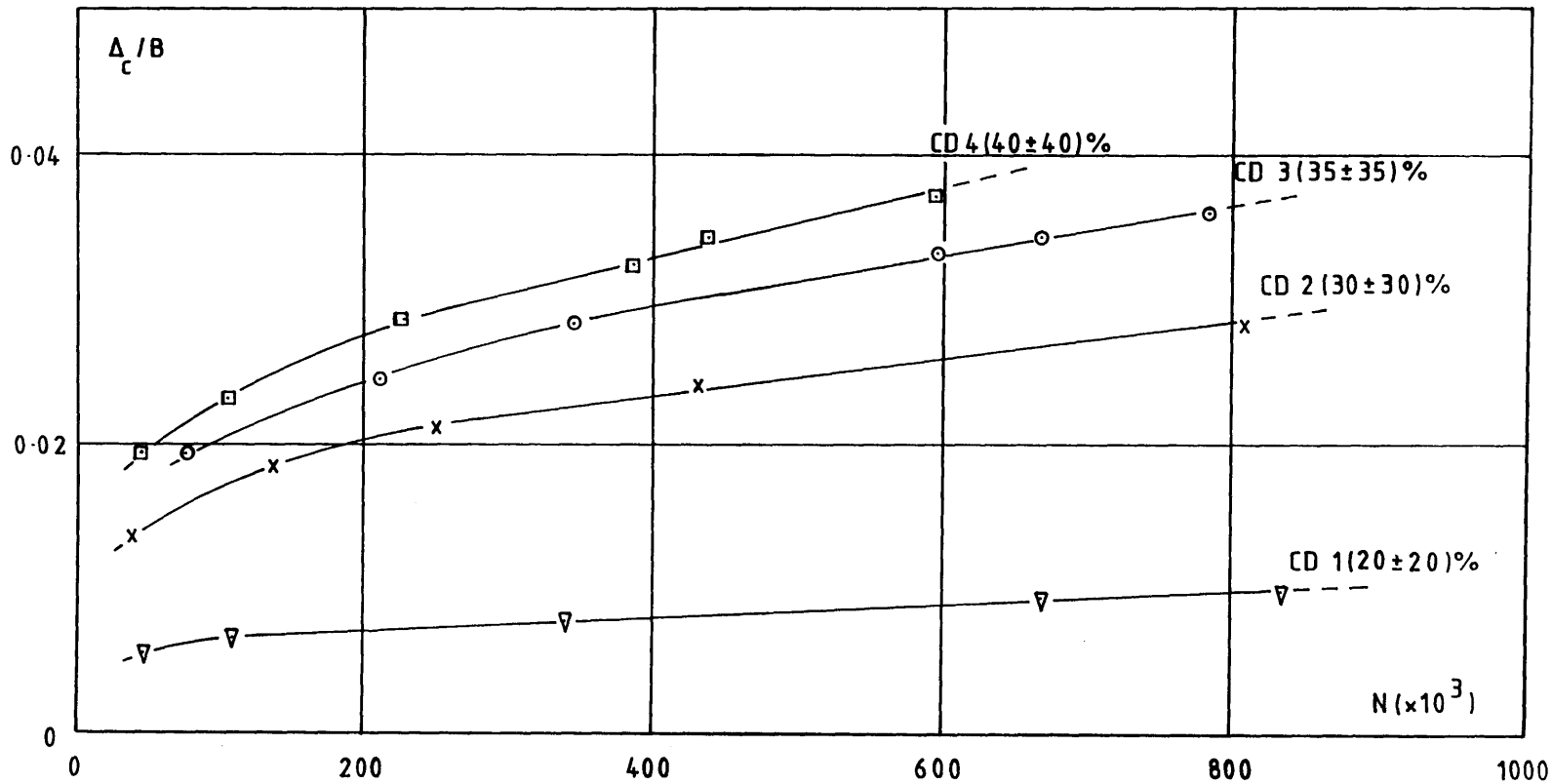

FIGURE 4.6 - Cyclic Test Results: Relative cyclic displacement versus number of cycles (linear scale). Tests CD1 to CD4.

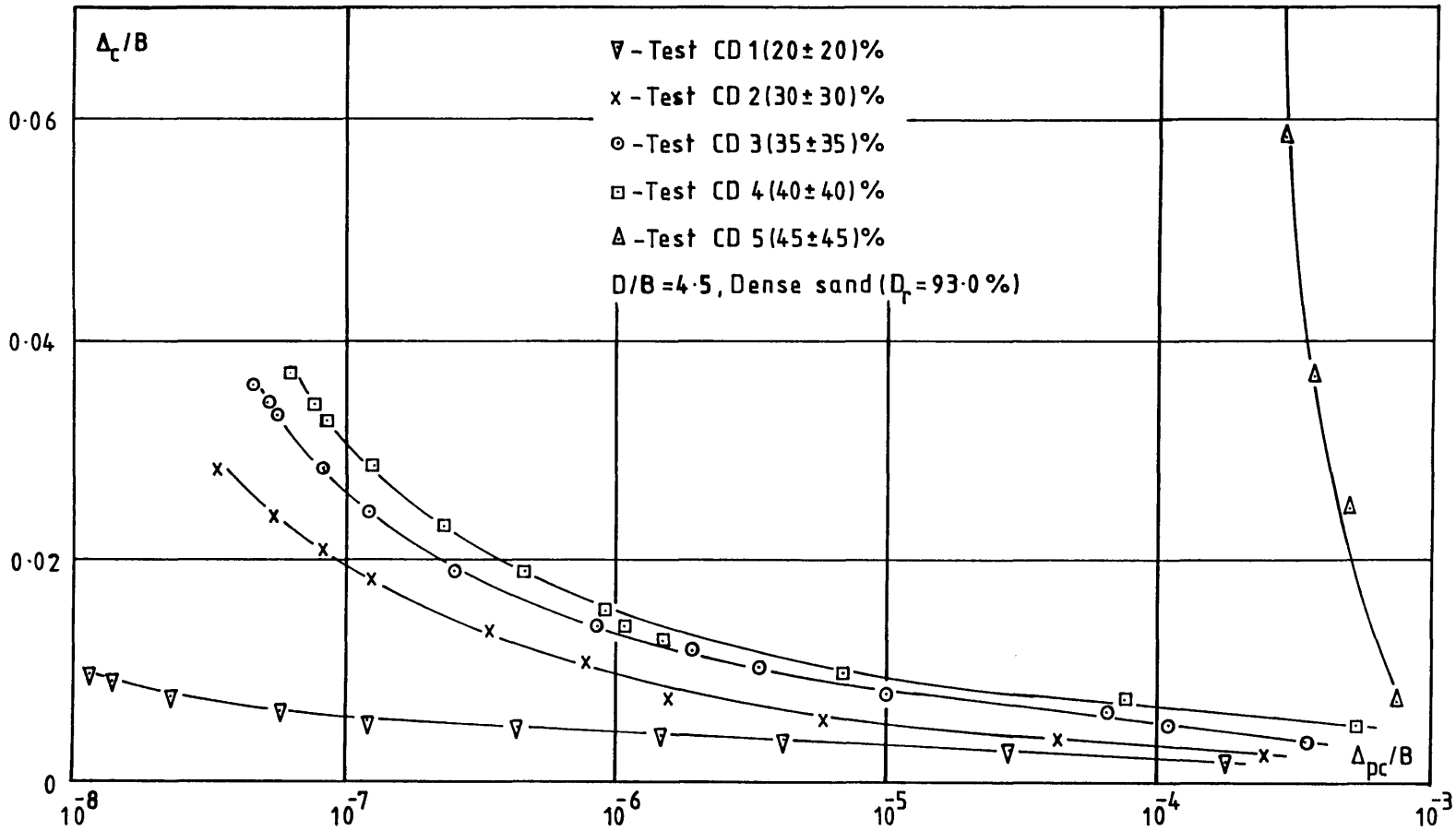

FIGURE 4.7 - Cyclic Test Results: Relative cyclic displacement versus relative displacement per cycle (Δ_{pc}/B) for tests CD1 to CD5.

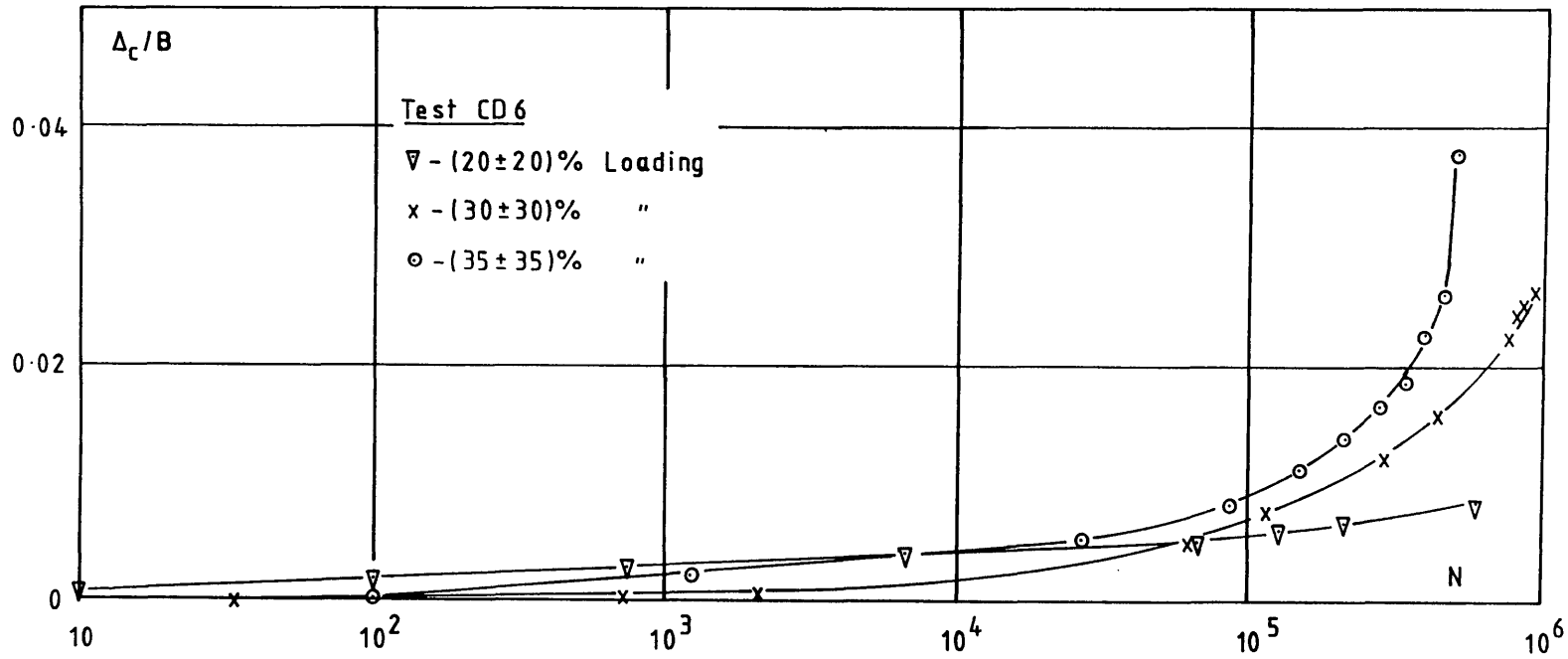

FIGURE 4.8 - Cyclic Test Results : Δ_c/B versus N for test CD6.

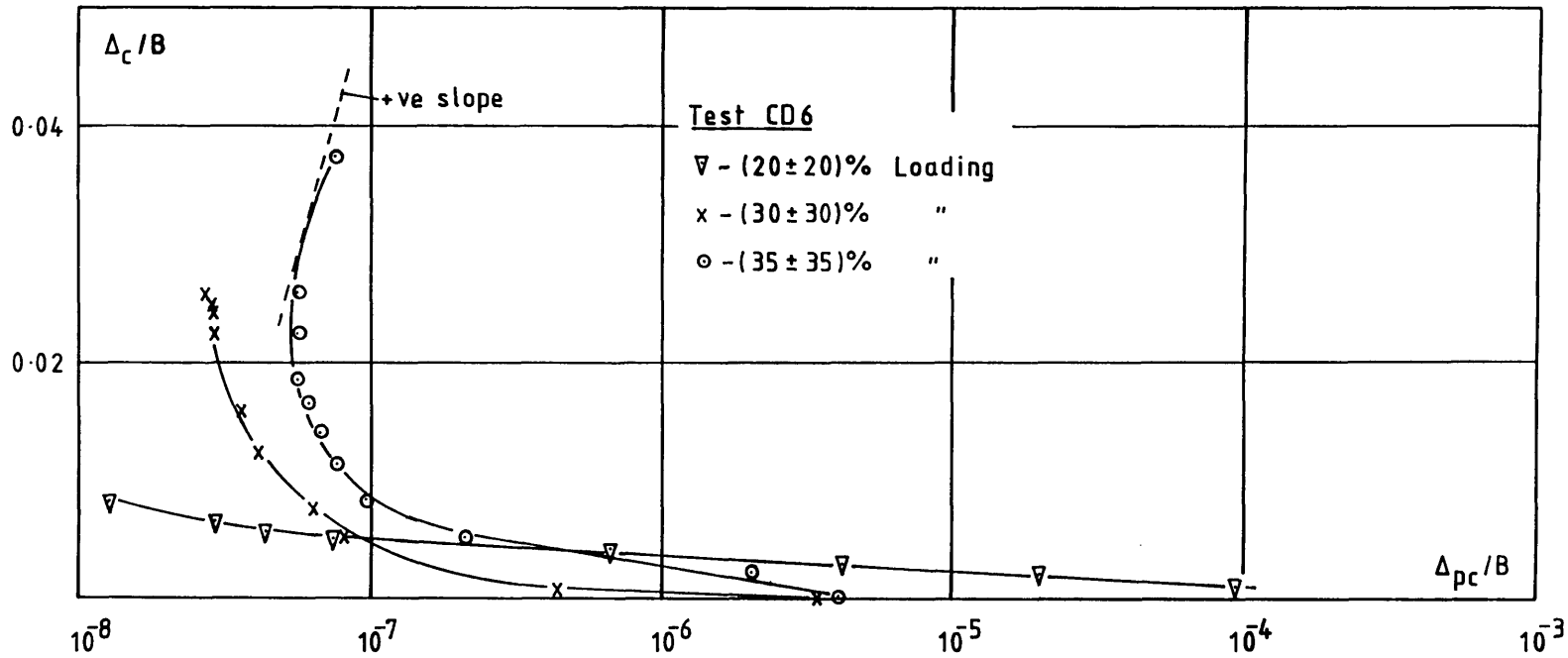

FIGURE 4.9 - Cyclic Test Results : Δ_c/B versus Δ_{pc}/B for test CD6.

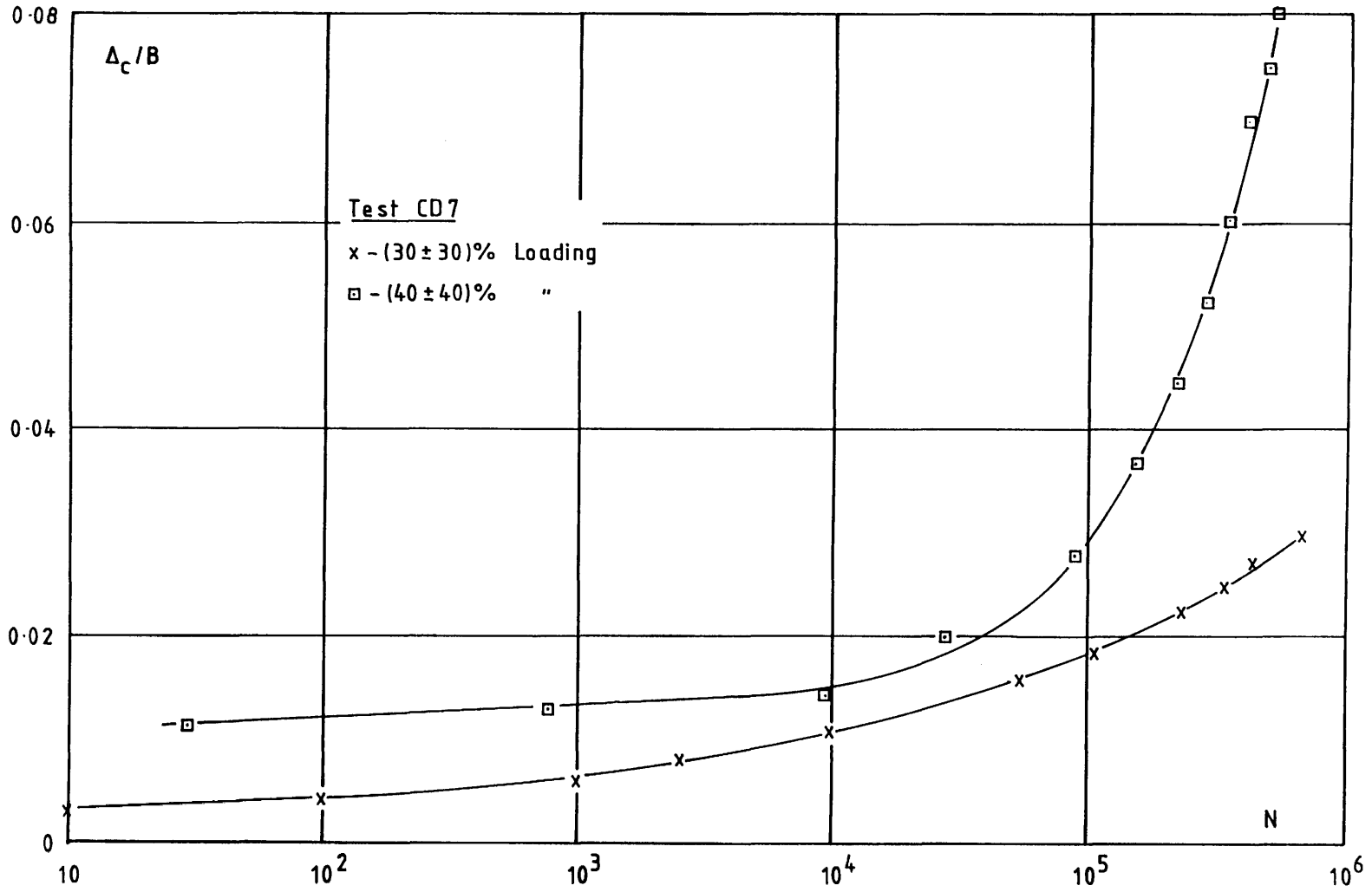

FIGURE 4.10 - Cyclic Test Results : Δ_c/B versus N for test CD7.

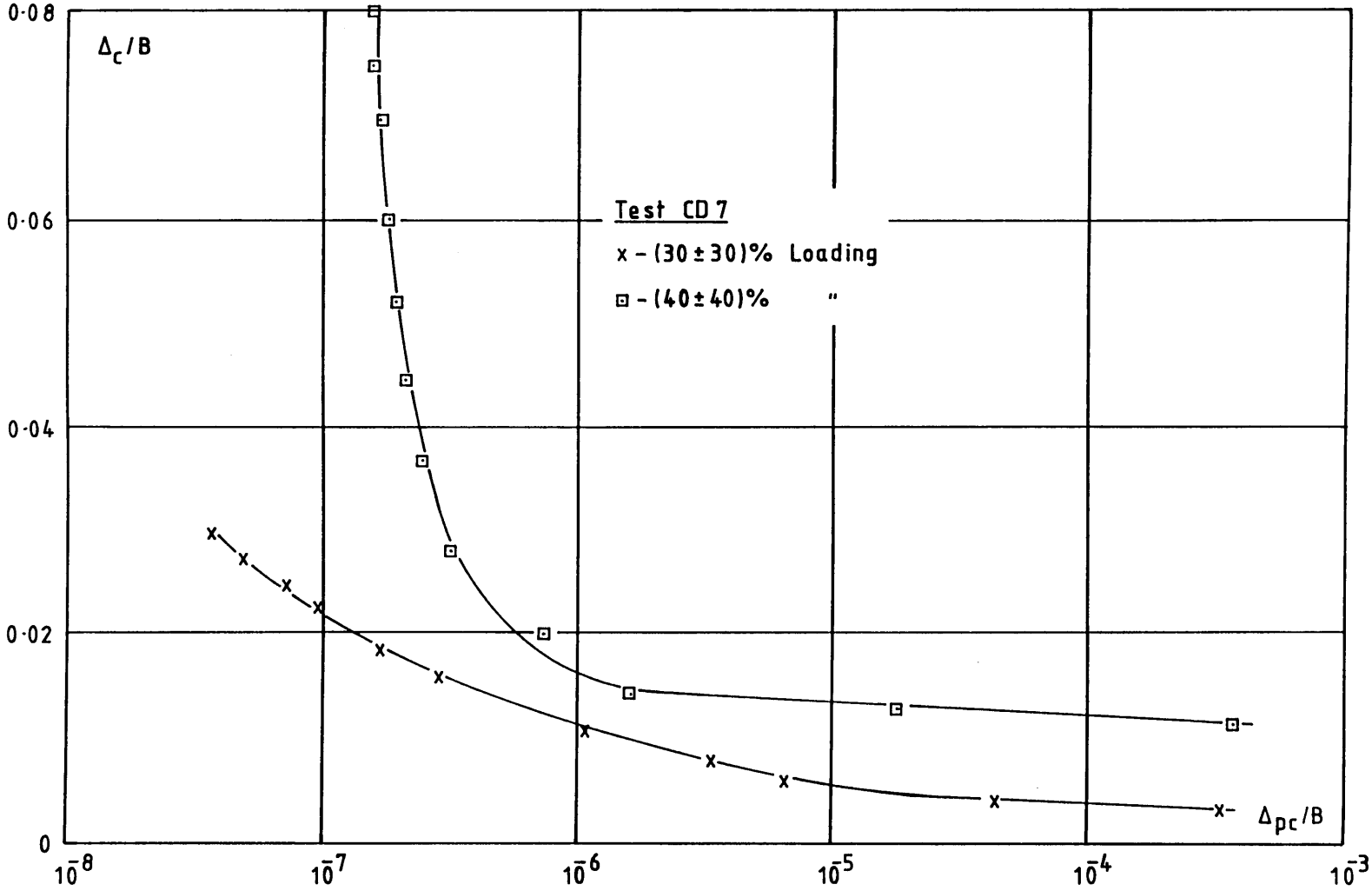

FIGURE 4.11 - Cyclic Test Results : Δ_c/B versus Δ_{pc}/B for test CD7.

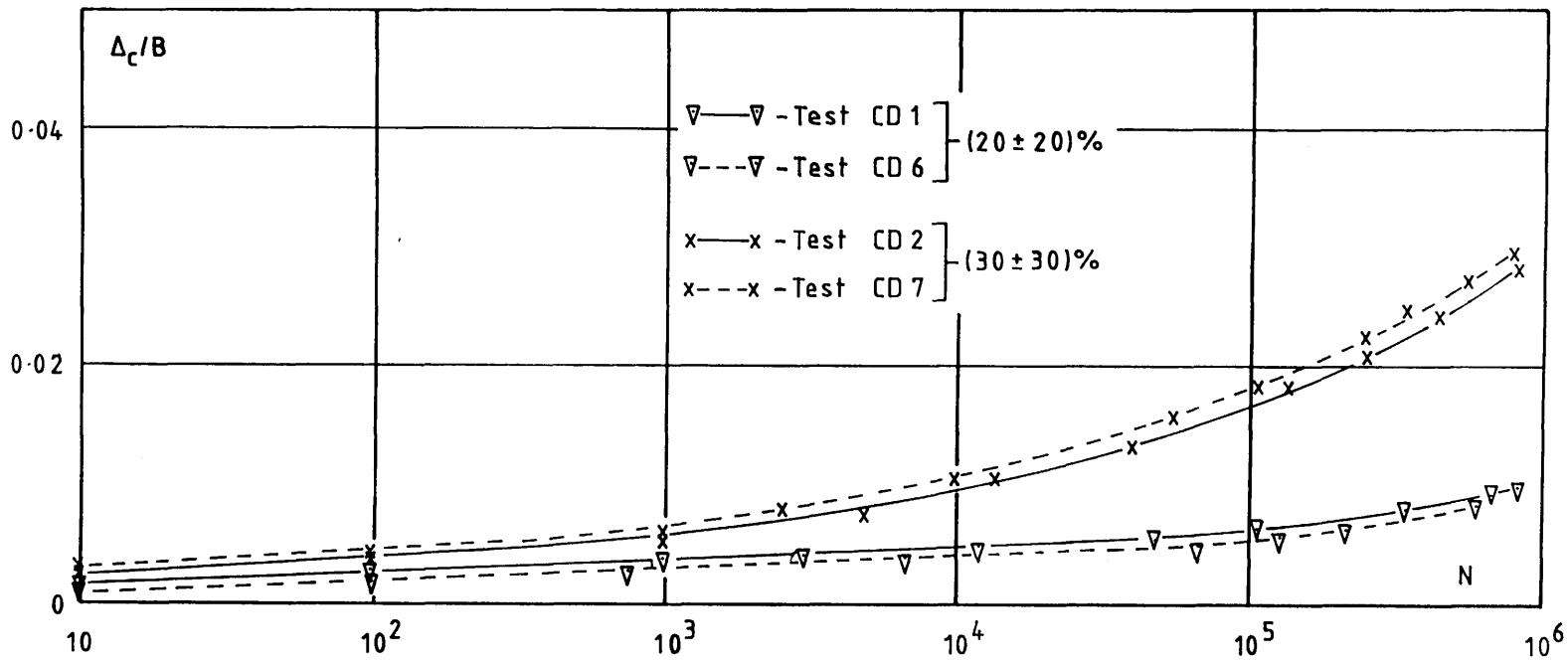

FIGURE 4.12 - Δ_c/B versus N : Comparison between tests subjected to the same cyclic loading.

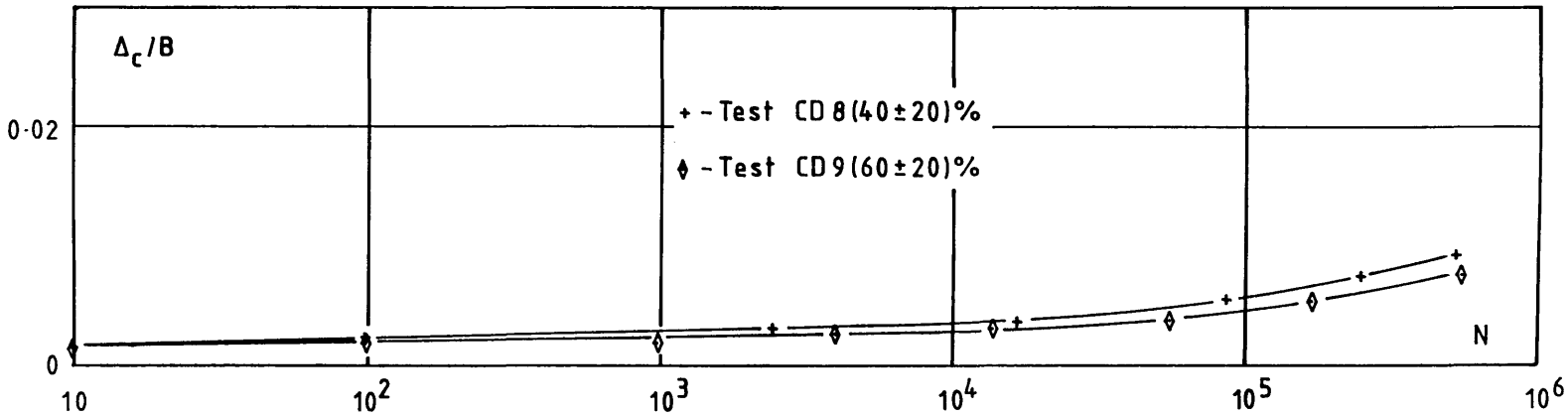

FIGURE 4.13 - Cyclic Test Results : Δ_c/B versus N for tests CD8 and CD9.

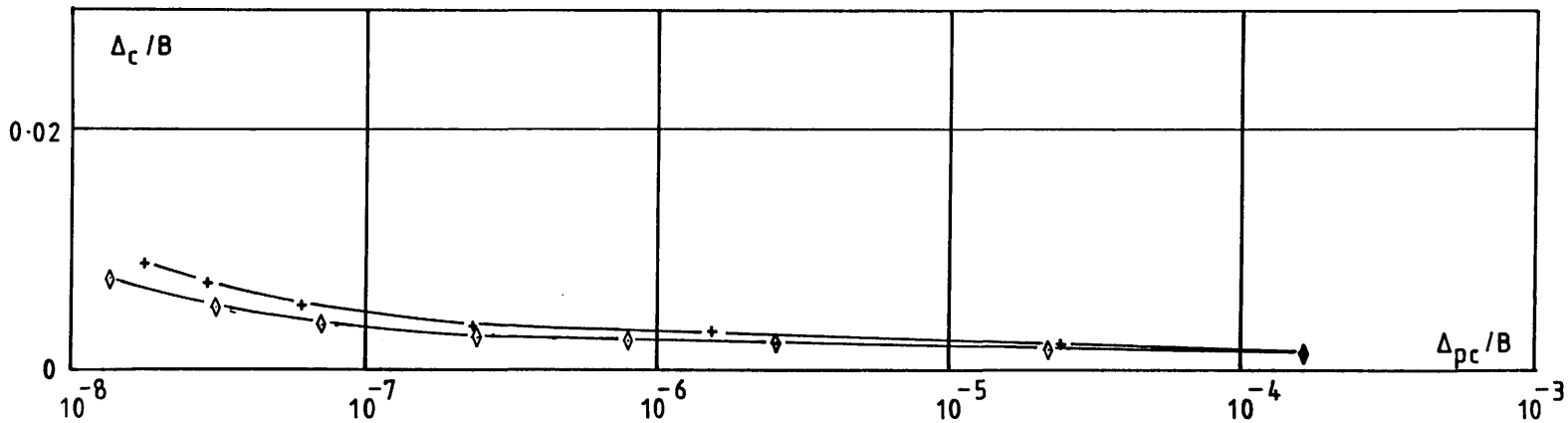

FIGURE 4.14 - Cyclic Test Results : Δ_c/B versus Δ_{pc}/B for tests CD8 and CD9.

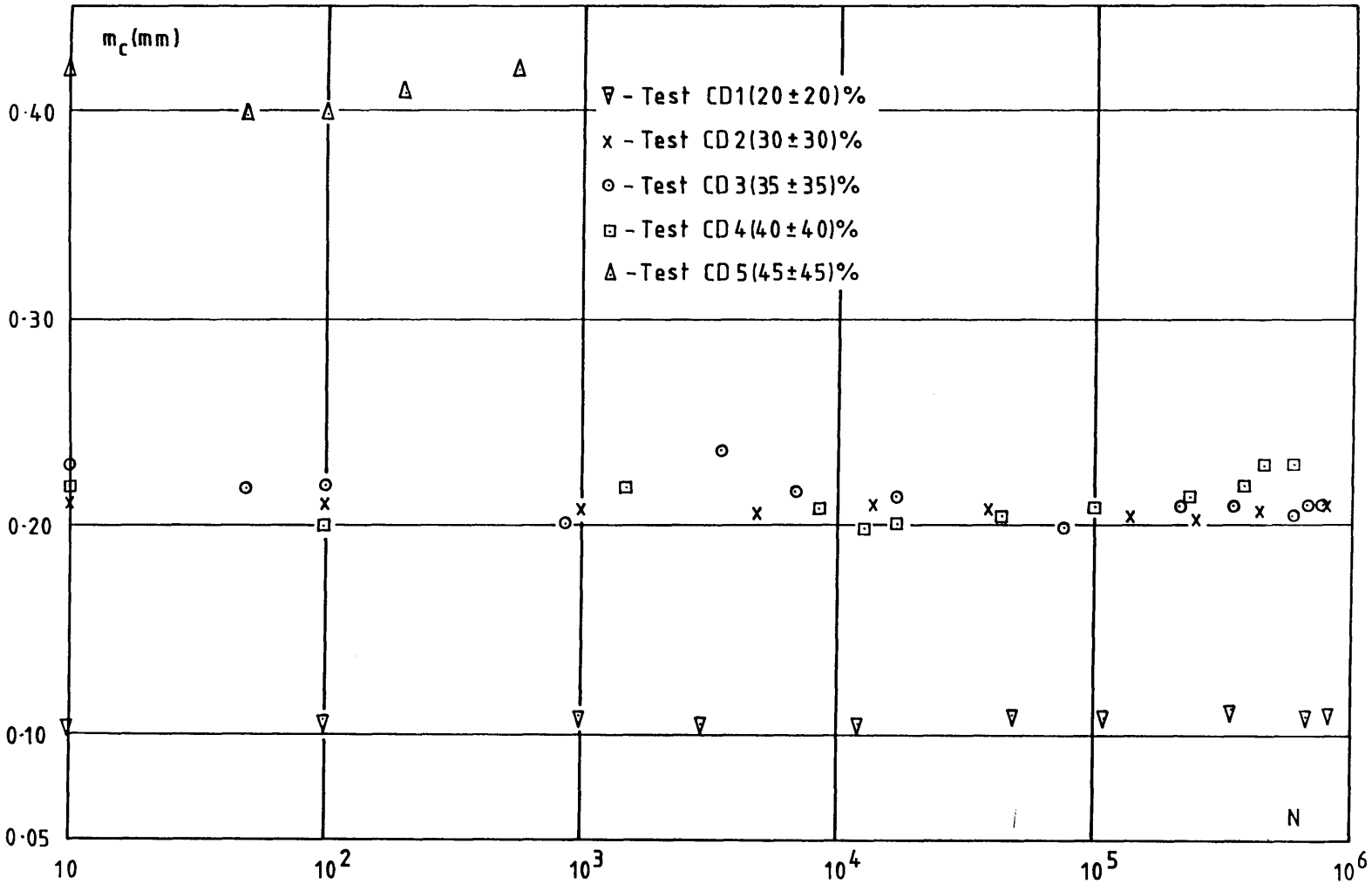

FIGURE 4.15 - Cyclic Test Results: Variation in anchor movement per cycle (m_c) for tests CD1 to CD5.

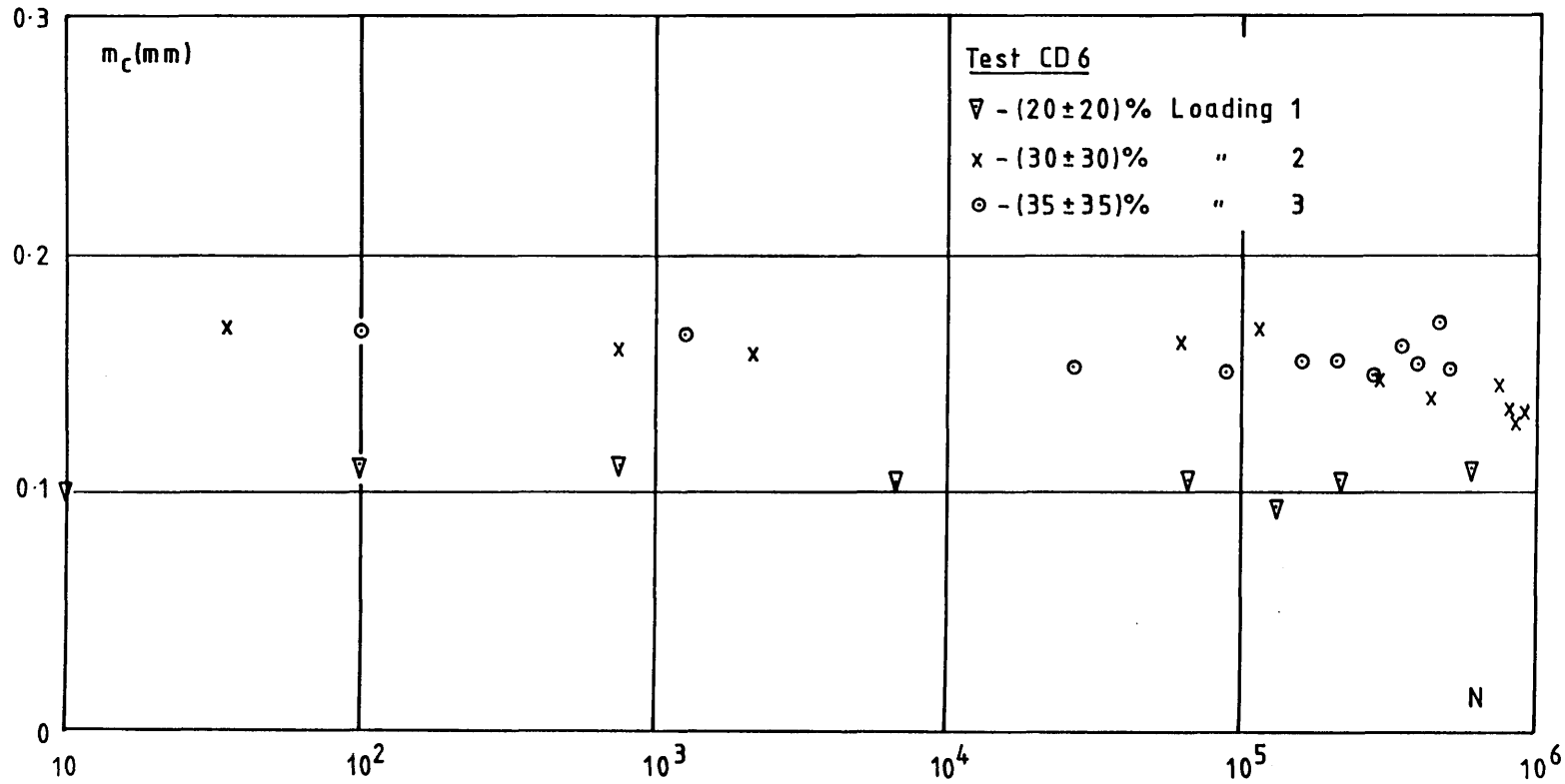

FIGURE 4.16 - Cyclic Test Results: Variation in m_c for test CD6.

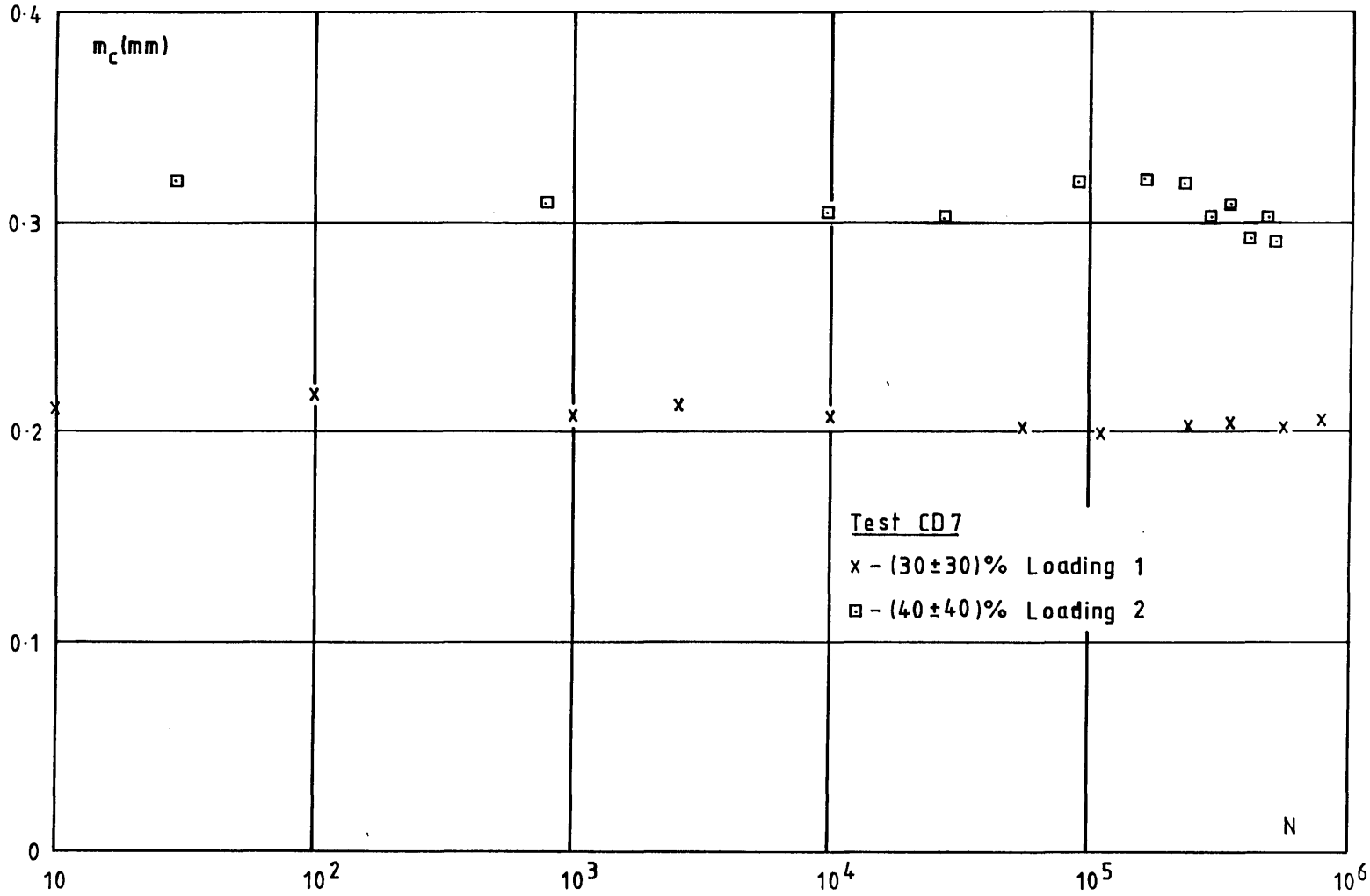

FIGURE 4.17 - Cyclic Test Results: Variation of m_c for test CD7.

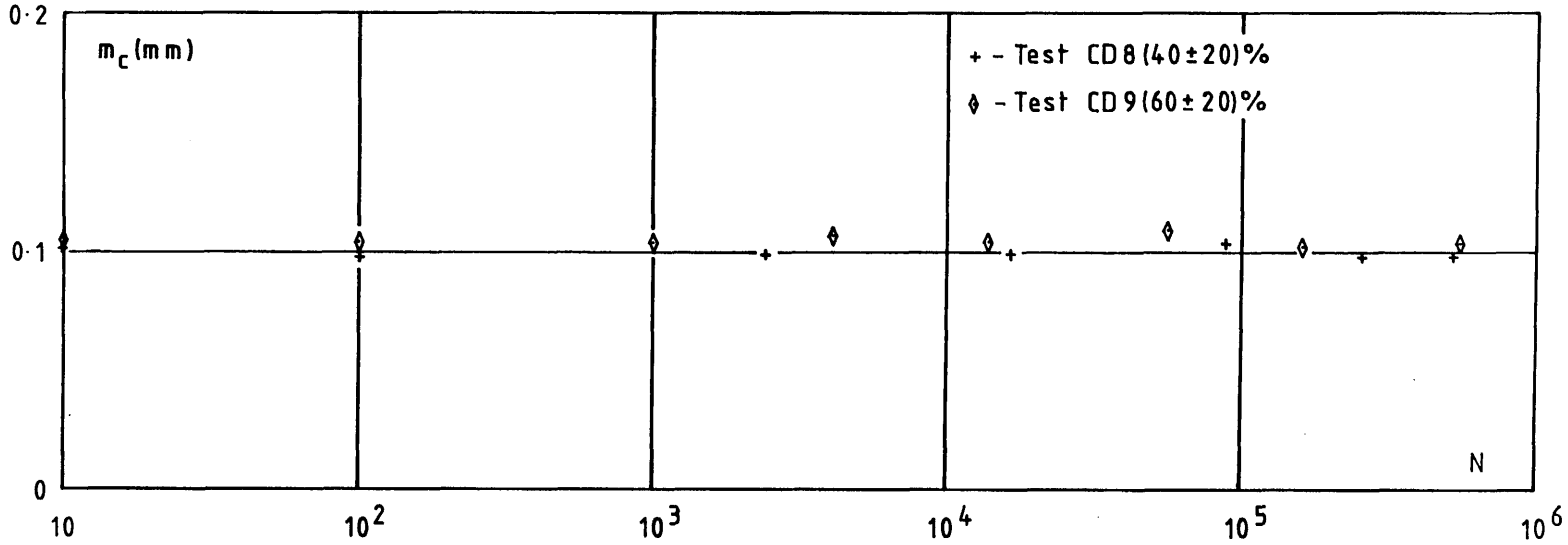

FIGURE 4.18 - Cyclic Test Results: Variation of m_c for tests CD8 and CD9.

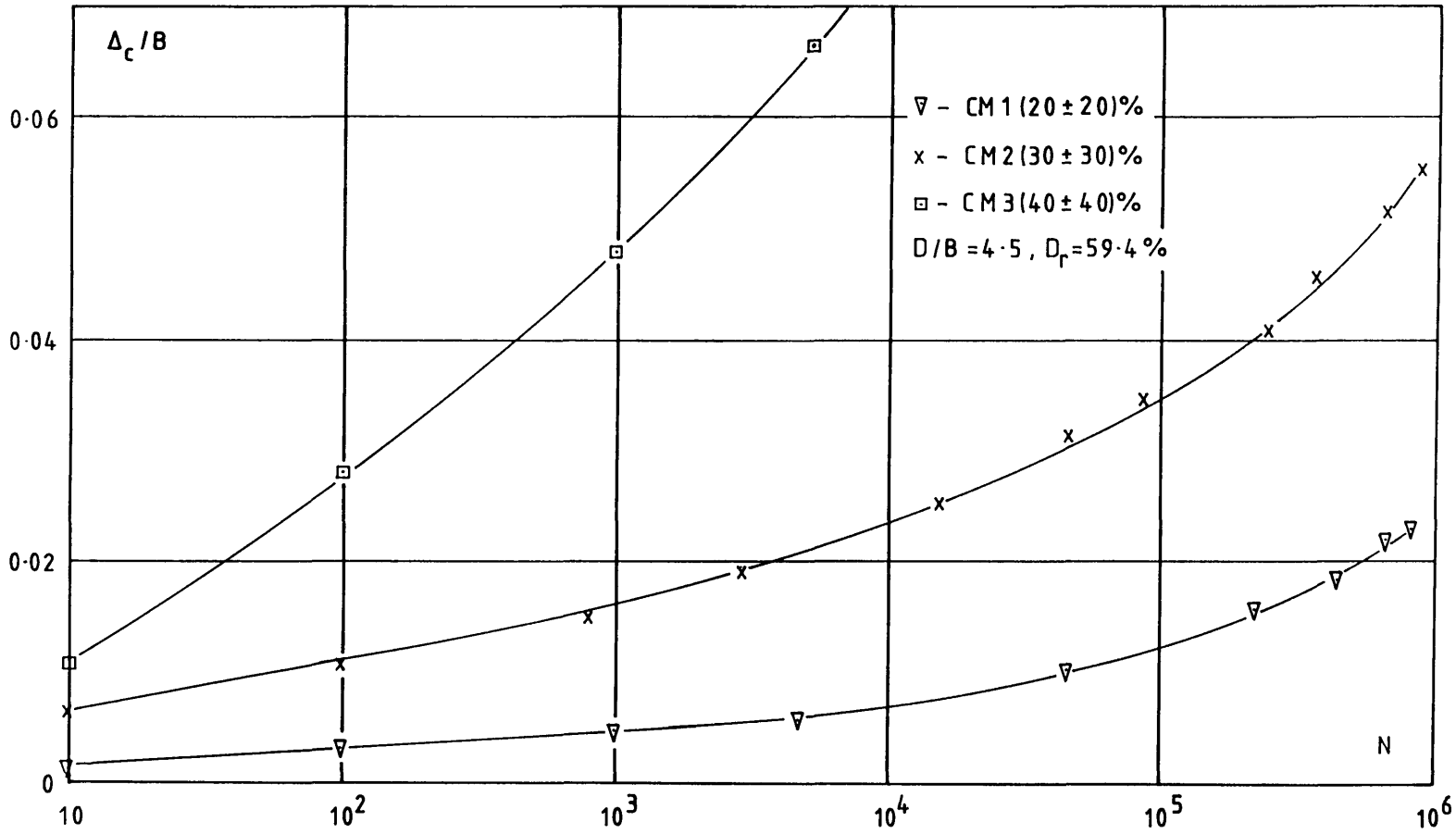

FIGURE 4.19 - Cyclic Test Rests: Δ_c/B versus N for tests CM1, CM2 and CM3.

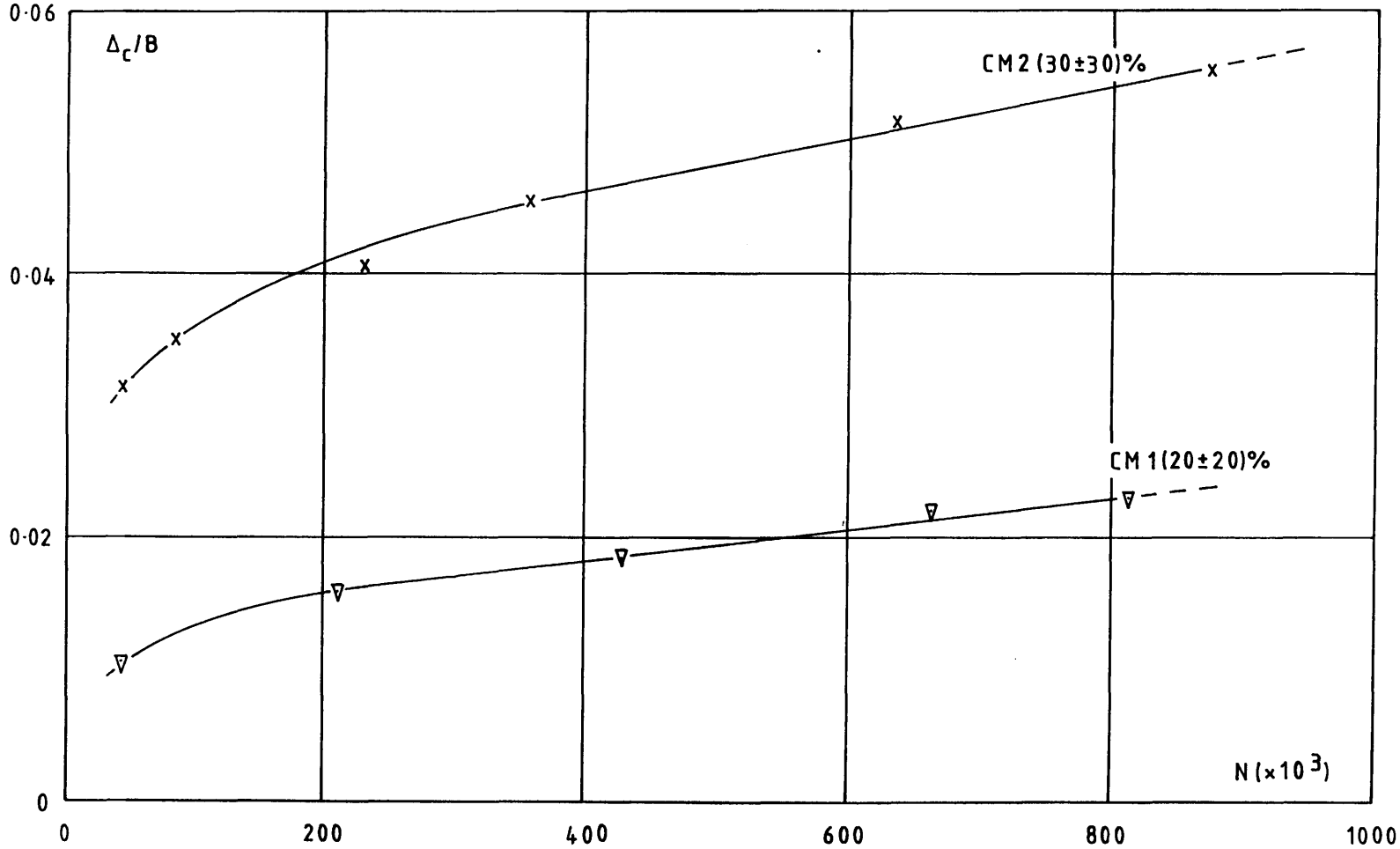

FIGURE 4.20 - Cyclic Test Results: Δ_c/B versus N (linear scale). Tests CM1 and CM2.

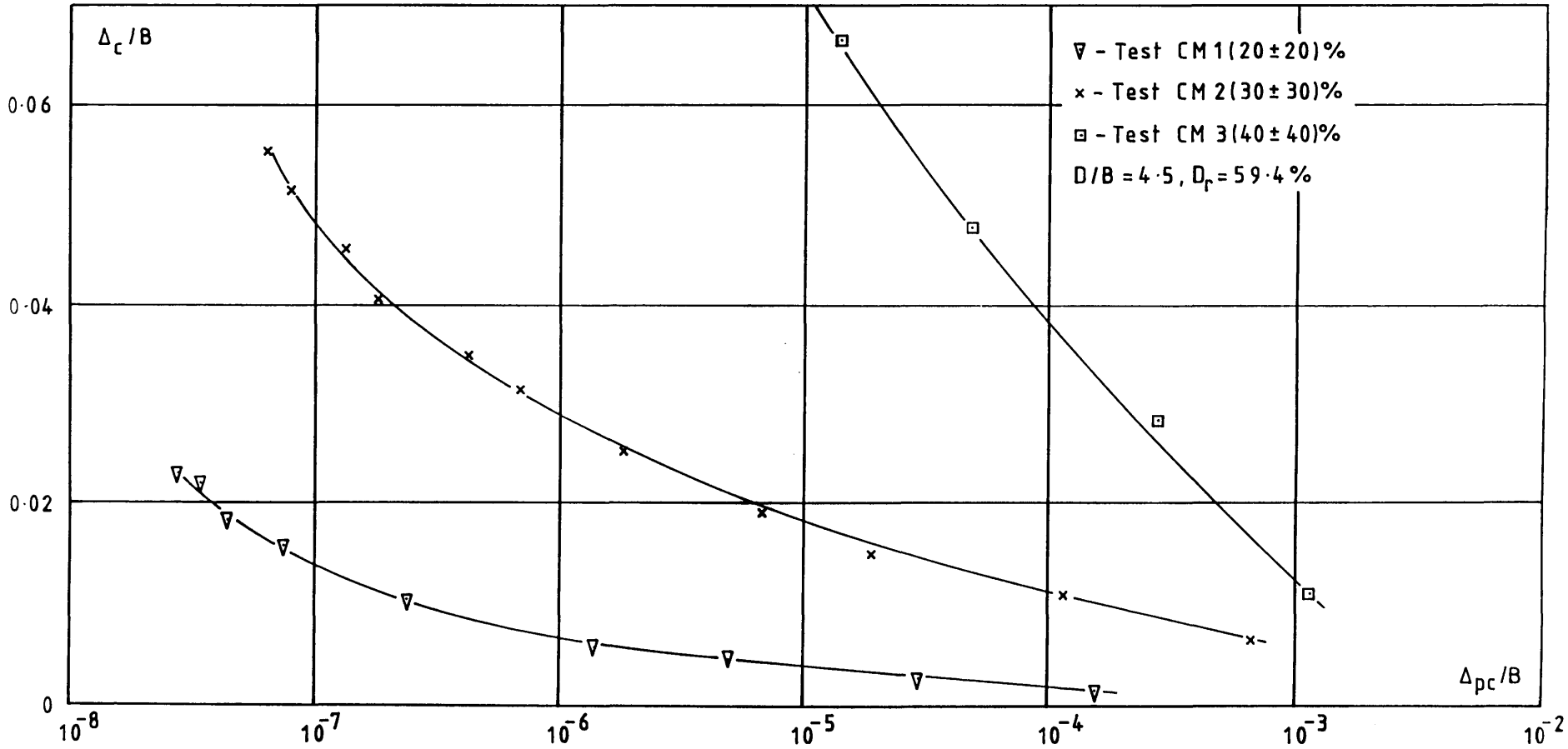

FIGURE 4.21 - Cyclic Test Results: Δ_c/B versus Δ_{pc}/B for tests CM1, CM2 and CM3.

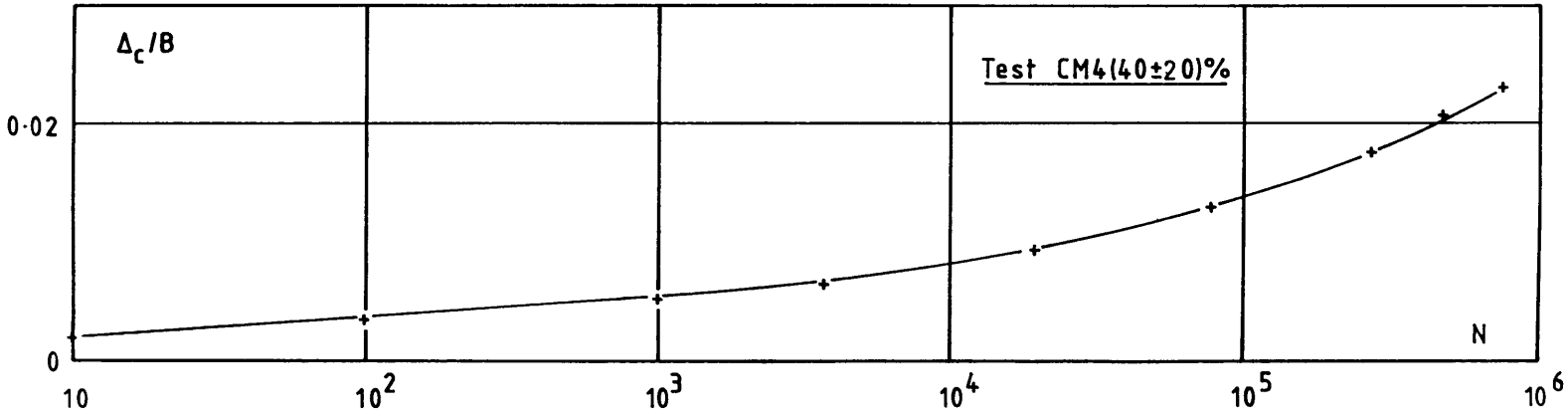

FIGURE 4.22 - Cyclic Test Results: Δ_c/B versus N for test CM4.

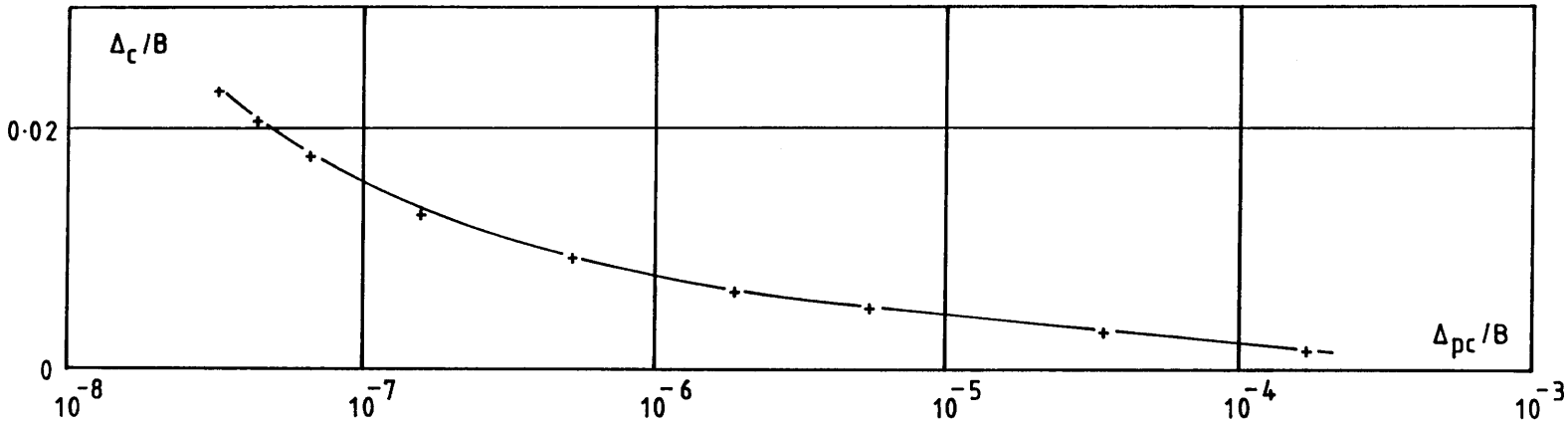

FIGURE 4.23 - Cyclic Test Results: Δ_c/B versus Δ_{pc}/B for test CM4.

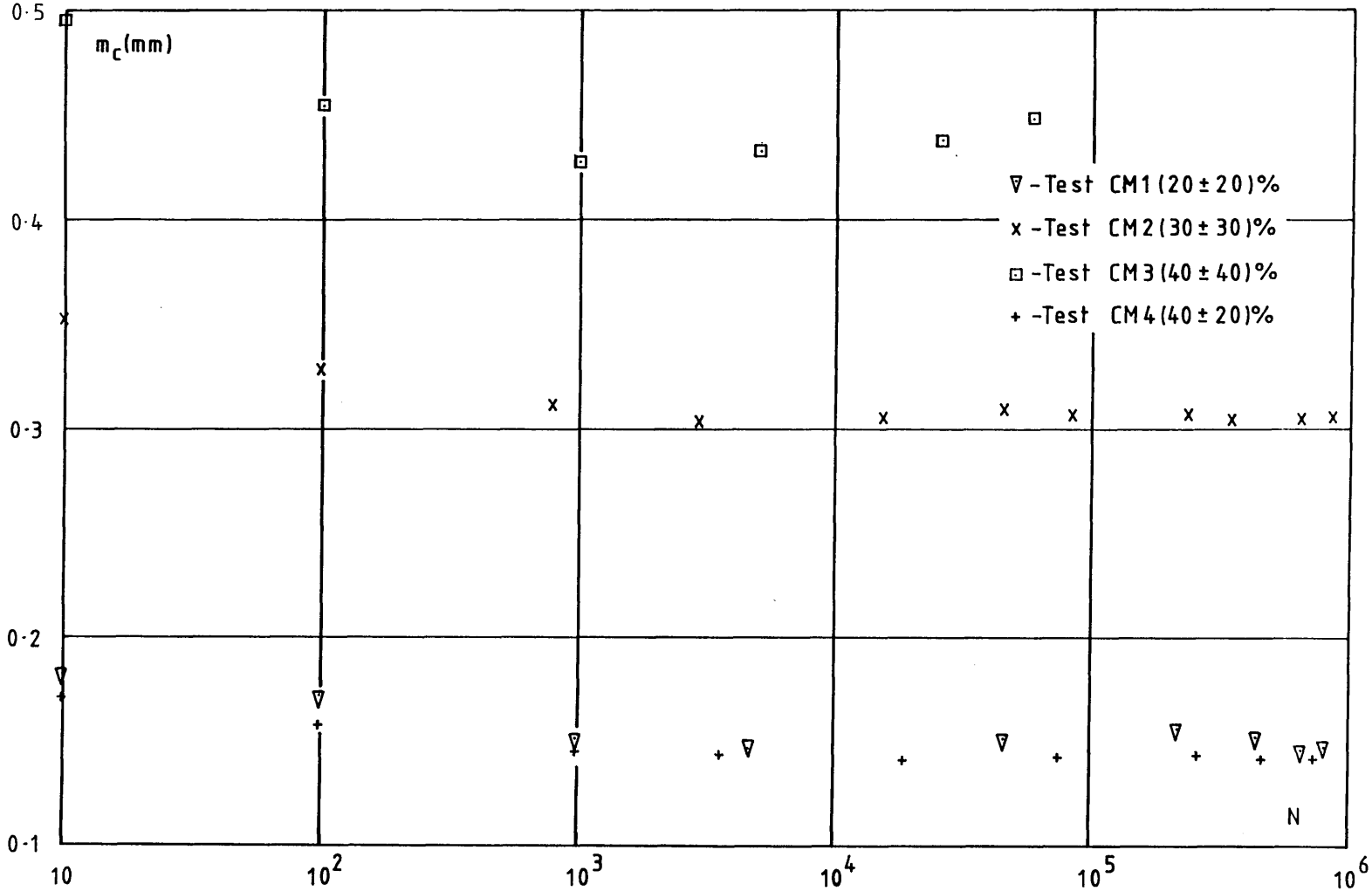

FIGURE 4.24: Cyclic Test Results: m_c versus N for tests CM1 to CM4.

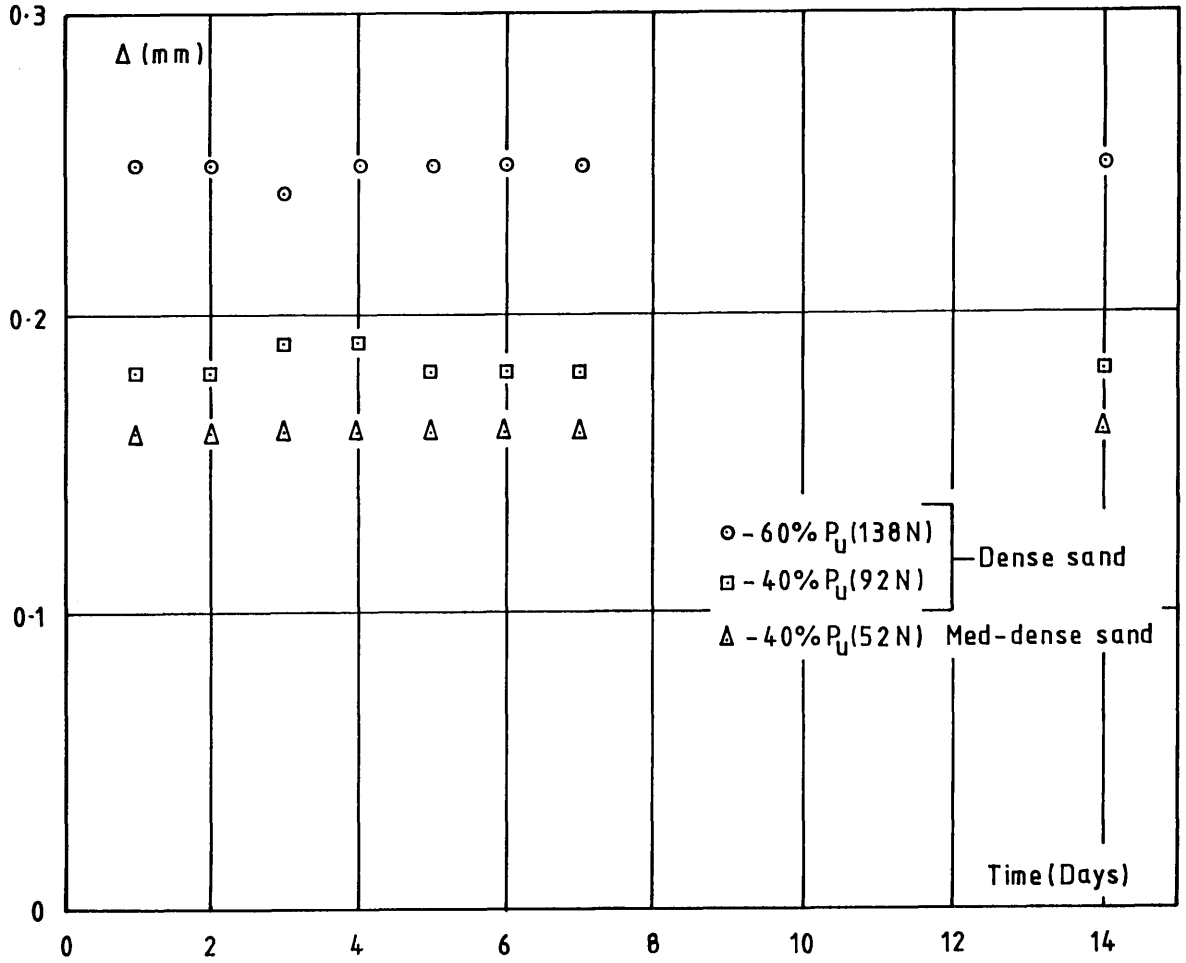

FIGURE 4.25 - Creep Test Results: Anchor displacement (Δ) versus time (in days).

CHAPTER 5 : FINITE ELEMENT ANALYSIS

5.1 INTRODUCTION

In Chapter 2, theoretical methods used in the analysis of embedded plate anchors were reviewed. The methods incorporated numerous assumptions regarding the behaviour of the soil and consisted of two basic types: those derived from elastic theory and those based on limit state concepts. In addition to these studies, a number of researchers have combined both analytical and numerical techniques to tackle the problem. Rowe and Booker (1979) described what is essentially an analytical technique for the analysis of horizontally embedded anchors in an elastic soil. In order to use the technique to predict the load–displacement behaviour of a rigid anchor, a numerical approximation regarding the number of sub–regions necessary to simulate rigid anchor behaviour is required. The analysis can take account of anchor shape, layer depth, anchor–soil interface condition, breakaway of the anchor from the underlying soil and interaction between groups of anchors. Further work by Rowe and Booker has investigated the behaviour of multiple underream anchors (Rowe and Booker 1980a) and single and multiple underream anchors in a Gibson soil (Rowe and Booker 1980b). Work by Butterfield and Banerjee (1971) and Davie and Merouani (1986) was concerned with the determination of stress and displacement fields around a rigid anchor embedded in an elastic half–space. A related study on the stress analysis of a deep, rigid, axially loaded cylindrical anchor in an elastic medium was reported by Luk and Keer (1980).

Although these further studies of anchor behaviour have become increasingly sophisticated, they have all been derived with respect to an elastic soil response. Unfortunately, the stress–strain behaviour of soils is distinctly non–linear and, although it may be argued that at working loads, obtained using a fairly large factor of safety, the soil response is elastic, or at least loadwise linear, this is certainly not the case when investigating ultimate conditions. For these investigations, non–linear methods have to be used and by far the most popular and powerful is the finite element method (FEM). Applicable to a huge range of problems in many fields of engineering, the method is becoming even more attractive as the relative cost of computing time reduces, due to continued advances in computer hardware and software design.

For the embedded anchor problem, the FEM offers the opportunity to investigate anchor behaviour using more realistic material parameters, without any assumptions regarding the position of the failure surface within the soil mass. A further attraction of the FEM is the ease with which parametric studies can be carried out. Once the basic geometric details have been established, the effect of varying different material parameters and/or boundary conditions can be easily investigated.

A brief review of previous FE analysis of plate anchors is presented in the next section, followed by a description of the FE analysis undertaken by the author. Results and discussion are presented at the end of the chapter.

5.2. FINITE ELEMENT ANALYSIS OF PLATE ANCHORS

Previous FE analysis have been carried out by Ashbee (1969), Davie (1973), Fadl (1981), Rowe and Davis (1982a,b), Tagaya, Tanaka and Aboshi (1983) and Ponniah (1984). A detailed review of all these investigations is outwith the scope of this thesis. However, the results reported by Rowe and Davis (1982b) for horizontal plate anchors embedded in cohesionless soil are more generally applicable and worthy of note.

They considered the effects of anchor embedment, friction angle, dilatancy, initial stress state K_o and anchor roughness on the ultimate uplift resistance which they defined as follows:

$$q_u = \gamma D F_{\gamma'} \qquad (5.1)$$

where q_u = ultimate pressure

γ = unit weight of soil

D = depth of soil above anchor

$F_{\gamma'}$ = anchor uplift factor

The anchor uplift factor $F_{\gamma'}$ was defined as a function of embedment ratio (D/B), angle of friction (φ) dilatancy (Ψ), initial stress state (K_o) and anchor roughness. $F_{\gamma'}$ was approximately expressed in terms of a basic anchor uplift factor F_γ and a number of correction factors, as follows:

$$F_{\gamma'} \simeq F_{\gamma}\ R_{\Psi}\ R_R\ R_K \qquad (5.2)$$

where F_{γ} = anchor uplift factor for the basic case of a smooth anchor in a soil which deforms plastically at constant volume ($\Psi = 0$) and with $K_o = 1$.

R_{Ψ}, R_R, R_K = correction factors for the effect of soil dilatancy, anchor roughness and initial stress state, respectively.

The numerical solutions presented for the basic anchor uplift factor, F_{γ} and the correction factors R_{Ψ}, R_R, R_K, were obtained using an elasto–plastic FE analysis based on the soil–structure interaction theory described by Rowe, Booker and Balaam (1978). The soil was assumed to have a Mohr–Coulomb failure criterion and Poisson's ratio was taken as 0.3.

Rowe and Davis found that soil dilatancy had a significant effect on anchor response, increasing appreciably the ultimate resistance for $D/B > 3$ in medium to dense sand ($\varphi > 30^0$). The effect of initial stress state on ultimate resistance was of less importance and significant only for soil exhibiting relatively little dilatancy. For these soils, the effect of K_o on ultimate resistance was usually less than 10%, and could be neglected for values of K_o between 0.4 and 1.0. Roughness had a negligible effect on the ultimate resistance of horizontal plate anchors.

5.3 NUMERICAL MODELLING USING FINEALE AND FINETAN

The finite element programs FINEALE (FINite Element Anisotropic Linear Elastic) & FINETAN (FINite Element TANgential stiffness) developed by Dr. David Naylor at the Institute for Numerical Methods in Engineering, University College, Swansea, were used by the author to model numerically the static loading anchor tests described in Chapter 3. The programs were run on the ICL 2966 computer at UCS during a short visit there by the author. Using the JANET system (Joint Academic NETwork), it was also possible to run the programs from a PAD terminal at Glasgow University.

5.3.1 Elastic Program (FINEALE 2D)

This is the two-dimensional version of FINEALE which was used on the axi-symmetric anchor problem. The material law is linear elastic, fully isotropic, defined by the elastic constants E and ν (Young's modulus and Poisson's ratio , respectively). Loading may be applied in any combination of discrete forces (applied at nodes), body forces (distributed over a region) or pressure/shear stresses (applied to element sides). The program can also handle anisotropic material behaviour, drained or undrained analysis and changes in porewater pressure, but these features are not required for the present study.

5.3.2 Data Input

The input data was given in records, each record comprising a line of data entered via a terminal. Figure 5.1 lists the record types used in FINEALE2D and the data input for each type. Detailed instructions on data input are given in the FINEALE User Guide (Naylor, 1981).

Record C gave the program basic information about the problem, e.g. number of nodes in mesh, number of elements in mesh, number of material property sets, etc.

Record G contained all the geometry data : node and element numbers, nodal coordinates, nodal fixities, etc. Rather than entering all this information by hand, a mesh generator program (FINEGEN) was used to establish the data input for record G (and record C). Figure 5.2 shows the half-mesh used in the present analysis. It consisted of 63 elements, only two of which represented the anchor (elements 4 and 13). Substantial stress concentrations were likely around the edge of the anchor and so the elements in this area were reduced in size. The combined thickness of the top three rows of elements was varied to match the D/B values used in the analysis (D/B= 6.0, 4.5 or 2.0). The geometry of the lower part of the mesh remained unchanged for D/B= 6.0 and D/B= 4.5, because the anchor diameter was 50mm in both cases. For D/B= 2.0, the anchor diameter was 76mm and the x co-ordinates of the mesh were altered accordingly. The anchor was taken as 6mm thick in all cases. Figure 5.3 shows the relative dimensions of the mesh for D/B= 6.0 and D/B= 2.0.

The tank boundary nodes were fixed in the x and y directions (rough interface assumed). The nodes on the axis of symmetry were fixed in the x direction only. The nodes along the base of the anchor were double–numbered in order that the anchor could move away freely from the underlying soil.

Two material property sets were defined in record M, one for the soil and one for the anchor. The anchor set was given typical values for brass, i.e. $E = 110{,}000$ kPa and $\upsilon = 0.3$, which were assigned to elements 4 and 13 only. These values remained unchanged throughout the FE study. Appropriate values for E and υ for the soil were much more difficult to ascertain. As a first attempt, the secant moduli obtained from the graphs of deviator stress versus strain for the triaxial tests on dense sand were used as E_{soil} (See Appendix I). Table 5.1 gives the values assigned to E_{soil} using the crude correlation of lowest cell pressure to lowest D/B value.

In dense sand at low confining pressure, Poisson's ratio very quickly increases to > 0.5 due to dilation in the specimen. Even during the very small range of strain for which the concepts from the theory of elasticity are applicable, Poisson's ratio can vary markedly. Thus it is very difficult to make an estimate of the value of υ to use in any problem. For computational reasons, υ must be < 0.5, and so values of 0.25 and 0.45 were chosen for comparison.

The element output control record (O1) allowed the user to specify the type and amount of ouput stored in the results file. Output of nodal forces and displacements occurred regardless of what was specified in record O1. Other output options included stress components, principal stresses and directions, stress invariants, etc.

Record GS contained details of gravity initial stresses, which included values for the soil bulk unit weight and horizontal to vertical initial stress ratio (K_o). The former was straightforward and was assigned a value of $17 kN/m^3$ (dense sand). The value assigned to K_o was much more problematical, being taken initially as 1.0.

Nodal forces and specified displacements were contained in record LD. As the analysis was elastic, absolute load values were not important. Based on the model test results, load values slightly below the ultimate were used. The load was applied at node 19 (Top left–hand corner node of element 9, see Figure 5.2).

The remaining records listed in Figure 5.1, i.e. S,B, P and W, were not relevant to the present study and therefore omitted.

5.3.3 Bi– Linear Program (FINETANBL)

This is the Bi– Linear version of the tangential stiffness finite element program FINETAN. The material stress– strain law assumes linear elasticity for all stress states below that corresponding to yield. If a yield stress state is reached, the tangential shear modulus is set to a very small, positive value (but not zero). The bi– linear stress– strain relationship is illustrated in Figure 5.4.

The material model incorporates the Mohr– Coulomb yield criterion and requires four parameters to define the material behaviour; two for elastic pre– yield behaviour and two to define the yield criterion. For the Mohr– Coulomb yield criterion, the latter two parameters are c and φ, the soil cohesion and friction angle respectively.

Defining

$$\sigma_d = (\sigma_1 - \sigma_3) \text{ and } \sigma_s = 1/2(\sigma_1 + \sigma_3),$$

then the yield criterion can be written as:

$$\sigma_d = 2\sigma_s \sin\varphi + 2c \cos\varphi \qquad (5.3)$$

Equation 5.3 represents the normal Mohr– Coulomb failure criterion.

The two elastic constants used by the program are the shear modulus, G, and the plane strain bulk modulus $\bar{K}$ ($= \bar{K} + G/3$). Axi– symmetric problems also use $\bar{K}$. The model differs from that described in Naylor et al (1981) in that K is replaced by $\bar{K}$. The practical significance of this is small since K and $\bar{K}$ are similar in magnitude. In the elastic state, the moduli are G_1 and $\bar{K}_1$. (The user, however, specifies E and υ). In the yielding state, the moduli are G_2 and $\bar{K}_2$.

The yield line represented by equation 5.3 is shown in Figure 5.5. Any stress state beneath the line is elastic (e.g. point B). On reaching the yield line, the value of G_2 assigned to an element depends on the stress path followed and is calculated to make the stresses adhere to the yield criterion insofar as this is possible with a postive value. If G_2 needs to be negative, it

is restricted to a small positive value. $\bar{K}_2$ is made equal to $\bar{K}_1$, which implies a small change in the bulk modulus, K, on yield.

The bi-linear soil model is suitable for investigating the development and spread of local yield. How this local yield occurred in the model anchor problem is discussed in section 5.5.2. Further information on this and other soil models for use with FINETAN is contained in Naylor et al (1981).

Data input for FINETANBL used most of the information already provided on the data records for FINEALE2D. Records C, M and O required some modifications and record LF (load fractions) was added. The latter record gave information on the number and magnitude of the loading increments. Details of data input are provided in the FINETAN User Guide (Naylor, 1983). Information from the triaxial tests was again used to provide initial values for input parameters. The soil cohesion was taken as zero, but for numerical reasons was assigned a small positive value (0.1kPa). As the failure criterion applied to all elements, a large cohesion value had to be assigned to the brass anchor elements (c = 10^6kPa). For the sand, a friction angle of $\varphi = 42^0$ was used (dense sand).

Data output consisted of the same options available when using FINEALE2D, plus, at the end of each increment, a summary output from which the spread of local yield could be assessed. The format for this output was $l = g_1\ g_2 \ldots g_n$, where l is the element number and g_1, g_2... are single digit numbers or letters which represent the state of stress at each gauss point as follows:

0,1,2,...9	Overstress ratio (OSR) x 10 (rounded down). Indicates elastic stress region (see below).
Y	Indicates yielding, OSR = 1.0
X	Stresses excessive, OSR > 1.1
T	Tension limit exceeded (i.e. negative stress values).

The overstress ratio is a number between 0 and 1.0 when the stress is in the pre-yield region, and should not exceed 1.0 when yielding occurs. It is defined as:

$$OSR = \frac{\sigma_d}{2\sigma_s \sin\varphi + 2c \cos\varphi} \qquad (5.4)$$

The eight– noded quadilateral elements used in the mesh had 4 gauss points each. The six– noded triangular elements had 3 gauss points each.

5.4 RESULTS

5.4.1 Elastic Analysis

a) Load– displacement relationship.

Figure 5.6 (a), (b) and (c) illustrates the effect of varying E and ν on the load– displacement graphs, for embedment ratios of 6.0, 4.5 and 2.0, respectively. Alternative soil stiffness values of x 2.0 and x 0.5 the values assigned in Table 5.1 were used for comparison. As expected, the slope of the load– displacement graph is proportional to Young's modulus, E. Increasing Poisson's ratio from 0.25 to 0.45 reduced the anchor displacements by approximately 15%, irrespective of the soil stiffness and embedment ratio. Varying the value of K_o (K_o= 0.5 or 1.0 or 2.0) or altering the position of the rigid boundary (x=160mm or 250mm or 400mm) had no effect on the load– displacement graphs.

The deformed mesh shown in Figure 5.7 is plotted to an exaggerated scale in order to emphasis the deformation which took place. The anchor displacement is 0.38mm and the maximum displacement at the surface is approximately 0.1mm.

b) Stress distribution

The stress distributions are reported in terms of the anchor pressure,p, for D/B= 6.0 only (E= 8700kPa, K_o= 1.0, P= 500N). Stress distributions for the other embedment ratios are very similar in form.

The variation of vertical normal stress (σ_y) on a vertical plane 3mm from the centreline of the anchor is shown in Figure 5.8. The maximum stress occurs just above the anchor, and reduces rapidly to a tensile value below the anchor. Increasing Poisson's ratio from 0.25 to 0.45 has little effect on the distribution.

The variation in vertical normal stress on a horizontal plane 2mm above the anchor is shown in Figure 5.9. The maximum stress occurs near the edge of the anchor, and this maximum increases with increasing Poisson's ratio. The stress over the central portion of the anchor is virtually constant and, at a distance of approximately B/4 from the edge of the anchor, the stress is comparable with the initial stress value.

Figure 5.10 shows the distribution of shear stress on a vertical section 2mm from the edge of the anchor (x= 27mm). There is a sharp peak to this distribution at anchor level, and the peak is reduced by increasing Poisson's ratio from 0.25 to 0.45.

c) Boundary effects

The distribution of horizontal stress (σ_x) is affected by the proximity of a rigid boundary. In Figure 5.11, the horizontal stress is plotted for a column of gauss points situated 147mm from the tank centreline, with rigid boundaries at 160mm, 250mm or 400mm. (i.e. 3mm, 103mm or 253mm from the column of gauss points). A linear variation of horizontal stress with depth is maintained in all cases, down to approximately one anchor diameter above the anchor. Below this level, the distributions are distinctly non– linear, but follow the same general trend. The stress values in the upper region are all slightly greater than the initial stress values.

5.4.2 Bi– Linear Analysis

The sensitivity of the load– displacement response and the spread of local yield were investigated by varying E, υ and φ. In the first instance, only results for D/B= 6.0 are reported.

a) Load– displacement relationship

The effect on the load– displacement relationship is illustrated in Figure 5.12. Each curve is clearly non– linear and, using the curve for E= 8700kPa, υ= 0.25, φ= 42°, and c= 0 for comparison, the effect of altering E or υ or φ is obvious and not unexpected. Halving the E– value almost exactly doubles the displacement at any level, which is similar to the elastic response. Increasing Poisson's ratio from 0.25 to 0.45 decreases the anchor displacement by about 25% at any load level. Reducing the φ value to 36° (medium dense sand) is equivalent to reducing the stiffness and therefore results in an increase in anchor

displacement. In this case, however, the increase becomes larger as the load increases. If the secant modulus for medium dense sand obtained from the triaxial tests (E= 4200kPa) was used as well, the displacements would increase further by a factor of two.

For the deformed mesh shown in Figure 5.13, the anchor displacement is 1.7mm and the maximum surface dispalcement is approximately 0.1mm.

b) Local yield

The sequence of meshes presented as Figure 5.14 shows how local yield progressed through the soil as the anchor load increased. The soil parameters were E= 8700kPa, υ= 0.25, φ= 42^0 (dense sand) and c= 0. Seven increments of load were applied, the first being extremely small (0.02P), thus ensuring elastic behaviour in all elements at the end of the first increment. White elements are elastic (OSR< 1.0), elements cross– hatched up to the right have yielded (OSR= 1.0), those cross– hatched up to the left are over– stressed (OSR> 1.1) and black elements signify areas of tension.

Figures 5.15 and 5.16 show sequences of local yield for φ= 36^0 (medium dense sand) and υ= 0.45, respectively, other parameters remaining constant. (Increments 2,4,6 and 7 only are presented). Changing Young's modulus did not alter the sequence of local yield.

5.5 DISCUSSION

Most of the results and discussion are presented for D/B= 6.0. The results for D/B= 4.5 and D/B= 2.0 show very similar trends and have not been considered separately. Any significant differences are highlighted when they occur.

5.5.1 Elastic Analysis

a) Load– displacement relationship.

For D/B= 6.0, the load– displacement graph from test SD10 is plotted in Figure 5.17. This graph has a maximum load of 511N at a displacement of 1.73mm. Clearly, using elastic analysis, it is possible to select a suitable value

of E such that the analysis produces the same load and displacement values at failure. In this case, taking E= 1920kPa gives the load– displacement line shown in Figure 5.17. Using the straight line portion of the experimental curve, the stiffness increases to 3320kPa. These values of E are less than those used in the analysis (see Figure 5.6 (c)) but, considering the very low confining pressure in the model tests, the soil stiffness may also be very low. The non– linear behaviour of the anchor as it approaches failure is very marked, and neither of the elastic versions shown in Figure 5.17 is able to model the anchor load– displacement behaviour accurately. It is therefore concluded that a linear elastic analysis is not suitable for modelling the anchor load– displacement relationship.

This is also true for surface dispalcements, as shown in Figure 5.18. At the tank centreline, the experimental surface displacement is approximately ten times greater than that predicted by elastic analysis. The experimental surface displacements fall off rapidly with distance from the centre of the tank, whereas the finite element values attenuate much more slowly. Increasing Poisson's ratio from 0.25 to 0.45 reduced the surface displacements by approximately 25%.

b) Stress distribution.

The variation in vertical normal stress on a horizontal plane shown in Figure 5.9 reveals a substantial stress concentration at the edge of the anchor. This is consistent with the analytical solution for the distribution of contact stress beneath a rigid circular foundation resting on an elastic medium (Borowicka, 1936). In the vicinity of the anchor, the stresses are considerably greater than the initial stresses caused by the overburden pressure. In the vertical plane (Figure 5.8), the variation of vertical normal stress above the anchor takes a similar form to the distribution of vertical stress beneath the centreline of a rigid circular disc buried at depth in an elastic half– space and subjected to a compressive vertical load (Butterfield and Banerjee, 1971). Figure 5.19 shows these distributions for comparison. The case for D/B= 0.0 by Butterfield and Banerjee in which there is no overburden effect, is physically similar to the deepest anchor case of D/B= 6.0, rotated through 180°: the distributions of vertical normal stress shown in Figure 5.19 are also similar.

Tensile stresses beneath the anchor are dependent on the local bonding conditions between the anchor and the soil. In their paper, Butterfield and Banerjee reported that tensile stresses would occur above rigid circular discs.

The shear stress distribution shown in Figure 5.10 confirms that the shear stress tends to zero at the free surface. The distribution again reveals substantial stress concentrations at the edge of the anchor which can lead to problems when using non– linear analyses (see discussion on FINETANBL).

In general, increasing Poisson's ratio resulted in greater values of normal stress and smaller values of shear stress (see Figures 5.9 and 5.10). Davies and Merouani (1986) reported a similar Poisson's ratio effect.

c) Boundary effects.

Referring to Figure 5.11, in the upper region the greatest increase in horizontal stress over the initial stress occurs with the rigid boundary at x= 160mm. The smallest increase occurs when the rigid boundary is at x= 400mm, but this increase is only marginally less than that associated with a rigid boundary at x= 250mm, the radius of the test container. In fact, the distributions for rigid boundaries at x= 250mm and x= 400mm are almost identical throughout the entire depth of soil. Increasing Poisson's ratio from 0.25 to 0.45 has virtually no effect in the upper region, but the horizontal stresses in the area immediately above and below the anchor are reduced by approximately 25%.

The results clearly indicate that the proximity of a rigid boundary affects the distribution of horizontal stresses. However, keeping all other parameters constant, the effect is not significant for the rigid boundary positions considered. Shear stresses on the vertical and horizontal boundaries were very small in all cases.

5.5.2 Bi– Linear Analysis

a) Load– displacement relationship.

In order to compare the results of the FE analysis and the anchor tests, the load– displacement curve for test SD10 and the finite element curves for E= 8700kPa are plotted in Figure 5.20. The experimental curve corresponds fairly well with the finite element curve for $\upsilon = 0.45$ and $\varphi = 42^0$, up to approximately 90% of the experimental failure load.

Similar comparisons are made for D/B= 4.5 and D/B= 2.0 in Figure 5.21, using the appropriate E– values from Table 5.1. The results for D/B= 2.0 are

particularly good, but in each of the comparisons it is clear that the FE analysis is unable to predict the failure load of the anchors. Only the results for D/B= 2.0 (Figure 5.21 (b)) show any sign of failure, in that the slope of the load– displacement curve reduces significantly above an anchor load of 80N.

This problem arises primarly because the program is unable to take account of the strain softening effect in the sand. The peak φ value of the sand was used, and this could not be varied during the loading increments. The choice of stiffness value in the FE analysis is critical, and the values listed in Table 5.1 give reasonable results with respect to the slope of the initial stage of the load– displacement graphs shown in Figures 5.20 and 5.21. For D/B= 4.5, the correspondence between test results and FE analysis could be improved by choosing a slightly higher value of sand stiffness. The good agreement obtained when using the secant moduli for D/B= 6.0 and D/B= 2.0 is probably fortuitous, but the results illustrate that, even for model tests where the confining pressures are low, the stiffness of the sand increases with confining pressure.

b) Local yield

The progression of local yield shown in Figure 5.14 is associated with a continual expansion of the yielded, over– stressed, and tension zones throughout the loading increments. After only the second increment there is a substantial zone around the anchor which is excessively stressed. The first small area of tensile stress is also apparent. An elastic wedge above the anchor is clearly defined at increment 2 and is still apparent at increment 7. The existence of an elastic wedge above the anchor has been reported by many researchers (e.g. Kupferman, 1974; Maddocks 1978), and is analagous to the wedge defined beneath a foundation in bearing capacity theory.

By increment 3, the soil in the surface elements begins to yield. In this area the stresses σ_d and σ_s have very small values, which places the stress state near the origin in Figure 5.5 (drawn for c= 0). Yielding occurs because the horizontal stresses become tensile (negative) and the stress state moves into the yielded zone. Tensile horizontal stresses in this area have been reported by Davies and Merouani (1986).

The sequence of meshes shown in Figure 5.15 for $\varphi = 36^0$ presents the same basic pattern as Figure 5.14 for $\varphi = 42^0$. With the lower value of φ, the slope of the yield line is less and, for the same loading, more elements would be expected to yield. This is confirmed by comparing meshes at appropriate

increments in Figures 5.14 and 5.15. It is also evident that, for high loading, the boundary of the yielded zone for $\varphi = 36^0$ has a more pronounced slope from the anchor to the soil surface.

Considering the sequence of meshes shown in Figure 5.16 for $\upsilon = 0.45$, the same basic pattern is apparent once again. However, there is a change in the stress distribution around the anchor and this is most obvious in increment 2 : there is a larger elastic area above the anchor and a larger yielded area below. Above the anchor the soil is in vertical compression and, because the soil has some lateral restraint, increasing Poisson's ratio effectively increases the lateral stress on the soil. Hence the stress state of the soil is moved away from the failure line. Conversely, below the anchor where the vertical compressive stress is reduced, increasing Poisson's ratio results in a reduction in lateral stress, thereby making failure more likely. The tensile zone is larger at all increments, with some elements near the surface also exceeding the tension limit.

For a comparison with the results of D/B= 6.0, Figure 5.22 shows the sequence of meshes for D/B= 2.0, with E= 2300kPa, $\upsilon = 0.25$, $\varphi = 42^0$ and c= 0. The elastic wedge is again clearly defined and relatively larger than the wedge defined for D/B= 6.0. For increments 5,6 and 7, the boundary of the yielded zone resembles a frustum of a cone, the shape assumed for the failure surface in some of the shallow anchor uplift theories mentioned in Chapter 2.

c) Stress distribution

The stress distributions are shown in Figures 5.23, 5.24 and 5.25 for the same situations as the elastic analysis. The elastic distributions are also plotted for comparison. In all cases, the anchor load is 500N. The general trends of the elastic and bi− linear distributions are similar. Considering the overall equilibrium of the anchor, the increase in vertical normal stresses in the bi− linear case is compensated by a corresponding reduction in the magnitude of the shear stresses compared with the elastic case. Hence equilibrium is maintained in both cases.

d) Surface displacements

These are very difficult to predict in non− linear analyses. The calculated displacements are very small, and hence any rounding errors in the computations are magnified and distort the results. The profile of surface

displacement obtained using the bi– linear program bore little relation to the measured surface displacements shown in Figure 5.18.

5.5.3 Closure

For such a complex, non– linear problem as anchor uplift resistance, an elastic analysis is clearly not relevant, although the stress distributions obtained took the form of established analytical and numerical solutions for analogous problems.

The bi– linear stress– strain model does not correspond to that associated with dense sand. It is unable to take account of the strain softening behaviour and also ignores the effect of dilatancy. This leads to large predicted failure loads of up to 3 times the experimental value. However, the analysis did identify two characteristics of shallow anchor behaviour : the elastic wedge of sand above the anchor and the shape of the failure surface, as defined by the shape of the boundary of the yielded elements.

Finally, the FINETAN program used by the author incorporates another soil model, the K– G model (FINETANKG). In this version the tangential moduli K and G vary continuously with stress. The stresses approach yield asymptotically and therefore over– stressed regions are not clearly defined as with the bi– linear model. The K– G model's strength is that it can reproduce more realistic stress– strain curves, although more parameters are required to define the model. An investigation of the anchor problem using this model will be pursued in the future

TABLE 5.1 – Values of Young's modulus used in FE study.

D/B	CELL PRESSURE (kPa)	SECANT MODULUS (kPa)
2.0	10	2300
4.5	20	4300
6.0	40	8700

Record Type	Data input
T1	Title (one or more records)
C1 C2 C3	Constants and control parameters (One record each).
G1 G2 G3	Mesh geometry and boundary fixity conditions.
M1 M2	Material properties and their distribution.
S1 S2	Initial stresses and other distribution.
01	Element output control.
GS	Data for generation of gravity and stress field (omit if not required).
LD	Nodal loads and/or specified displacements.
B1 B2	Body forces (omit if none)
P1 P2	Surface tractions (omit if none)
W1 W2	Final pore pressures for known - p.p. - change analysis (omit if none).

FIGURE 5.1. - List of record types for FINEALE2D.

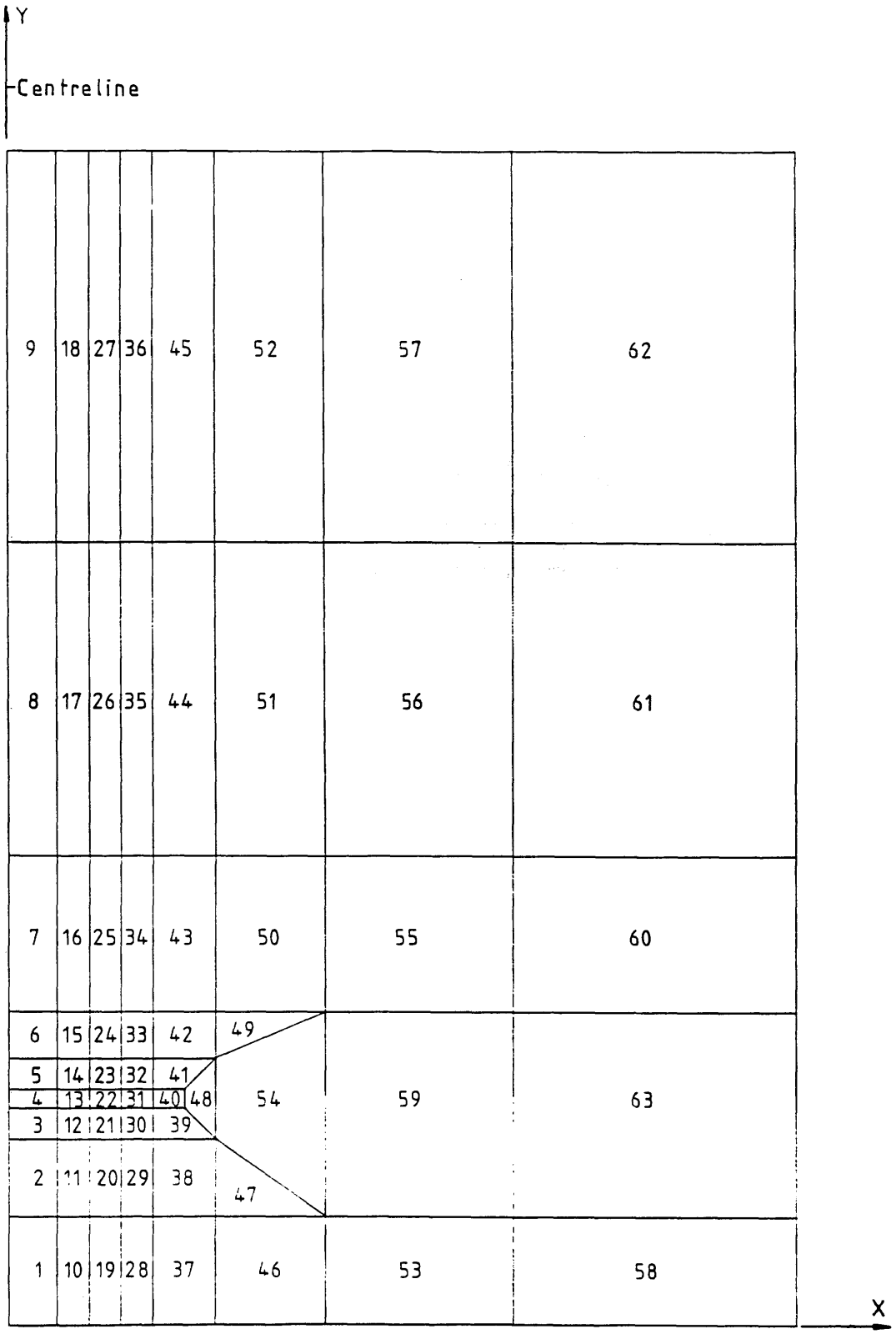

FIGURE 5.2 - Finite Element Mesh (symmetrical about centreline).

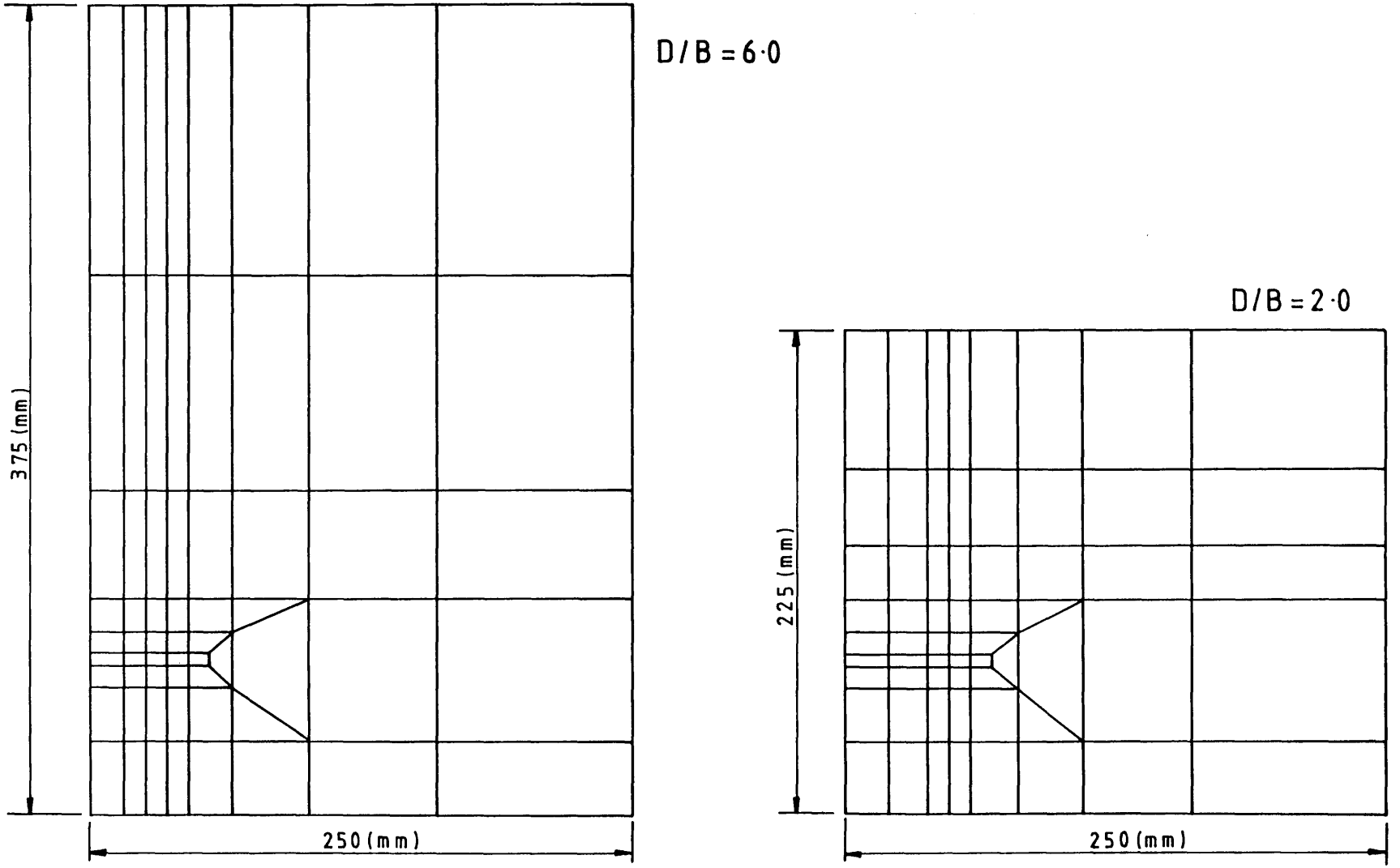

FIGURE 5.3 - Relative dimensions of mesh for $^{D}/_{B}$ = 6.0 and $^{D}/_{B}$ = 2.0

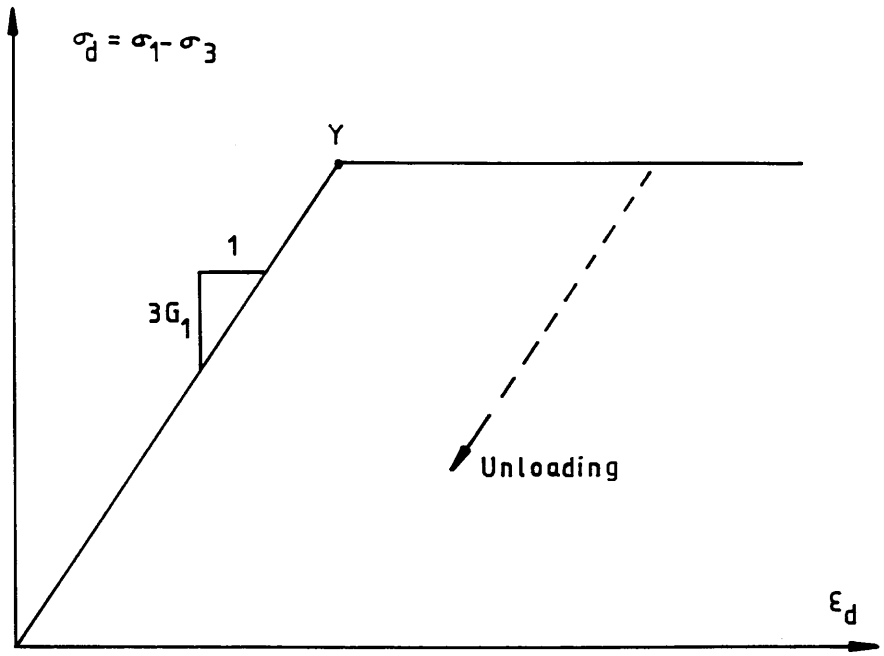

FIGURE 5.4 - Bi-linear stress-strain relationship.

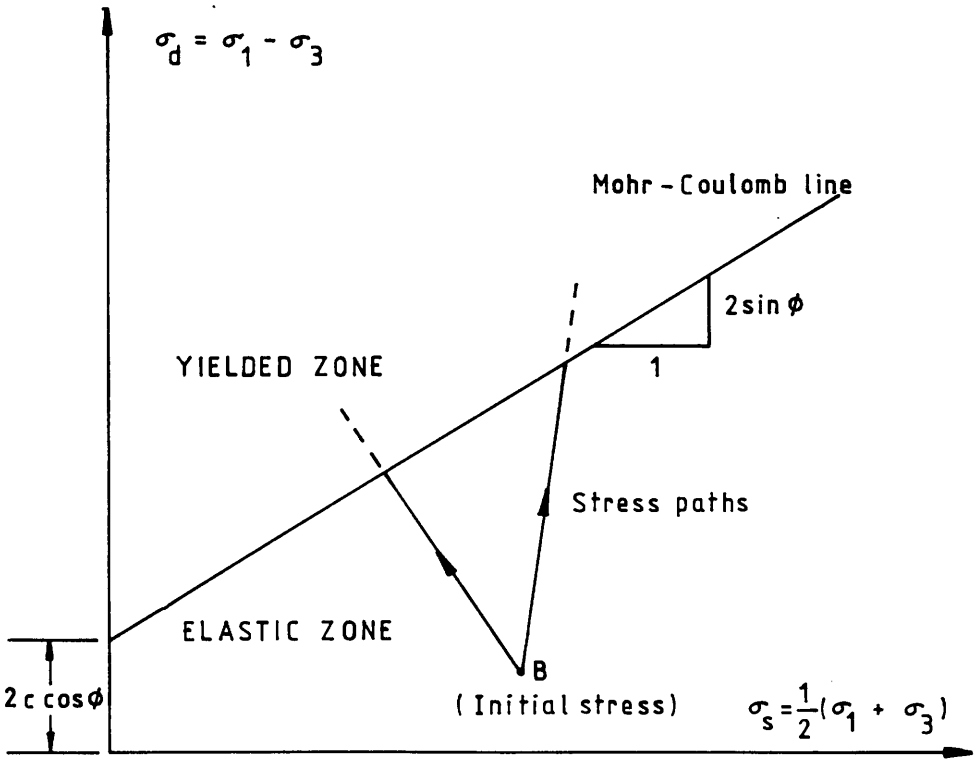

FIGURE 5.5 - Yield line for bi-linear model showing possible stress paths.

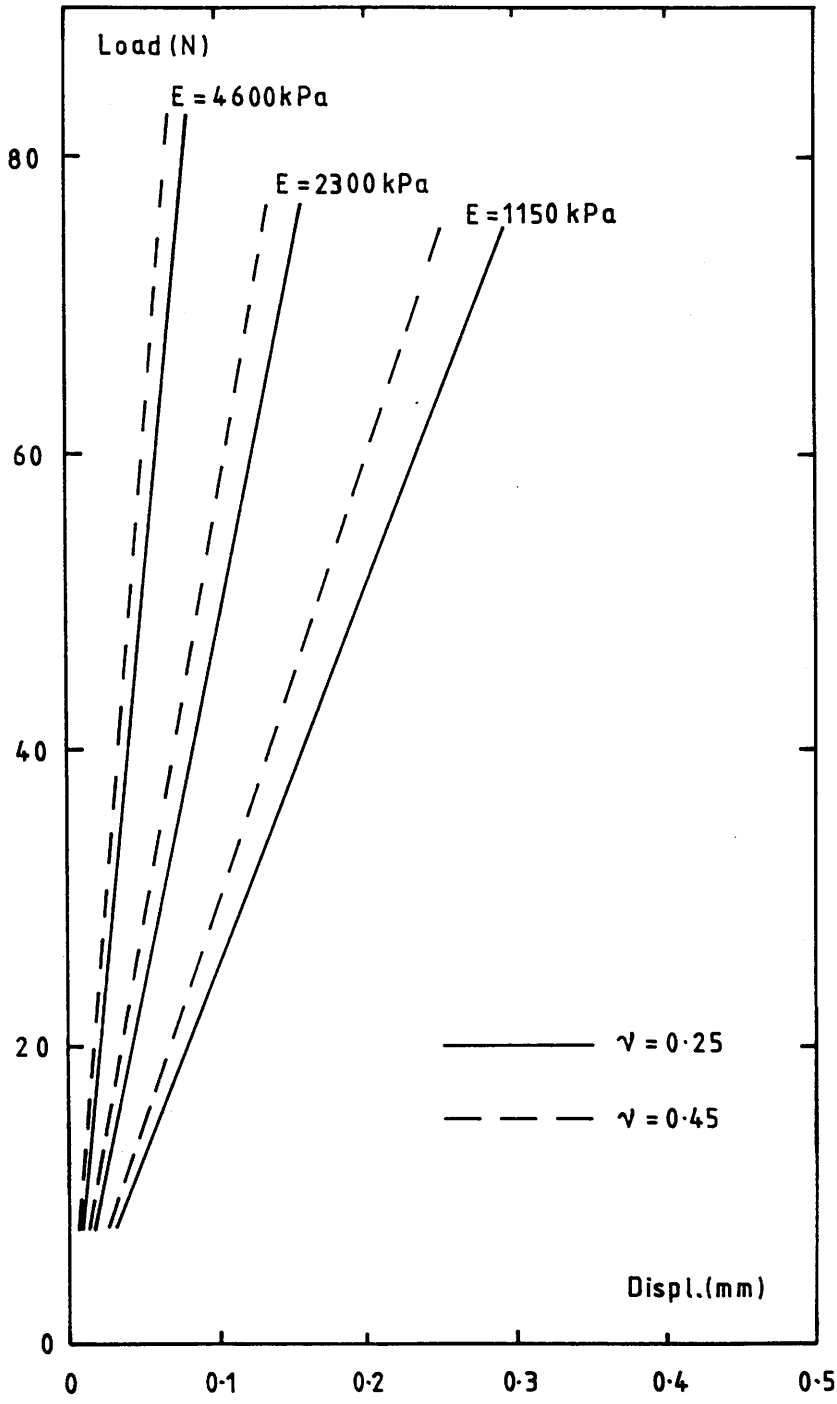

FIGURE 5.6(a) - Elastic Analysis: Effect of varying E and ν on load-displacement ($^{D}/_{B}$ = 2.0)

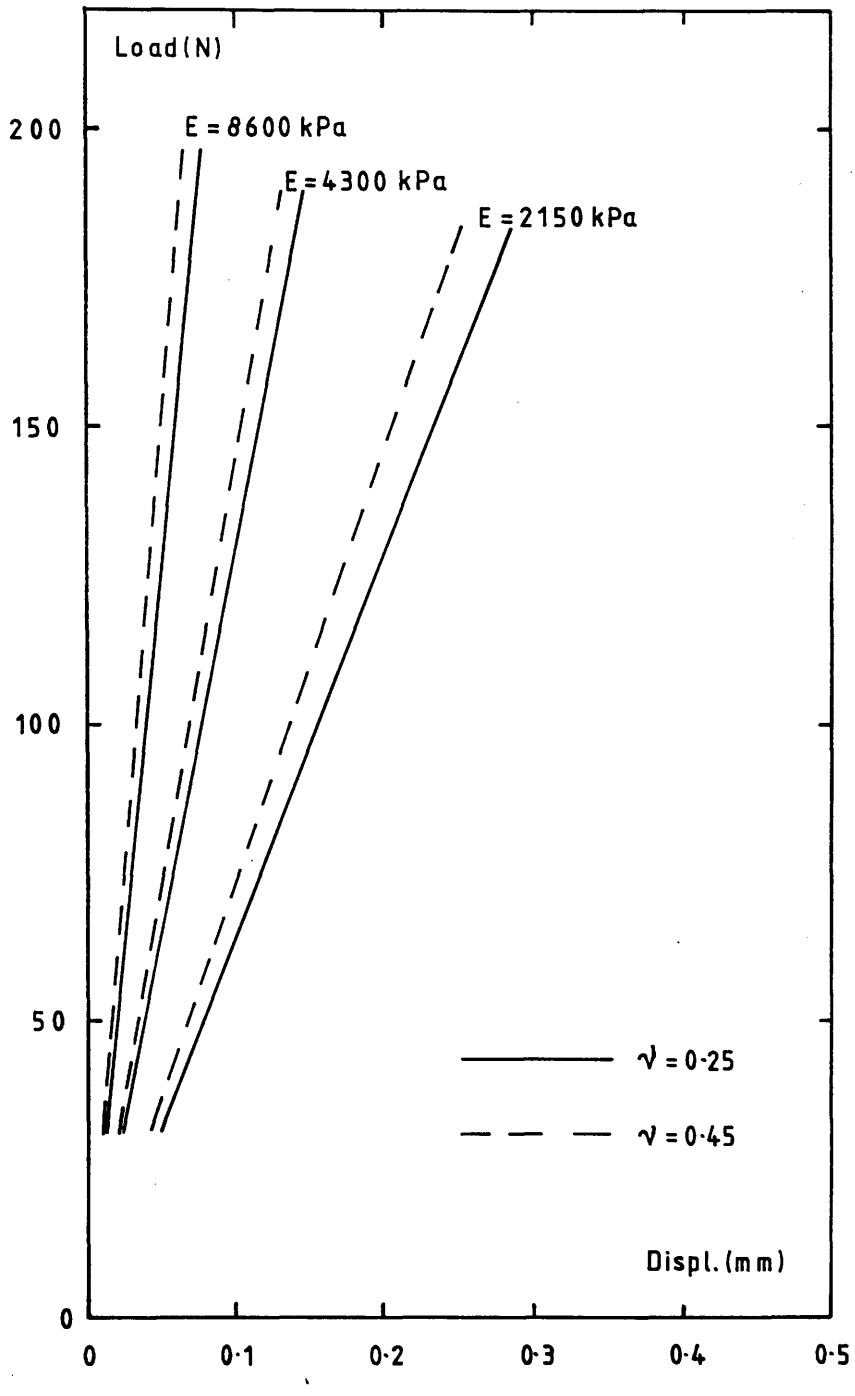

FIGURE 5.6(b) - Elastic Analysis: Effect of varying E and ν on load-displacement. ($^{D}/_{B}$ = 4.5).

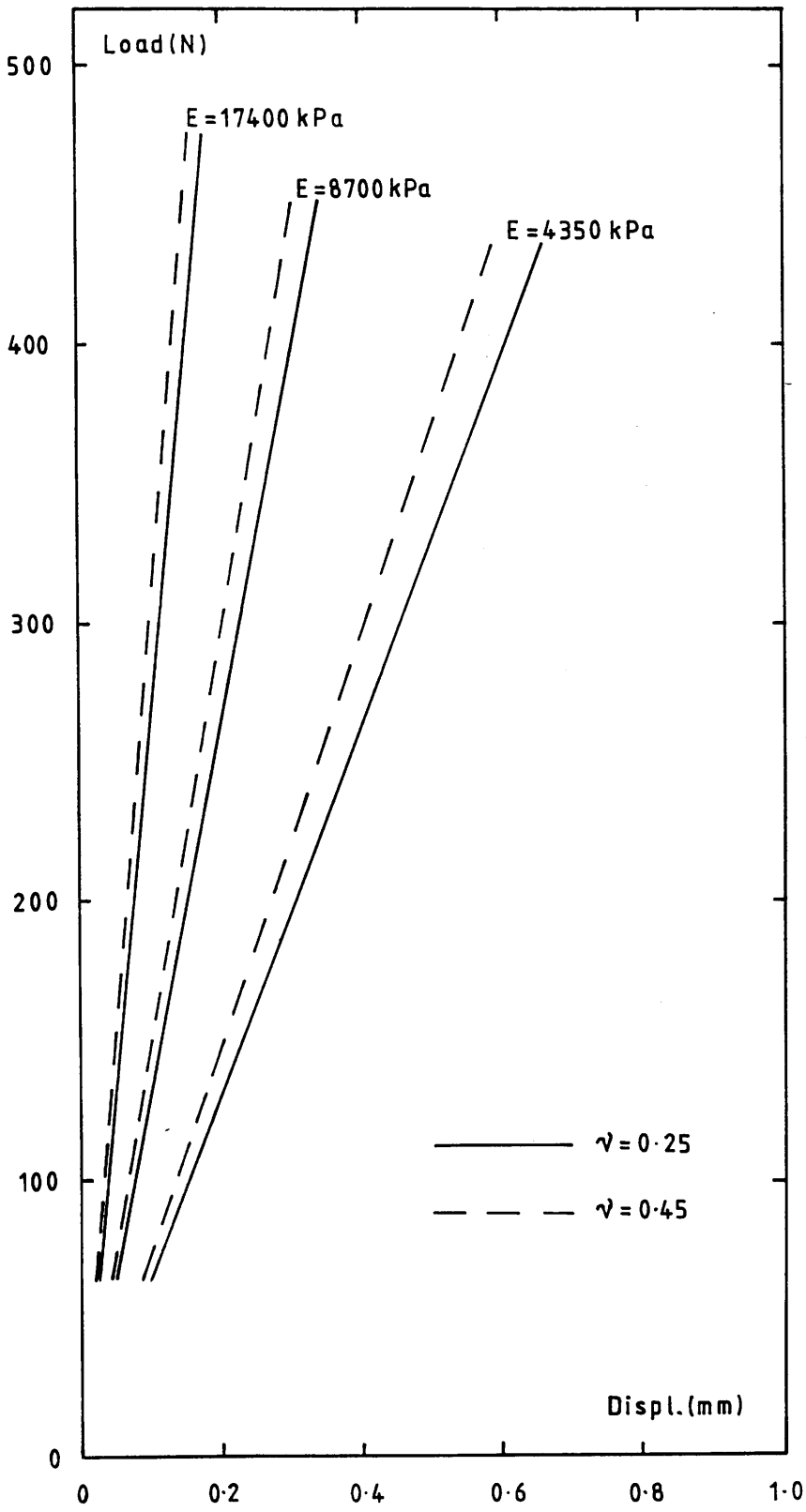

FIGURE 5.6(c) - Elastic Analysis: Effect of varying E and ν on load-displacement. ($^{D}/_{B}$ = 6.0).

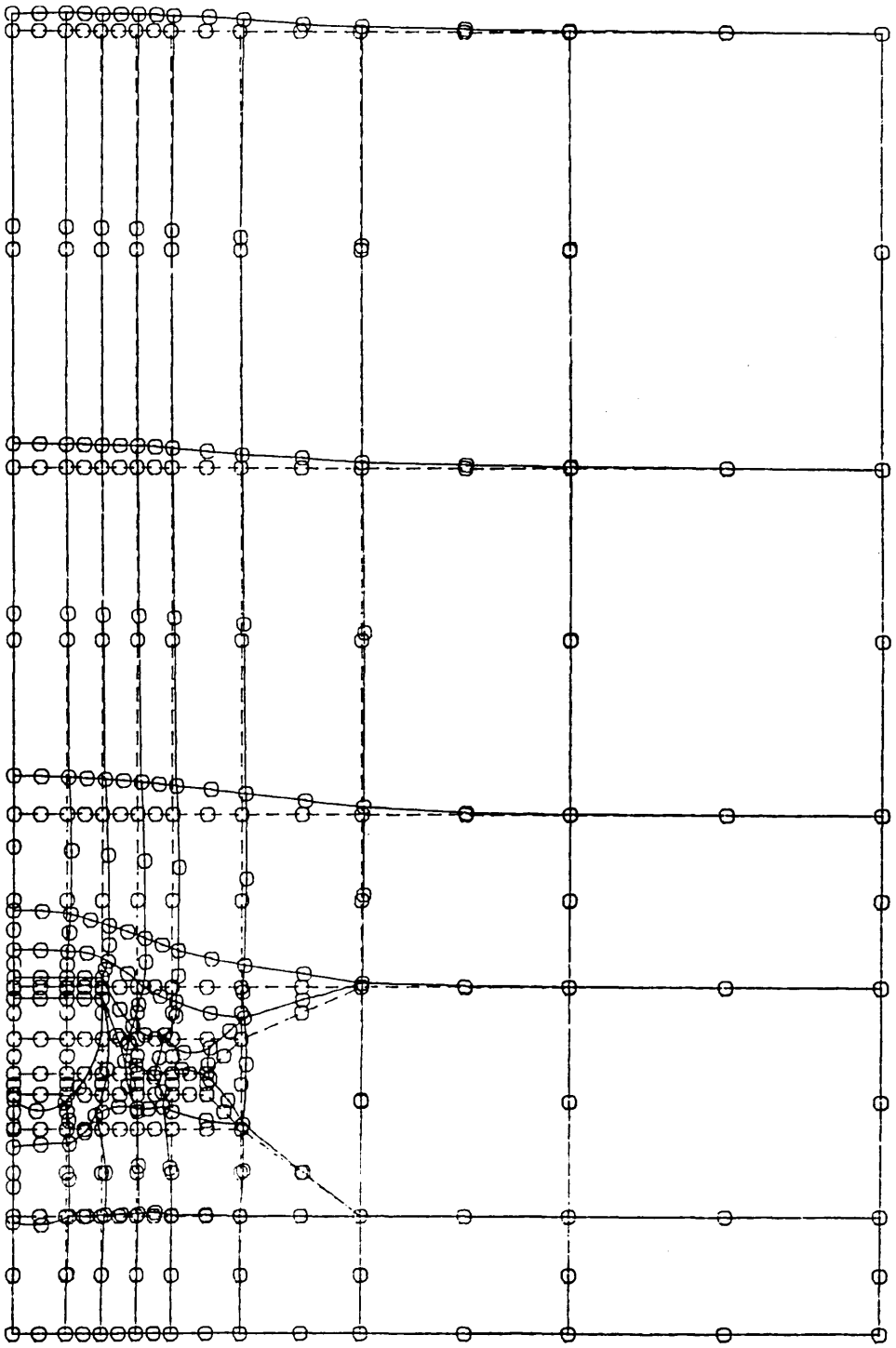

FIGURE 5.7 - Elastic Analysis: Deformed mesh for $D/B = 6.0$.
Anchor displacement = 0.38 mm.
(E = 8700 kPa, ν = 0.25, P = 500N).

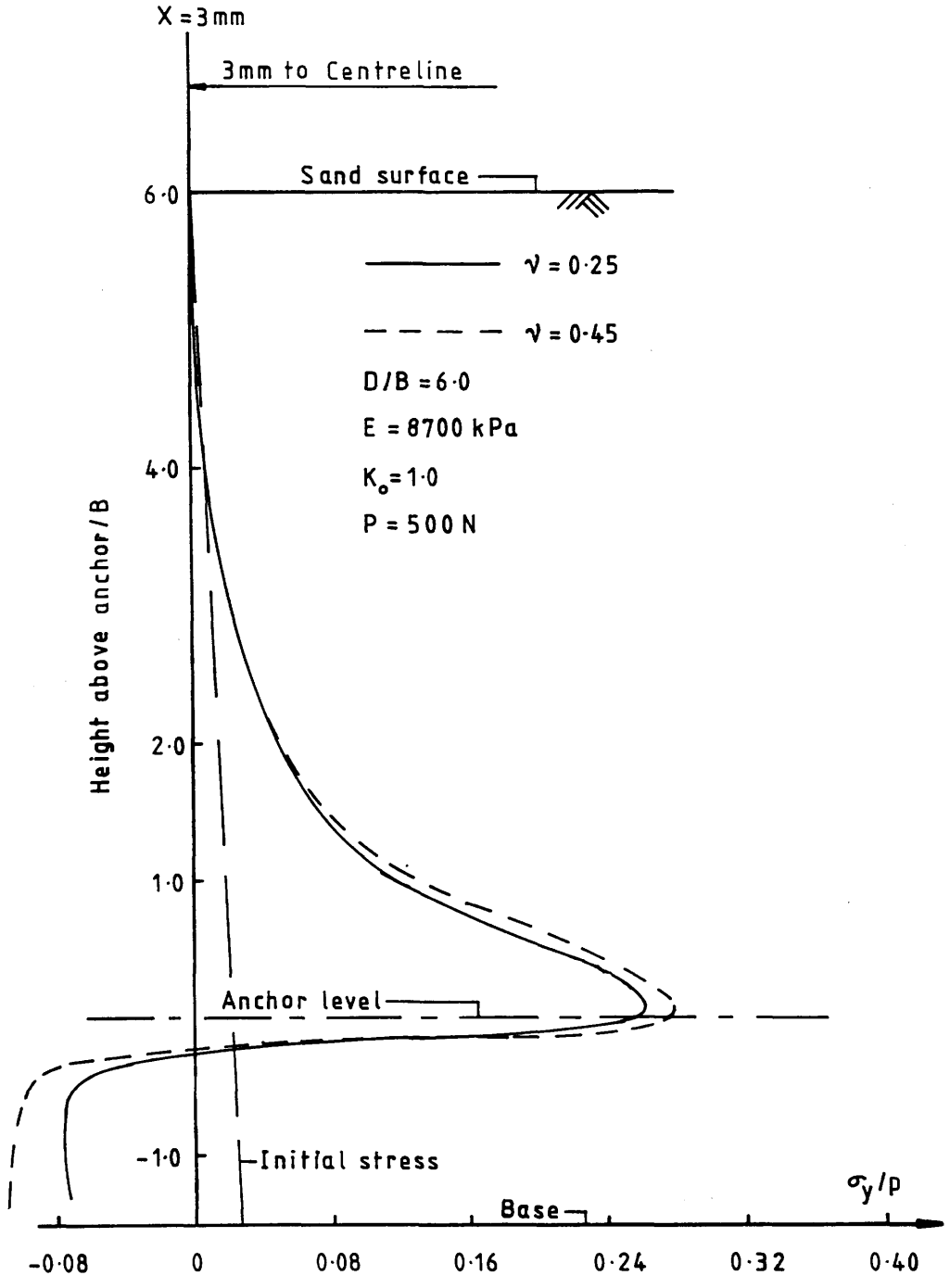

FIGURE 5.8 - Elastic Analysis: Variation of vertical normal stress on vertical plane at x = 3 mm.

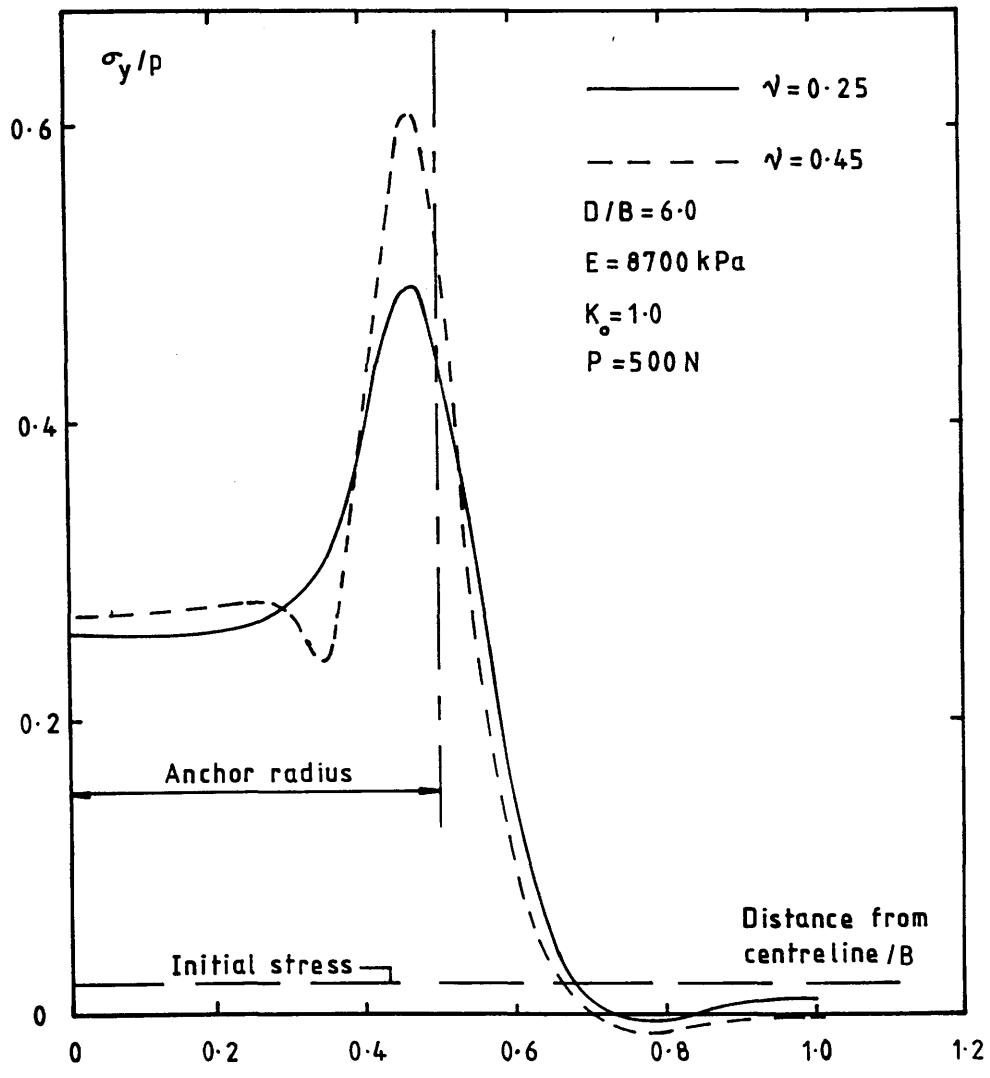

FIGURE 5.9 - Elastic Analysis: Variation of vertical normal stress on a horizontal plane 2 mm above the anchor.

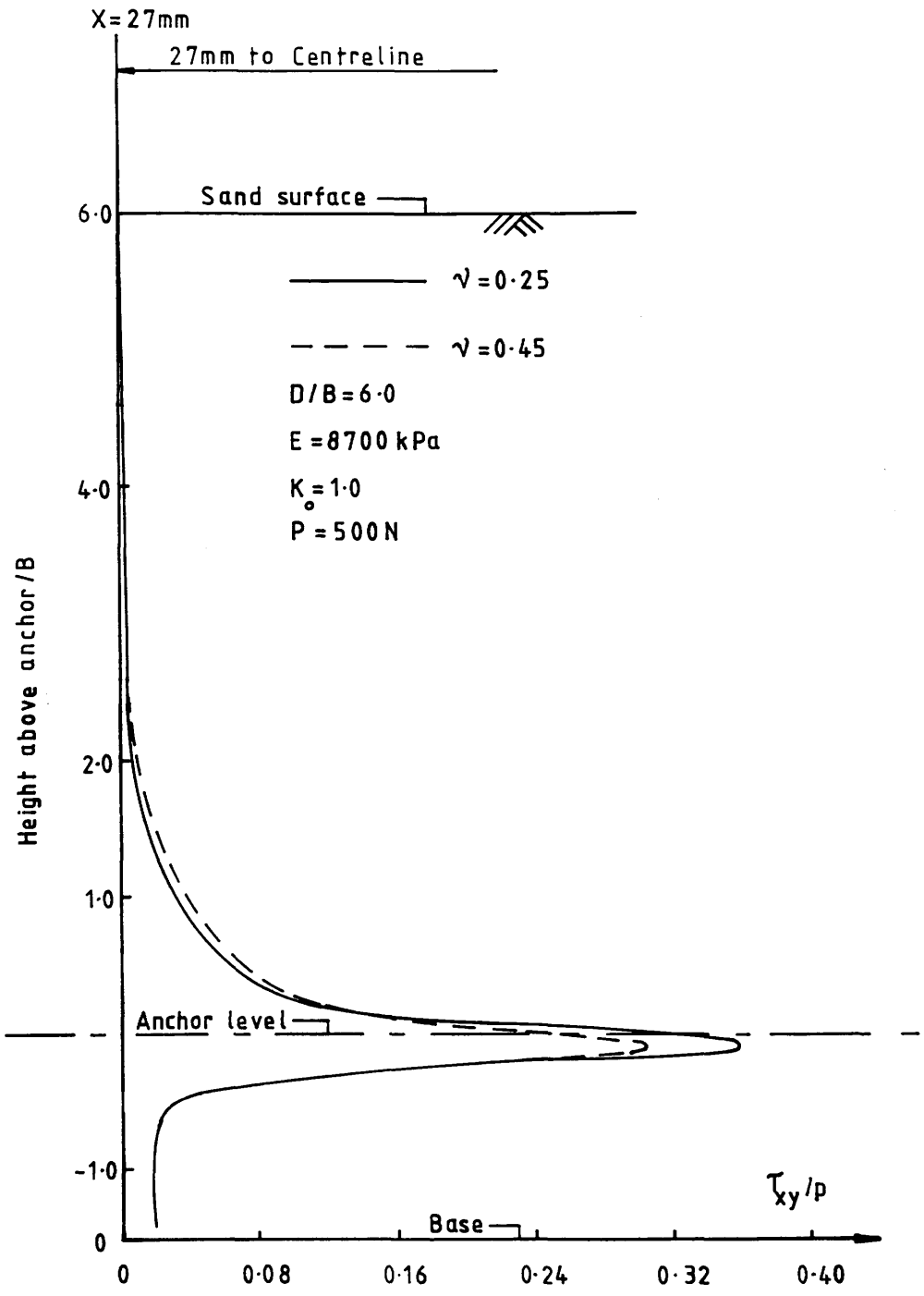

FIGURE 5.10 - Elastic Analysis: Variation of shear stress on vertical plane at x = 27 mm.

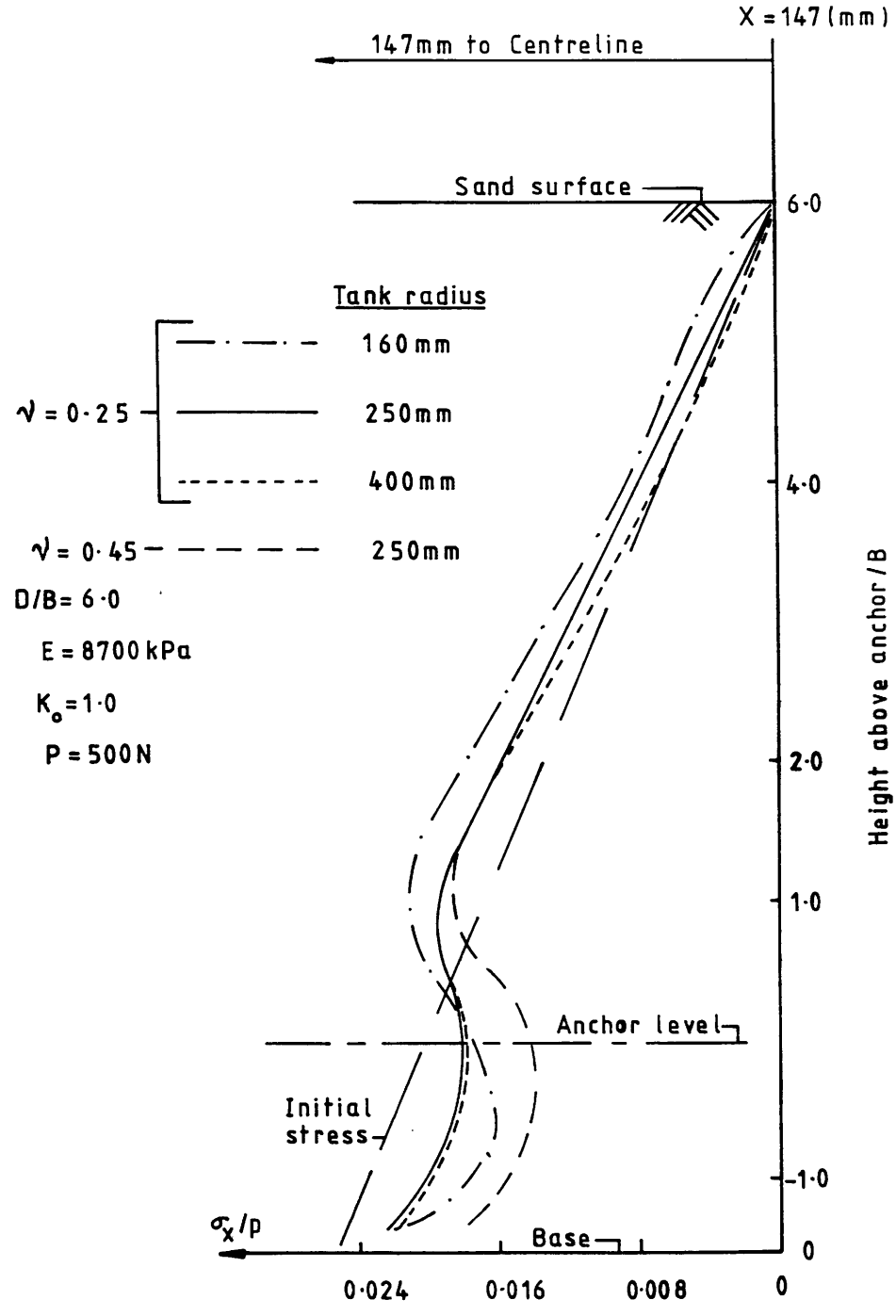

FIGURE 5.11 - Elastic Analysis: Horizontal stresses at position x = 147 mm for different tank radii.

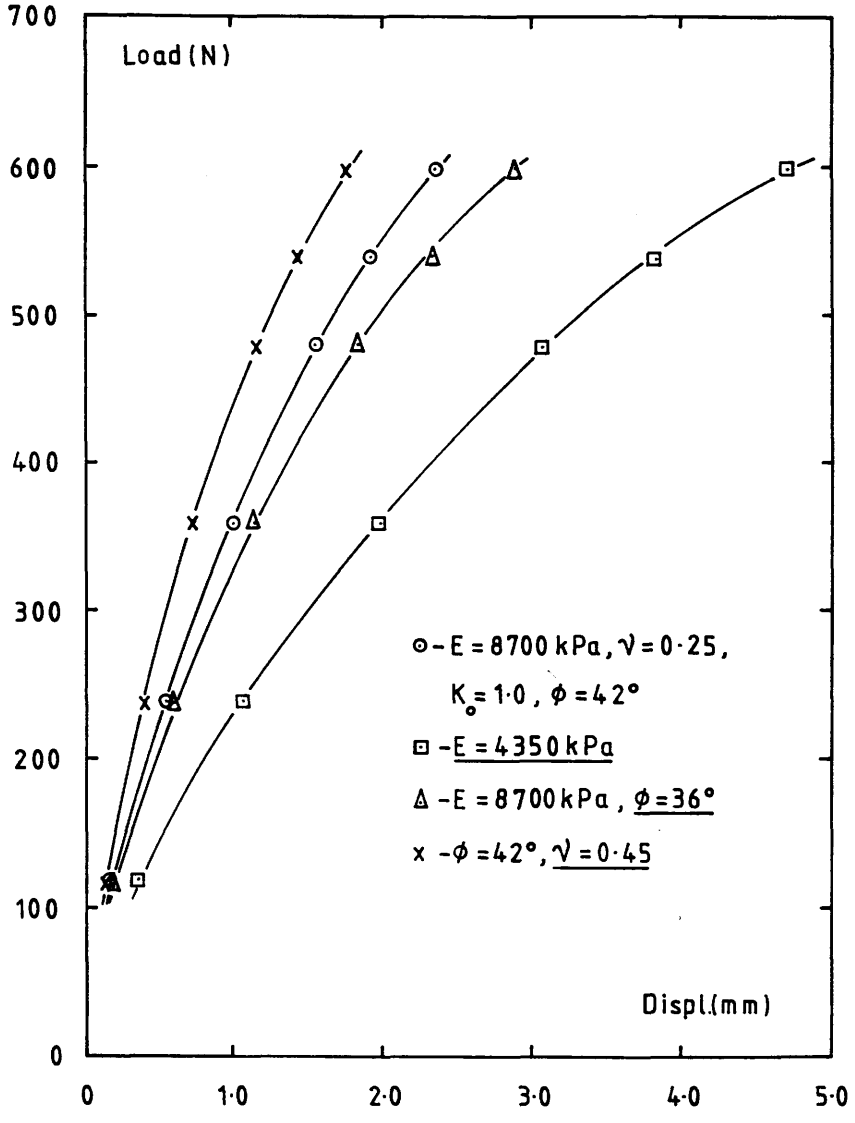

FIGURE 5.12 - Bi-linear Analysis: Effect of varying E, ν or φ on load-displacement ($^{D}/_{B}$ = 6.0).

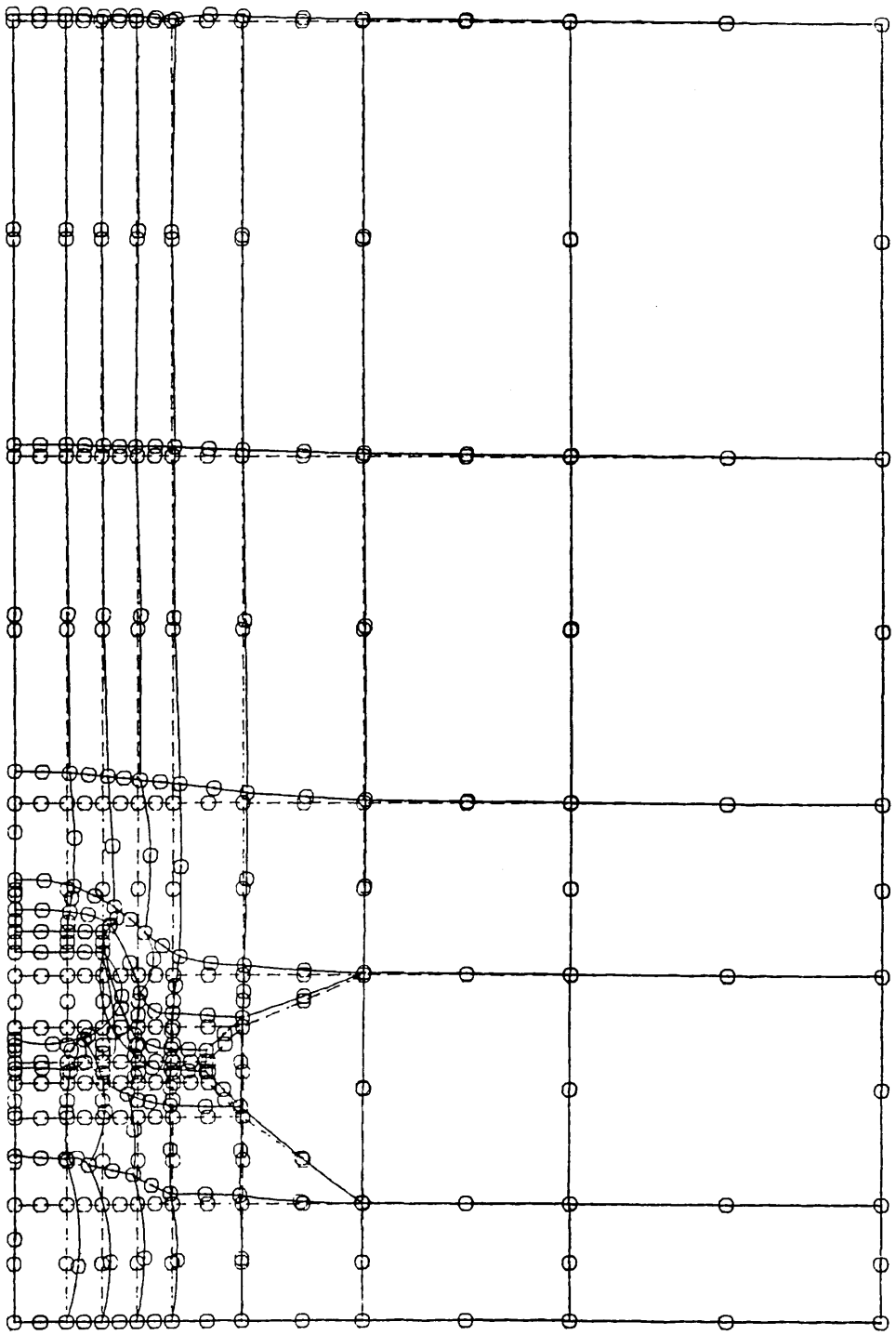

FIGURE 5.13 - Bi-linear Analysis: Deformed mesh for D/B = 6.0. Anchor displacement = 1.7 mm (P = 500N, E = 8700 kPa, ν = 0.25, ϕ = 42°, K_o = 1.0).

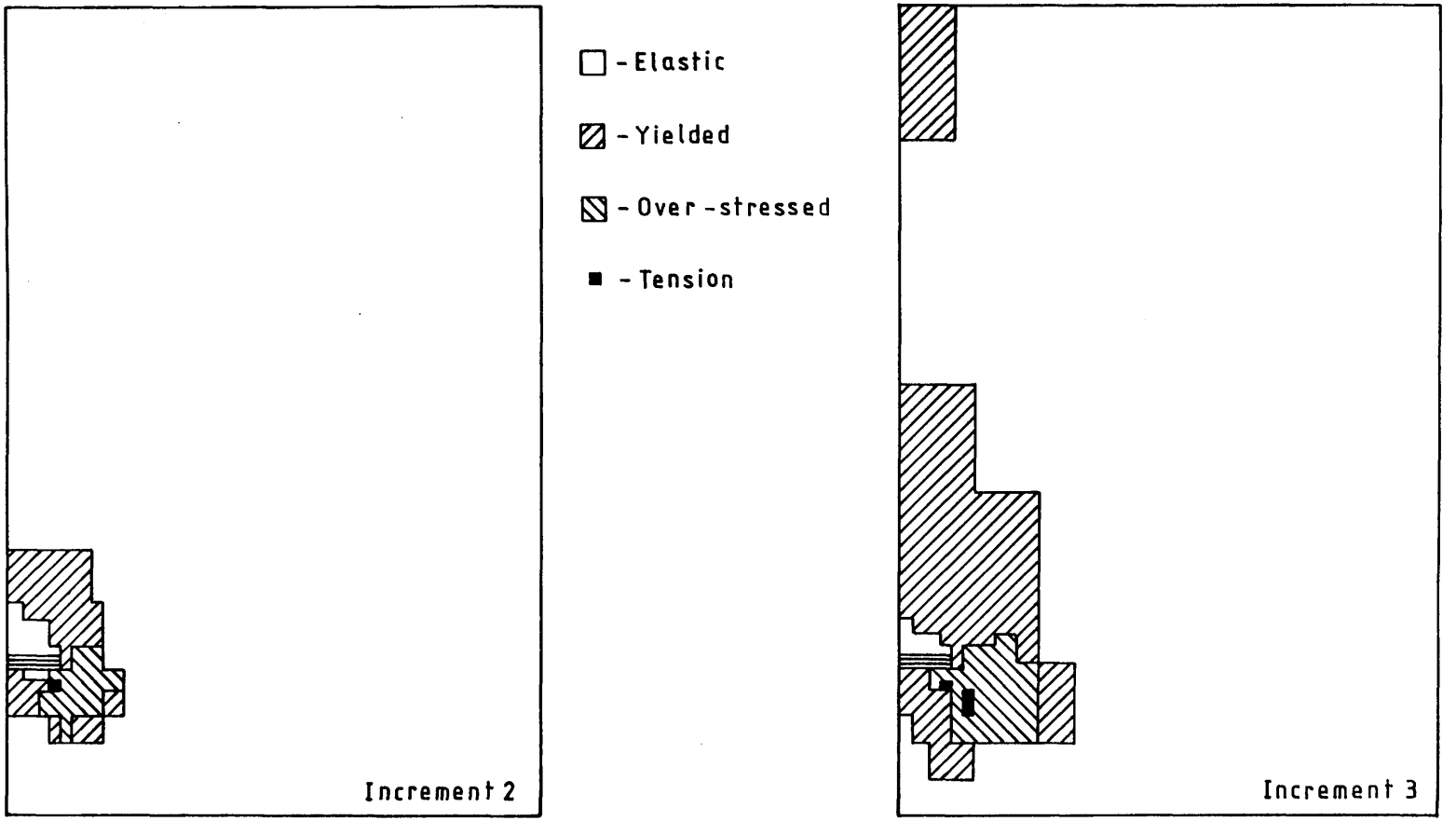

FIGURE 5.14 - Bi-linear Analysis: Progression of yield for $^{D}/_{B}$ = 6.0, ν = 0.25, ϕ = 42°, E = 8700 kPa.

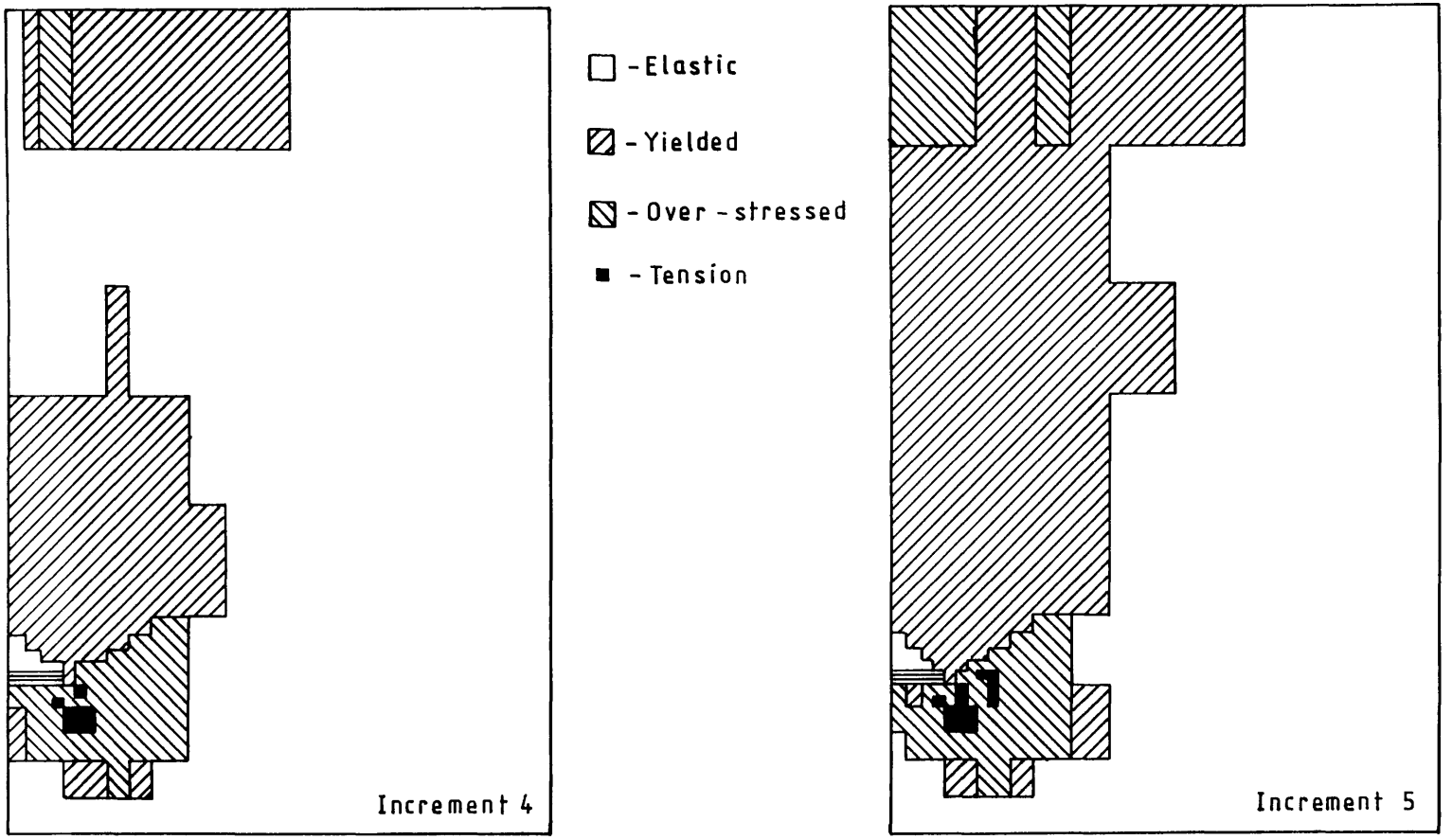

FIGURE 5.14 (cont'd.)

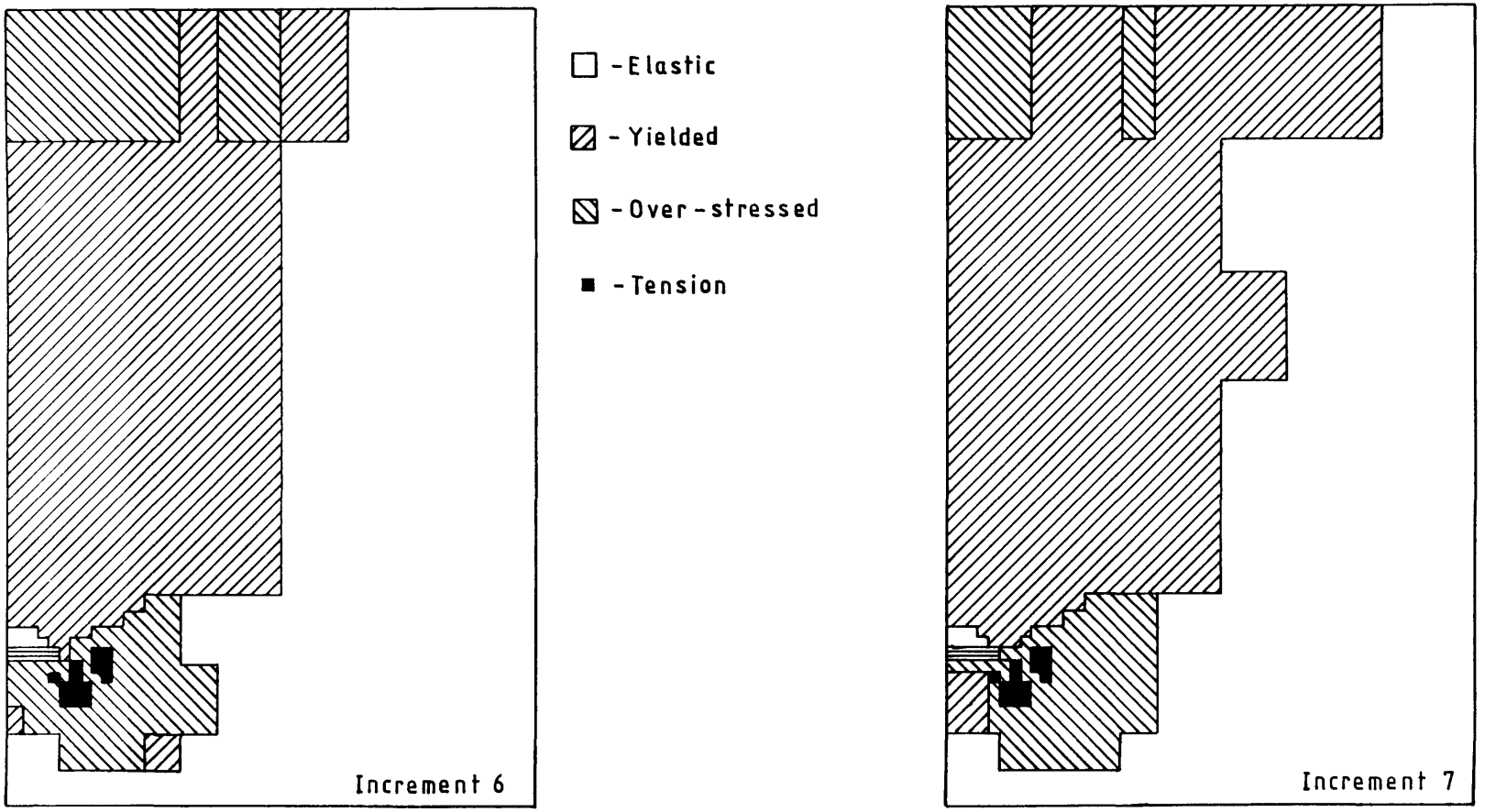

FIGURE 5.14 (cont'd).

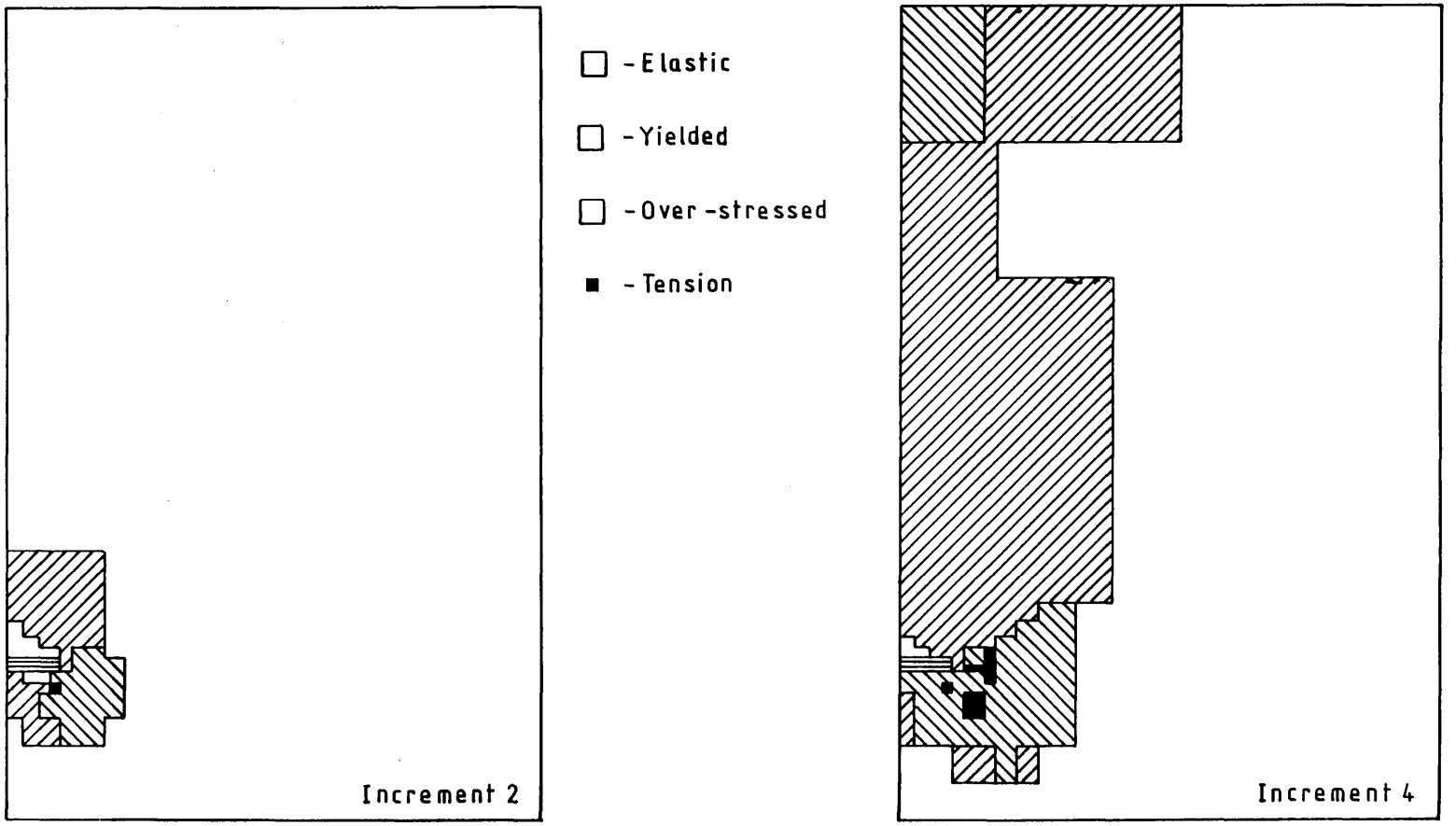

FIGURE 5.15 - Bi-linear Analysis: Progression of yield for $^{D}/_{B}$ = 6.0, ν = 0.25, ϕ = 36°, E = 8700 kPa.

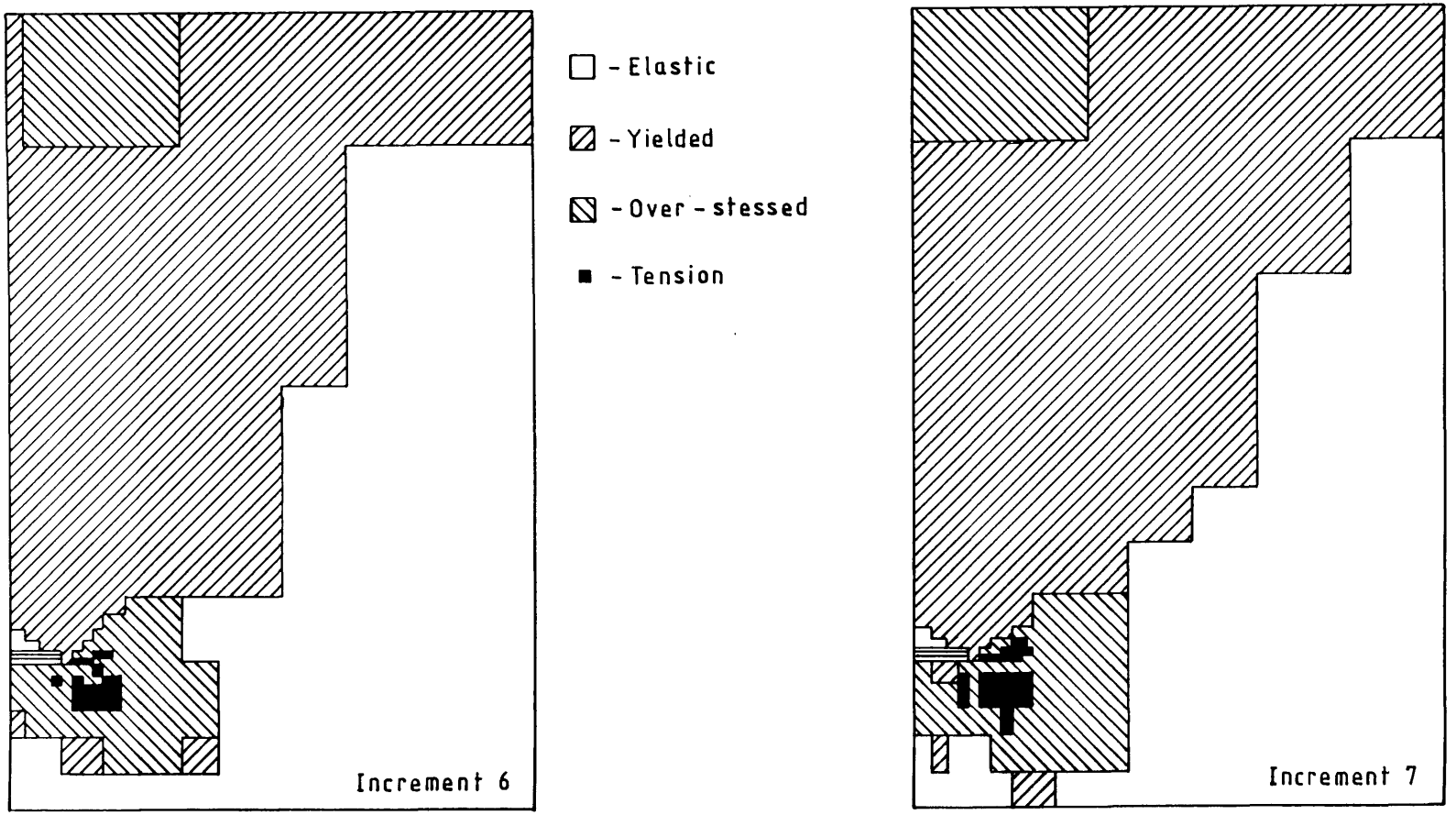

FIGURE 5.15 (cont'd).

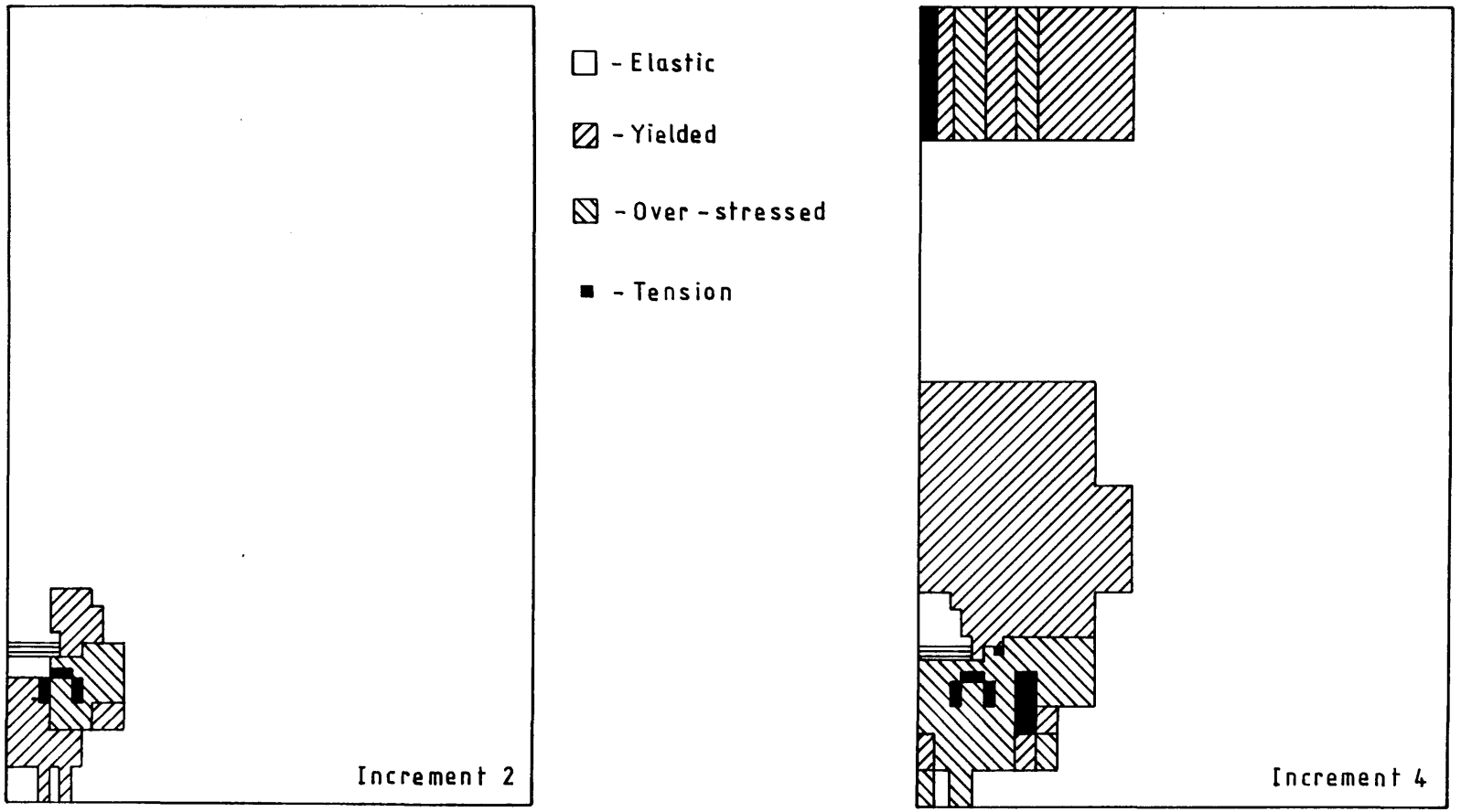

FIGURE 5.16 - Bi-linear Analyais: Progression of yield for $^{D}/_{B}$ = 6.0, ν = 0.45, ϕ = 42°, E = 8700 kPa.

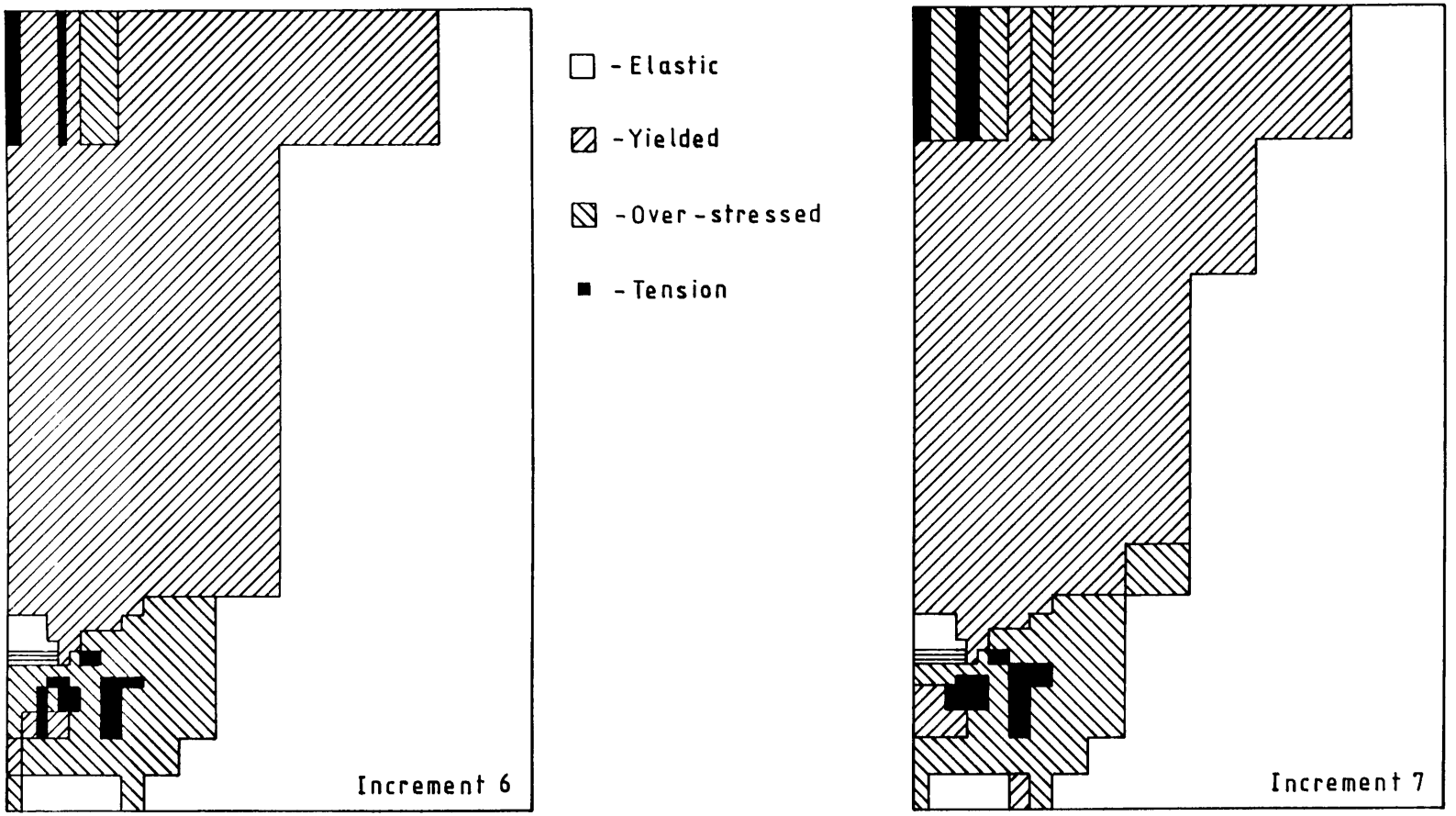

FIGURE 5.16 (contd).

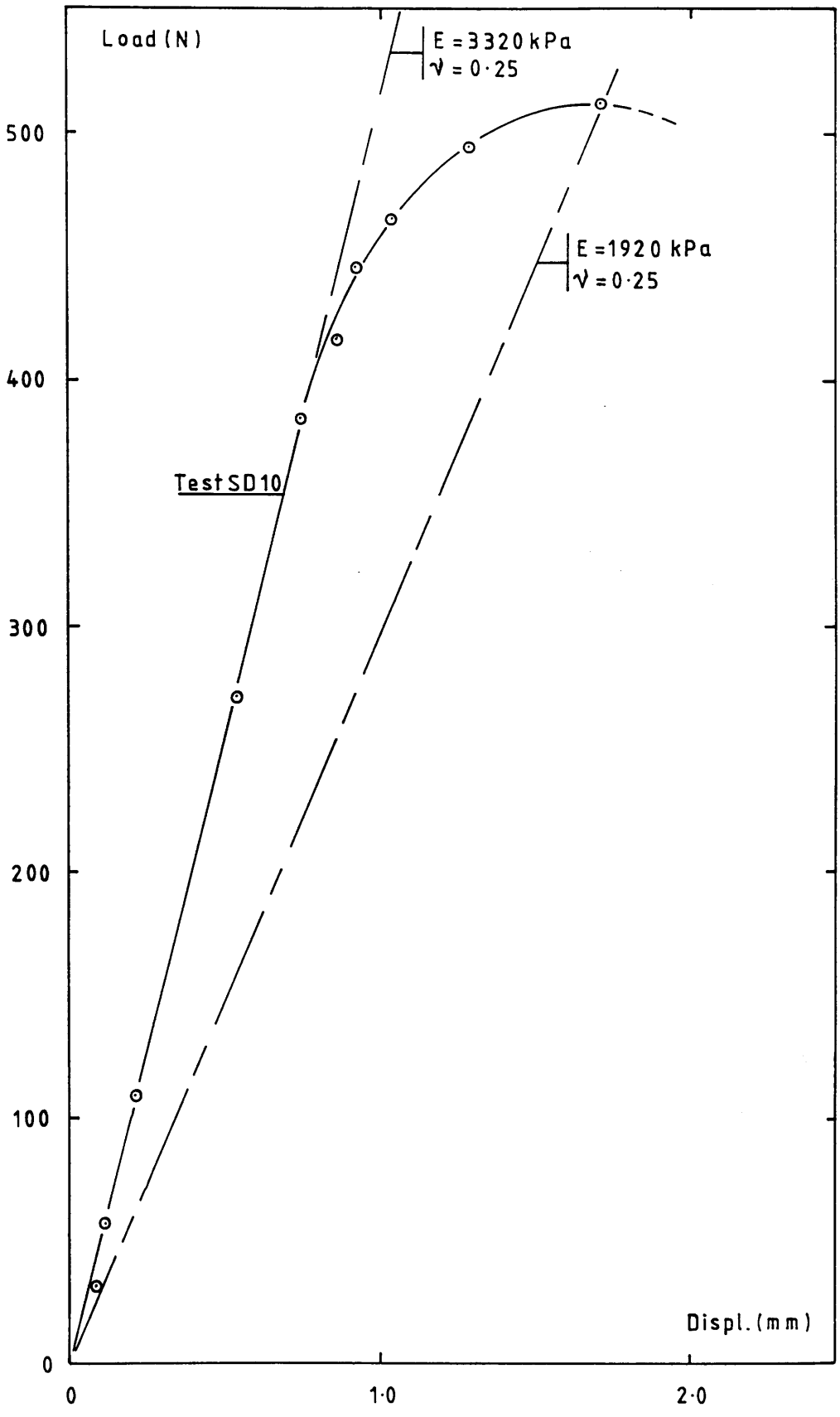

FIGURE 5.17 - Load-diaplacement relationship: Comparison between test SD 10 and elastic analysis ($^{D}/_{B}$ = 6.0).

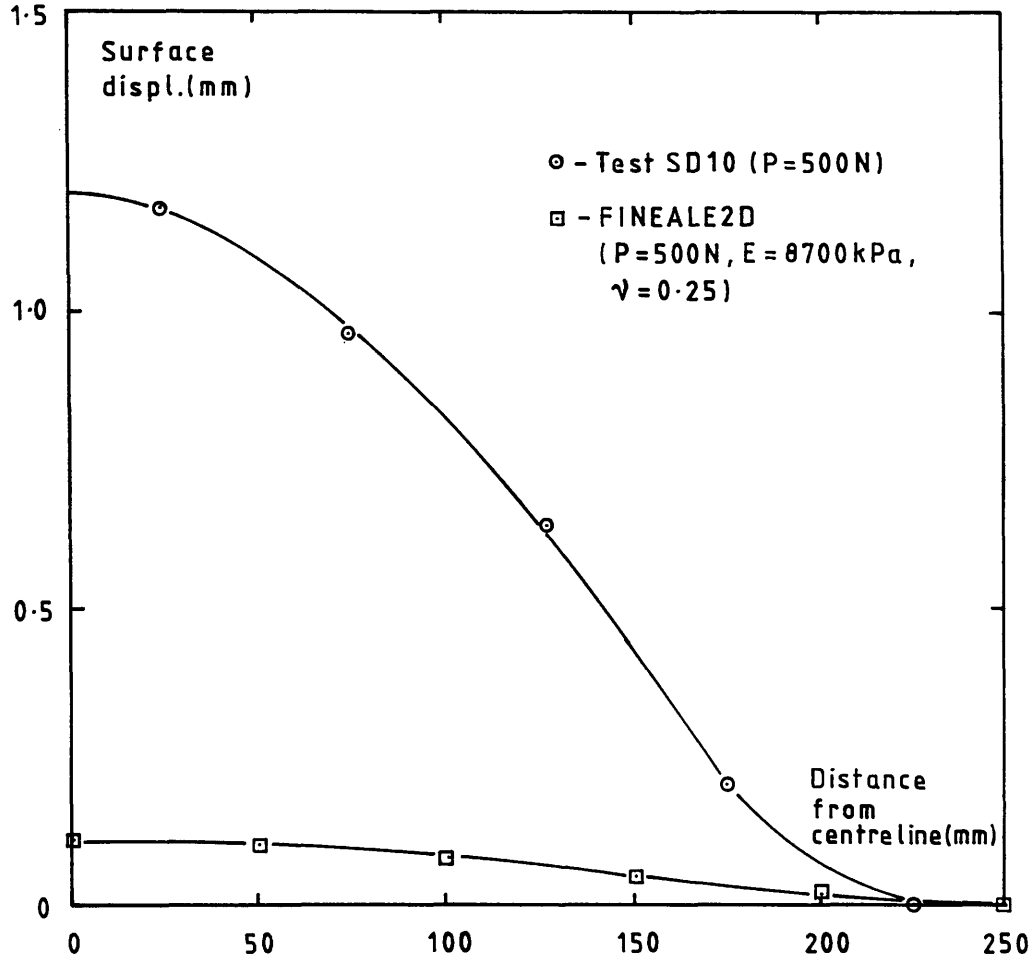

FIGURE 5.18 - Surface displacements: Comparison between test SD 10 and elastic analysis ($^{D}/_{B}$ = 6.0).

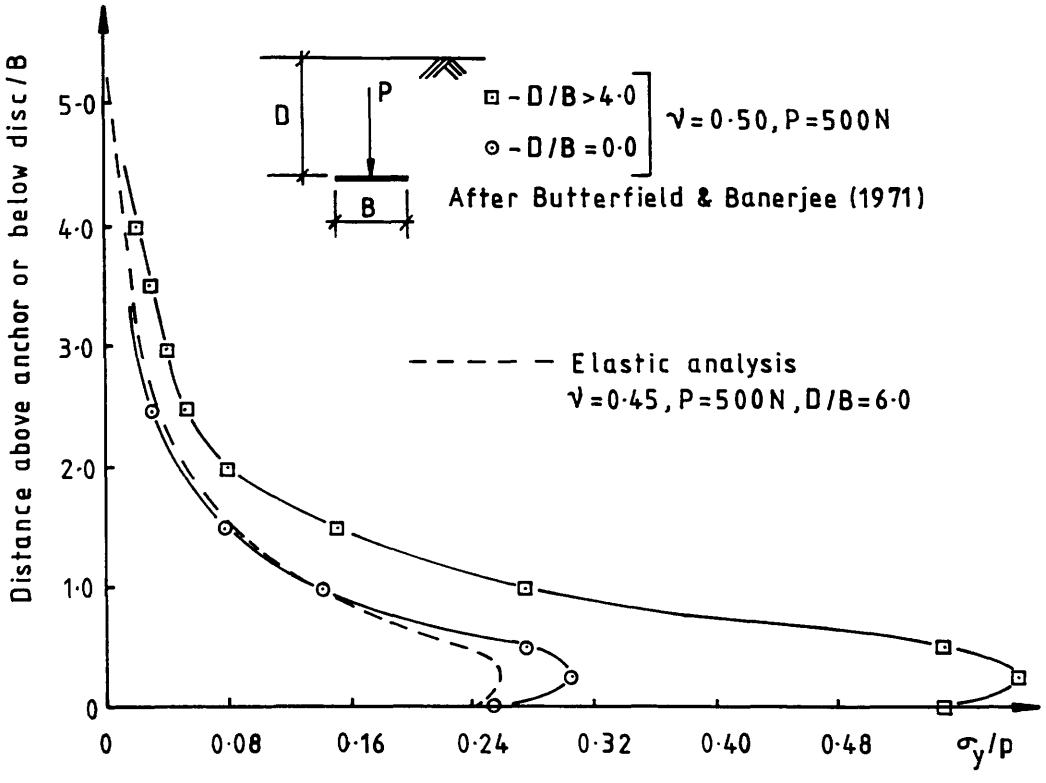

FIGURE 5.19 - Elastic Analysis: Comparison of vertical normal stress above an anchor and below a rigid disc.

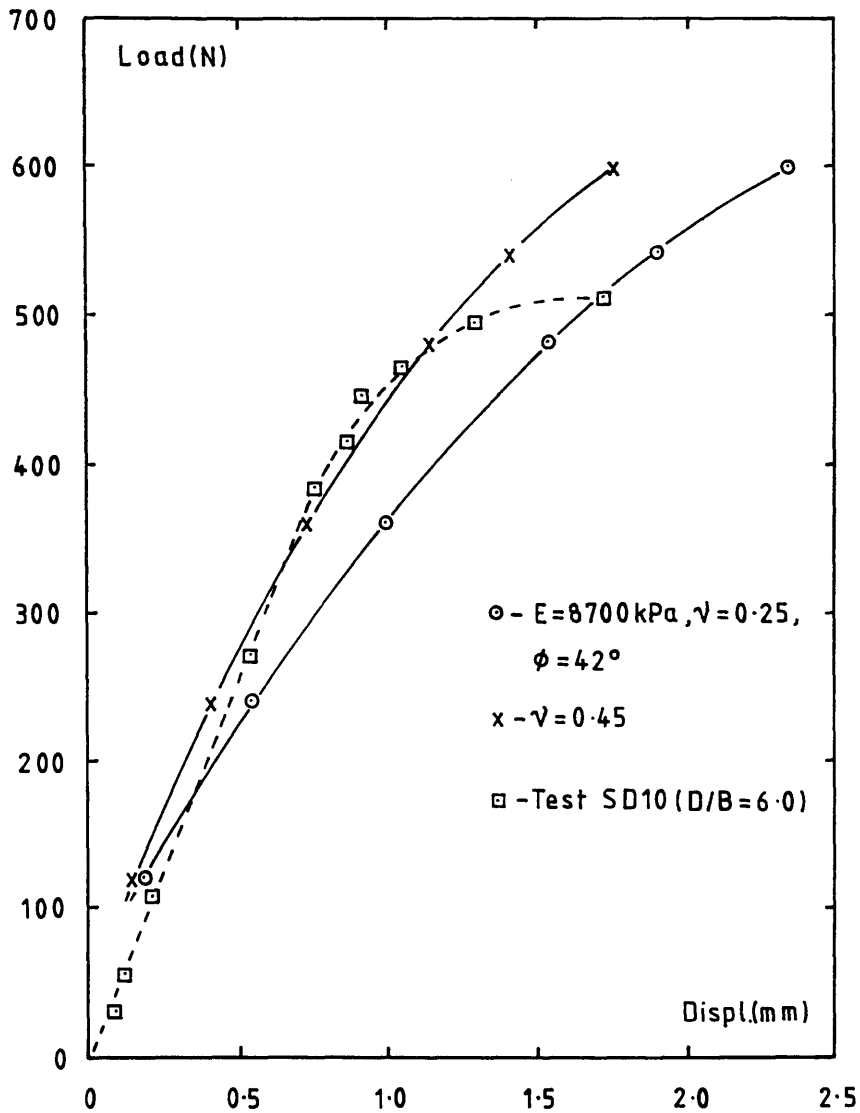

FIGURE 5.20 - Load-displacement relationship: Comparison between test SD 10 and bi-linear analysis ($^{D}/_{B}$ = 6.0).

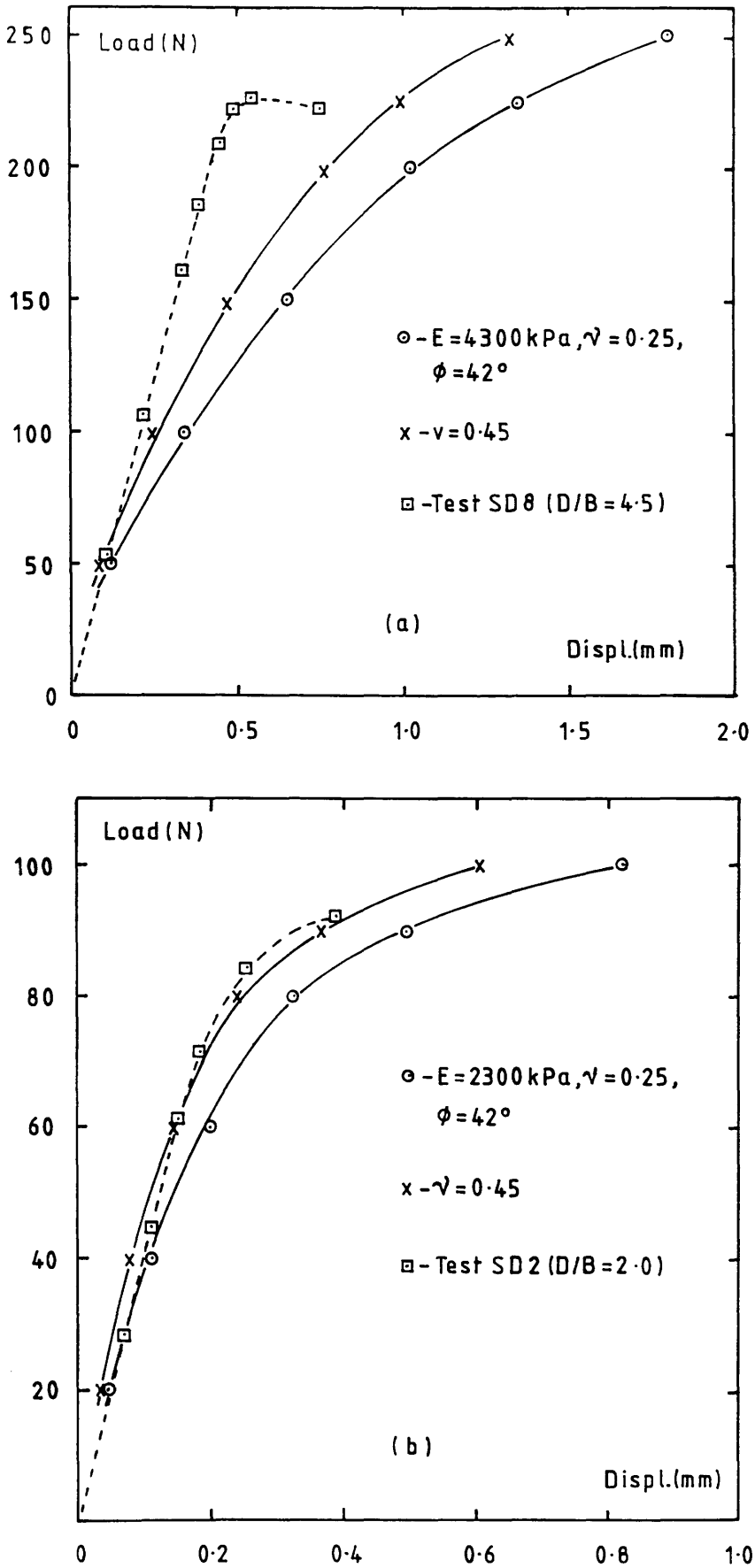

FIGURE 5.21 - Load-displacement relationship: Comparison between bi-linear analysis and (a) test SD 8 ($^{D}/_{B}$ = 4.5) and (b) test SD 2 ($^{D}/_{B}$ = 2.0).

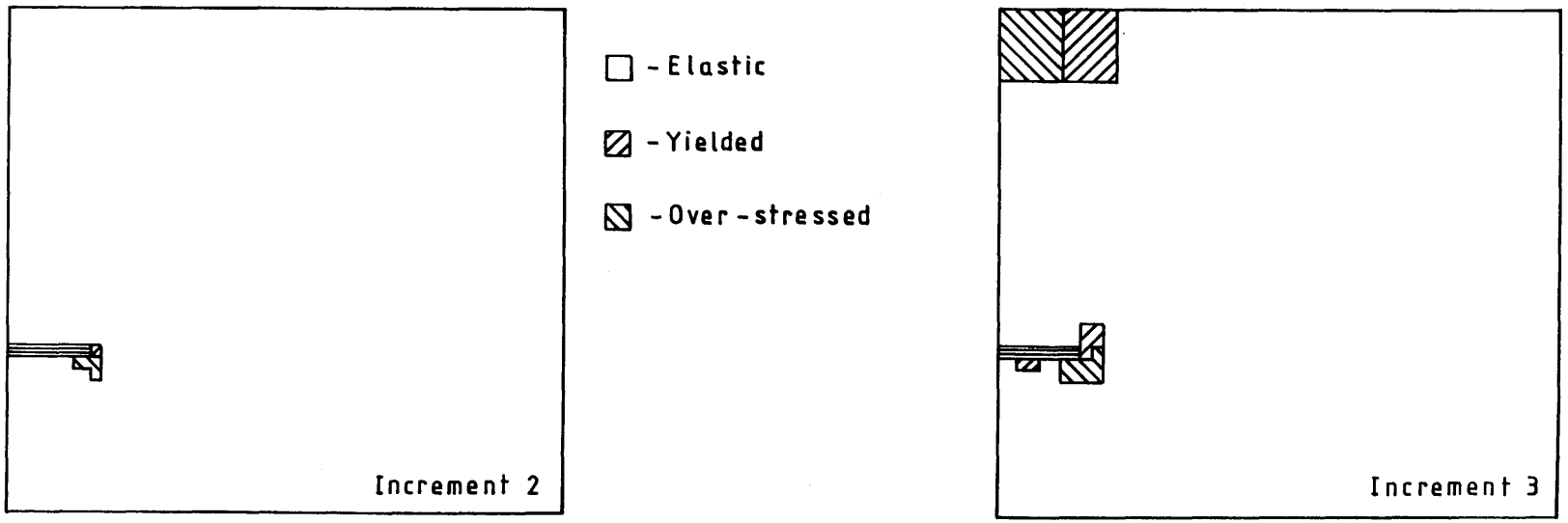

FIGURE 5.22 - Bi-linear Analysis: Progression of yield for $^{D}/_{B}$ = 2.0, ν = 0.25, ϕ = 42°, E = 8700 kPa.

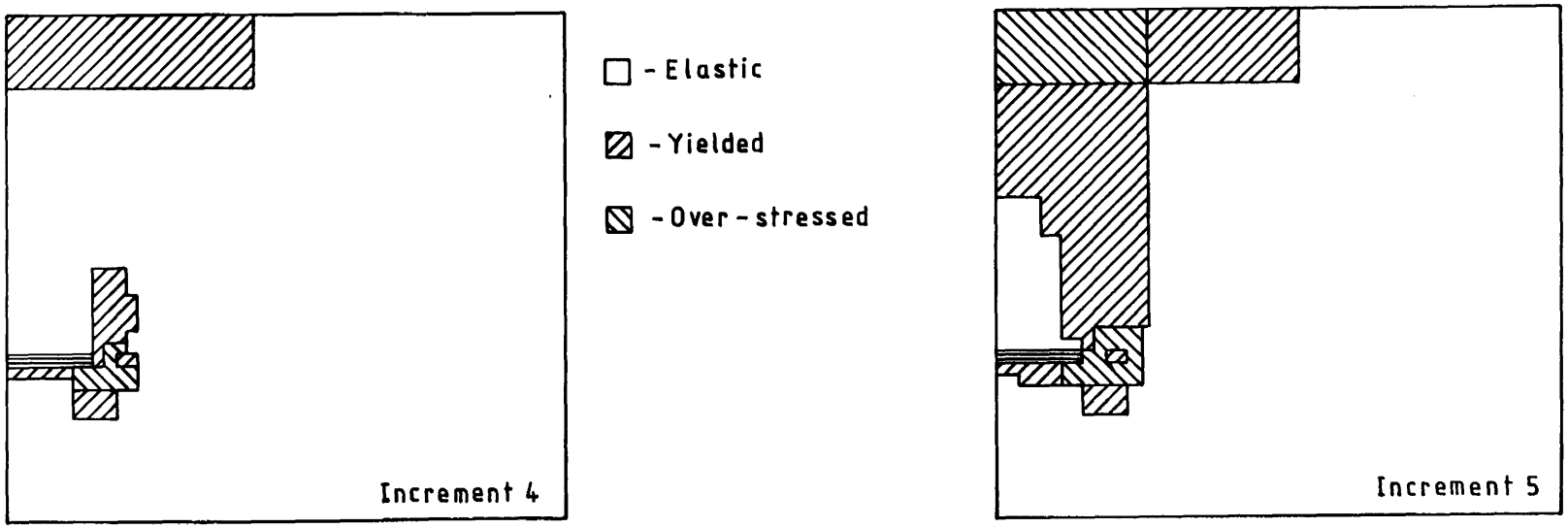

FIGURE 5.22 (cont'd).

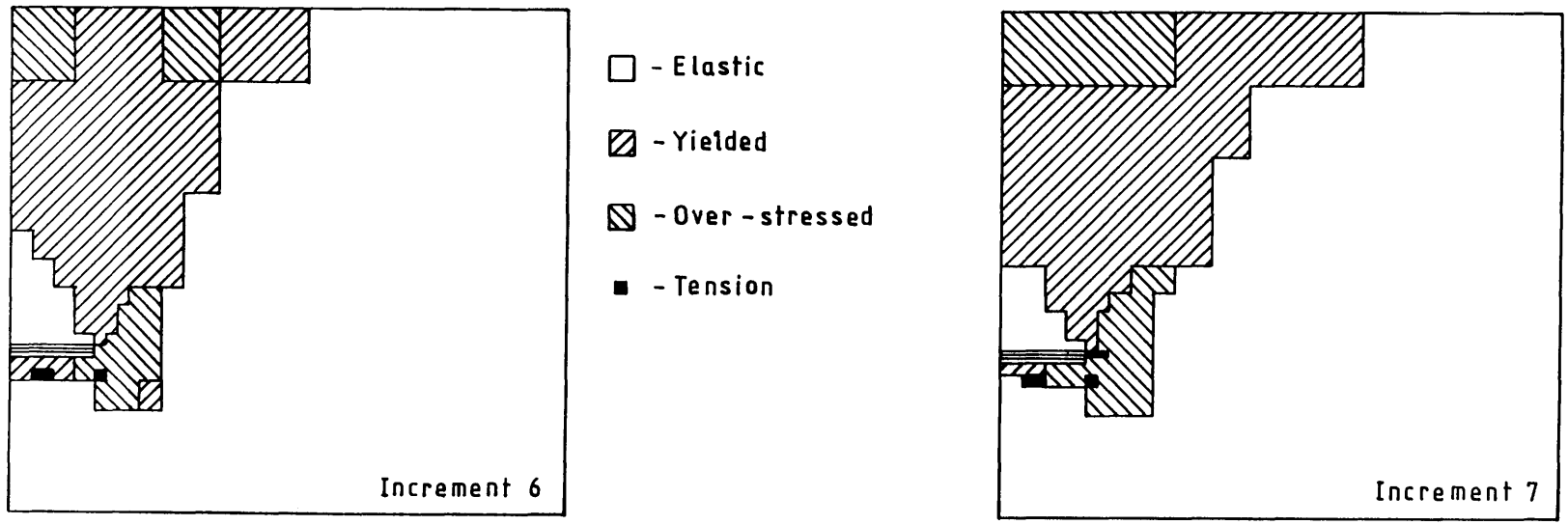

FIGURE 5.22 (cont'd).

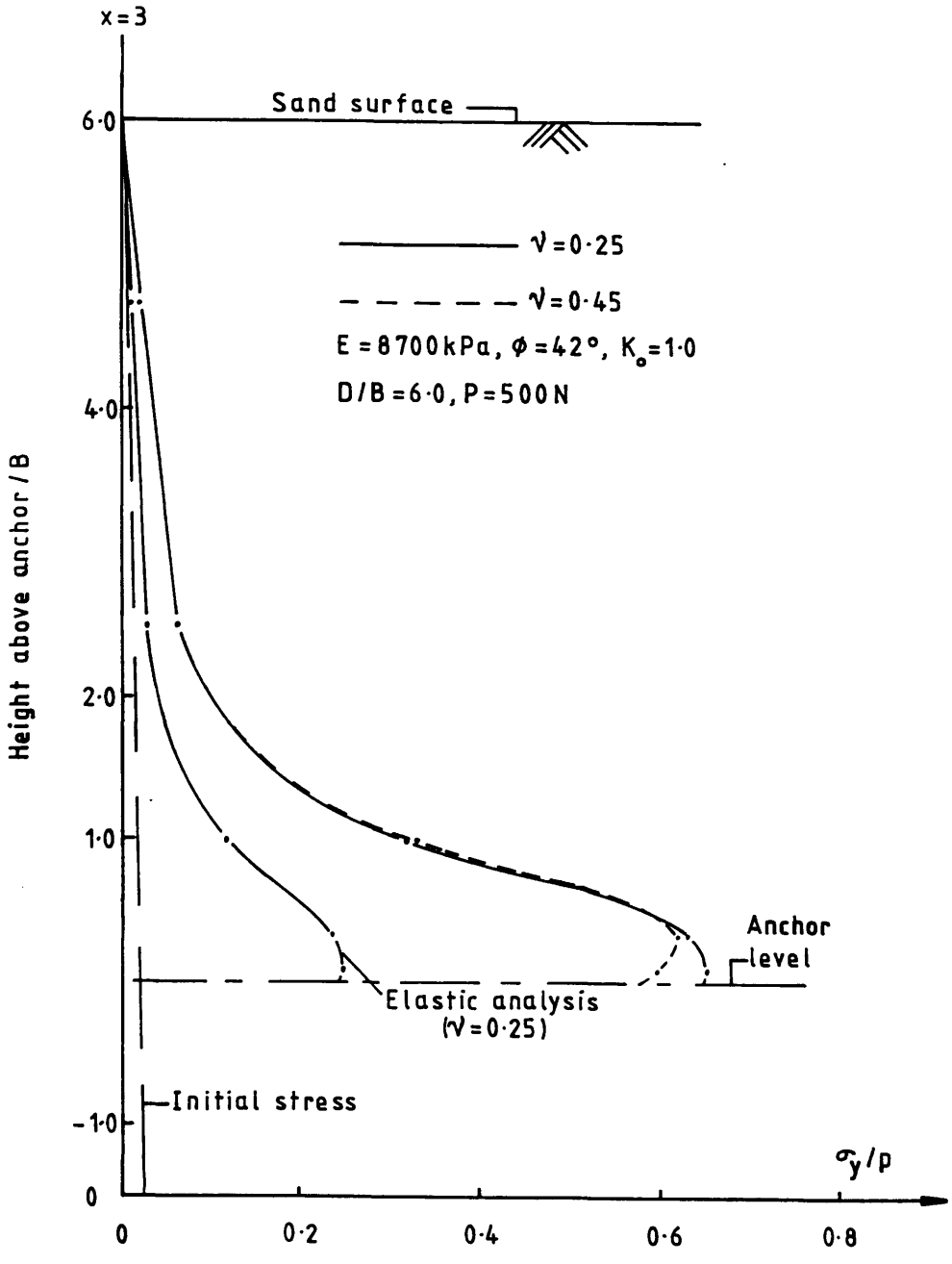

FIGURE 5.23 - Bi-Linear Analysis: Variation of vertical normal stress on vertical plane at x = 3 mm.

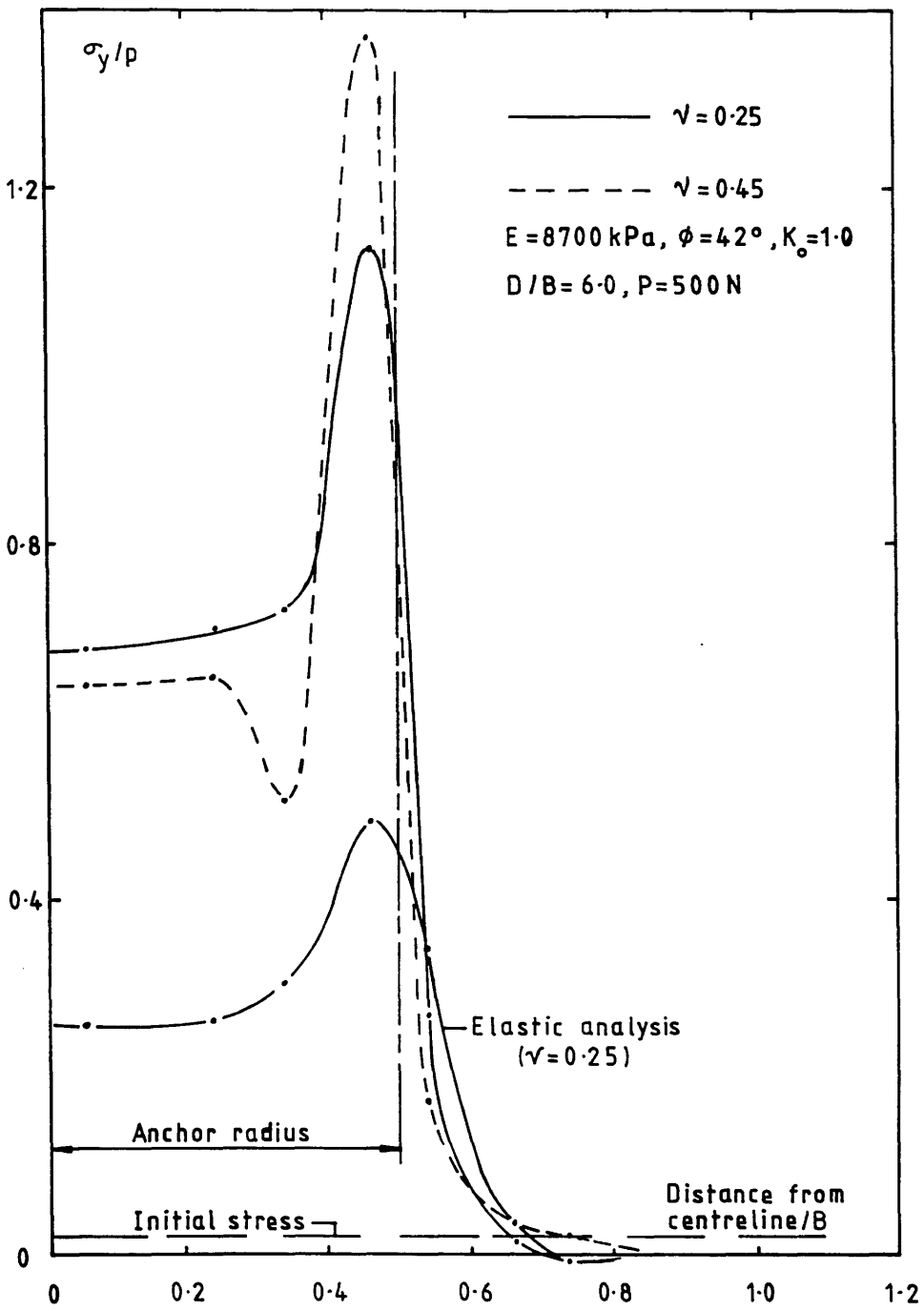

FIGURE 5.24 - Bi-linear Analysis: Variation of vertical normal stress on a horizontal plane 2 mm above the anchor.

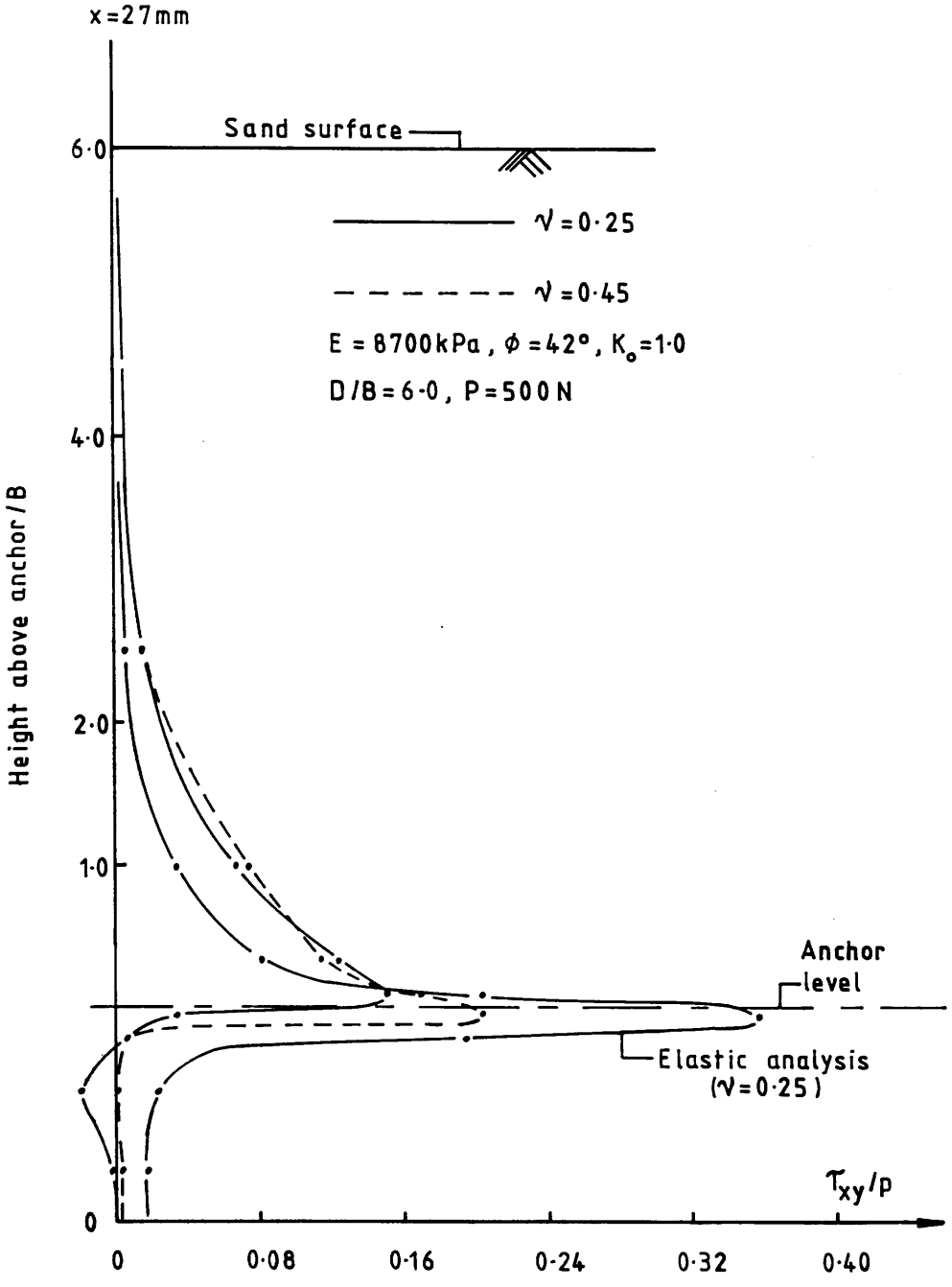

FIGURE 5.25 - Bi-linear Analysis: Variation of shear stress on vertical plane at x = 27 mm.

CHAPTER 6 – DISCUSSION

6.1 INTRODUCTION

The discussion encompasses the results of this and previous investigations into the static and cyclic loading of circular plate–type anchors buried in cohesionless soil. Firstly, the static loading behaviour is considered, including a subsection on boundary and scale effects associated with anchor uplift tests. Discussion on the cyclic loading behaviour follows, and this is principally concerned with the anchor displacement and how it is affected by the form of loading applied to the anchor. Hysteresis effect, post–cyclic loading behaviour and the effect of sand density are also considered.

Conclusions are listed in Chapter 7, together with suggestions for further investigations.

6.2 STATIC LOADING

6.2.1 General

Using the standard plot of uplift factor (N_u) versus embedment ratio (D/B), Figure 6.1 compares the author's results in dense sand with those of previous investigations at Glasgow University which used the same grade of Leighton–Buzzard sand. The density and relative density (to the nearest whole number) for each set of results are given in Figure 6.1.

For the results of Hutchison (1982), Zakaria (1986) and the author, there is very good agreement up to an embedment ratio of approximately 8. The discrepancies in N_u at greater embedment ratios are associated with boundary and scale effects (see sub–section 6.2.2)

The results of Fadl (1981) reflect the lower relative density of the sand, giving consistently lower values of uplift factor for the range of embedment depths considered.

The influence of relative density is again obvious in the results for medium–dense sand shown in Figure 6.2, in which Fadl's N_u values for $D_r = 50\%$ are considerably lower than Zakaria's for $D_r = 68\%$. The results of

Hutchison, Wang (1986) and the author, at D_r values of 60%, 58% and 59%, respectively, show good agreement for embedment ratios up to 10.5, the maximum used in the present study.

Figure 6.3 shows how the author's test results in dense and medium–dense sand compare with the range of previous investigations presented by Andreadis (1979), and referred to in Chapter 2 (see Figure 2.15, page 67). For the most part the results are comfortably within the range defined in Figure 6.3, only moving outwith the top of the range at embedment ratios greater than eight. These particularly high values of uplift factor are the result of boundary effects in the dense sand anchor tests. (see below) Also shown in Figure 6.3 are the shallow anchor theoretical curves after Fadl (1981), for dense sand ($\varphi = 42^0, D_r = 93\%$) and medium–dense sand ($\varphi = 36^0$, $D_r = 59\%$). The dense sand curve is in good agreement with the author's test results, up to an embedment ratio of 8. The correspondence for medium–dense sand begins to deteriorate for $D/B > 4.0$. The relationship between Fadl's theoretical curves and those of other authors was discussed in Chapter 2.

6.2.2 Boundary and Scale Effects

The presence of boundary and scale effects in model anchor tests was highlighted in Chapter 2. Results from previous investigations indicated that boundary effects were related to the ratio of container diameter to anchor diameter, B_c/B. Below a limiting value of B_c/B, boundary effects resulted in an increase in uplift resistance factor with decreasing B_c/B. Boundary effects diminished considerably for anchors with $D/B < 10$, approximately.

Scale effects depended primarily on the anchor diameter, B, which was used in terms of the dimensionless parameter B/d_{50}, the ratio of anchor diameter to average grain size for the sand. Below a limiting value of B/d_{50}, scale effects resulted in an increase in N_u with decreasing B/d_{50} (or B, for any given sand). Scale effects became more severe as the embedment ratio increased.

These conclusions are illustrated clearly in Figures 6.4. and 6.5, which plot the uplift resistance factor, N_u, against anchor diameter, B, for tests in dense Leighton–Buzzard sand. The points plotted in these figures were taken from the results of the author's tests and those undertaken by Hutchison (1982), and are listed in Table 6.1. Where duplicate tests were carried out, the

average value of N_u has been plotted. The density and relative density of the sand used in both sets of tests were very similar. The number adjacent to each of the points is the ratio of B_c/B for that test, rounded to the nearest whole number.

Considering firstly Figure 6.4, a scale effect is evident for anchors at D/B= 6.0 and D/B= 8.0. This results in an increase in N_u as the anchor diameter reduces. (The ratio B/d_{50} reduces from 63 to 31). No scale effect is evident for an anchor at D/B= 2.0 and $B/d_{50} > 83$. The comparisons made earlier using Figure 6.1 are not invalidated by this effect, at least not up to embedment ratios of D/B= 8.0, approximately. In this region, the scale effect is relatively small and, in any case, many of the test results were obtained using identical anchor diameters at the same (or similar) embedment ratios. Referring to the values of B_c/B shown in Figure 6.4, there is no evidence of boundary effects at any of the embedment ratios considered (D/B= 2.0, 6.0, 8.0).

This is certainly not the case in Figure 6.5, where the results for anchors at D/B= 10.0 and D/B= 12.0 exhibit substantial boundary effects. Assuming that a constant value of B_c/B implies no change in boundary effects, and a constant value of B implies no change in scale effects, the separate contributions of boundary and scale effects can be assessed from Figure 6.5 and Table 6.1. For D/B= 10.0 and B_c/B= 20, the scale effect between a 38mm diameter anchor and a 25mm diameter anchor leads to 16% increase in uplift resistance factor, from 124 to 144 (to nearest whole number). The parameter B/d_{50} reduces from 48 to 31. For the same embedment ratio and B= 38mm, the boundary effect between B_c/B= 20 and B_c/B= 13 increases N_u from 124 to 176 (42%).

Using the same comparative values for B_c/B and B, the scale and boundary effects for D/B= 12.0 increase N_u from 143 to 196 (37%), and from 143 to 209 (46%), respectively. The boundary effect for a 25mm diameter anchor between B_c/B= 30 and B_c/B= 20 increases N_u from 174 to 196 (13%).

The results confirm that both boundary and scale effects increase with embedment ratio. This characteristic was reported by Tsangarides (1978) and Ovesen (1981) for boundary and scale effects, respectively. In the present study, boundary effects disappeared below D/B= 8.0, approximately, whilst scale effects persisted down to embedment ratios of 6 or less. Boundary effects were evident even at B_c/B= 30, thus supporting the conclusion of Tsangarides (1978) and Andreadis et al (1981) that a large mass of sand is affected by anchor testing.

It is clear from the results presented that boundary and scale effects can have a considerable influence on the value of uplift resistance factor obtained from model anchor tests in dense sand. For deeply buried anchors ($D/B \geqslant 10$), the effects are particularly marked, making comparison between results of different investigations more uncertain than before. This is the case even for tests carried out in the same sand, as illustrated by the results presented in Figure 6.5.

There was insufficient data available to investigate boundary and scale effects in medium–dense sand, but it is considered likely that boundary effects would be less severe in this case.

6.2.3 Summary

The static tests were undertaken principally to establish a data base of anchor failure loads in dense and medium–dense Leighton–Buzzard sand for use in subsequent cyclic loading tests. Expressed in terms of the anchor uplift resistance factor, N_u, the results for dense sand ($D/B < 8$) and medium–dense sand($D/B < 4$) compared well with those of previous investigations which used Leighton–Buzzard sand and with the theoretical method of Fadl (1981). In dense sand at $D/B > 8$, the results were seriously affected by boundary and scale effects, leading to substantial differences in N_u values for the same embedment ratio. It is therefore important that the influence of boundary and scale effects be borne in mind when comparison is made between the results of deep anchor tests in dense sand.

6.3 CYCLIC LOADING

6.3.1 General

As mentioned in Chapter 2, comparisons between the actual test results of cyclic loading investigations are fraught with problems, because the combined effects of the various parameter values used means that each investigation is unique in itself. This being the case, it would be extremely difficult to draw valid conclusions from such comparisons. However, this does not apply to the general trends and characteristics identified in previous investigations, nor does it apply to the comparative aspects of the present study. These and other features of anchor cyclic loading behaviour are discussed in the following sections, dealing initially with anchors in dense sand.

6.3.2 Cyclic Displacement

a)Tests CD1 to CD5

Referring to the results presented in Figure 4.5 (page 137), the relative cyclic displacement, Δ_c/B, continued to accumulate throughout each test. The family of curves shown in Figure 4.5 is similar in form to those obtained by Hanna, et al (1978), Andreadis, et al (1981) and others, and illustrates the dependency of Δ_c/B on the applied loading level. For cyclic loading from a lower limit of zero, the cyclic displacement increases with the upper load limit.

The curves of Figure 4.5 are also similar to those reported by Morgan (1966) for axial deformation during cyclic loading in triaxial tests. For the case of constant confining pressure and cyclic deviator stress (Figure 2.17(a),page 69), the zone immediately above the anchor plate is subjected to a similar stress regime. The results for tests CD2 (30±30), CD3 (35±35) and CD4 (40±40)are grouped closely together, indicating that the rate of increase in Δ_c/B reduces as the maximum load level increases. A reduced rate of increase in axial deformation with increasing deviator stress is apparent in Figure 2.17(a).

The close grouping of the anchor tests may be explained by considering the results of Figure 4.15 (page 146), in which the anchor movement per cycle, m_c, is plotted for tests CD1 to CD5. The three tests CD2, CD3 and CD4 show consistently similar values for m_c, in the range 0.20– 0.24mm. This would lead to similar stiffening and cyclic creep effects for all three tests. The fifth test, CD5, which failed after <600 cycles, had an upper limit of 90%sfl and an anchor movement per cycle of approximately double that of tests CD2, CD3 and CD4, with upper limits of 60%, 70% and 80%sfl, respectively.

The significant reduction in time to failure in test CD5 is primarily caused by the increase in load (stress) level. However, another important factor may be the increase in anchor movement per cycle, leading to a rapid increase in cyclic creep rate.

Considering, firstly, the load level, Figure 6.6 compares the upper limits used in the cyclic loading with the static load– displacement graph of test SD8 (D/B= 4.5, dense sand). The upper load limits for tests CD1 to CD5 are marked on the load axis and correspond to anchor displacements of 0.19, 0.28, 0.33, 0.37 and 0.43mm respectively. The highest load limit of 90%sfl intersects

at the very top of the linear portion of the load–displacement graph. For shallow anchors, potential failure surfaces extend from the edge of the anchor to the ground surface (Chapter 2). In test CD5, within the narrow band of sand forming the failure surface, cyclic shear strains will be developed due to the anchor movement, and these shear strains will be relatively large. Referring to the work of Wood and Budhu (1981) from Chapter 2, large cyclic shear strains applied to dense Leighton–Buzzard sand result in a net increase in volume. In the cyclic anchor tests, this dilatational effect will take place in the sand adjacent to the failure surface, leading to a reduction in resistance to strain along the failure surface. Dilatancy effects will be encouraged by the low confining pressure in the model tests. Also from Chapter 2, Silver and Seed (1971(a)) reported a reduction in shear modulus during cyclic loading in simple shear.

Considering the anchor movement per cycle, Figure 4.15 shows that m_c for test CD5 did not diminish as the test progressed. Instead it remained at approximately 0.4mm until very close to complete failure, when it increased dramatically. Hence the cyclic shear strain developed on the failure surface would be sustained throughout the test, thus maintaining the dilatational effect on the failure surface. An additional point to note is the effect of cyclic creep on the failure of test CD5. Figure 6.7 shows the position of m_c for tests CD1 to CD5 relative to the particle size distribution curve of the sand used in the tests. The potential for cyclic creep is greatest in test CD5, and the presence of additional sand grains beneath the anchor would enhance the upward displacement of the anchor by decreasing the amount of recoverable displacement during each cycle.

Therefore the rapid failure of test CD5 is caused by the combined effects of cyclic shear strain, dilation and cyclic creep.

By comparison, test CD4 exhibited a substantial stiffening effect over the first few cycles, despite the relatively small reduction in upper load limit to 80%sfl. The anchor movement per cycle quickly stabilised at approximately 0.2mm, and subsequent load cycles behaved in an essentially elastic manner. This is similar to the behaviour of triaxial samples reported by Morgan (1966), some of which were loaded up to 83% of their equivalent static failure load and survived many cycles of loading.

Due to the smaller anchor movement per cycle, the cyclic shear strain on any potential failure surface is less, and for moderately small cyclic shear

strains there is a decrease in volume of the sand adjacent to the failure surface (After Wood and Budhu, 1981). Therefore, in test CD4, during the initial period of cyclic loading the sand particles are able to re-arrange themselves into more stable positions, thus increasing the resistance to further deformation.

The basically stable nature of test CD4 (and tests CD3, CD2 and CD1) is illustrated in Figure 4.6 (page 138), which shows the relative cyclic displacement, Δ_c/B, increasing at a constant rate for $N \geqslant 250{,}000$ cycles. The steadily increasing cyclic displacement is caused partly by the small, permanent deformations taking place in the sand, partly by attrition of the sand grains themselves and partly by the cyclic creep effect.

b)Tests CD6 and CD7

In tests CD6 and CD7, the repeated loading was increased as the tests progressed. The initial loading in test CD6 was (20±20), which was increased to (30±30) after 609,000 cycles, and increased again to (35±35) after a further 919,000 cycles. The effect of these changes on the anchor displacement is illustrated in Figure 6.8. The first change in loading occurred at a relative displacement of 0.0082 ($\Delta_c = 0.41$mm) ; the second at a relative displacement of 0.0343 ($\Delta_c = 1.72$mm). Clearly the increase in loading accelerated the cyclic displacement, but the initial response of the anchor to an increase in loading was actually stiffer than the response to the same loading applied for the first time. However, as the number of cycles increased, the anchor response became less stiff, and the rate of cyclic displacement increased beyond that obtained in the "first time" tests.

This behaviour is shown in Figure 6.9, in which the results of tests CD2 and CD3 are used as the "first time" tests for comparison. Referring to Figure 6.9, the anchor response to both the second and third loading stages results in lower rates of cyclic displacement for $N < 100{,}000$ cycles (approximately). The reduction in cyclic displacement rate is a result of the previous cyclic loading applied to the anchor. In Chapter 2, the densification and stiffening effect of cyclic loading on even dense sand was reported for triaxial tests (Morgan, 1966), simple shear tests (Youd 1971, Moussa 1975, Wood and Budhu, 1981) and anchor tests (Hanna, et al, 1978, Maddocks 1978, Andreadis, et al, 1981).

However, by comparing the slopes of the corresponding curves in the region $N > 100{,}000$ cycles, it is clear that the rate of cyclic displacement is greater in the second and third loading stages of test CD6 than the "first time"

tests CD2 and CD3. The change from stiffer to less stiff response is illustrated in Figure 6.10, which plots Δ_c/B versus Δ_{pc}/B for tests CD2, CD3 and the second and third stages of test CD6. The curves for the latter begin at a much lower value of Δ_{pc}/B than the corresponding curves for tests CD2 and CD3, but rise sharply as the number of cycles increases (decreasing Δ_{pc}/B). The curve for the third loading stage (35±35) eventually obtains a positive slope, indicating that failure is imminent. This definition of failure was proposed by Andreadis (1979), and test CD6 did, in fact, fail after 510,000 cycles of the third stage loading.

Now consider the anchor movement per cycle, m_c, in test CD6. Figure 6.11 plots the variation in m_c with N for the three loading stages of test CD6 plus tests CD1, CD2 and CD3. The value of m_c during the latter two stages of test CD6 was consistently less than the "first time" values for tests CD2 and CD3. The reduction in m_c is small but is consistent with the densification and stiffening effect of the cyclic pre–loading. However, the increase in cyclic displacement rate over the latter part of the second and third stage loadings is not consistent with this reduced anchor movement response. The combination of sand densification and attrition of the sand grains is thought to be the reason for this apparent contradiction.

After the initial loading stage of (20±20), the sand around the anchor is more dense and provides greater resistance to any applied load. Hence the smaller values of m_c in Figure 6.11 for the second stage loading compared to test CD2. However, also due to the initial loading, a greater amount of attrition will have taken place in test CD6 at any stage after the increase in loading. Hence, a greater amount of smaller particles will be present in the vicinity of the anchor to fuel the cyclic creep mechanism, leading to a decrease in recoverable displacement during each cycle and consequently a greater upward displacement of the anchor. Therefore, despite the smaller anchor movement per cycle in test CD6 (second stage), cyclic creep eventually takes place at a faster rate than test CD2. The same reasoning holds for the cyclic displacement behaviour during the third stage of test CD6 compared to the 'first time' test CD3.

Morgan (1968) and Tanimoto and Nishi (1970) suggested that attrition of sand grains took place in triaxial samples subjected to very many cycles of loading. In the particular case of plate anchors, Hanna and Al Mosawe (1981) reported a change in gradation of the sand near the anchor, caused by attrition of the sand grains.

The situation in test CD7 was somewhat different from that in test CD6. The initial loading of (30±30) was increased to (40±40) after 795,000 cycles ($\Delta c/_B$= 0.0296, Δ_c= 1.48mm). This resulted in an anchor movement per cycle greater than that obtained for the "first time" loading of (40±40) in test CD4, as shown in Figure 6.12 Hence, the cyclic displacement accumulated at a faster rate than test CD4. This is clearly illustrated by comparing the results for tests CD7 and CD4, plotted in Figures 6.13 and 6.14. The combination of a larger anchor movement per cycle and a greater amount of attrition leads to a more rapid increase in cyclic displacement. Test CD7 failed after approximately 500,000 cycles of (40±40) loading.

The initial loading stages of tests CD6 and CD7 served as a check on the reproducibility of the results at repeated load levels of (20±20) and (30±30). The variation of m_c during these initial stages is compared with that of tests CD1 and CD2 in Figures 6.11 and 6.12, respectively. Taken together with the cyclic displacement results for the same tests shown in Figure 4.12 (page 144), there is good agreement between tests subjected to the same repeated loading.

c)Tests CD8 and CD9

The sustained–repeated tests, CD8 and CD9, were undertaken to assess the influence of load amplitude on the cyclic displacement. Figure 6.15 compares the response of anchors which were subjected to the same maximum load per cycle, but different load amplitudes. Tests CD2, CD7 (first stage loading) and CD8 all had a maximum load level of 60%sfl, but the load amplitude in the first two tests was ±30%sfl, whilst in the latter test it was ±20%sfl. Figure 6.15 clearly shows that for any value of N, the cyclic displacement is greater in the test with greater load amplitude. This effect is even more marked when comparing tests CD4 and CD9. Again the maximum load level is the same in each test (80%sfl), but the load amplitude is ±40%sfl and ±20%sfl in tests CD4 and CD9, respectively. After 100,000 cycles, the cyclic displacement in test CD4 is approximately 5 times that of test CD9.

Hence, repeated loading has a more detrimental effect on the anchor response than sustained–repeated loading, to the same maximum load. Creep effects during the sustained–repeated tests had no influence on the results. Figure 4.25 (page 155) shows a plot of anchor displacement versus time for anchors loaded to the mean values set in tests CD8 and CD9, i.e. 40%sfl and 60%sfl, respectively. No creep effect is evident at either load level.

The variation in anchor movement per cycle for all tests with an amplitude of ±20%sfl is shown in Figure 6.16. The range of movement is quite small, clustering around an approximate average of 0.1mm. Given that the anchor movement per cycle and the variation in load per cycle are similar for tests CD1, CD6 (first stage), CD8 and CD9, it is reasonable to suppose that the cyclic displacement behaviour is also similar. The results plotted in Figure 6.17 support this conclusion. Note that the vertical scale for Δ_c/B has been increased (x 6, approximately).

6.3.3 Anchor Hysteresis

After the initial few cycles of loading, the anchor hysteresis in dense sand was extremely small. Typical results obtained from pen–recorder plots are shown in Figure 6.18 for cycles 1, 10 and 100 of test CD2 (30±30). By the tenth cycle the response had stabilised into a near–elastic form, and further cycles of loading reproduced a very similar response. Permanent deformation continued to accumulate, however, but at a very slow rate.

The hysteresis behaviour of the anchor illustrates the stiffening effect of cyclic loading on the sand, and is very similar to that reported by Morgan (1966) and others for triaxial samples and Hanna, et al (1978) and Andreadis, et al (1981) for anchors. A reduction in hysteresis effect with number of cycles has also been reported for cyclic simple shear tests (see Figure 2.25, page 76, after Silver and Seed, 1971a). Note that the stiffening effect on the sand takes place over a relatively small number of cycles from the beginning of the test.

The exception to this behaviour is test CD5. After an initial decrease in loop area over the first few cycles, the amount of permanent displacement per cycle begins to increase (Compare cycles 10 and 100 in Figure 6.19). With the movement per cycle remaining essentially constant, the loop area increases and the anchor moves rapidly upwards to failure. Any stiffening effect is very slight and is quickly counteracted by the more dominant dilatational effects in each cycle of loading, as explained in sub–section 6.3.2.

The hysteresis behaviour of anchors in medium–dense sand is presented in sub–section 6.3.5.

6.3.4 Post–Cyclic Behaviour

At the end of the cyclic tests in dense sand, the anchors which were still in place were loaded to failure statically. This was possible for tests CD1 to CD4, CD8 and CD9. In all cases, the anchor response was stiffer than the original static load tests.

Referring to Figure 6.20, the increase in stiffness is represented by the change in slope of the linear portion of the load–displacement graph compared with that of the original static test (Test SD8). The increase in stiffness is modest and very similar for each of the post–cyclic tests. For clarity, only the point representing the failure load has been plotted for each test, with a single straight line drawn for all tests. The modest increase is stiffness is consistent with the hysteresis behaviour of the anchors described in the previous sub–section, and with the knowledge that the initial relative density of the sand was $>90\%$. Consequently, there is little scope for substantial densification of the sand because the capacity of the sand to densify must be reduced as the structure of the sand becomes denser. A stiffer anchor response to post–cyclic static loading was reported by Maddocks (1978), Hanna, et al, (1978) and Andreadis (1979)

The similarity in post–cyclic stiffness indicates that, irrespective of the form of the cyclic loading, the sand attains an ultimate stiffness and further cyclic loading does not increase the stiffness of the sand. Andreadis (1979) reported the same characteristic for his tests in a medium–dense sand ($D_r = 66\%$) and Figure 2.20 (page 71, after Youd, 1972) illustrates the same limiting stiffness effect in cyclic simple shear tests.

The ultimate load in each of the post–cyclic tests is higher than the original test, although the difference is fairly small. The maximum increase in test CD3 is approximately 10%. The increase in P_u seems to be unrelated to the magnitude of the repeated load applied to the anchors in tests CD1 to CD4.

6.3.5 Effect of Sand Density

Figure 6.21 compares the relative cyclic displacement of anchors subjected to repeated loading in dense and medium–dense sand. For corresponding repeated load levels, the displacement is greater at any stage of

the test in medium–dense sand. This is not an unexpected result, and is consistent with the values of m_c plotted in Figure 6·22 for dense and medium–dense sand. Note that the anchor movement per cycle reduces slightly over the first 1000 or so cycles in each of the medium–dense tests, indicating that the sand around the anchor has densified during this period, leading to a stiffer response from the sand. The stiffening effect is illustrated by considering the anchor hysteresis behaviour of test CM2, as shown in Figure 6.23. The loop area reduces with increasing N, and the average slope of the loop increases slightly. As with the dense sand tests, the anchor eventually behaves in a near–elastic manner during each cycle of load.

Test CM3 was the only test in the medium–dense sand to fail during the loading period. The response stiffened somewhat over the first 1000 or so cycles, and stabilised at an anchor movement per cycle of approximately 0.42mm, similar to that in test CD5, the failure test in dense sand. Assuming the same failure mechanism as described for test CD5, at this stage in test CM3 the dilatational effect present during each cycle of load begins to dominate, possibly benefitting from the initial densification of the sand and the low confining pressure in the model test. Consequently, the sand adjacent to the failure surface begins to dilate, the resistance to deformation is reduced and, with cyclic creep going on apace, the anchor rapidly approaches failure.

The results of the post–cyclic loading tests for CM1 CM2, CM4 and CM5 are shown in Figure 6.24, together with the original static test (Test SM7). Note that the loading in test CM5 (30±30) was deliberately stopped after 10,000 cycles. Despite this, the slope of the load–displacement curve for test CM5 is very similar to that of the other post–cyclic tests, falling within the wedge shown in Figure 6.24. This supports the finding that most of the stiffening arising from cyclic loading occurs during a relatively small number of cycles from the beginning of a test (Silver and Seed, 1971(a); Youd, 1972).

The post–cyclic response of the anchors in dense and medium–dense sand display the same basic characteristics: the response is stiffer than the original static load test; the increase in stiffness is independent of the form of cyclic loading applied to the anchor; the post–cyclic ultimate load is greater than the original test value. The increase in stiffness in the medium–dense sand is more pronounced, and consequently the increase in P_u is also greater. The maximum increase in P_u is approximately 18%, in test CM2 (c.f. a 10% increase in test CD3).

Test CM5 also served as a check on the repeatability of the results of (30±30) loading, but only up to 10,000 cycles. No significant difference in behaviour was observed between tests CM2 and CM5 for $N < 10{,}000$ cycles.

The results of test CM4, a sustained–repeated load test, are shown in Figure 6.25, together with the results of test CM1 (same amplitude) and test CM2 (same maximum load). Comparison of these results confirms the conclusions obtained from similar tests in dense sand, i.e. repeated loading has a more detrimental effect on anchor response than sustained–repeated loading, to the same maximum load; for the same load amplitude, the cyclic displacement is independent of the mean load; and creep effects may be ignored (see Figure 4.25, page 155). These conclusions apply to anchors which had a relative cyclic displacement of < 0.05 after 500,000 cycles of loading.

6.3.6 Summary

Within the range of parameter values used in this investigation, the main findings of the cyclic loading tests are as follows:

i) Attrition of the sand grains takes place around the anchor and is an important factor in maintaining cyclic creep. Due to this attrition, pre–cycling at a lower repeated load level has a detrimental effect on the anchor cyclic displacement, when the repeated load level is increased.

ii) When cycling to the same maximum load level, the greater the load amplitude, the greater the cyclic displacement. In tests with the same load amplitude, the anchor cyclic displacement is similar.

iii) Apart from the anchors which failed during cycling, the load–displacement hysteresis of the anchors is very small. The response quickly stabilises into a near–elastic form which continues for the rest of the test.

iv) The post–cyclic static loading response is stiffer than the original static load test. The increase in stiffness takes place over the initial part of the test and is independent of the form of cyclic loading applied to the anchor. The ultimate resistance in the post–cyclic test is greater than that in the original test.

v) A reduction in sand density leads to an increase in cyclic displacement, for anchors subjected to the same relative loading levels.

vi) For the anchors which failed during cycling, the failure mechanism can be described in terms of the behaviour of simple shear samples of sand subjected to cyclic loading. The onset of failure can be identified by an increase in the anchor displacement per cycle, as proposed by Andreadis (1979).

6.4 DESIGN CONSIDERATIONS

Some of the many design situations for anchors were described in Chapter 1, and a particularly important one involving cyclic loading is the foundation design for tethered buoyant platforms or guyed towers. The tension leg platform (TLP) of Conoco's Hutton field in the U.K. sector of the North Sea was the first of this type to be deployed. Tension piles were used to resist the uplift forces, and the arrangement at one of the four foundation templates is shown in Figure 6.26 . The template is anchored to the seabed by eight tubular steel pipes, 1830mm in diameter and driven to a minimum penetation of 58metres. (Tetlow, et al, 1983).

The behaviour of piles under repeated or sustained–repeated tensile loads, and the consequent design considerations, have been the subject of intensive research in recent years (e.g. Puech, 1982 ; St. John, et al, 1983 ; Nauroy, et al, 1985; Jardine, et al, 1985). The loss of shaft capacity during cycling of a pile in sand is associated with grain repacking and attrition, and is critically dependent upon the mineralogy of the sand grains. Even if the sand is initially dense, cycling can cause dramatic reductions in radial effective stress. Chan and Hanna (1980) and Low (1986) reported that substantial cyclic displacement occurred in model tests on single piles in sand, even when the maximum load level during repeated loading was only 30% of the equivalent static failure load in tension (see Figure 6.27). The general trends in cyclic displacement behaviour reported by Chan and Hanna (1980), Puech (1982), Nauroy, et al (1985) and Low (1986) for tension piles are similar to those for plate anchors identified in section 6.3.

For both plate anchors and tension piles, cyclic displacement results in a progressive reduction in capacity, and any definition of failure must be related

to the amount of irrecoverable displacement which takes places, and whether or not it is "allowable". The allowable displacement for shallow anchors (or short piles) may be much less than that for deep anchors (or long piles) and the cyclic displacement will continue to accumulate during the design life of the structure. The Hutton TLP has a design life of 20 years (approximately 100 million load reversals), and a monitoring system has been installed to measure the vertical displacement of the pile groups during this time (Jardine, et al, 1985).

Any assessment of the design uplift resistance of prototype plate anchors based on the model test results reported herein would have to take account of a number of factors, for example:

i) if multiple anchors were used, the interaction effects of anchors placed in groups (Yilmaz, 1971; Wang, 1986),

ii) the effects of anchor installation, which loosens the sand and can lead to substantial reductions in static pullout capacity (Andreadis, 1979; Zakaria, 1986). Subsequent cyclic loading would help to densify the sand in the vicinity of the anchor,

iii) the true nature of the loading applied to the anchor. In an offshore context, this would involve periods of calm, steady-state cyclic loading and storm loading. There may also be a horizontal cyclic load component,

iv) scale effects associated with confining pressure and particle size.

The latter two factors are particularly relevant to the anchor cyclic displacement.

At the present time, using plate anchors in a similar manner to the tension piles of the Hutton TLP is not a practical proposition. The quoted maximum uplift resistance of the largest propellant embedment anchor (270T in sand, McCormick, 1979) is considerably less than the uplift force on a single Hutton pile (1140T, Tetlow, et al, 1983) under the most adverse loading conditions. The principal use for plate-type anchors offshore will continue to be in the provision of single surface or sub-surface moorings.

TABLE 6.1 - Boundary and Scale Effects: Values of Nu for Figures 6.4 and 6.5.

D/B	Bc/B	31 25	48 38	63 50	83 66	94 75	125 100	130 104	B/d_{50} † B(mm)
2	5	-	-	-	-	-	8.0 7.9	-	
	7	-	-	-	-	8.4 8.1	-	8.3*	
	11	-	-	-	8.1* 8.3*	-	-	-	
6	10	-	-	51.4 50.5					
	15	-	-	51.1*					
	20	57.5* 58.6*	53.1*	-					
8	10	-	-	83.4					
	13	-	88.5	-					
	20	94.8*	87.6*	-					
10	13	-	172.4 179.6						
	20	143.8*	123.7* 125.2*						
12	13	-	209.2						
	20	195.7	140.8* 144.3*						
	30	173.3* 174.0*	-						

* - Results after Hutchison (1982). Those for D/B = 2.0 have been estimated from test results reported for D/B = 2.27 (66 mm ϕ anchor) and D/B = 2.16 (104 mm ϕ anchor).

† - Mean diameter of sand grains, d_{50} = 0.80 mm.

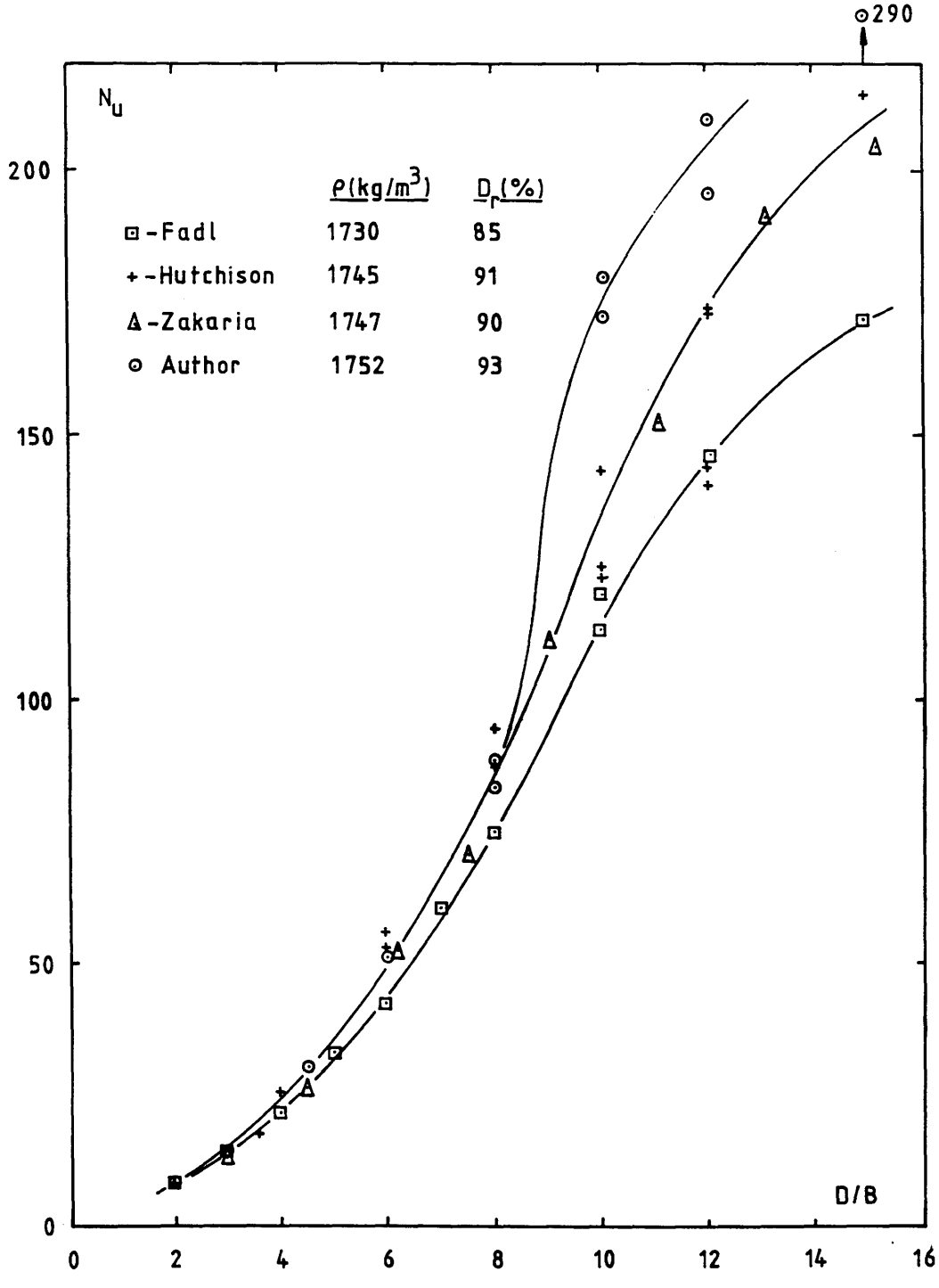

FIGURE 6.1 - Static Test Results: Comparison with previous investigations in dense Leighton Buzzard sand.

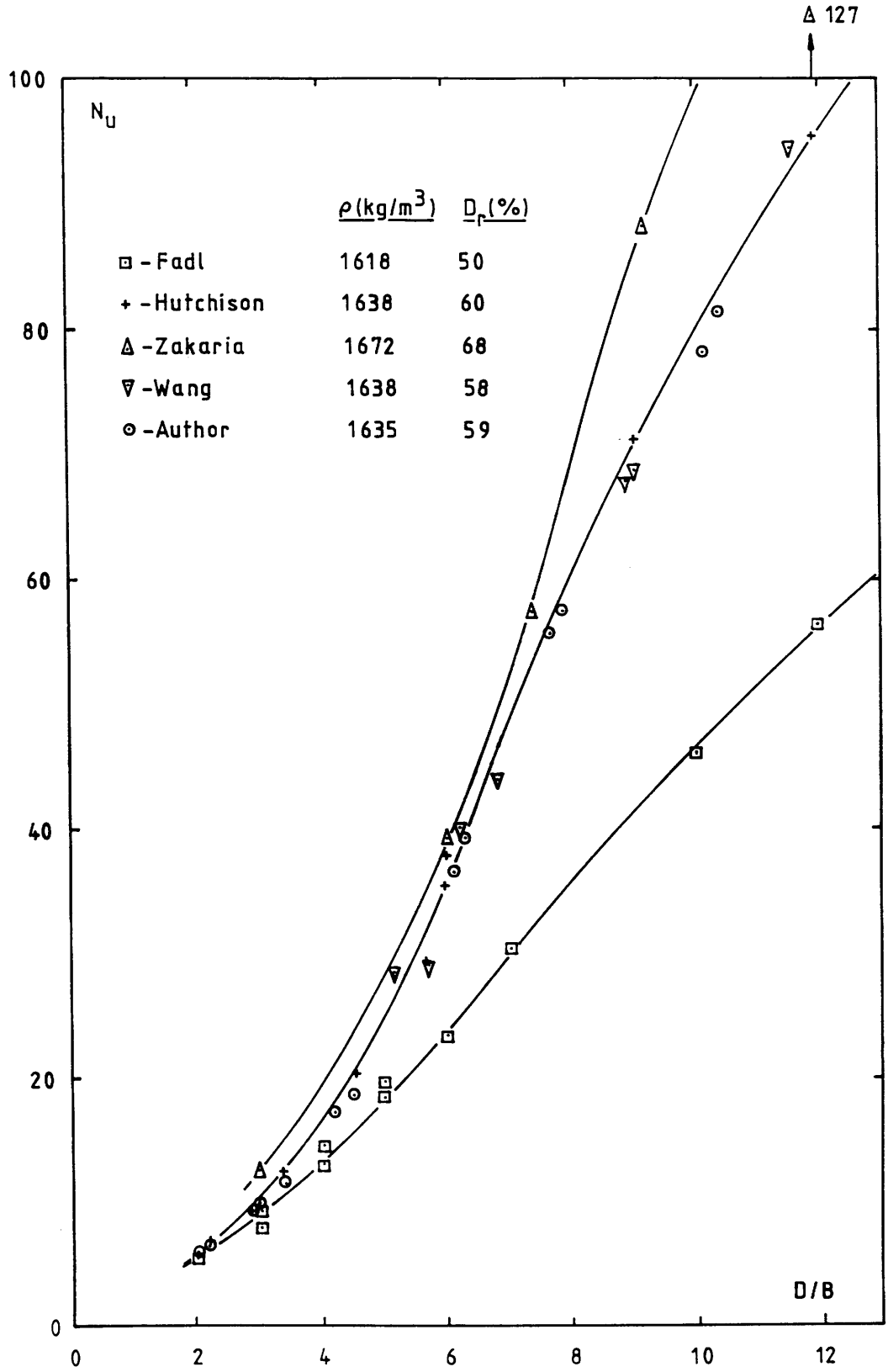

FIGURE 6.2 - Static Test Results: Comparison with previous investigations in medium-dense Leighton Buzzard sand.

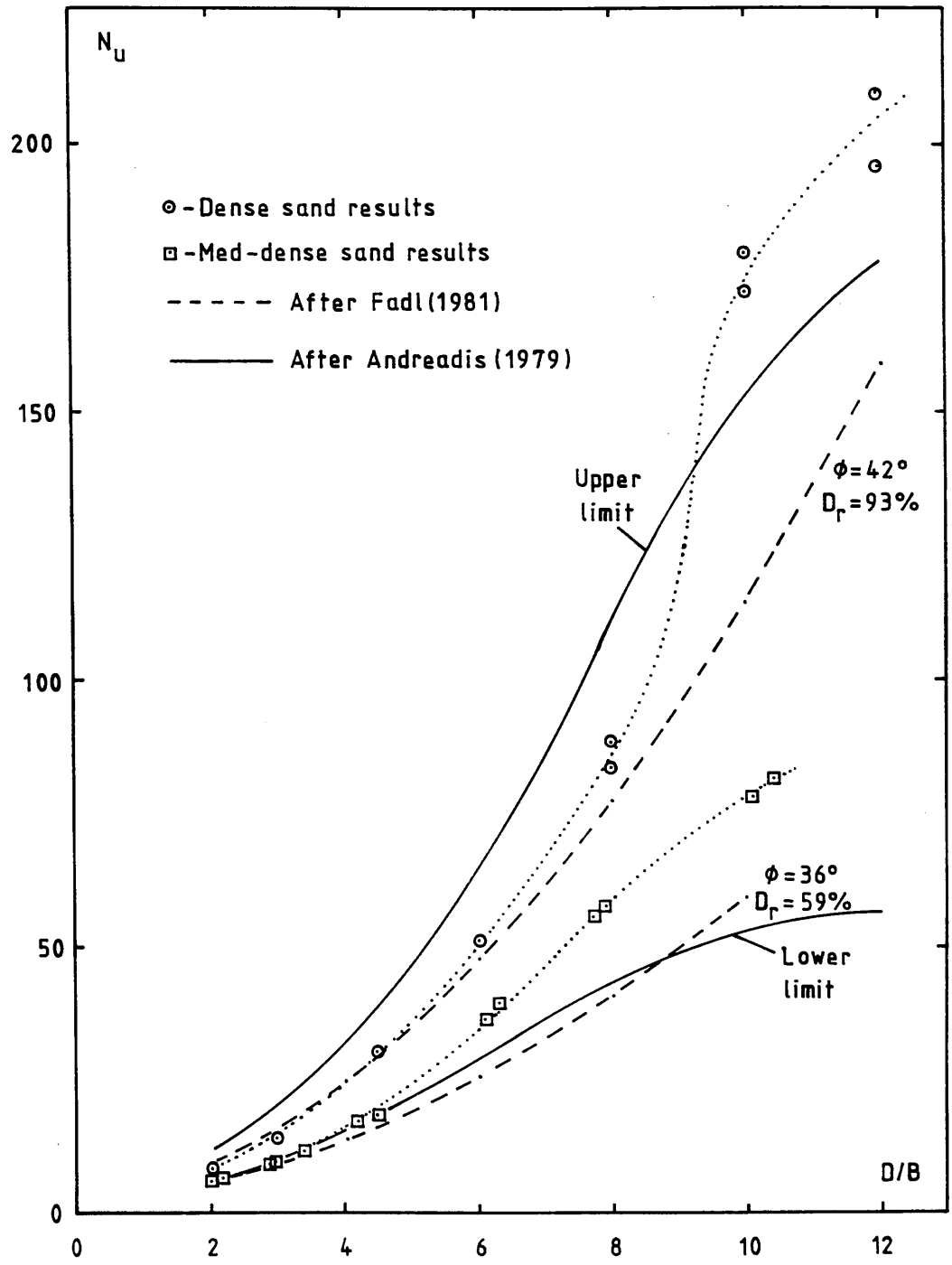

FIGURE 6.3 - Static Test Results: Comparison with previous investigations and Fadl's shallow anchor theory.

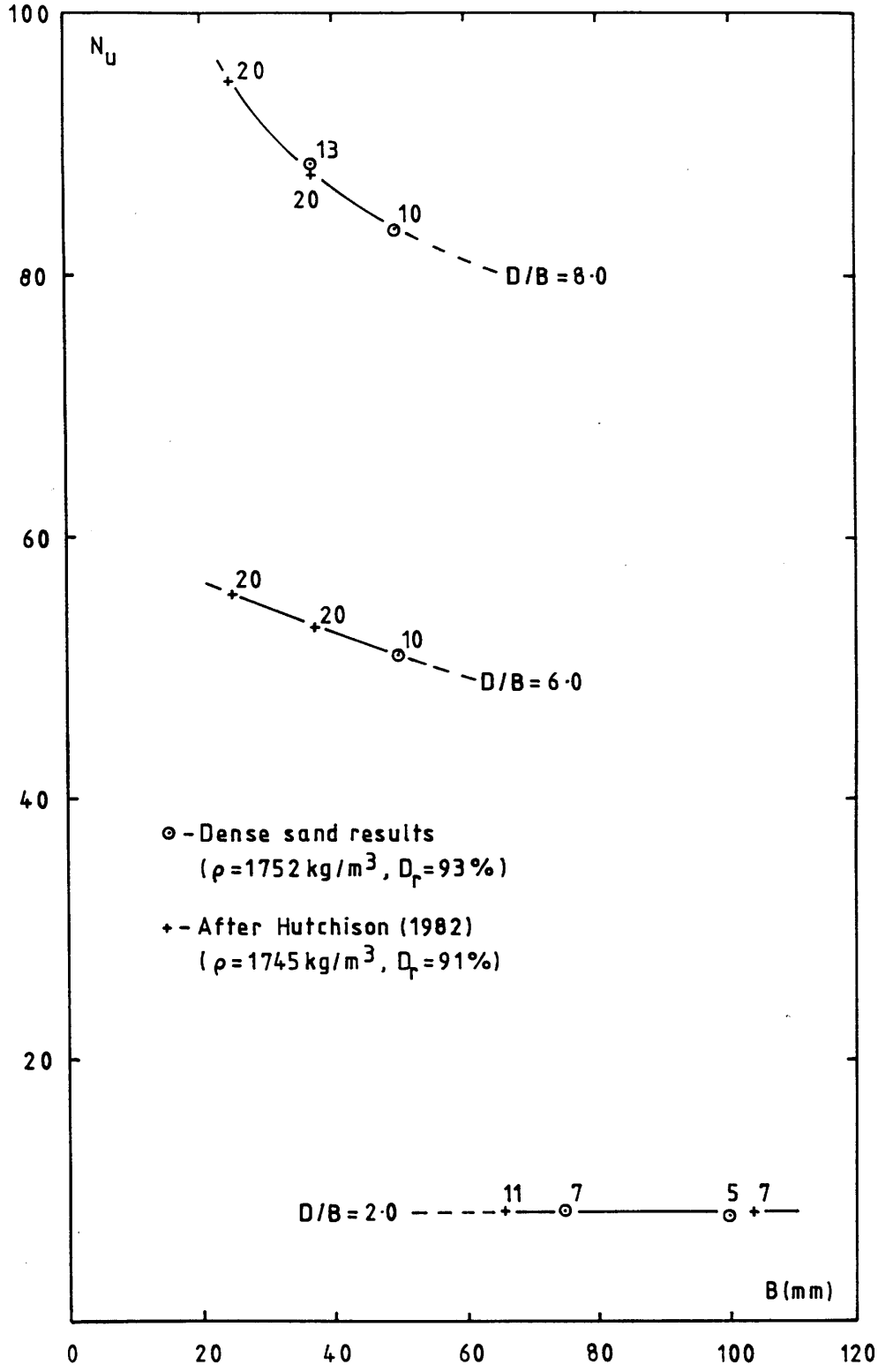

FIGURE 6.4 - Static Test Results: Scale effect at D/B = 2.0, 6.0, 8.0.

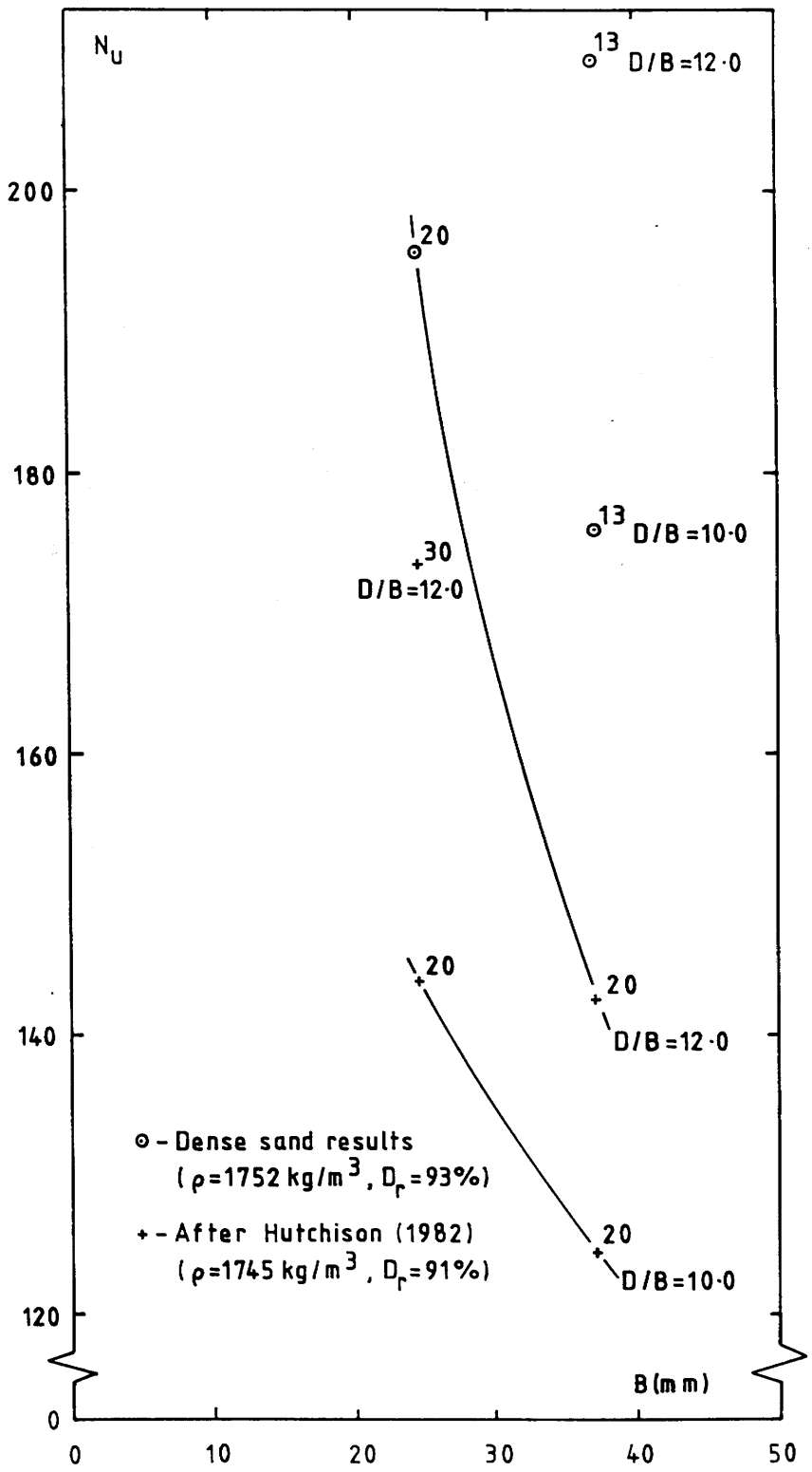

FIGURE 6.5 - Static Test Results: Scale and boundary effects at D/B = 10.0, 12.0.

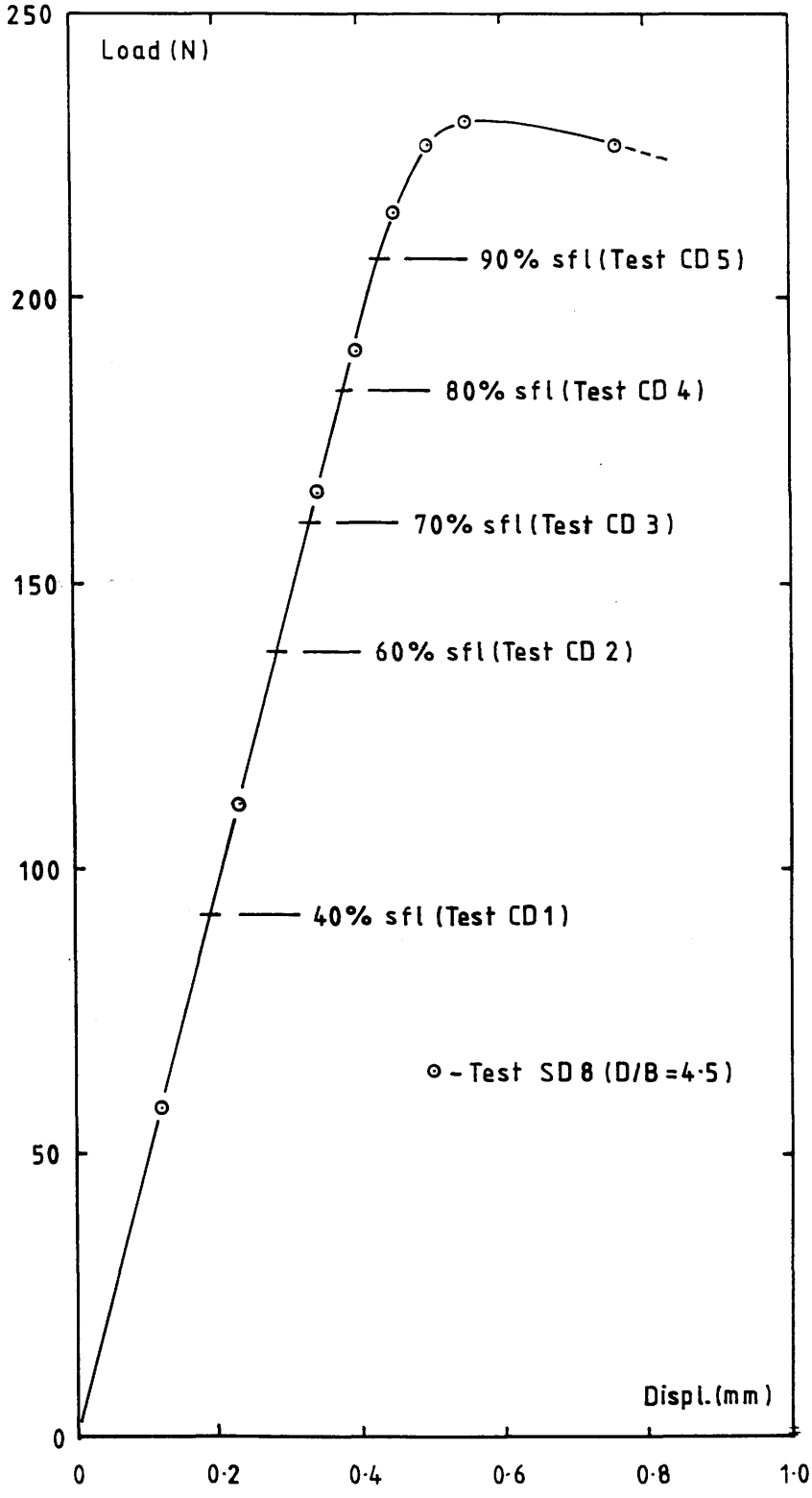

FIGURE 6.6 - Relative position of upper load limits used in repeated load tests CD1 to CD5 with respect to load-displacement graph of test SD8.

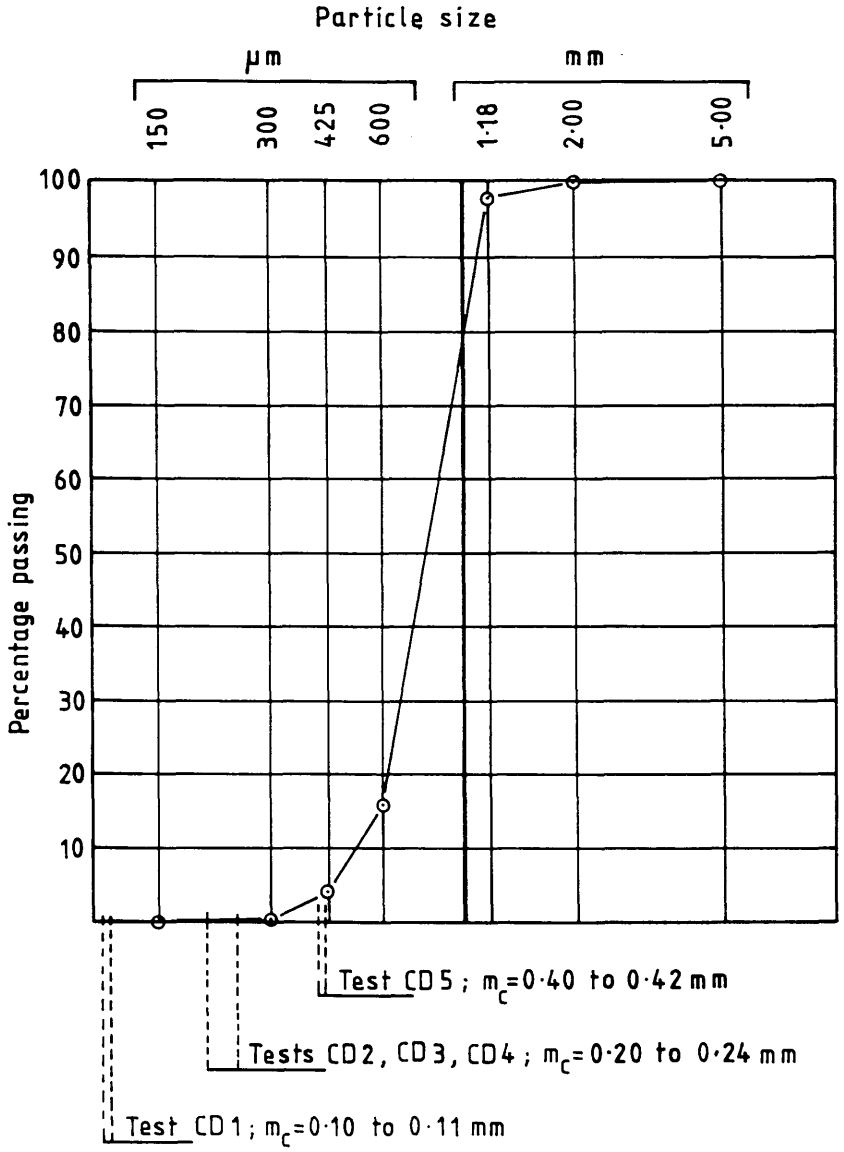

FIGURE 6.7 - Position of m_c for tests CD1 to CD5 relative to PSD curve for grade 1630 Leighton Buzzard sand.

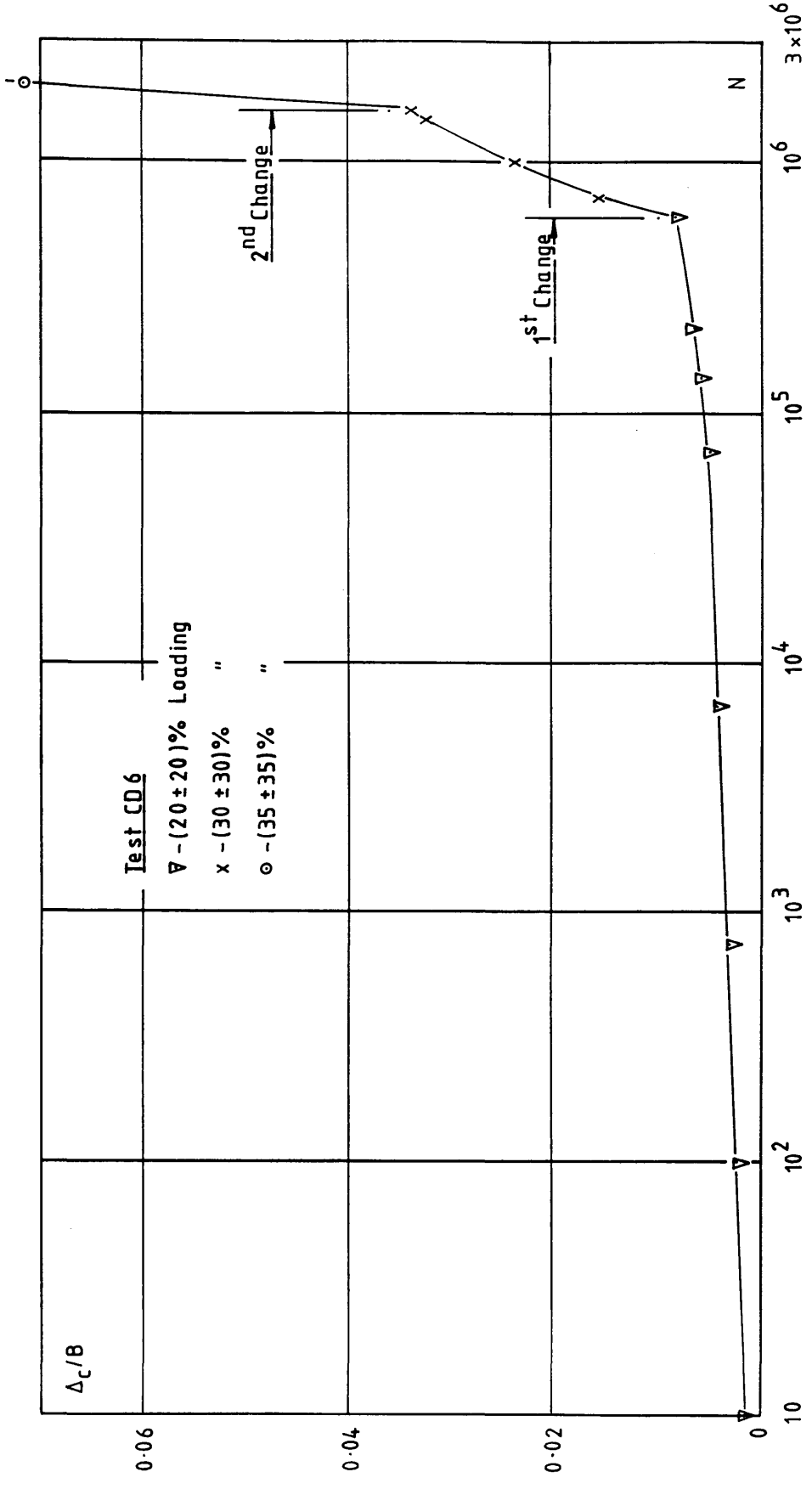

FIGURE 6.8 - Test CD6 : Cumulative plot of Δ_c/B versus N.

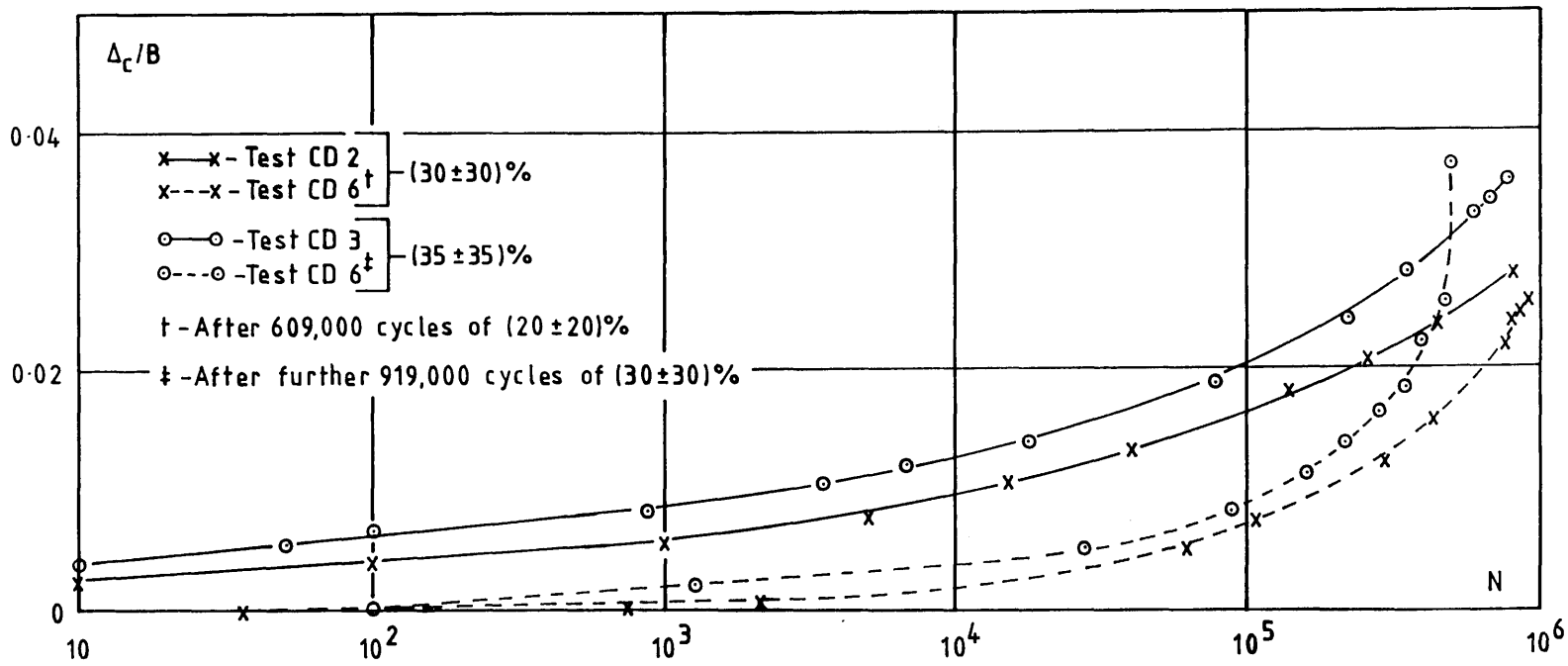

FIGURE 6.9 - Test CD6: Comparison with tests CD2 and CD3 (Δ_c/B versus N).

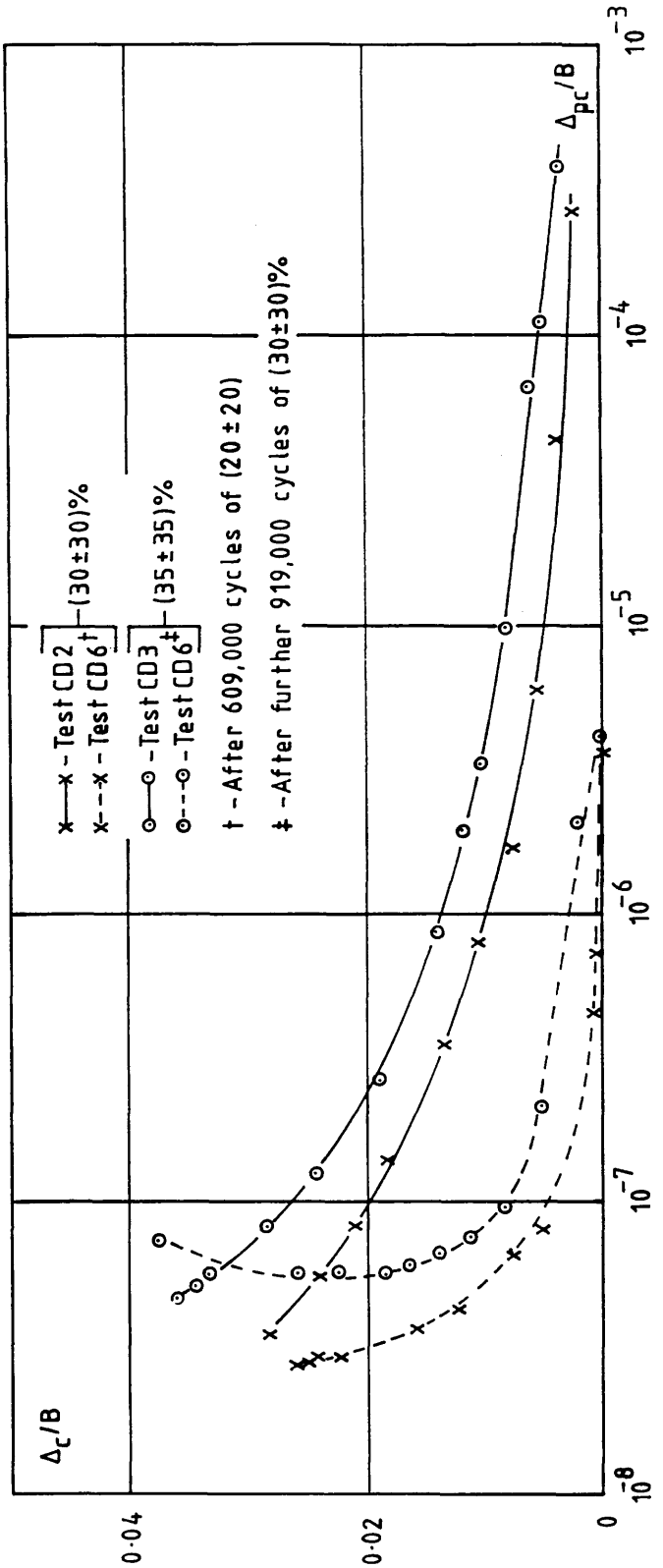

FIGURE 6.10 - Test CD6: Comparison with tests CD2 and CD3 (Δ_c/B versus Δ_{pc}/B).

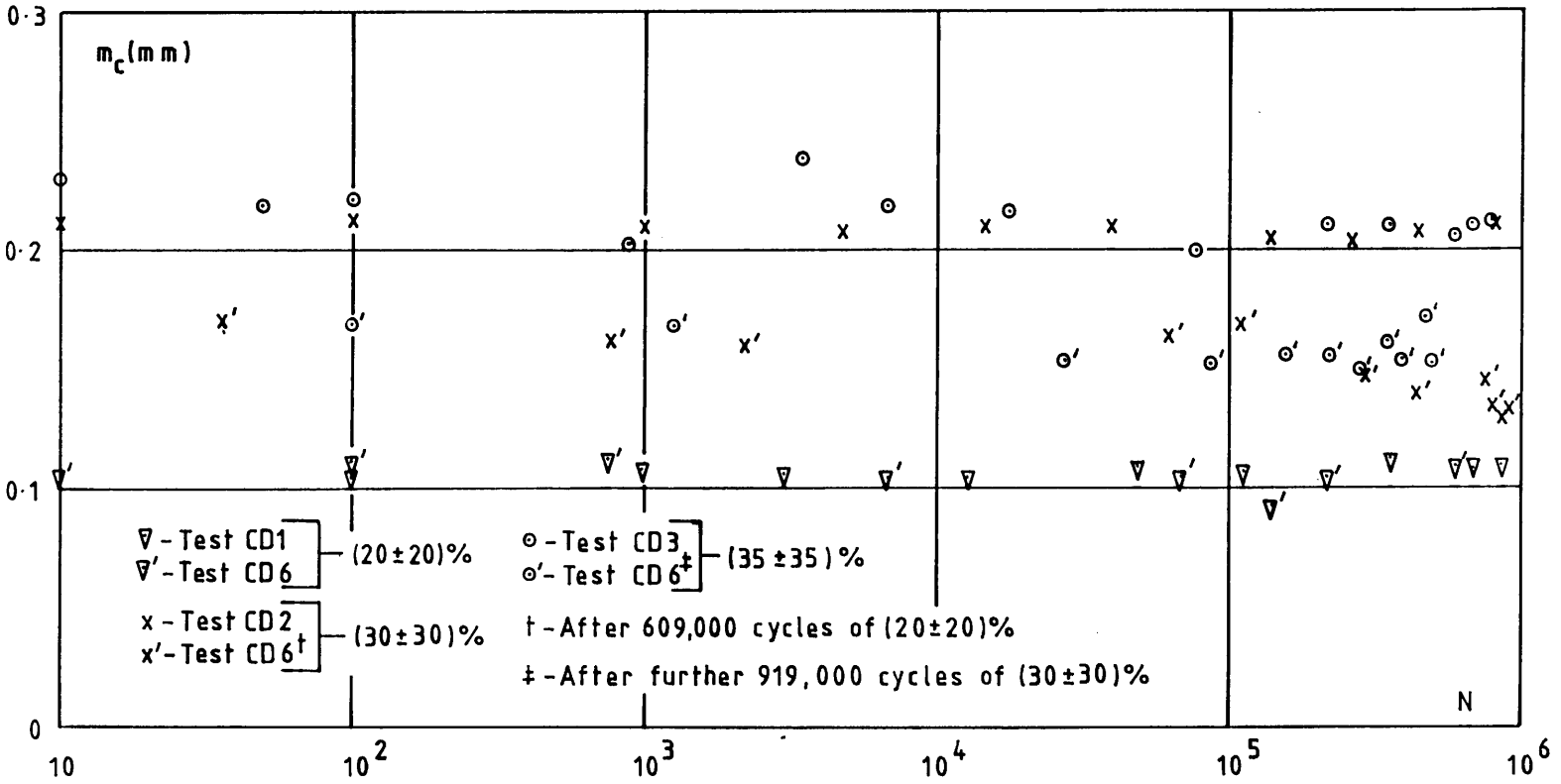

FIGURE 6.11 - Test CD6: Comparison with tests CD1, CD2 and CD3 (m_c versus N).

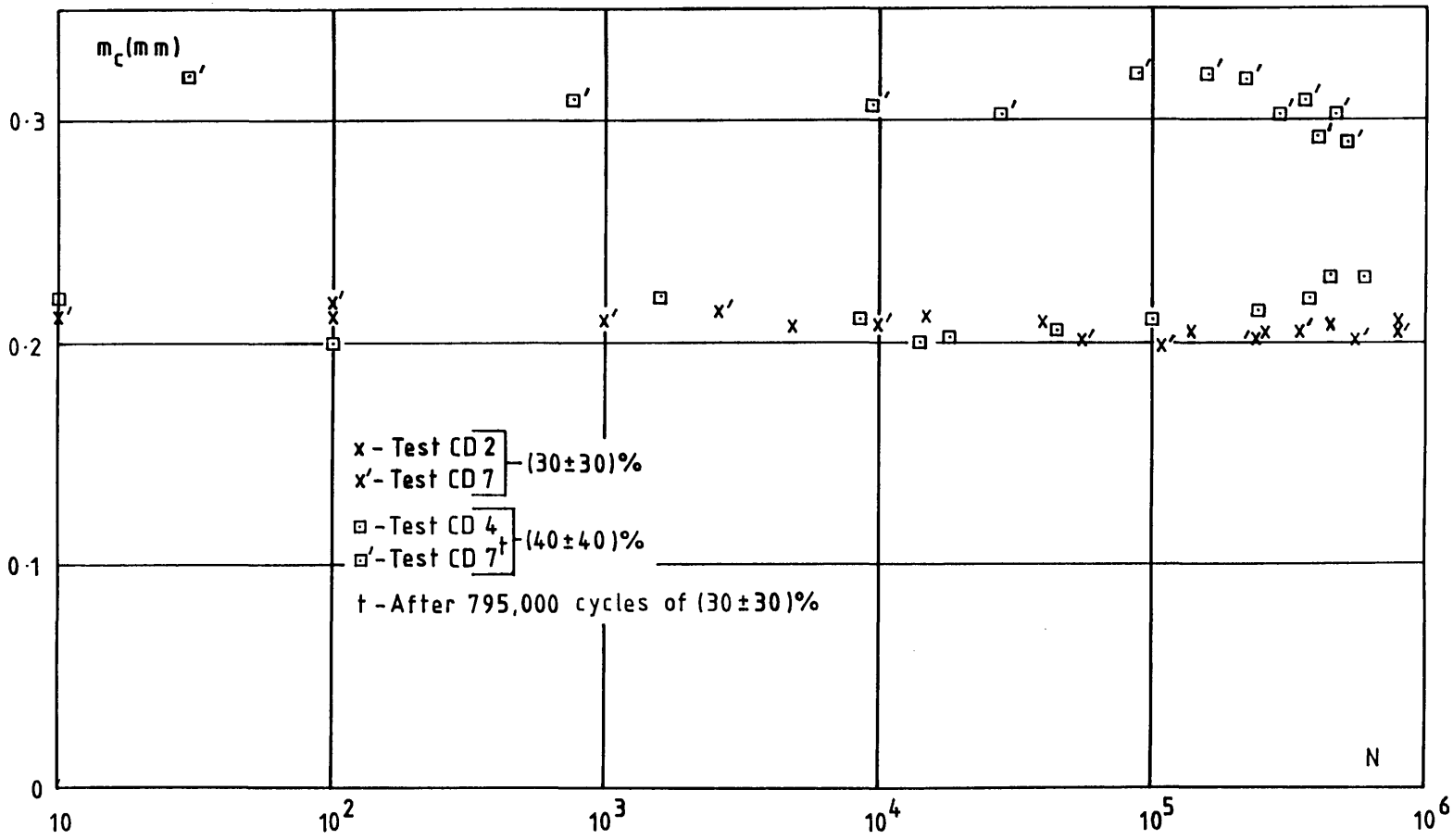

FIGURE 6.12 - Test CD7: Comparison with tests CD2 and CD4 (m_c versus N).

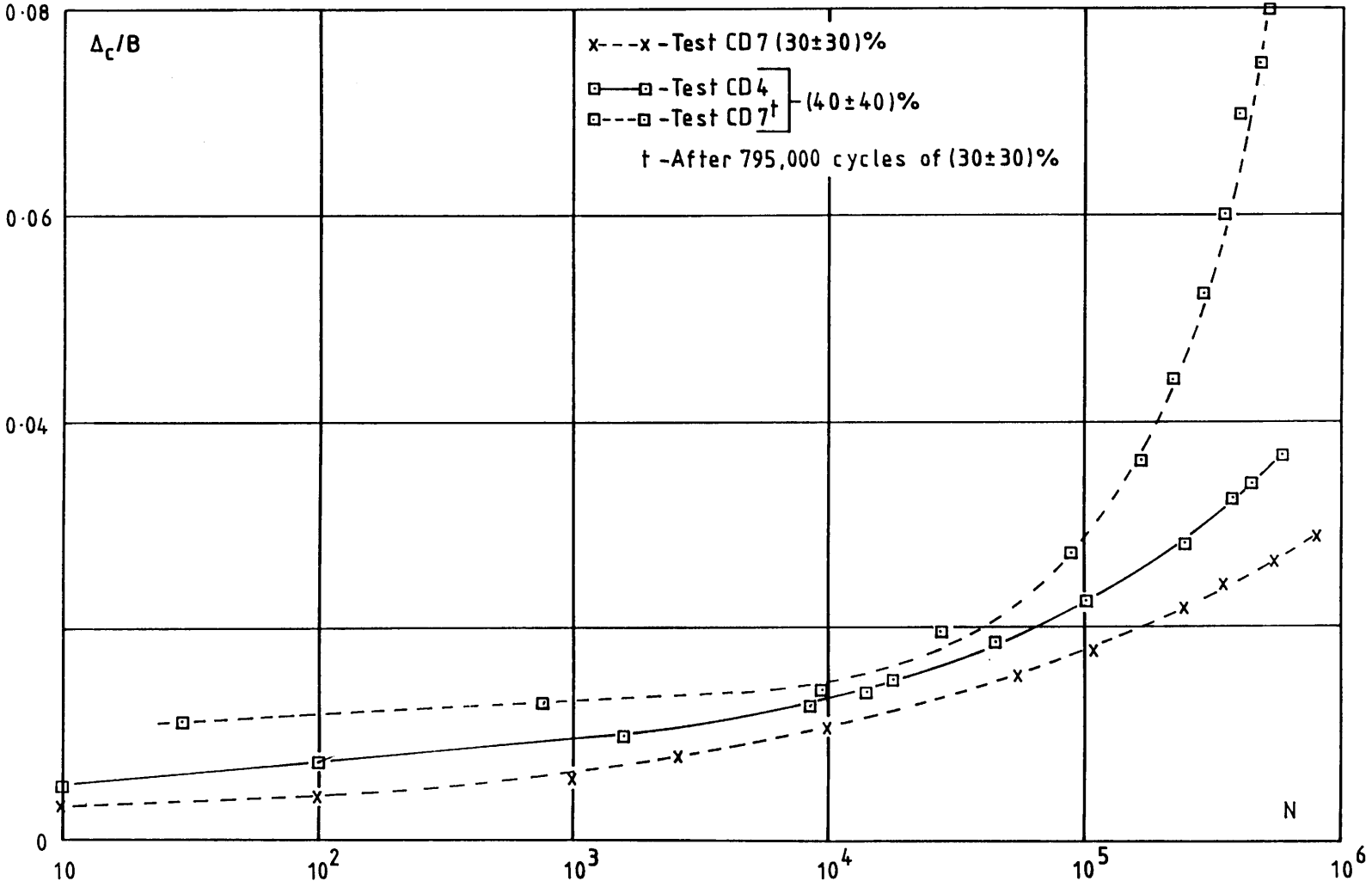

FIGURE 6.13 - Test CD7: Comparison with test CD4 (Δ_c/B versus N).

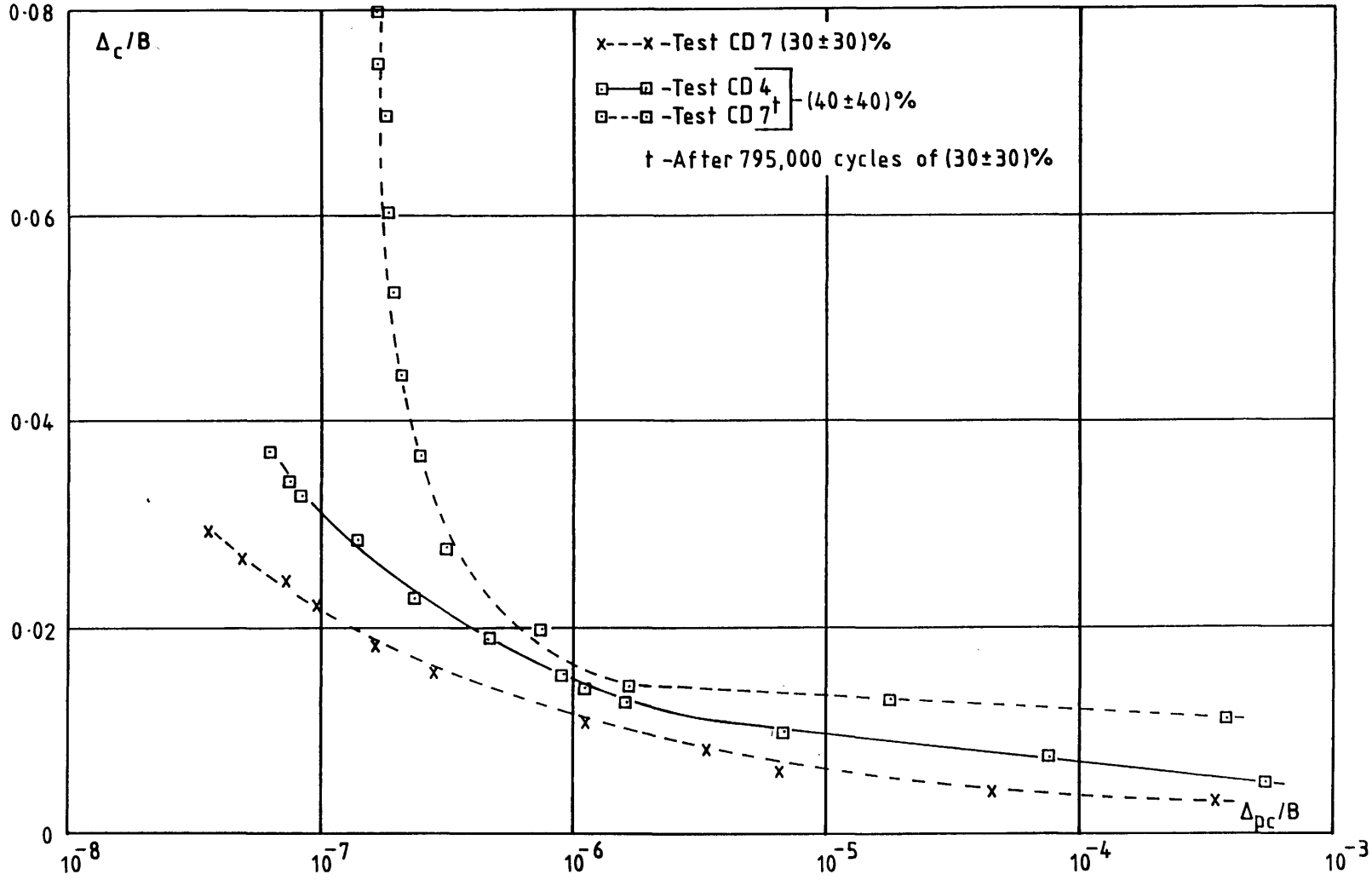

FIGURE 6.14 - Test CD7 : Comparison with test CD4 (Δ_c/B versus Δ_{pc}/B).

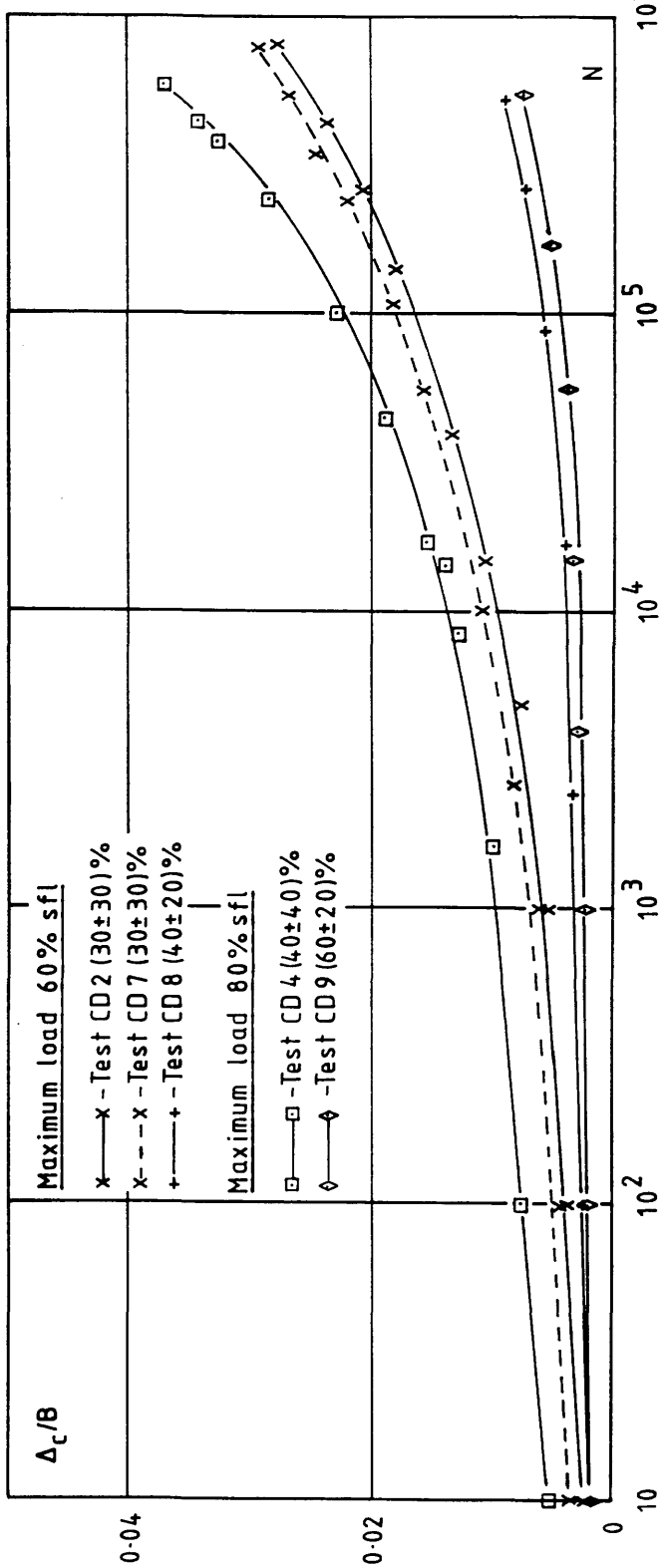

FIGURE 6.15 - Δ_c/B versus N : Amplitude effect on tests with same maximum load.

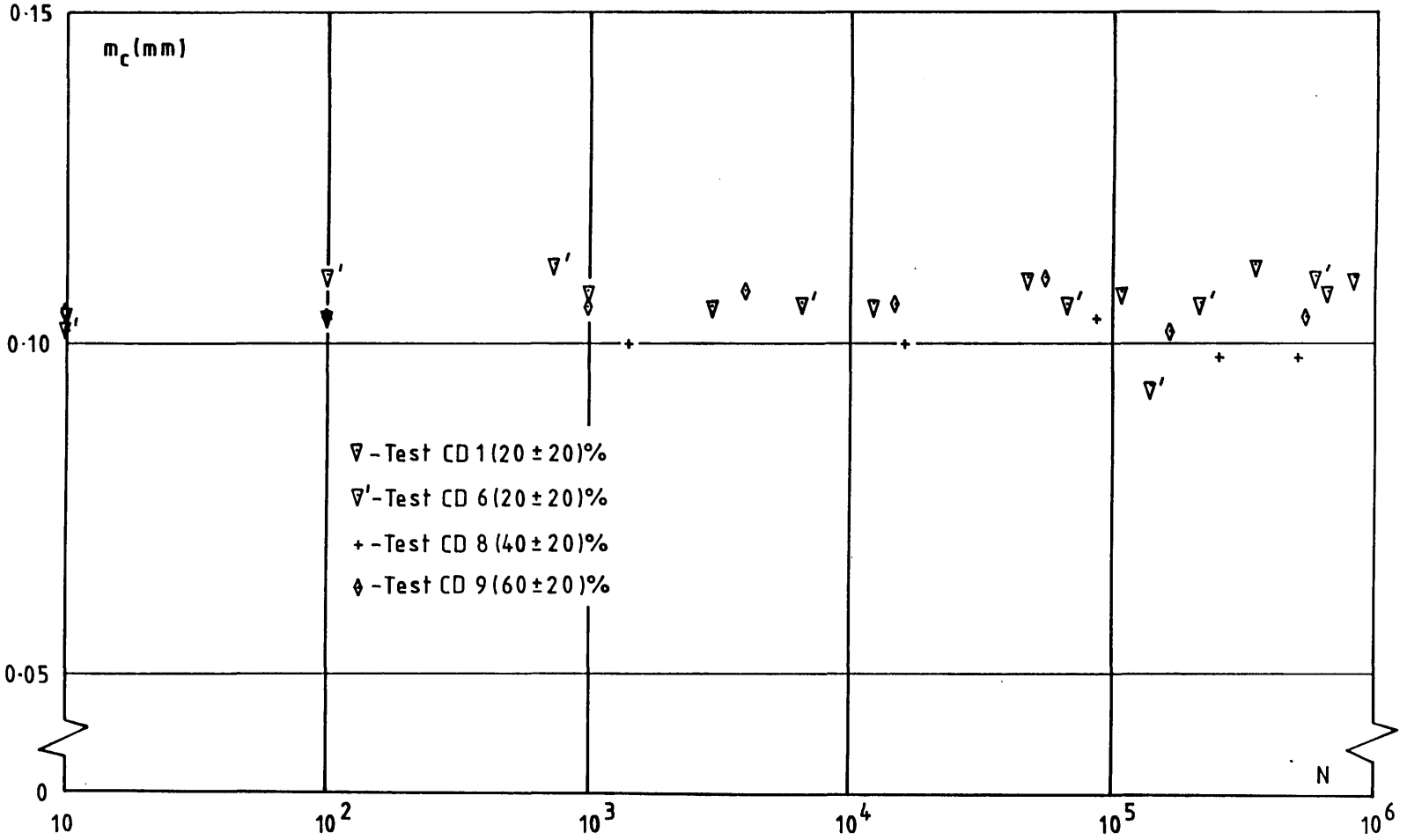

FIGURE 6.16 - m_c versus N : All tests with load amplitude of ± 20% sfl.

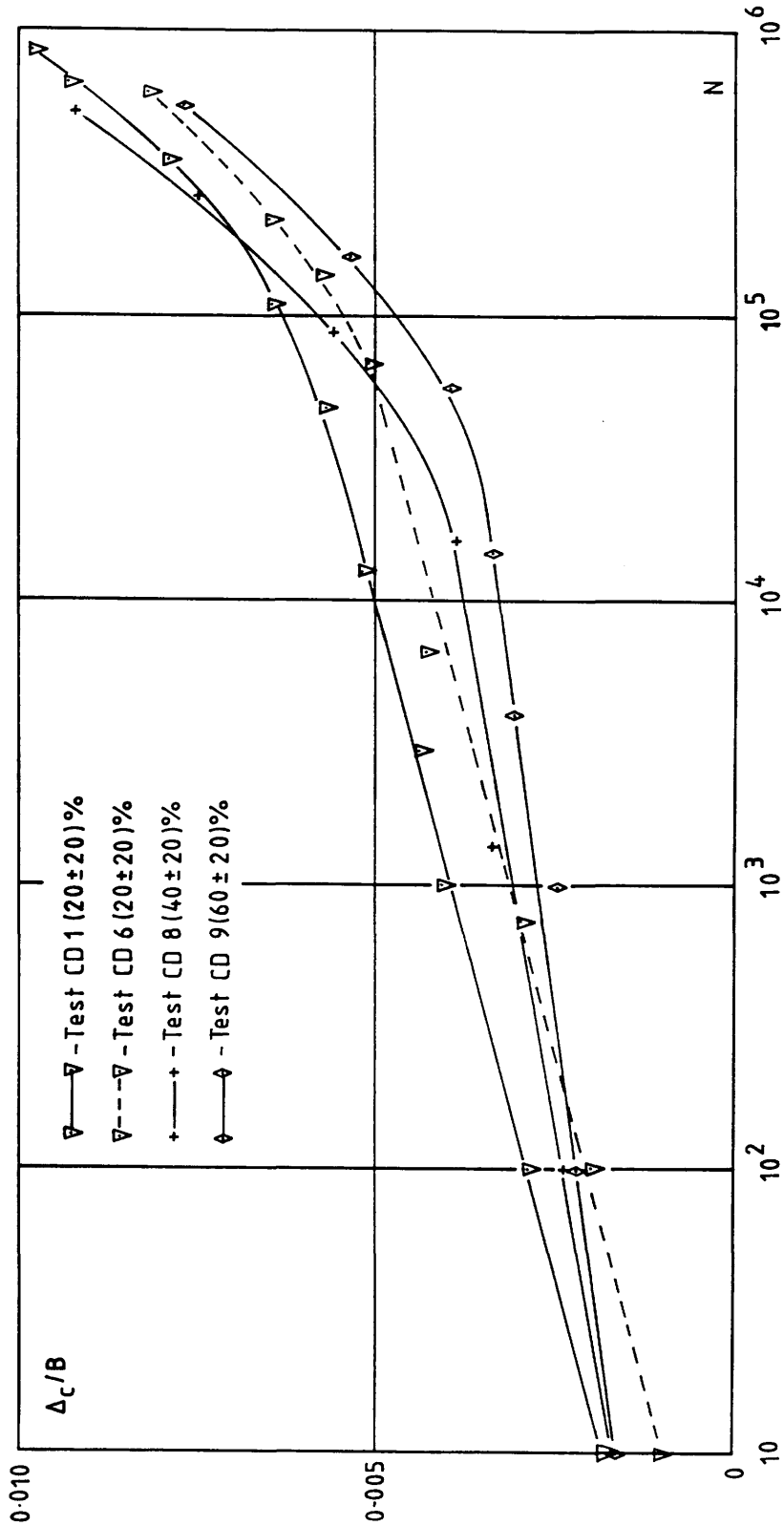

FIGURE 6.17 - Δ_c/B versus N : All tests with load amplitude of $\pm$ 20% sfl.

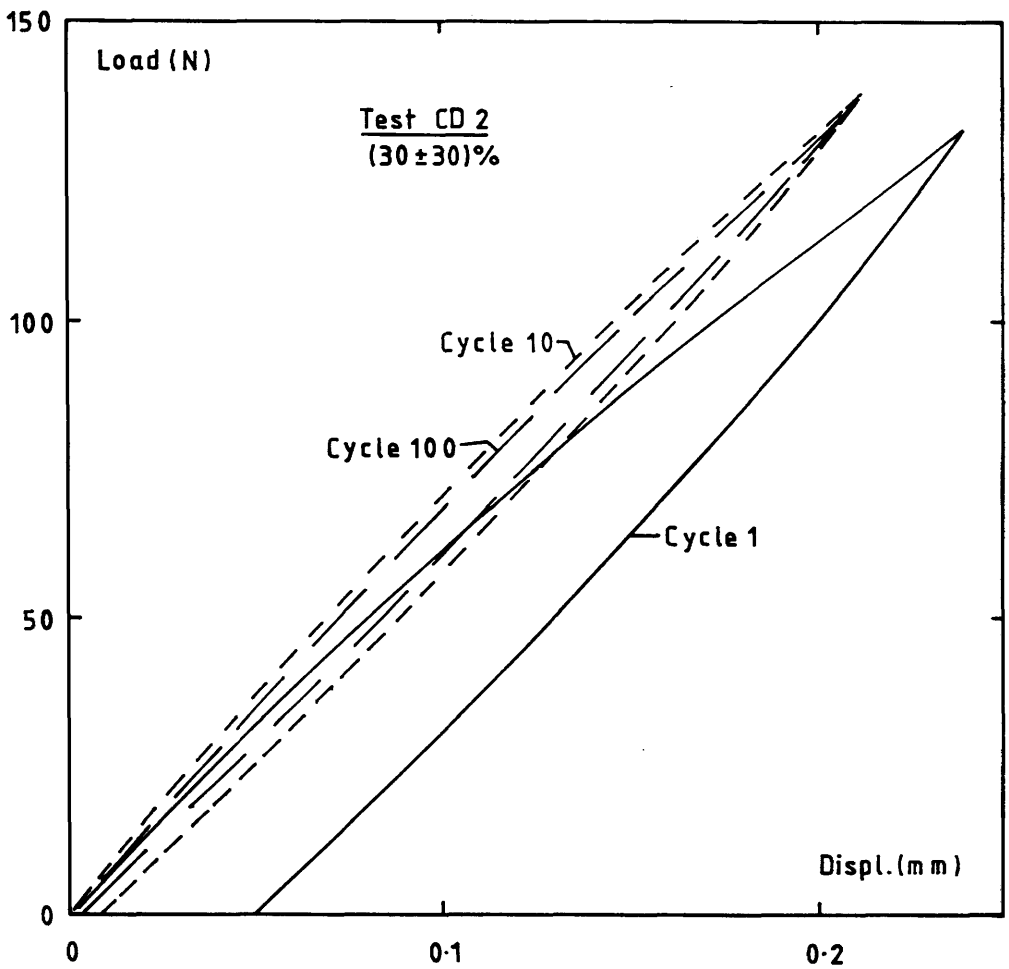

FIGURE 6.18 - Anchor Hysteresis: Typical results for tests in dense sand.

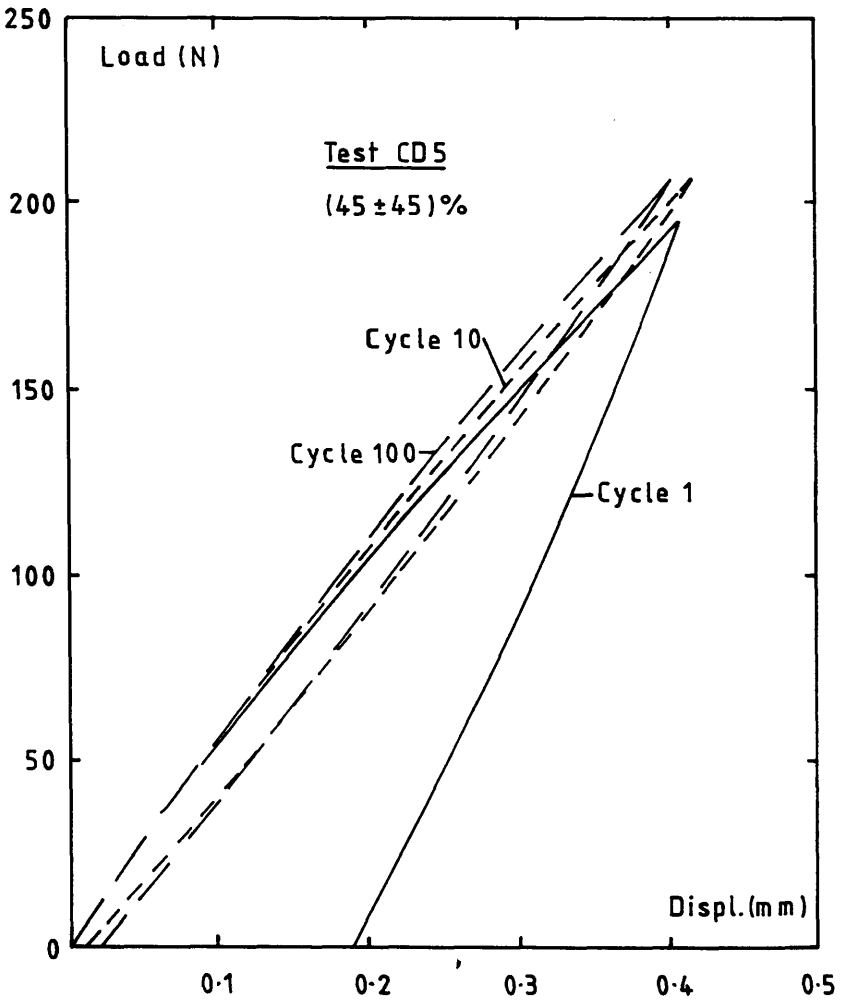

FIGURE 6.19 - Anchor Hysteresis: Results for test CD5.

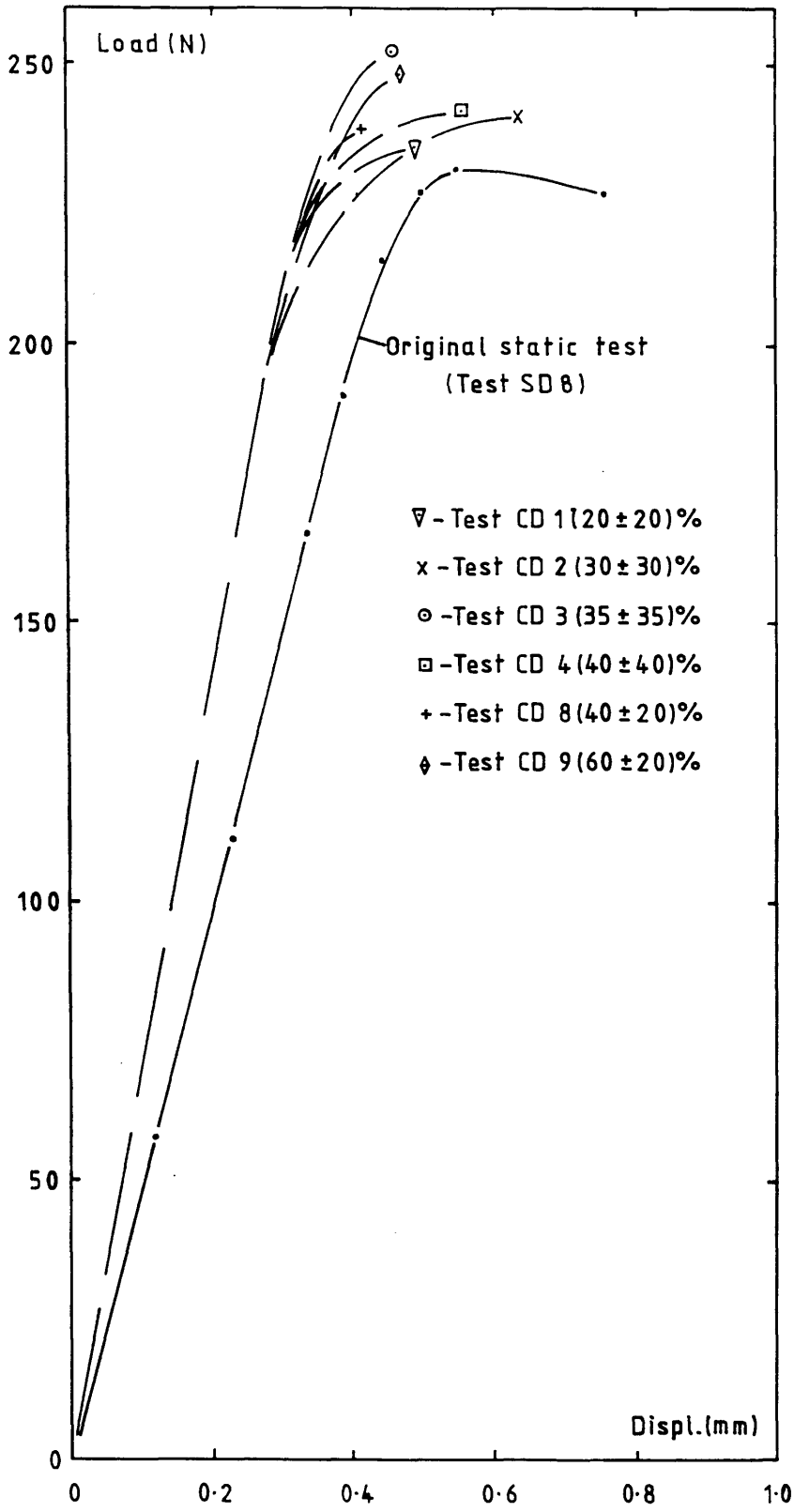

FIGURE 6.20 - Post-Cyclic Results: Load-displacement curves for tests in dense sand (D/B = 4.5).

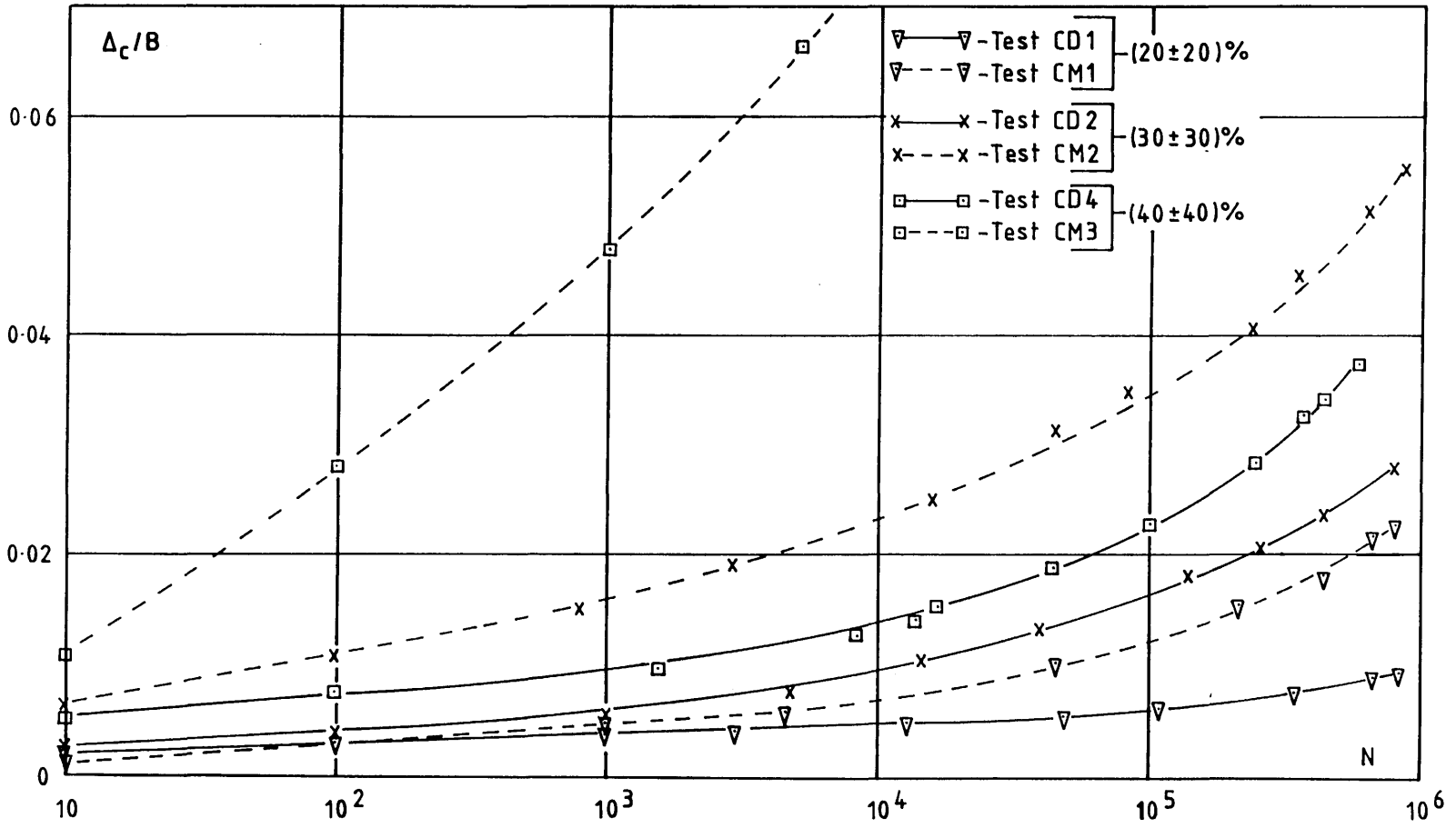

FIGURE 6.21 - Δ_c/B versus N : Comparison between dense sand (D_r = 93.0%) and medium-dense sand (D_r = 59.4%) test results.

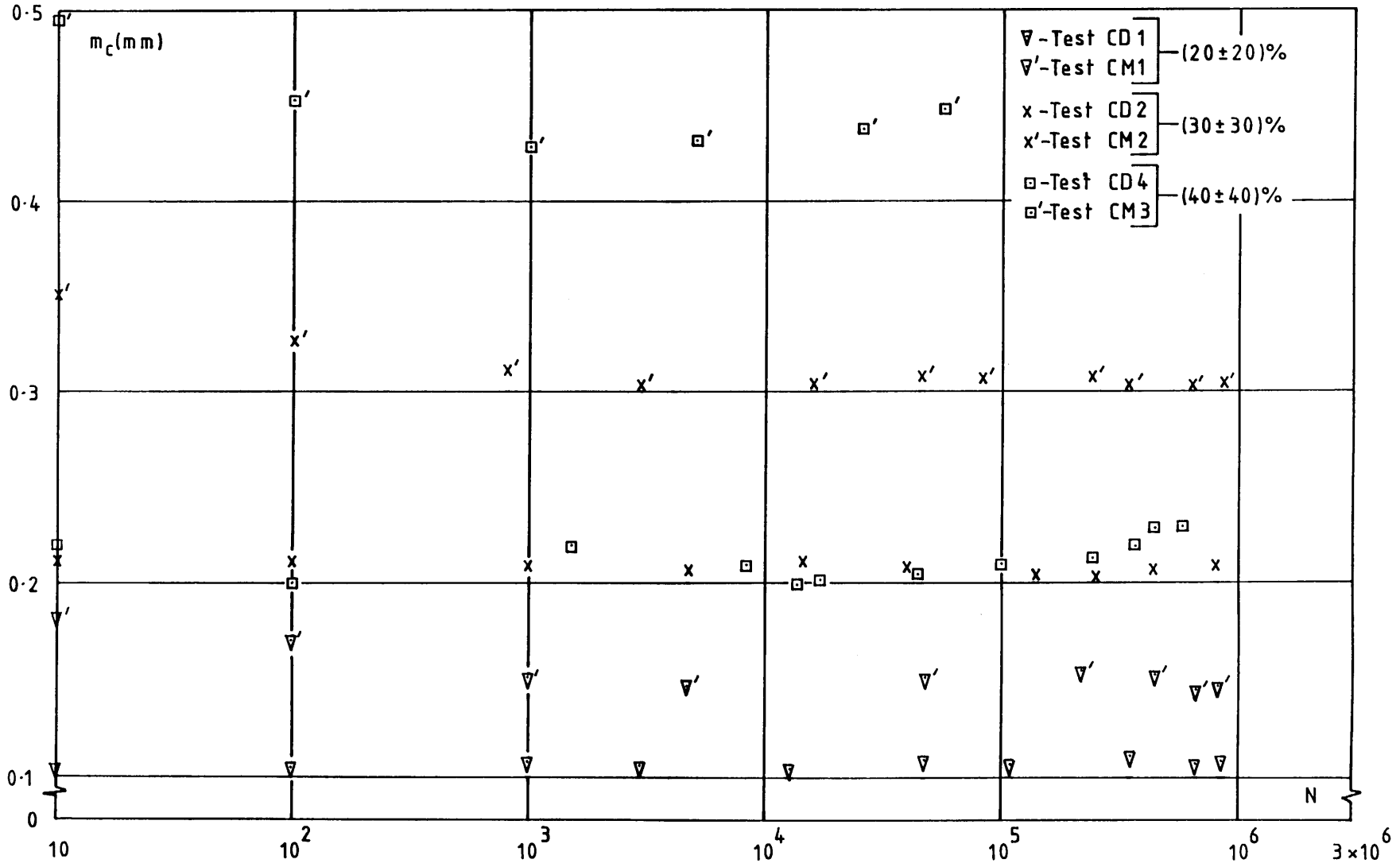

FIGURE 6.22 - m_c versus N : Comparison between dense and medium-dense test results.

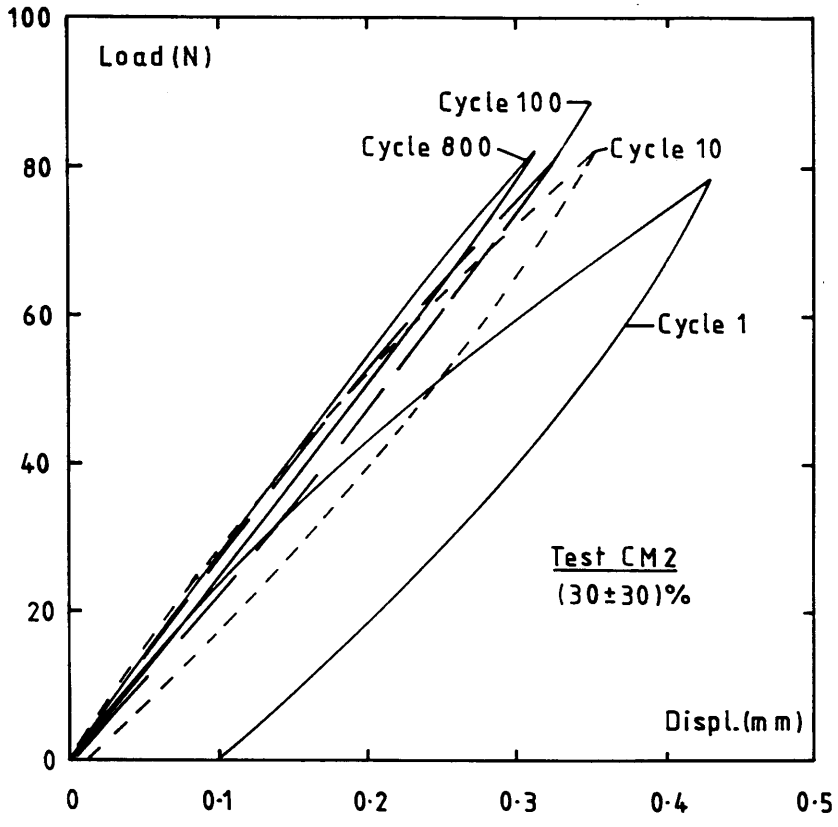

FIGURE 6.23 - Anchor Hysteresis: Typical results for tests in medium-dense sand.

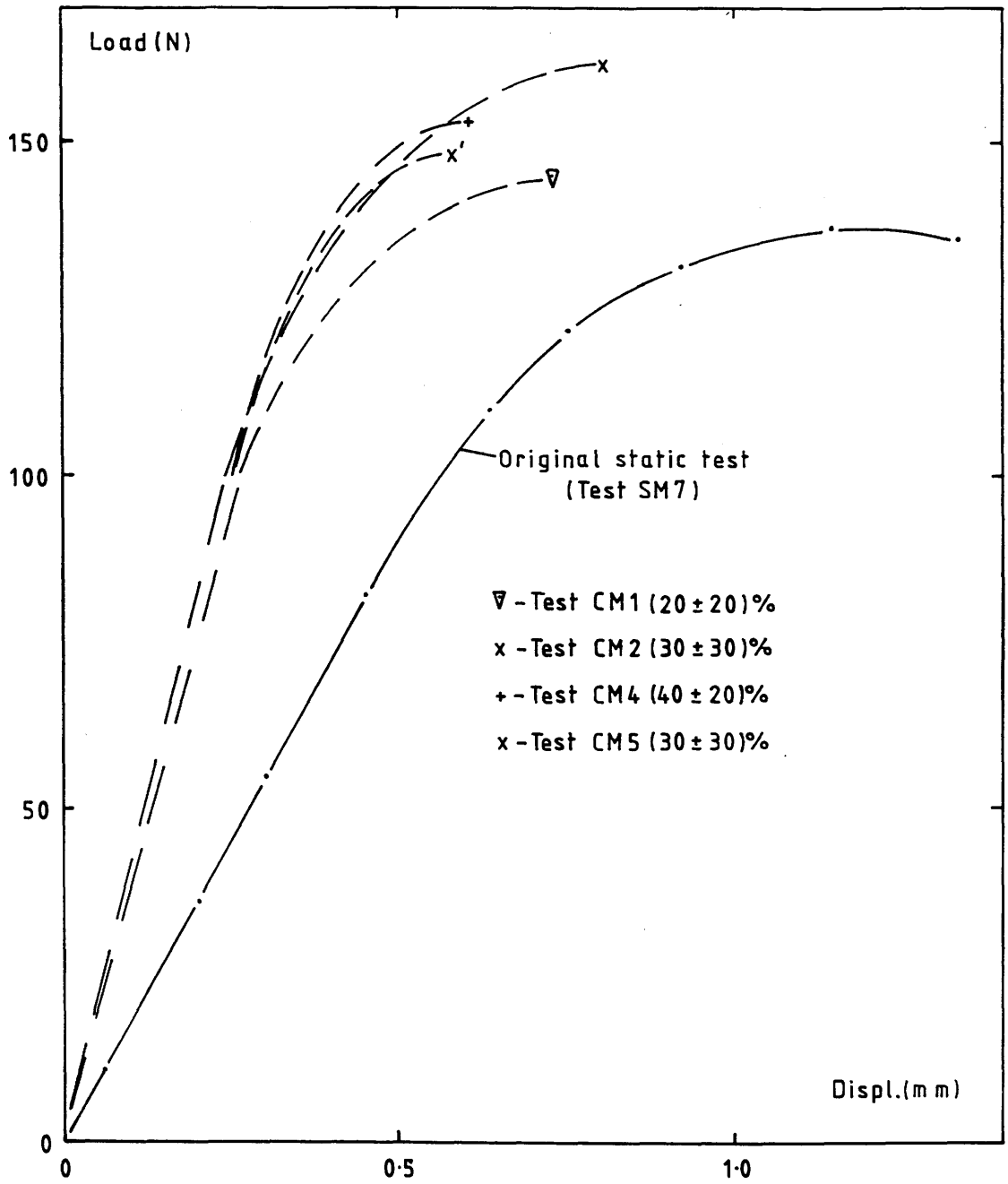

FIGURE 6.24 - Post-Cyclic Results: Load-displacement curves for tests in medium-dense sand (D/B = 4.5).

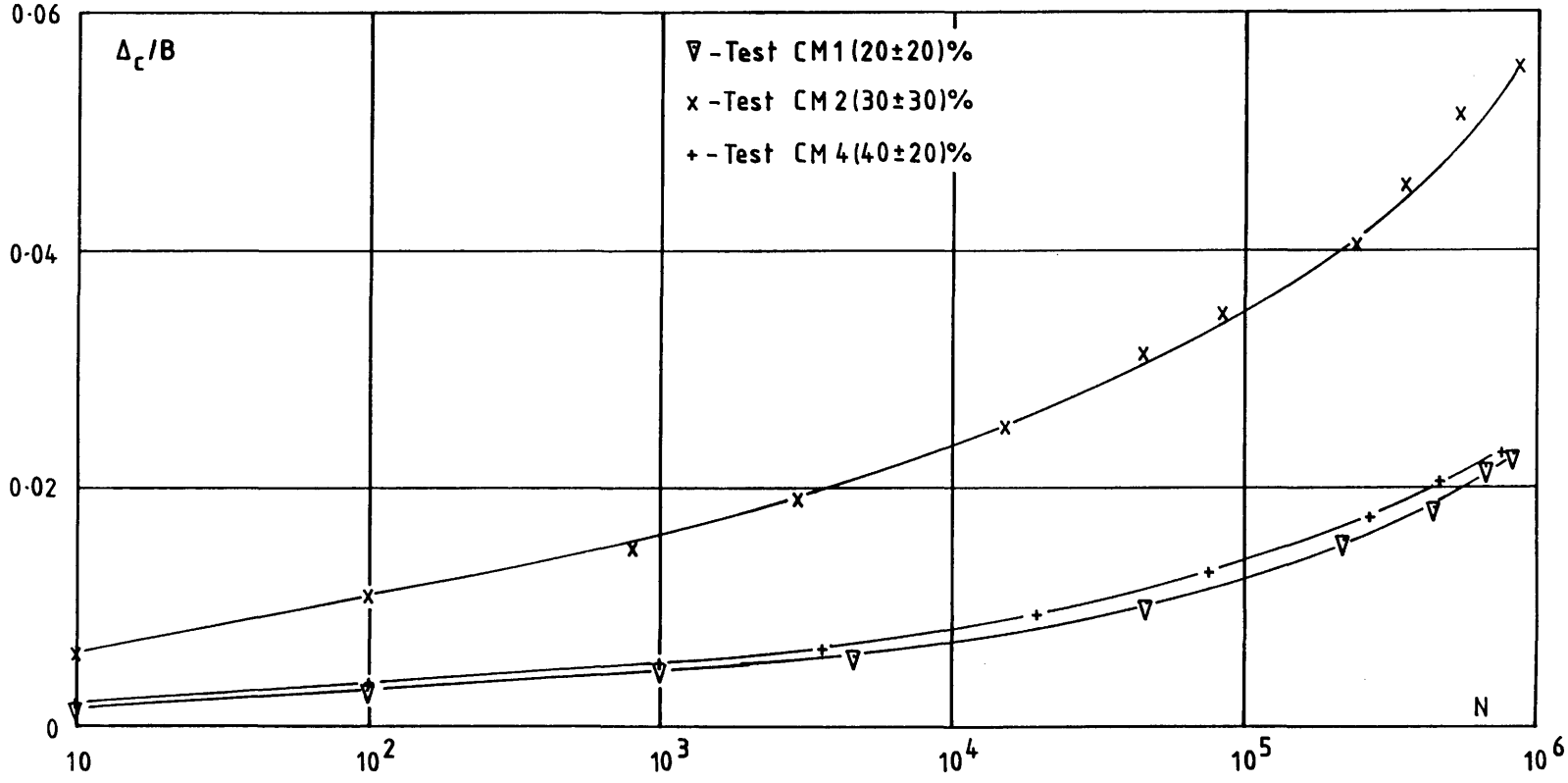

FIGURE 6.25 - Δ_c/B versus N: Amplitude effect on tests in medium-dense sand.

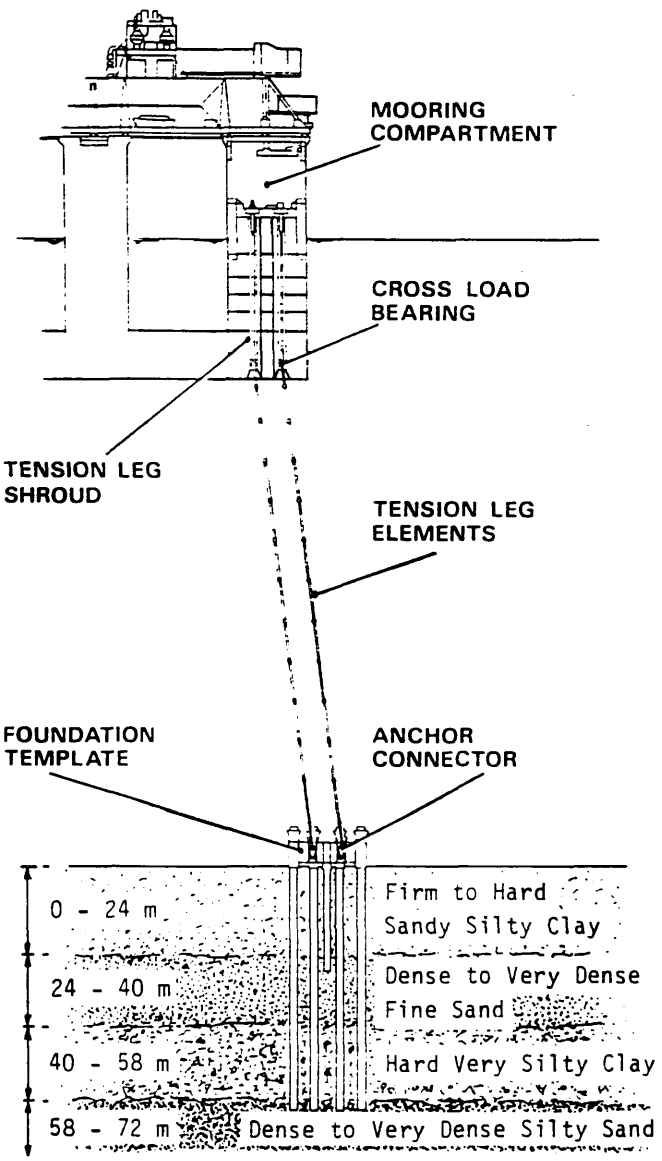

FIGURE 6.26 : Foundation arrangement for Hutton TLP (After Tetlow, et al, 1983).

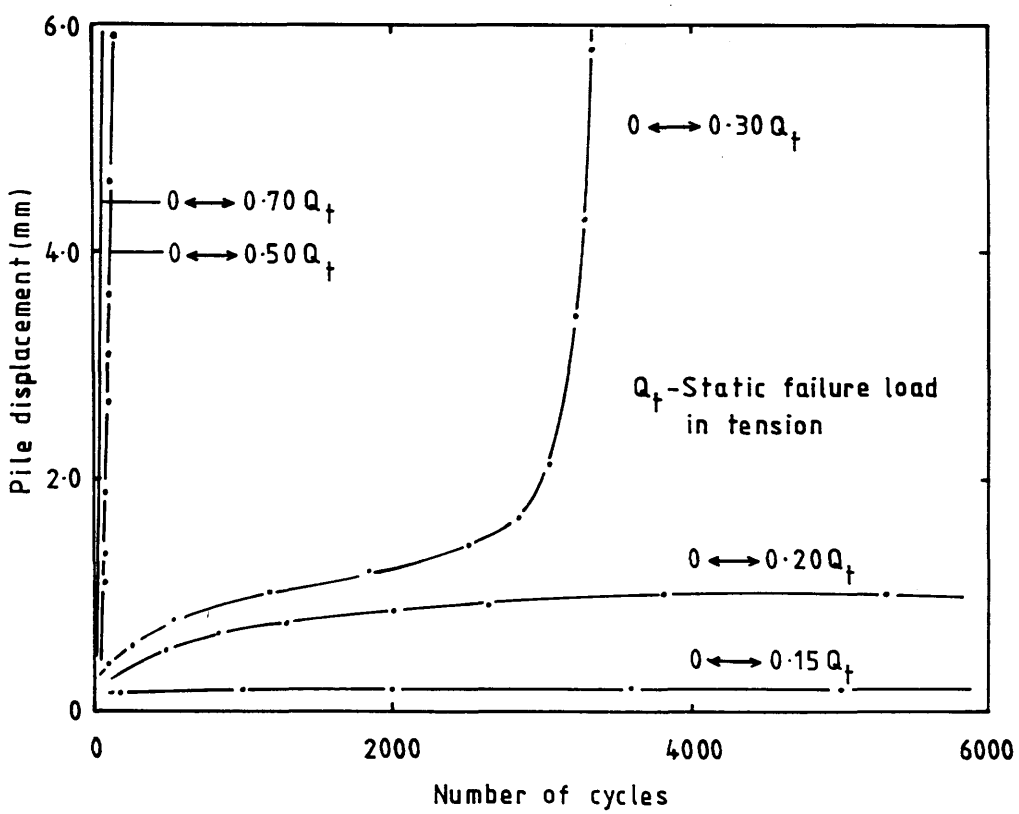

FIGURE 6.27 - Effect of cyclic loading on model pile displacement (After Chan and Hanna, 1980).

CHAPTER 7 – CONCLUSIONS

The apparatus and measurement equipment used in this investigation worked satisfactorily throughout the test period. When checked, the repeatability of the results from both the static and cyclic tests was good.

a) Static loading tests

The following conclusions are made with respect to the results from the static loading tests:

i) Expressed in terms of the uplift resistance factor, Nu, the results for dense sand ($D/B < 8$) and medium–dense sand ($D/B < 4$) compared well with those of previous investigations which used Leighton–Buzzard sand and with the theoretical method of Fadl (1981).

ii) In dense sand at $D/B > 8$, the results were seriously affected by boundary and scale effects, leading to substantial differences in Nu values for the same embedment ratio. It is therefore important that the influence of boundary and scale effects be borne in mind when comparison is made between the results of deep anchor tests in dense sand.

b) Cyclic loading tests

Within the range of parameter values used in this investigation, the following conclusions are made with respect to the results from the cyclic loading tests:

i) Attrition of the sand grains takes place around the anchor and is an important factor in maintaining cyclic creep. Due to this attrition, pre–cycling at a lower repeated load level has a detrimental effect on the anchor cyclic displacement when the repeated load level is increased.

ii) When cycling to the same maximum load level, the greater the load amplitude, the greater the cyclic displacement. For tests with the same load amplitude, the anchor cyclic displacement is similar.

iii) Apart from the anchors which failed during cycling, the load–displacement hysteresis of the anchors is very small. The response quickly stabilises into a near–elastic form which continues for the rest of the test.

iv) The post–cyclic static loading response is stiffer than the original static load test. The increase in stiffness takes place over the initial part of the test and is independent of the form of cyclic loading applied to the anchor. The ultimate resistance in the post–cyclic test is greater than that in the original.

v) A reduction in sand density leads to an increase in cyclic displacement, for anchors subjected to the same relative loading levels.

vi) For the anchors which failed during cycling, the failure mechanism can be described in terms of the behaviour of simple shear samples of sand subjected to cyclic loading. The onset of failure can be identified by an increase in the anchor displacement per cycle (Δ_{pc}), as proposed by Andreadis (1979).

c) Finite element study

The following conclusions are made with respect to the finite element study:

i) The stress distributions obtained using the elastic program (FINEALE2D) took the form of established analytical and numerical solution for analogous problems. However, in general, an elastic analysis is inappropriate for modelling the behaviour of plate anchors up to failure.

ii) Using the bi–linear program (FINETANBL), good correspondence with experimental load–displacement graphs was achieved for $P \leq 0.9 P_u$, but the inability of the bi–linear program to model strain softening behaviour leads to predicted failure loads of up to 3 times the experimental values.

iii) The local yield patterns obtained using the bi–linear program

confirmed two characteristics of shallow anchor behaviour: the presence of an elastic wedge of soil above the anchor and the truncated cone shape of the failure surface, as defined by the shape of the boundary of the yielded elements.

d) Suggestions for further study

i) Investigation of scale effects in model anchors subjected to cyclic loading. Considering the nature of the cyclic displacement mechanism, scale effects associated with confining pressure and particle size are particularly relevant in this respect. The investigation would seek to establish parameter limits to minimise any scale effects.

ii) Investigation of the cyclic displacement characteristics of groups of anchors. This is a logical extension of the static loading work done on anchor groups (Yilmaz, 1971 ; Wang 1986) and has important implications for any large–scale offshore deployment of plate–type anchors.

iii) Investigation of the effects of ground disturbance during placing on the cyclic displacement characteristics of single/group anchors. This would complement the static work done on ground disturbance using single anchors (Andreadis, 1979 ; Zakaria, 1986), and the work carried out in (ii) above. Once again, there are important practical implications for the offshore deployment of plate–type anchors.

iv) Continue the finite element work using more realistic stress–strain models for sand, in order to predict the ultimate uplift resistance. This would be carried out in conjunction with further model tests on more fully instrumented anchors. The material properties of the sand would also require further investigation.

v) Study of the anchor uplift problem using discrete element techniques. With the continuing development of computing power, the discrete element method (DEM) is potentially a very useful numerical tool for investigating the behaviour of particulate material (Cundall and Strack, 1979). The method has recently been applied to the problem of break–up in jointed rock (Lemos, et al, 1985), a process analogous to the attrition of sand grains during cyclic loading.

APPENDIX I

TRIAXIAL TEST RESULTS

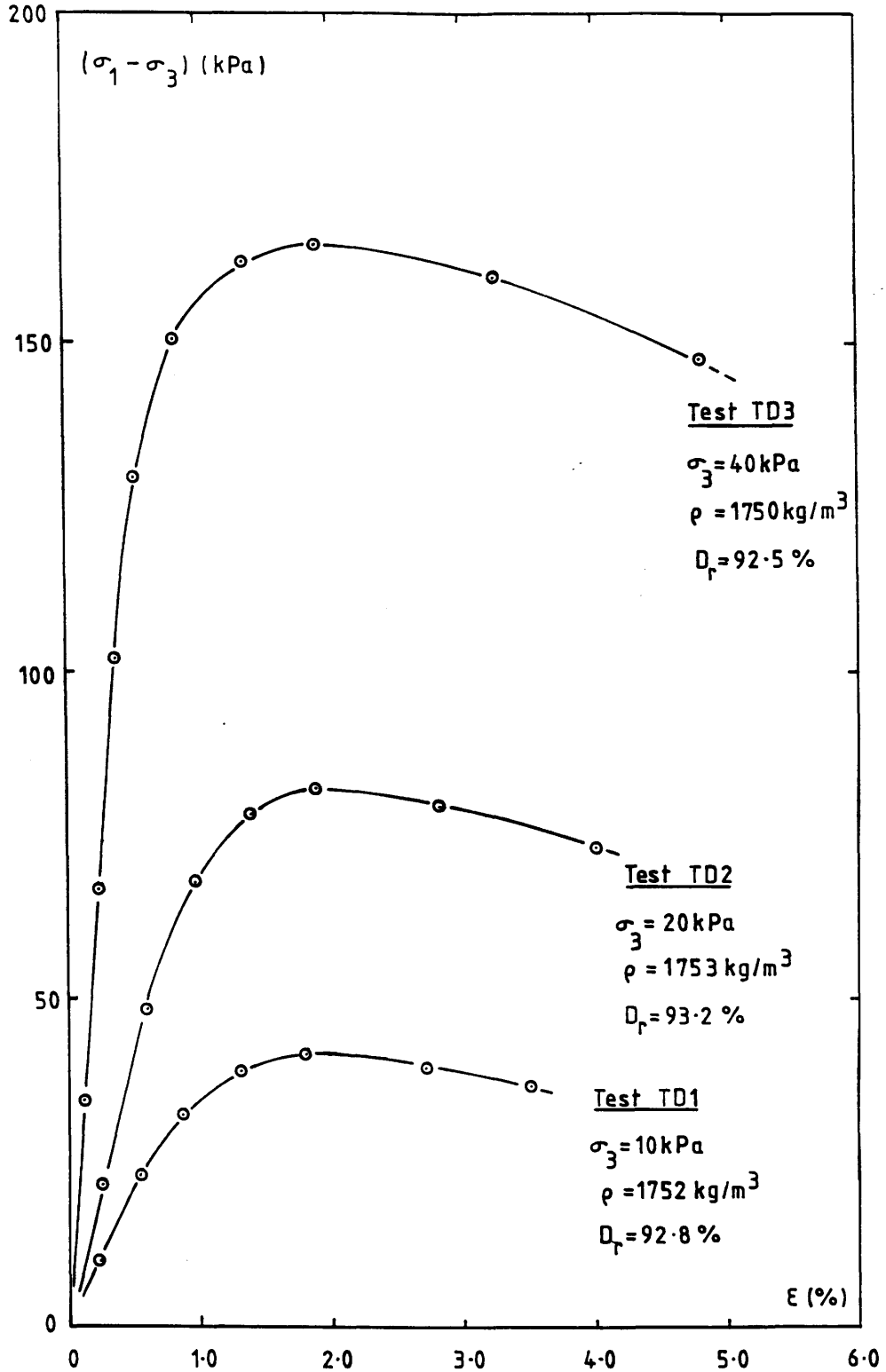

FIGURE A1.1 - Triaxial Test Results: Deviator stress versus strain for dense sand.

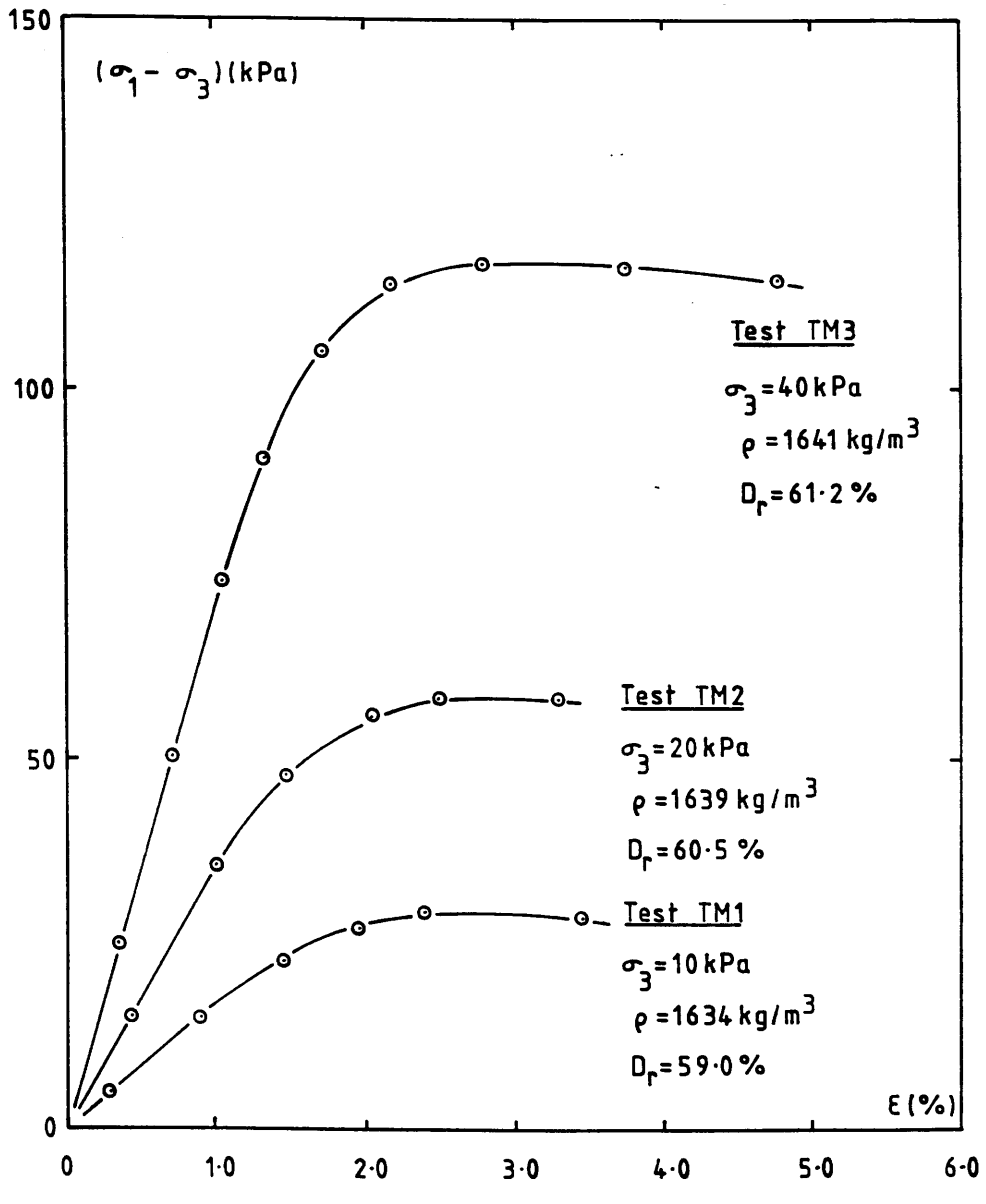

FIGURE A1.2 - Triaxial Test Results: Deviator stress versus strain for medium-dense sand.

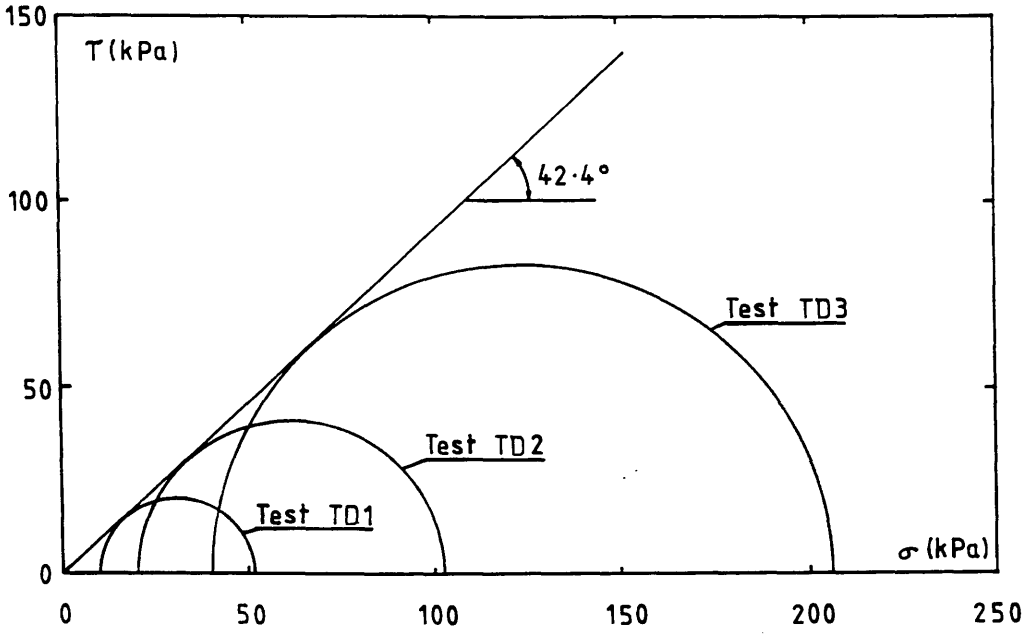

FIGURE A1.3 - Triaxial Test Results: Mohr circles for dense sand.

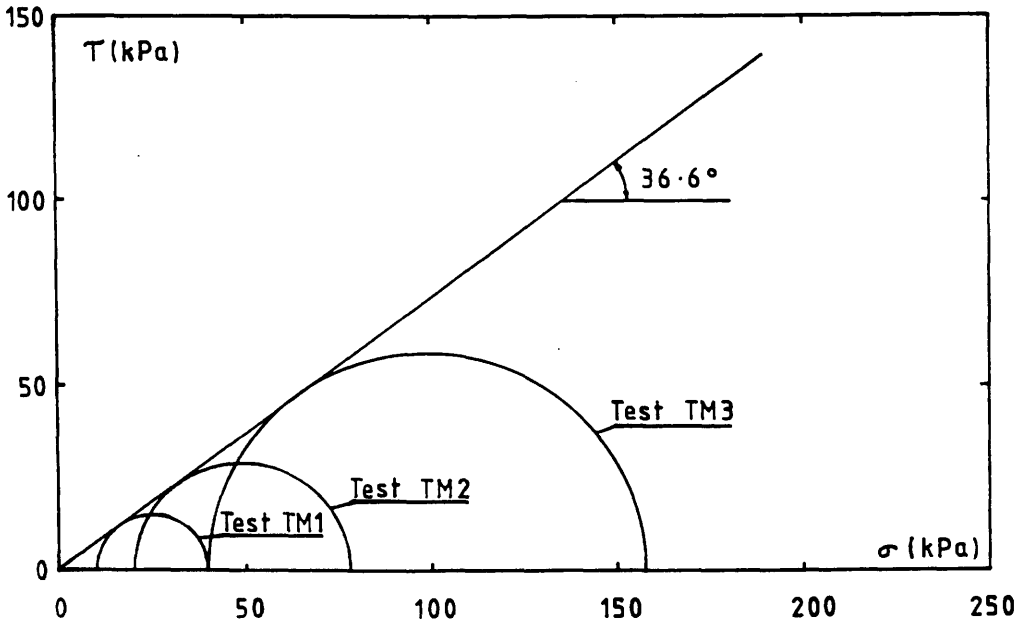

FIGURE A1.4 - Triaxial Test Results: Mohr circles for medium-dense sand.

APPENDIX II

EQUIPMENT INFORMATION

Equipment Information

RIG No. 1

Air Cylinder

Type: Schrader Pneumatics
Diameter: 100mm
Stroke: 100mm
Force at 1 bar pressure: 700N (approximately)

E– P Transducer

Type: GEC– Elliot Series 77
Supply pressure: 1– 4bar
Electrical input: 1– 5mA from signal generator
Minimum output pressure: zero

Load Cell

Type: Sangamo D91
Range: 0– 445N
Sensitivity: 1.0N/division (at DVM)

Displacement Transducers

Type: Sensonic SR
Stroke: ±25mm
Sensitivity: 0.02mm/division (at DVM)

RIG No. 2

Air Cylinder

Type: Schrader Pneumatics
Diameter: 150mm
Stroke: 150mm
Force at 1 bar pressure: 1600N (approximately)

E– P Transducer

Type: GEC– Elliot Series 77
Supply pressure: 1– 4bar
Electrical input: 1– 5mA from signal generator
Minimum output pressure: zero

Load Cell

Type: Sangamo D91
Range: 0– 2225N
Sensitivity: 1.0N/division (at DVM)

Displacement Transducers

Type: Sensonic SR
Stroke: ±25mm
Sensitivity: 0.02mm/division (at DVM)

RIG No. 3

Air Cylinder

Type: Schrader Pneumatics
Diameter: 80mm
Stroke: 150mm
Force at 1 bar pressure: 450N (approximately)

E– P Transducer

Type: GEC– Elliot Series 77
Supply pressure: 1.4bar
Electrical input: 1– 5mA from signal generator
Minimum output pressure: zero.

Load Cell

Type: Sangamo D91
Range: 0– 445N
Sensitivity: 1.0N/division (at DVM)

Displacement Transducers

Type: Sensonics SR
Stroke: ±25mm
Sensitivity: 0.02mm/division (at DVM)

Air filters, lubricators and regulators supplied by Schrader Pneumatics. Air pressure gauges supplied by Budenberg.

SUPPLIERS

George Garside (Sand) Ltd.,
39 Hockcliffe Street,
Leighton– Buzzard,
LU7 8HB.
0525– 372201.

Sangamo Schlumberger,
Southern Cross Industrial Estate,
Bognor Regis,
Sussex, PO22 9ST.
0243– 825011.

Sensonics,
Chartridge Lane,
Chartridge,
Chesham,
Bucks, HP5 2SH.
0494– 774251.

GEC– Elliott Automation Ltd.,
1 Stanhope Gate,
London, W1A 1EH.
01– 493– 8484

Schrader Pneumatics,
Walkmill Lane,
Bridgtown,
Cannock,
Staffordshire, WS11 3LR.
0543– 462644.

Budenberg Gauge Ltd.,
59 Berkeley Street,
Glasgow, G3 7DX.
041– 248– 6847.

APPENDIX III

LOAD– DISPLACEMENT GRAPHS FOR STATIC TESTS

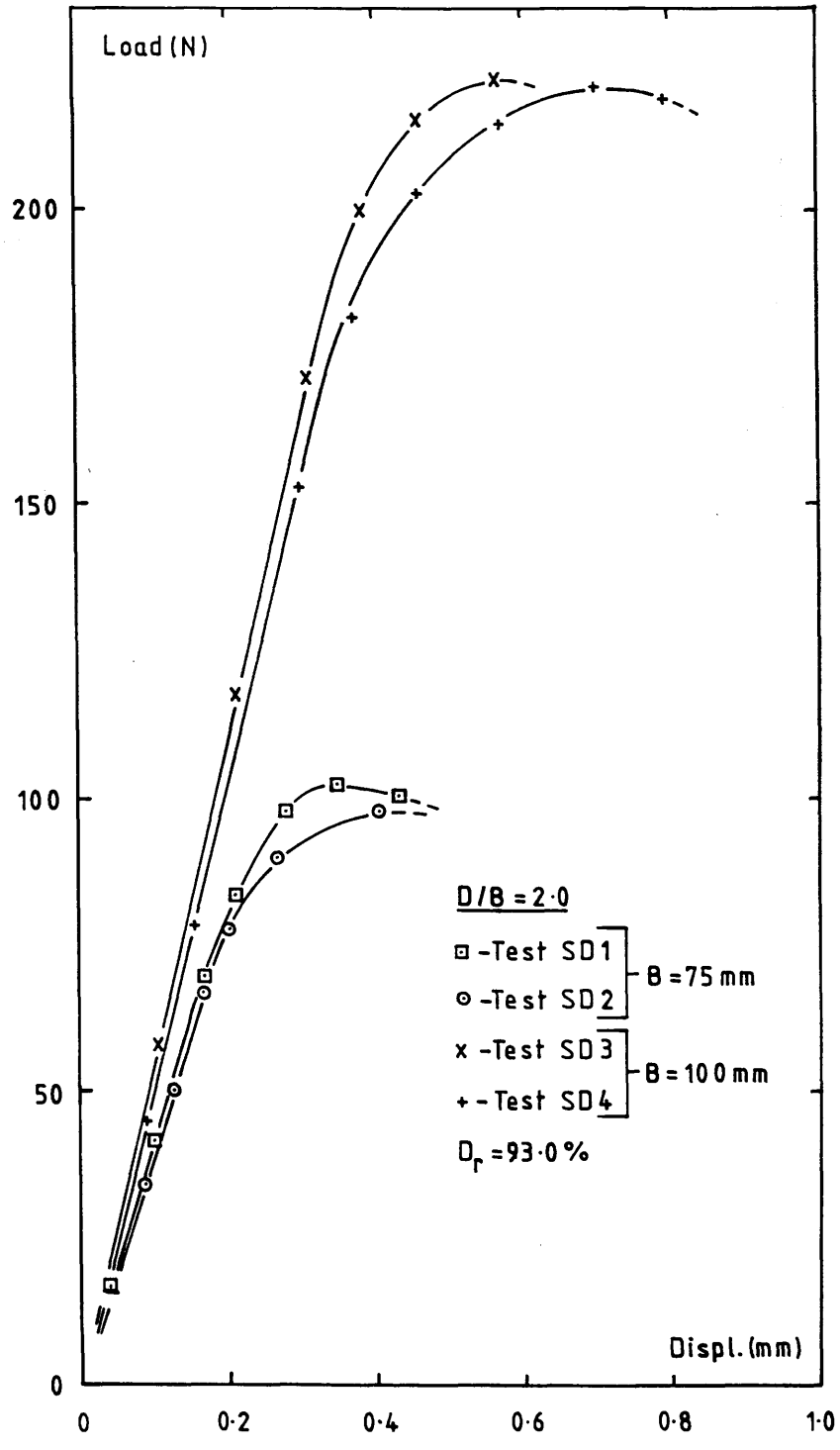

FIGURE A3.1 - Dense Sand Results: Load-displacement for tests SD1, SD2, SD3 and SD4.

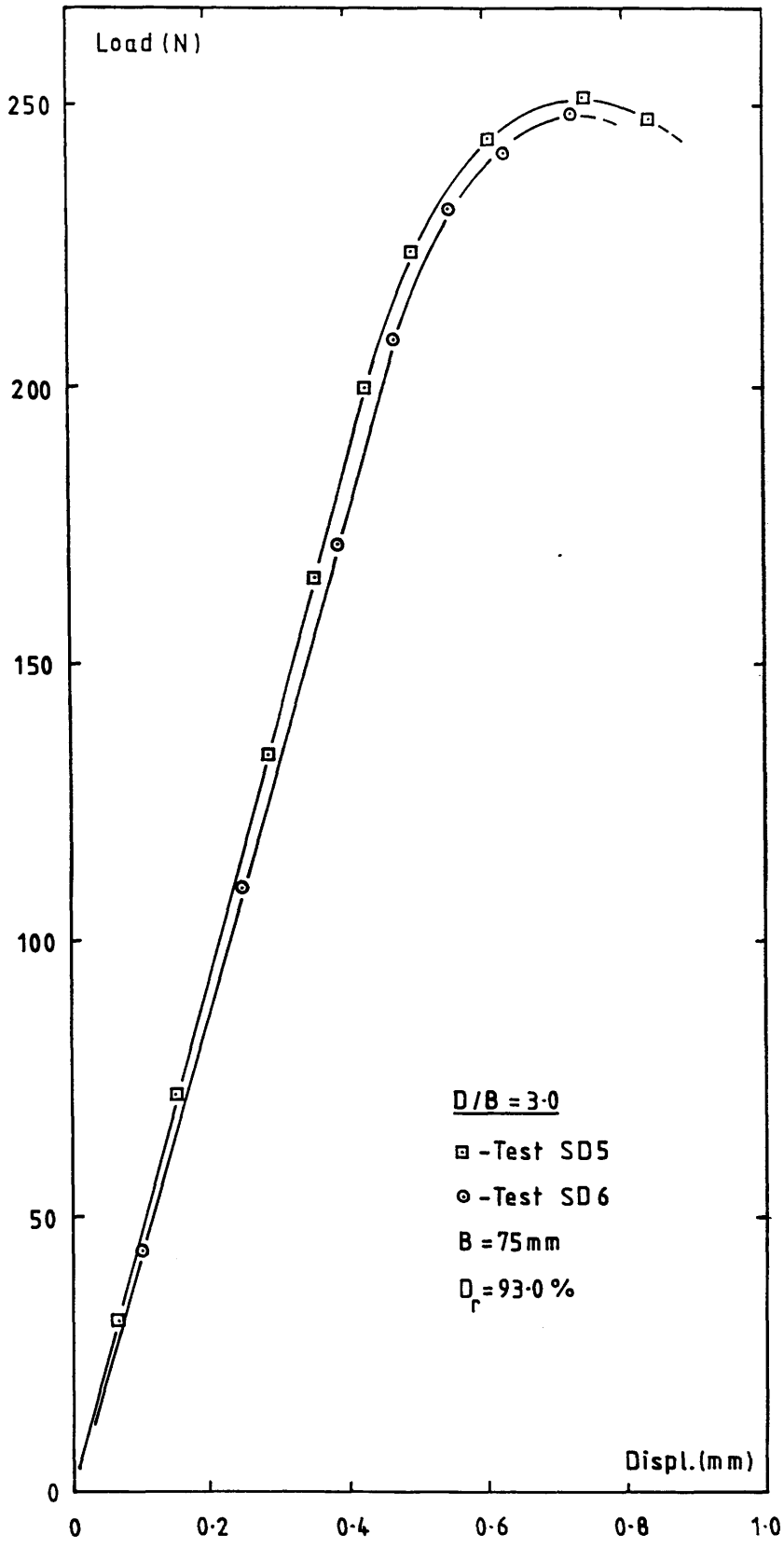

FIGURE A3.2 - Dense Sand Results: Load-displacement for tests SD5 and SD6.

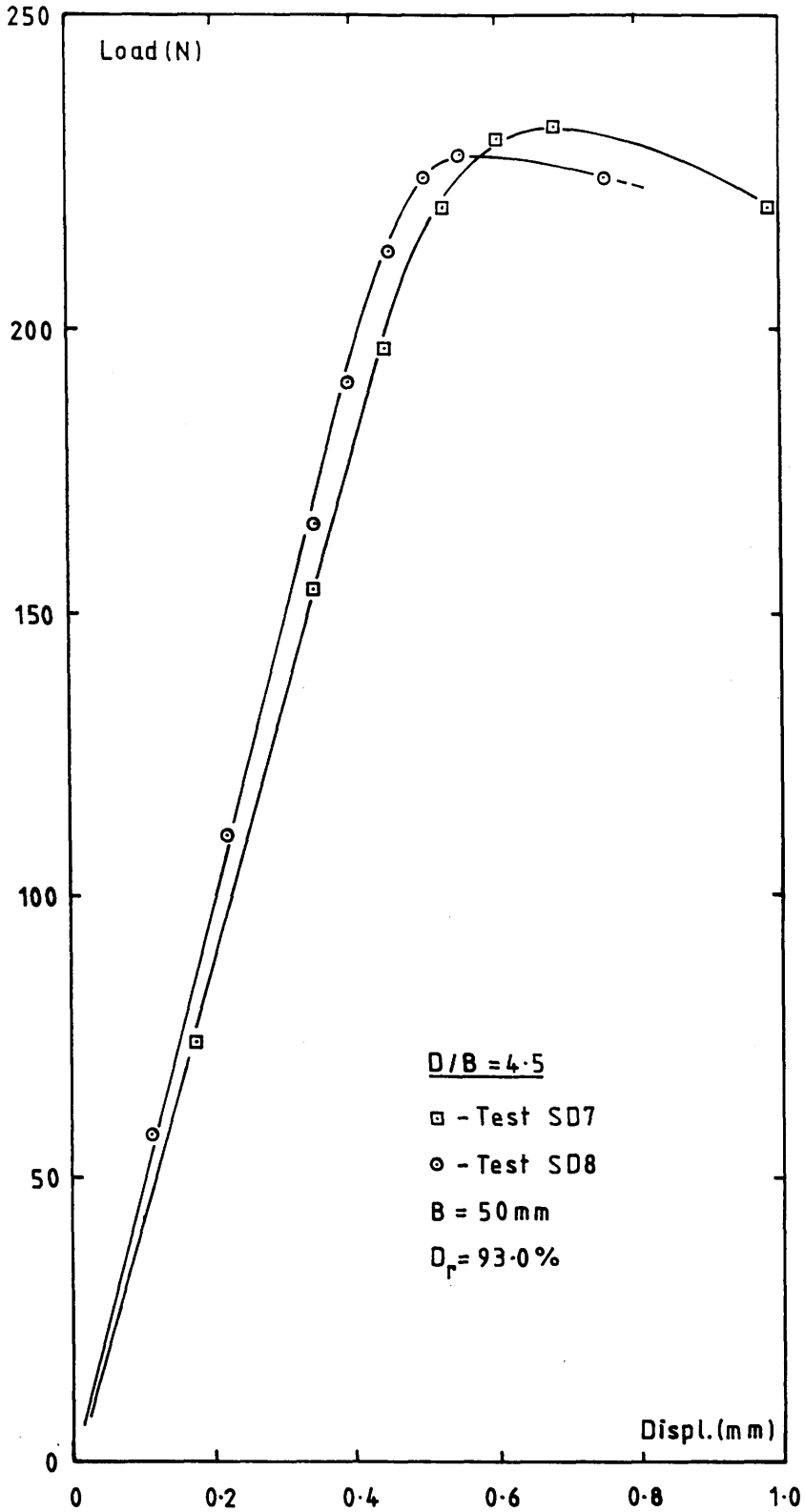

FIGURE A3.3 - Dense Sand Results: Load-displacement for tests SD7 and SD8.

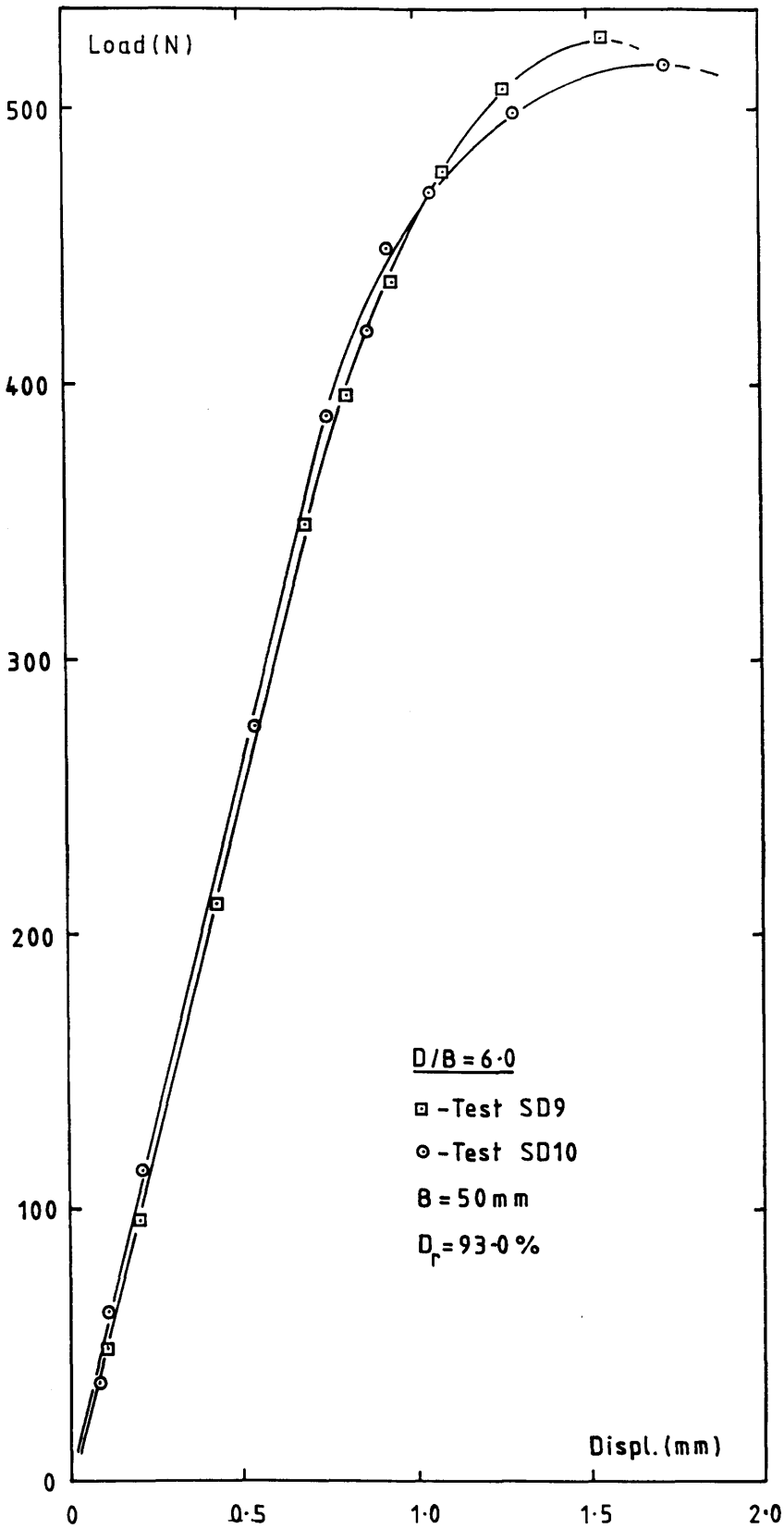

FIGURE A3.4 - Dense Sand Results: Load-displacement for tests SD9 and SD10.

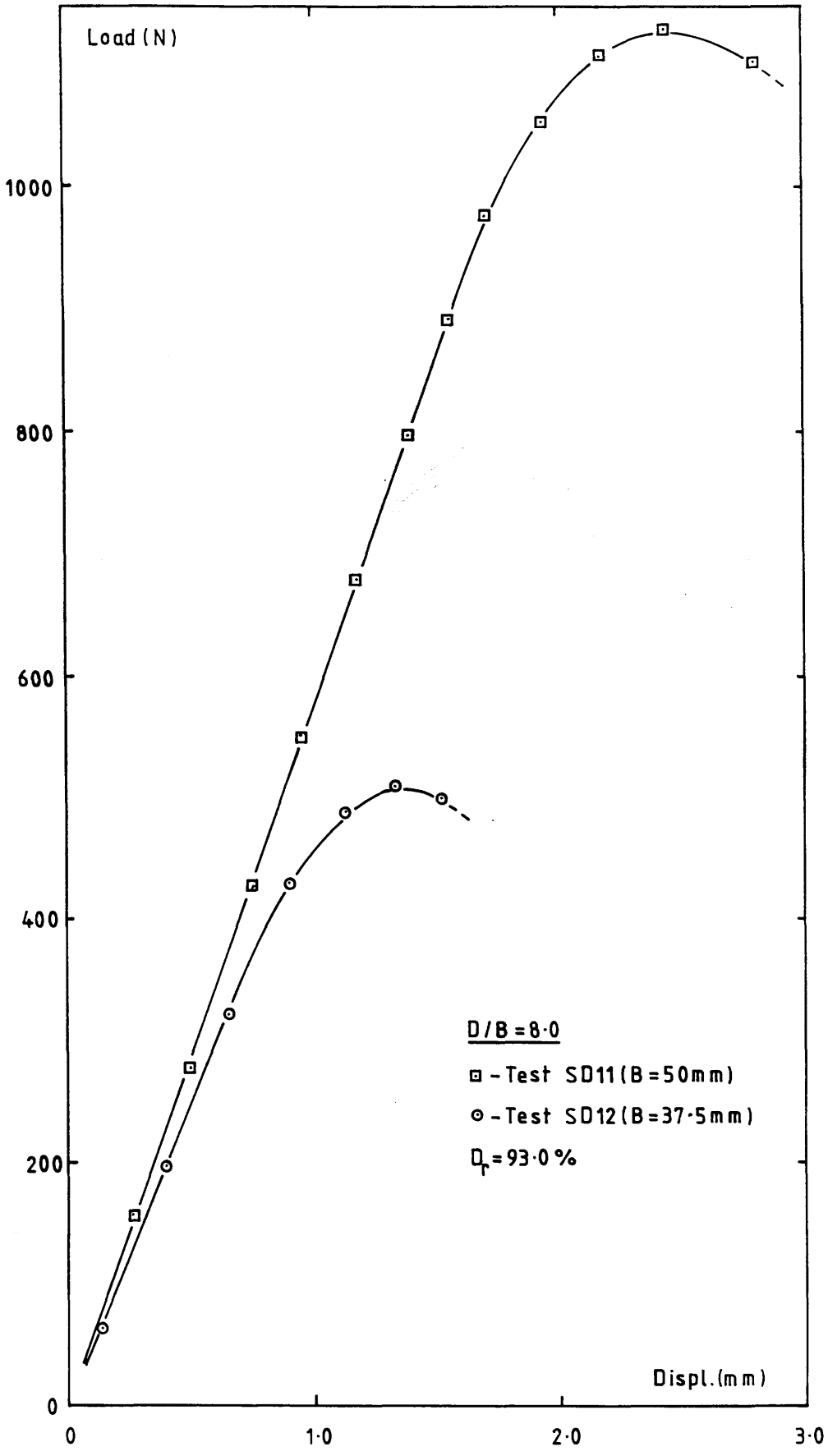

FIGURE A3.5 - Dense Sand Results: Load-displacement for tests SD11 and SD12.

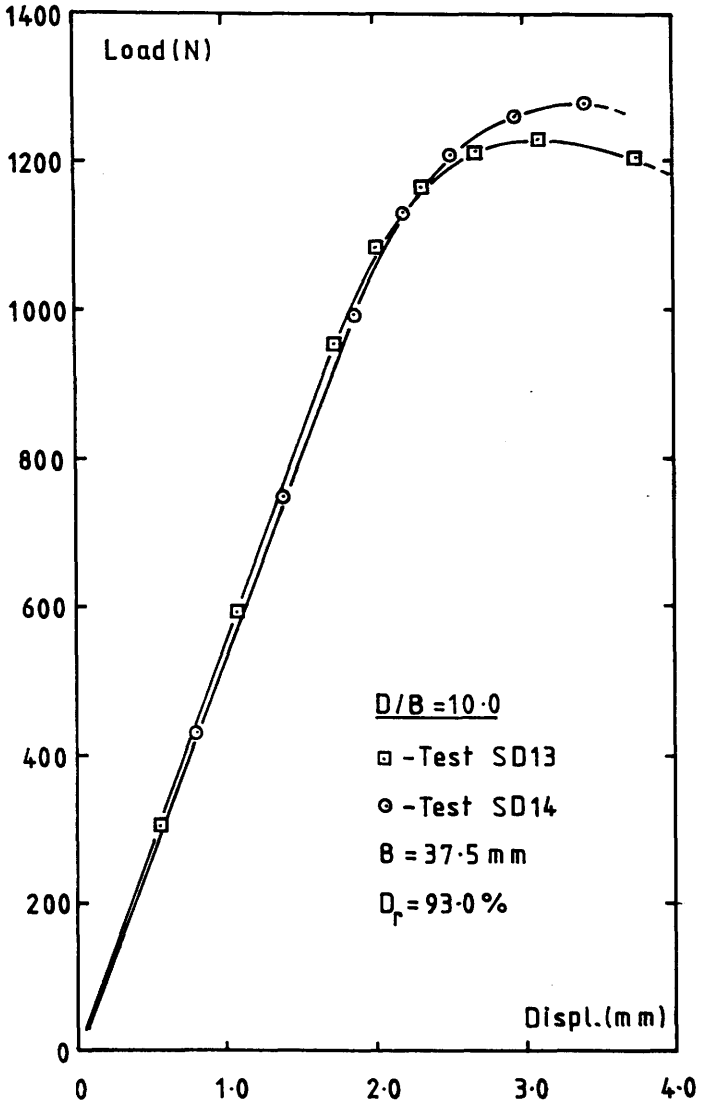

FIGURE A3.6 - Dense Sand Results: Load-displacement for tests SD13 and SD14.

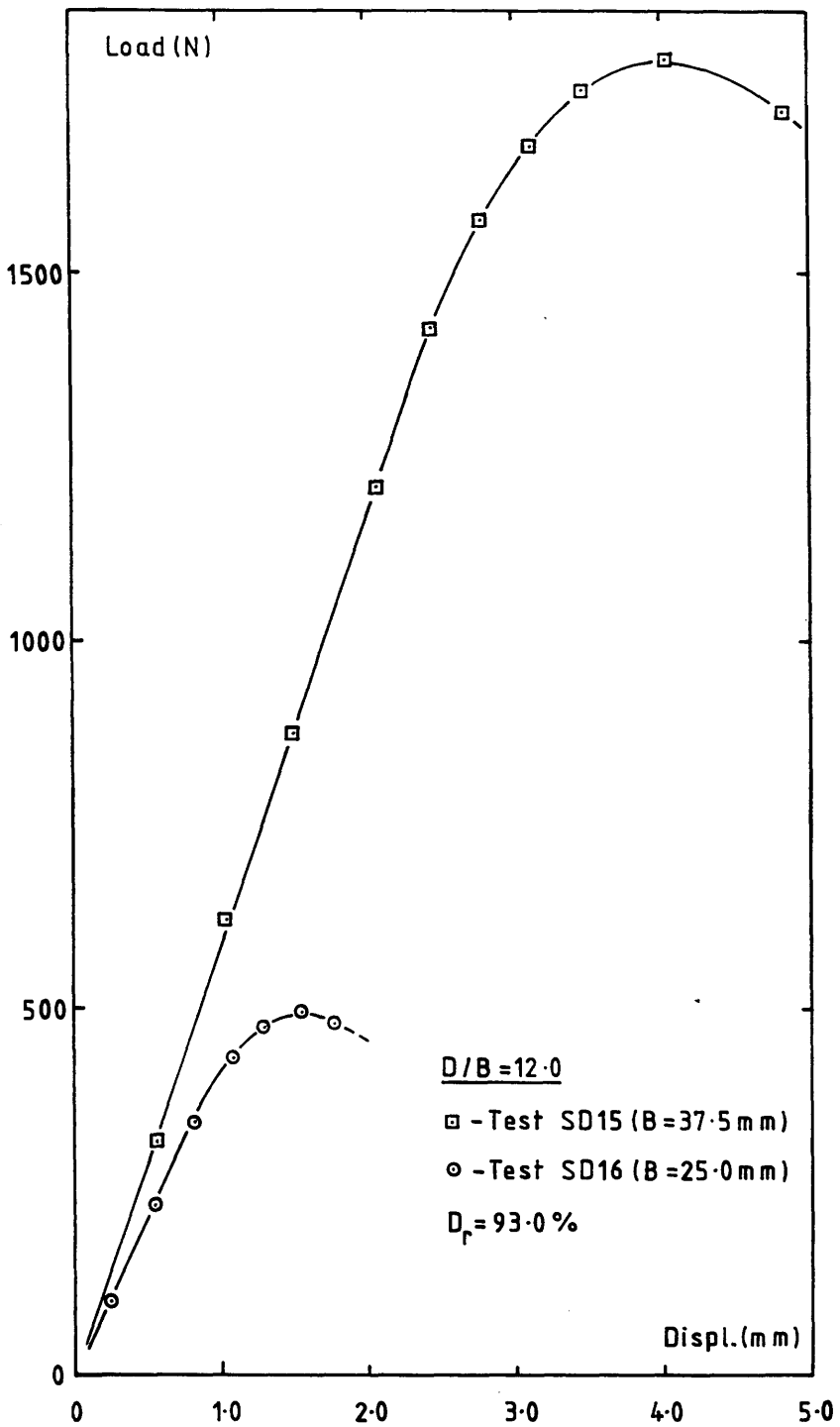

FIGURE A3.7 - Dense Sand Results: Load-displacement for tests SD15 and SD16.

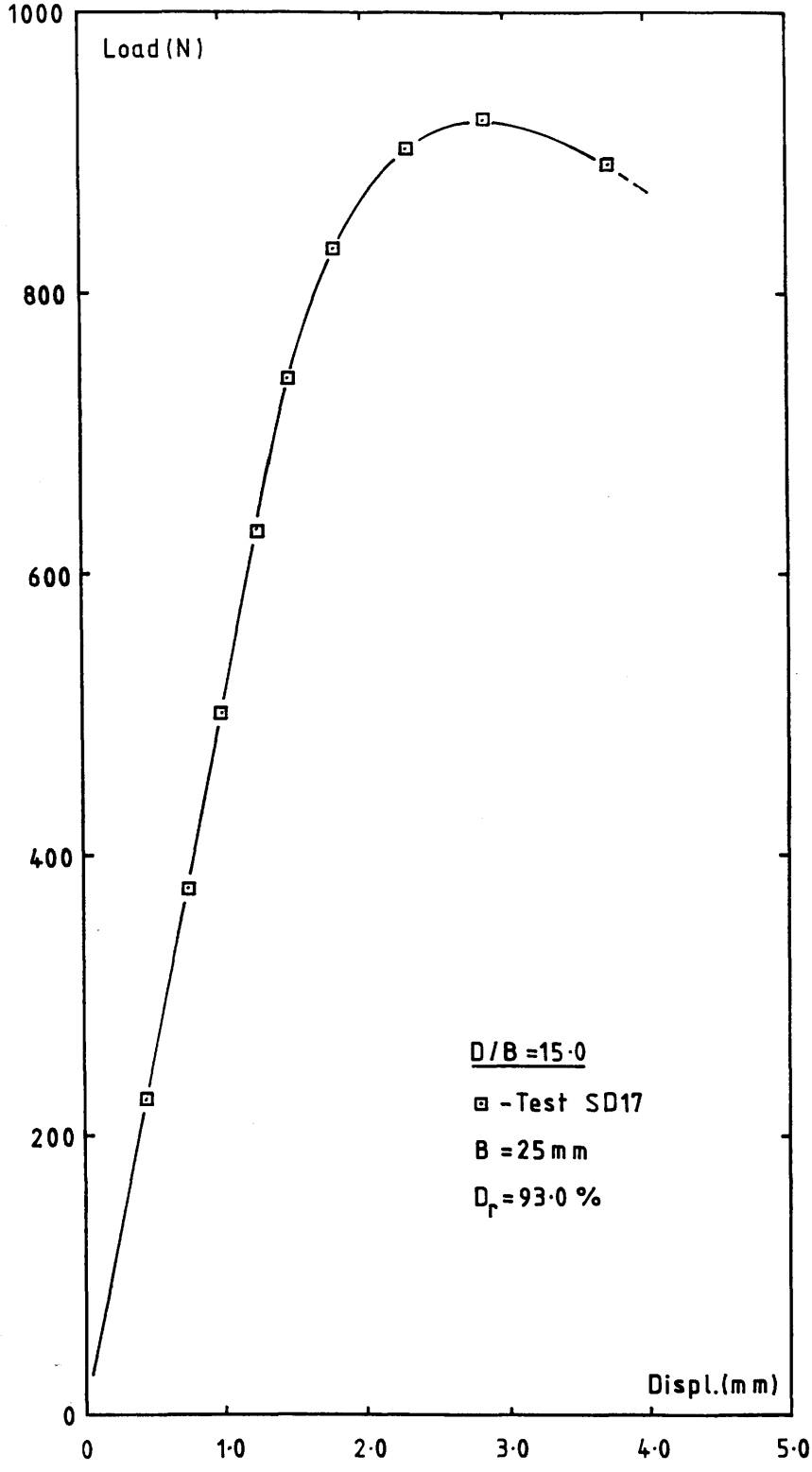

FIGURE A3.8 - Dense Sand Results: Load-displacement for test SD17.

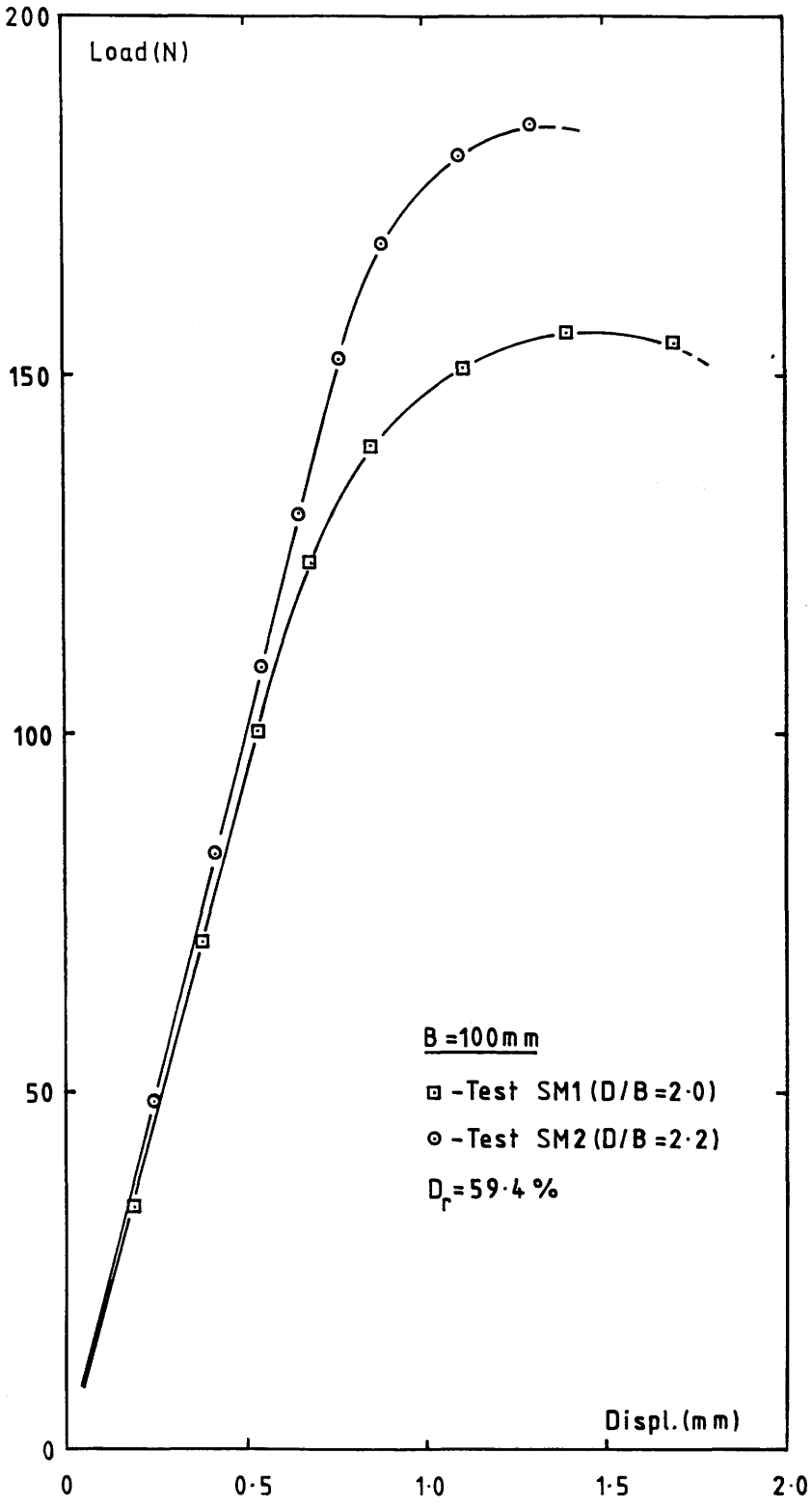

FIGURE A3.9 - Medium-Dense Sand Results: Load-displacement for tests SM1 and SM2.

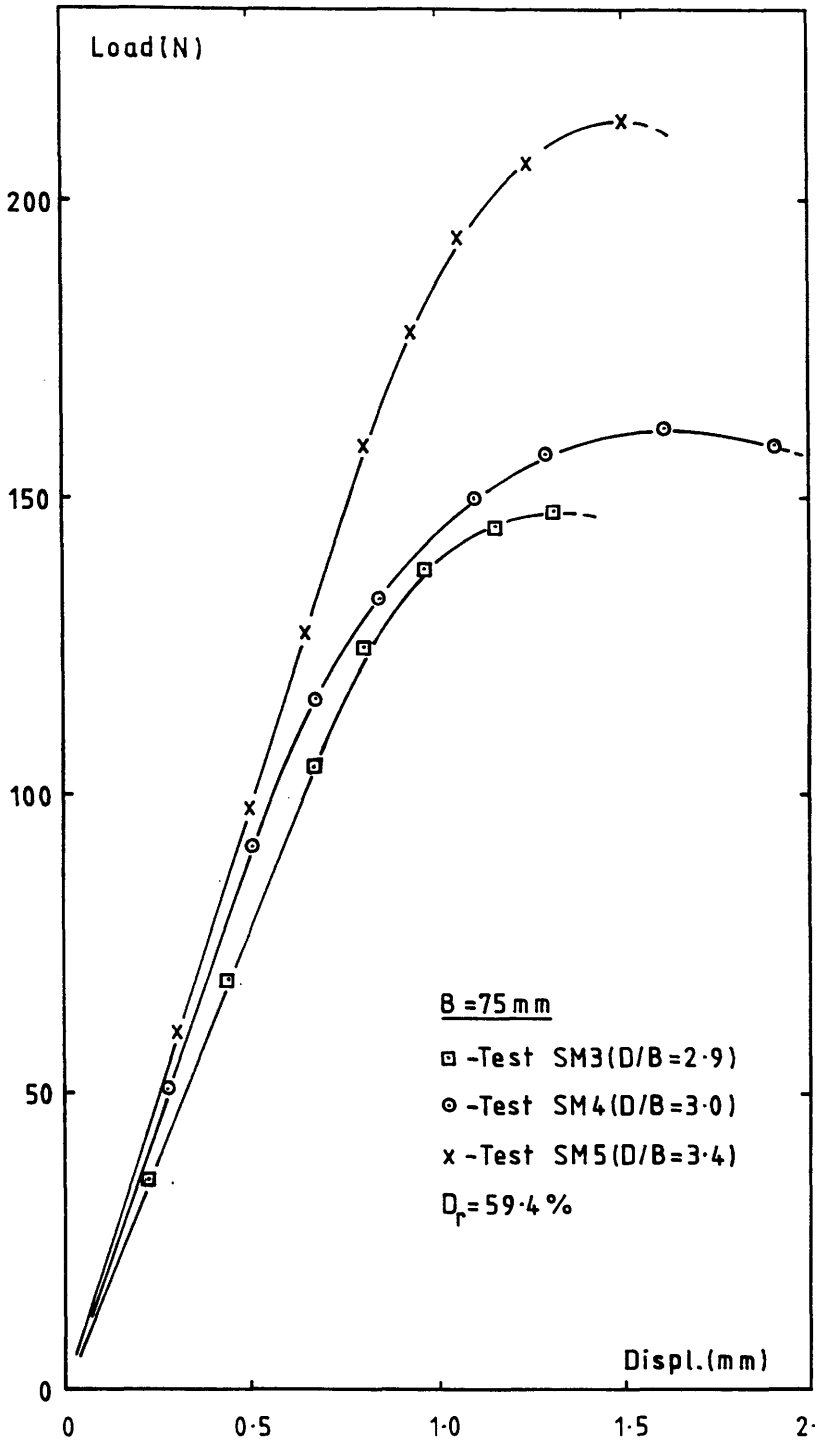

FIGURE A3.10 - Medium-Dense Sand Results: Load-displacement for tests SM3, SM4 and SM5.

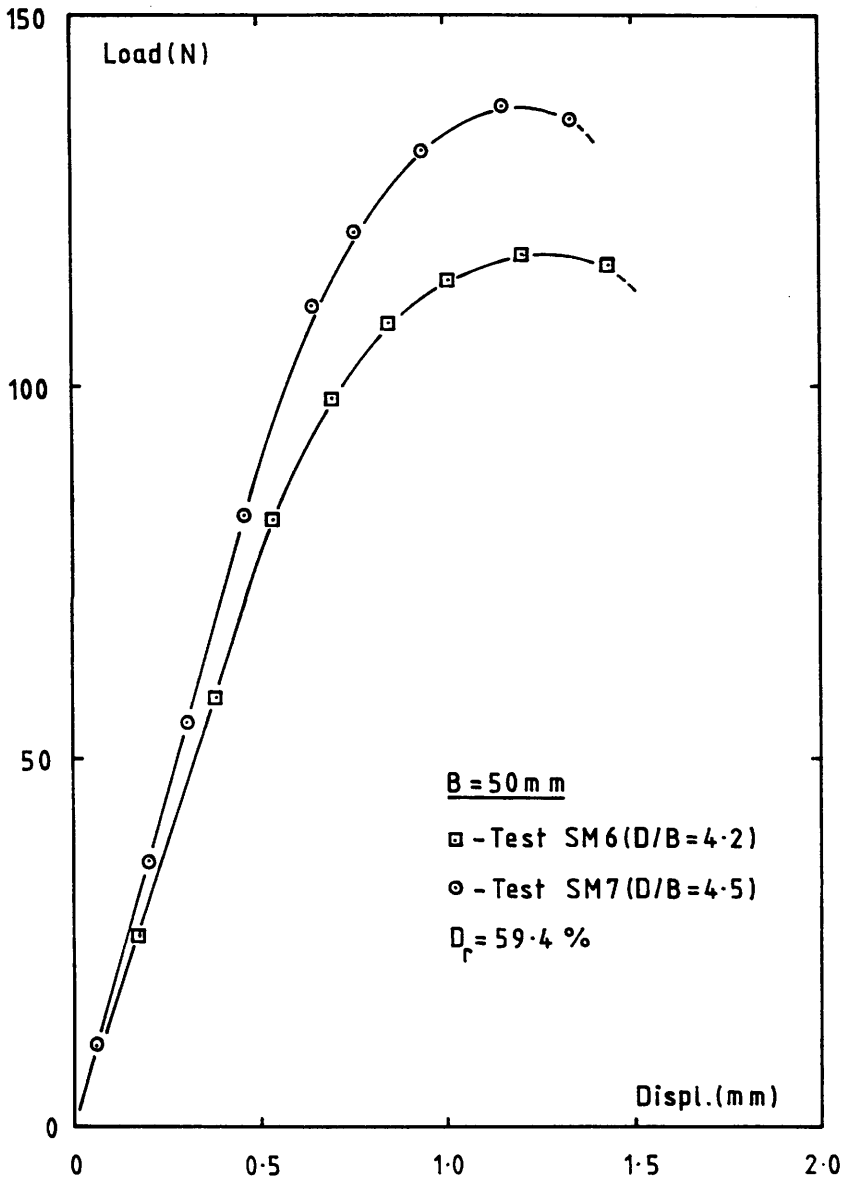

FIGURE A3.11 - Medium-Dense Sand Results: Load-displacement for tests SM6 and SM7.

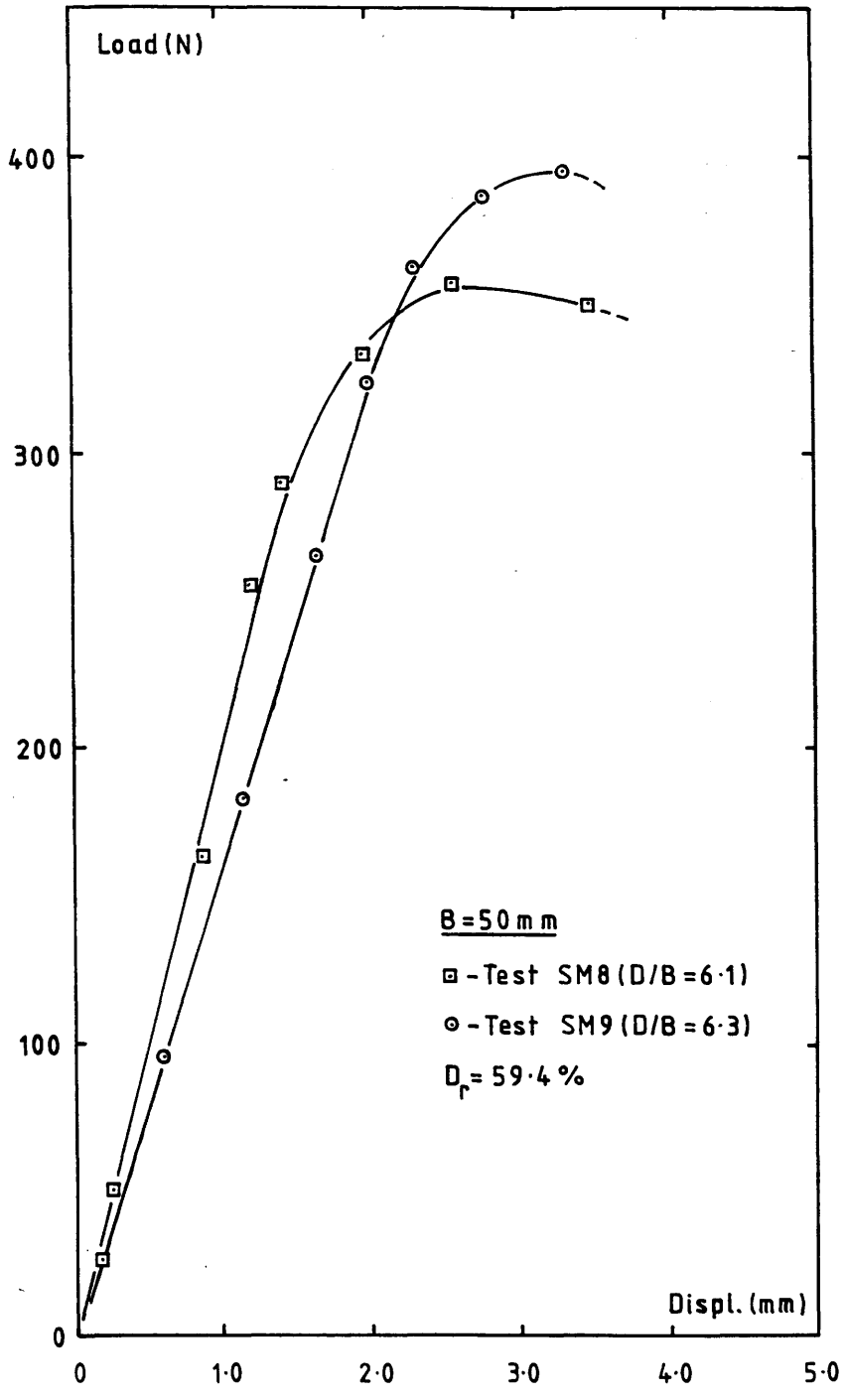

FIGURE A3.12 - Medium-Dense Sand Results: Load-displacement for tests SM8 and SM9.

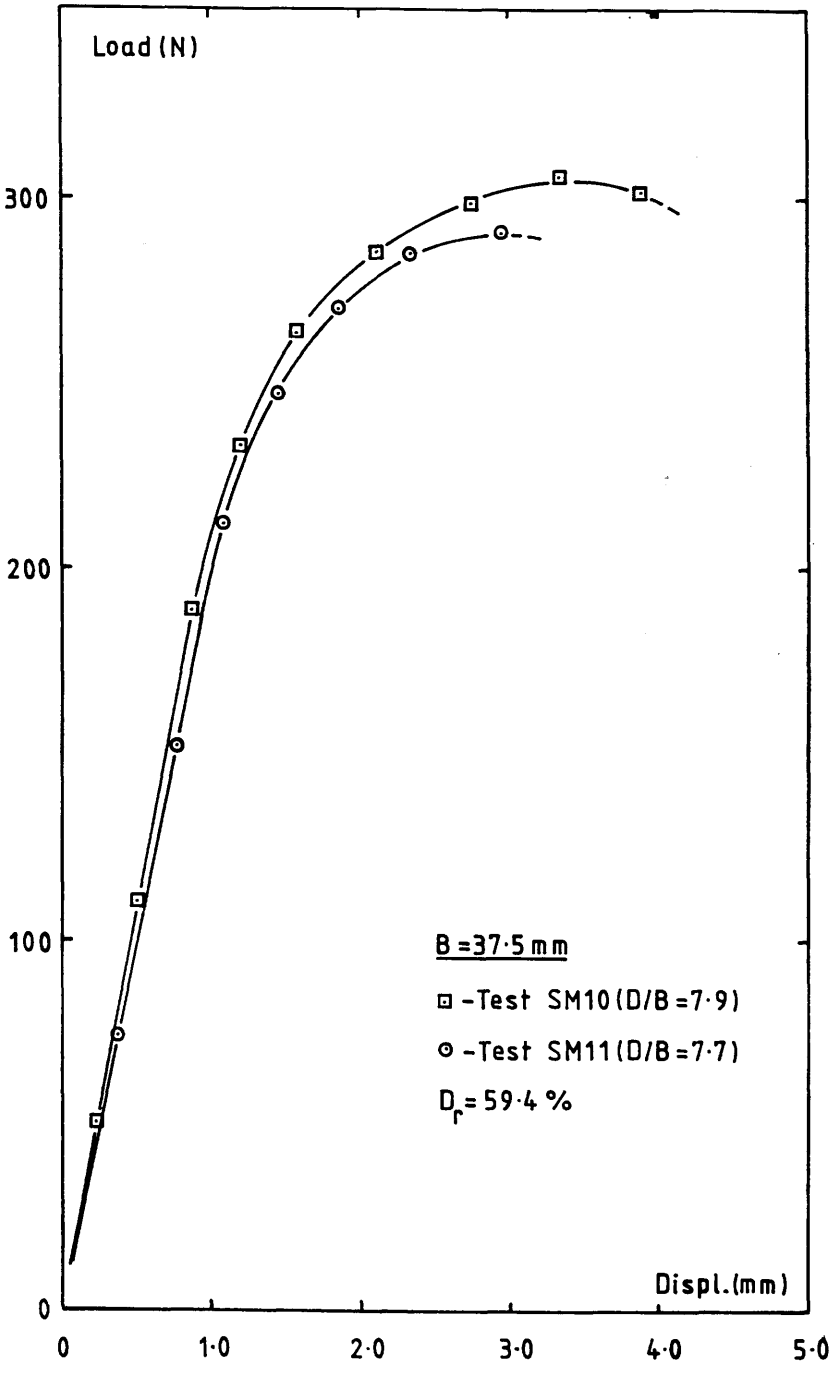

FIGURE A3.13 - Medium-Dense Sand Results: Load-displacement for tests SM10 and SM11.

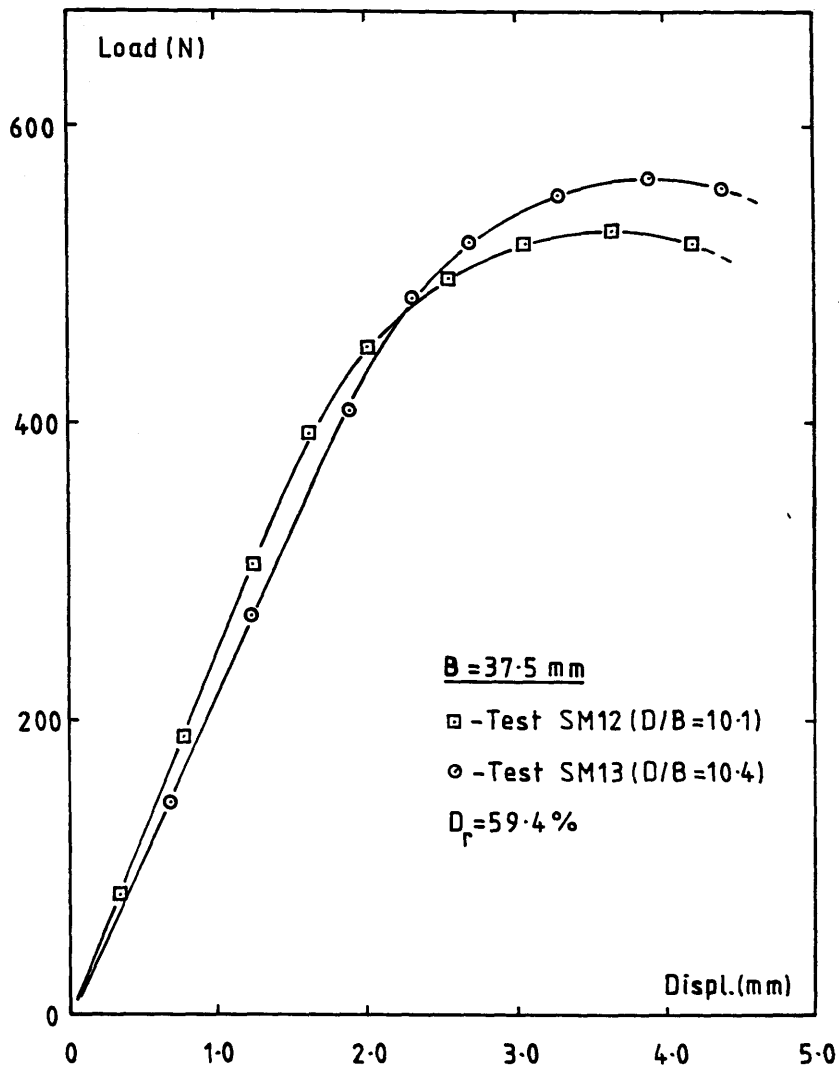

FIGURE A3.14 - Medium-Dense Sand Results: Load-displacement for tests SM12 and SM13.

REFERENCES

Abu–Taleb, M.G.A. (1974), "The behaviour of anchors in sand", Ph.D. Thesis, University of Sheffield.

Andreadis, A. (1979), "Uplift resistance of embedded sea bed anchors", Ph.D. Thesis, Queen Mary College, University of London.

Andreadis, A., Harvey, R.C. and Burley, E. (1981), "Embedded anchor response to uplift loading", Proc. ASCE., Jour. Geot. Div., Vol.107, No.GT1 (Jan.), pp. 59–78.

Ashbee, R.A. (1969), "A uniaxial analysis for use in uplift foundation calculations", Central Electricity Research Laboratories, Report No.RD/L/R 1608.

Balla, A. (1961), "The resistance to breaking out of mushroom foundations for pylons". Proc. 5th ICSMFE (Paris), Vol.1, pp. 569–576.

Bea, R.G., Dover,.A.R. and Audibert, J.M.E. (1982), "Pile foundation design considerations for deepwater fixed structures", Proc. Conf. Behaviour of Offshore Structures (MIT), Vol.1, pp. 125–140.

Bemben, S.M. and Kupferman, M. (1975), "The vertical holding capacity of marine anchor flukes subjected to static and cyclic loading", Proc. 7th Offshore Technology Conf., Vol.1, Paper No.OTC 2185, pp. 363–374.

Bemben, S.M., Kalajian, E.H. and Kupferman, M. (1973), "The vertical holding capacity of marine anchors in sand and clay subjected to static and cylic loading", Proc. 5th Offshore Technology Conf., Vol.1, Paper No. OTC 1912, pp. 871–880.

Bishop, A.W. and Henkel, D.J. (1962), "The measurement of soil properties in the triaxial test", 2nd Edition, Publ. by Edward Arnold.

Bolton, M.D., Engish, R.J., Hird, C.C. and Schofield, A.N. (1973), "Modelling", Proc. Symp. Role of Plasticity in Soil Mechanics (Cambridge), pp. 251–262.

Borowicka, H. (1936), "Influence of rigidity of a circular foundation slab on the distribution of pressures over the contact surface", Proc. 1st ICSMFE, Vol.2, pp. 144–149.

British Geotechnical Society (1980), Proc. Conf. Design Parameters in Geotechnical Engng. (London), Session 9: "The use of physical models in design", pp. 315–360.

Butterfield, R. and Andrawes, K.Z. (1970), "An air activated sand spreader for forming uniform sand beds", Geotechnique, Vol.20, pp. 97–100.

Butterfield, R. and Banerjee, P.K. (1971), "A rigid disc embedded in an elastic half space", Geotechnical Engng., Vol.2, pp. 35–52.

Carr, R.W. (1970), "An experimental investigation of plate anchors in sand", Ph.D. Thesis, University of Sheffield.

Chan, S.F. and Hanna, T.H. (1980), "Repeated loading on single piles in sand", Proc. ASCE., Jour. Geot. Div., Vol.106, No.GT2 (Feb)., pp. 171–188.

Clemence, S.P. and Smithling, A.P. (1983), "Dynamic uplift capacity of helical anchors in sand", Civil Engng., for Practicing and Design Engineers, Vol.2, pp.345–367.

Clemence, S.P. and Veesaert, C.J. (1977), "Dynamic pullout resistance of anchors in sand", Proc. Int. Symp. Soil–Structure Interaction (Univ. of Roorkee, India), pp.389–397.

Colp, J.L. and Herbich, J.B. (1975), "Inclined pullout forces for embedded plate anchors", Proc. 7th Offshore Technology Conf., Vol.1, Paper No. OTC 2182, pp. 333–342.

Cundall, P.A. and Strack, O.D.L. (1979), "A discrete numerical model for granular assemblies", Geotechnique, Vo.29, No.1, pp. 47–65.

Das, B.M. and Seeley, G.R. (1975a), "Inclined load resistance of anchors in sand", Proc. ASCE, Jour. Geot. Div., Vol. 101, No.GT9, pp. 995–998.

Das, B.M. and Seeley, G.R. (1975b), "Breakout resistance of shallow horizontal anchors", Proc. ASCE, Jour. Geot. Div., Vol.101, No.GT9, pp. 999–1003.

Das, B.M. and Seeley, G.R. (1976), "Shallow anchor resistance to eccentric uplift load", Proc. ASCE, Jour. Geot. Div., Vol.102, No. GT4., pp.389–393.

Davie, J.R. (1973), "Behaviour of cohesive soils under uplift forces", Ph.D. Thesis, University of Glasgow.

Davies, T.G. and Merouani, Z.E. (1986), "Elastic stress distribution around embedded anchors", Internal Research Report GT/1986/1/TGD, Dept. of Civil Engng., University of Glasgow.

El–Rayes, M.K. (1965), "Behaviour of cohesionless soils under uplift forces", Ph.D. Thesis, University of Glasgow.

Fadl, M.O. (1981), "The behaviour of plate anchors in sand", Ph.D. Thesis, University of Glasgow.

Gibbs, H.J. and Holtz, W.G. (1957), "Research on determining the density of sands by spoon penetration testing", Proc. 4th ICSMFE (London), Vol.1, pp.35–39.

Hanna, T.H.(1980), "Design and construction of ground anchors", CIRIA Report 65 (Second edition).

Hanna, T.H. and Al–Mosawe, M.J. (1981), "Performance of prestressed anchors under slow repeated loadings", Proc. 10th ICSMFE. (Stockholm), Vol.2, pp.127–132.

Hanna, T.H., Sivapalan, E. and Senturk, A. (1978), "The behaviour of dead anchors subjected to repeated and alternating loads", Ground Engineering, April, pp. 28–34.

Hutchison, N.J. (1982), "Groups of plate anchors in sand", Internal Research Report CE1/1982, Dept. of Civil Engng., University of Glasgow.

James, J.P. (1967), "Stress–displacement relationship for sand subjected to passive pressure", Ph.D. Thesis, University of Manchester.

James, R.G. (1971), "Some aspects of soil mechanics model testing", Proc. Roscoe Memorial Symp. Stress–Strain Behaviour of Soils (Camb.), pp.417–440.

Jardine, R.J., Potts, D.M., Hight, D.W. and Burland, J.B. (1985), "Assessing the safety of offshore piles by displacement monitoring", Proc. Conf. Behaviour of Offshore Structures, pp. 611–622.

Kalajian, E.H. (1971), "The vertical holding capacity of marine anchors in sand subjected to static and cyclic loading", Ph.D. Thesis, University fo Massachusetts (Amherst), U.S.A.

Karal, K. (1982), "Anchors for wave energy converters", Proc. 2nd Int. Symp. Wave Energy Utilization (Trondheim), pp. 211–228.

Kerr, N. (1976), "A self–burying anchor of considerable holding power", Proc. 8th Offshore Technology Conf., Paper No.OTC 2466, pp. 447–458.

Ko, H.Y. and Scott, R.F. (1967), "Deformation of sand in hydrostatic compression", Proc. ASCE, Jour. Soil Mech. and Founds. Div., Vol.93, No.SM3, pp. 137–156.

Kolbuszewski, J.J. (1948), "An experimental study of the maximum and minimum porosities of sands", Proc. 2nd ICSMFE (Rotterdam), Vol.1, pp.158–165.

Kolbuszweski, J.J. and Jones, R.H. (1961), "The preparation of sand samples for laboratory testing", Proc. Midland SMFE Society, Vol.4, pp.107–123.

Kulhawy, F.H. (1985), "Uplift behaviour of shallow soil anchors – an overview", Geot. Engng. Div., (ASCE) Special Technical Publication, pp. 1–25.

Kupferman, M. (1974), "The behaviour of embedded marine anchor flukes subjected to static and cyclic loading", Ph.D. Thesis, University of Massachusetts (Amherst), U.S.A.

Kwasnieski, J., Sulikowska, I. and Walter, A. (1975), "Anchors with vertical tie rods", Proc. 1st Baltic Conf. SMFE, Vol.3, pp. 121–133.

Lambe, T.W. and Whitman, R.V. (1979), "Soil Mechanics (S.I. version), Publ. by John Wiley and Sons, Inc., ISBN 0–471–02491–0.

Lemos, J.V., Hart, R.D. and Cundall, P.A. (1985), "A generalized distinct element program for modelling jointed rock mass", Proc. Int. Symp. Fundamentals of Rock Joints (Bjorkliden), pp. 335–343.

Littlejohn, G.S. and Bruce, D.A. (1977), "Rock anchors – state of the art", Foundation Publications Ltd., England. Also in Ground Engng., Part 1, May 1975, pp. 25–32, July 1975, pp. 41–48 ; Part 2, Sept. 1975, pp. 34–35, Nov. 1975, pp. 36–45 ; Part 3, March 1976, pp. 20–29, April 1976, pp. 55–60, May 1976, pp. 23–45.

Low, K.S. (1986), "Pile–anchor response to monotonic and repeated loading", Ph.D. Thesis, Sunderland Polytechnic.

Luk, V.M. and Keer, L.M. (1980), "Stress analysis of a deep rigid axially–loaded cylindrical anchor in an elastic medium", Int. Jour. Numer. Anal. Method. Geomech., Vol.4, No.3, pp. 215–232.

Maddocks, D.V. (1978), "The behaviour of model ground anchors installed in sand and subjected to pull–out and repeated loading", Ph.D. Thesis, University of Bristol.

Mariupolskii, L.G. (1965), "The bearing capacity of anchor foundations", Soil Mech. and Found. Engng., Vol.2 No.1, pp. 26–32. Translated from Osnovaniya, Fundamenty i Mekhanika Gruntov.

Marr, W.A. and Christian, J.T., (1981), "Permanent displacements due to cyclic wave loading", Proc. ASCE, Jour. Geot. Div., Vol.107, No.GT8, pp.1129–1149.

Matsuo, M. (1967), "Study on the uplift resistance of footings (I)", Proc. Japanese Soc. SMFE, Soils and Founds., Vol.7, No. 4, pp. 1–37.

Matsuo, M. (1968), "Study on the uplift resistance of footings (II)", Proc. Japanese Soc., SMFE, Soils and Founds., Vol.8, No.1, pp. 18–48.

Maus, L.D., Finn, L.D. and Turner, J.W. (1985), "Development of the guyed tower", Jour. Petroleum, Engineers, April, 647–654.

McCormick, M.E. (1979), Editor, "Anchoring Systems", Pub. by Pergamon Press, ISBN 0–08–022694–9

Meyerhof, G.G. and Adams, J.I. (1968), "The ultimate uplift capacity of foundations", Canadian Geot. Jour., Vol.5, No.4, pp. 225–244.

Mitsch, M.P. and Clemence, S.P. (1985), "The uplift capacity of helix anchors in sand", Geot. Engng., Div. (ASCE), Special Technical Publ., pp. 26–47.

Mooney, J.S., Adamczak, S. and Clemence, S. (1985), "Uplift capacity of helical anchors in clay and silt", Geot. Engng., Div. (ASCE), Special Technical Publ., pp. 48–72.

Morgan, J.R. (1966), "The response of granular materials to repeated loading", Proc. Australian Road Research Board, Vol.3, No.2, pp. 1178–1192.

Motherwell, J.T. and Wright, S.G. (1978), "Cyclic apparatus using frictionless air piston", Proc. ASCE, Jour. Geot. Div., Vol.104, No.GT7, pp. 1036–1039.

Moussa, A.A. (1975), "Equivalent drained–undrained shearing resistance of sand to cyclic simple shear loading", Geotechnique, Vol.25, No.3, pp. 485–494.

Nauroy, J.F., Brucy, F. and Le Tirant, P. (1985), "Static and cyclic load tests on a drilled and grouted pile in calcareous sand", Proc. Conf. Behaviour of Offshore Structures, pp. 577–587.

Naylor, D.J. (1981), "FINEALE User Guide", Institute for Numer. Methods in Engng., University of Swansea.

Naylor, D.J. (1983), "FINETAN User Guide", Institute for Numer. Methods in Engng., University of Swansea.

Ostermayer, H. (1974), "Construction, carrying behaviour and creep characteristics of ground anchors", Proc. ICE Conf. Diaphragm Walls and Anchorages (London), pp. 141–151.

Ovesen, N.K. (1962), "Cellular cofferdams, calculation methods and model tests", Danish Geotechnical Institute, Bulletin No.14

Ovesen, N.K. (1981), "Centrifuge tests of the uplift capacity of anchors", Proc. 10th ICSMFE (Stockholm), Vol.1, pp. 717–722.

Ponce, V.M. and Bell, J.M. (1971), "Shear strength of sand at extremely low pressures", Proc. ASCE, Jour. Soil Mech. and Founds. Div., Vol.97, No. SM4, pp. 625–638.

Ponniah, D.A. (1984), "Behaviour of plate anchors in cohesive soils under static and cyclic loads", Ph.D. Thesis, University of Glasgow.

Puech, A.A. (1982), "Basic data for the design of tension piles in silty soils", Proc. Conf. Behaviour of Offshore Structures (MIT), Vol.1, pp.141–157.

Rocha, M. (1957), "The possibility of solving soil mechanics problems by the use of models", Proc. 4th ICSMFE (London), Vol.1, pp. 183–188.

Roscoe, K. (1968), "Soils and model tests", Jour. Strain Analysis, Vol.3, No.1, pp. 57–64.

Rowe, R.K. and Booker, J.R. (1979), "A method of analysis for horizontally embedded anchors in an elastic soil", Int. Jour. Numer. Anal. Meth. Geomech., Vol.3, No.2, pp. 187–203.

Rowe, R.K. and Booker, J.R. (1980a), "The elastic response of multiple underream anchors", Research Report No.R369, School of Civil Engng., University of Sydney, Australia.

Rowe, R.K. and Booker, J.R. (1980b), "The behaviour of single and multiple underream anchors in a Gibson soil", Research Report No.R373, School of Civil Engng., University of Sydney, Australia.

Rowe, R.K., Booker, J.R. and Balaam, N.P. (1978), "Application of the initial stress method to soil–structure interaction", Int. Jour. Numer. Meth. in Engng., Vol.12, No.5, pp. 873–880.

Rowe, R.K. and Davis, E.H. (1982a), "The behaviour of plate anchors in clay", Geotechnique, Vol.32, No.1, pp. 9–23.

Rowe, R.K. and Davis, E.H. (1982b), "The behaviour of plate anchors in sand", Geotechnique, Vol.32, No.1, pp. 25–41.

Saeedy, H.S. (1975), "Analytical determination of anchor capacity in sand", Proc. 1st Baltic Conf. SMFE, Vo.3, pp. 199–212.

Senturk, A. (1977), "The behaviour of plate anchors subjected to repeated loading", M. Eng. Thesis, University of Sheffield.

Silver, M. L. and Seed, H.B. (1971a), "Deformation characteristics of sands under cyclic loading", Proc. ASCE, Jour. Soil Mech. and Founds. Div., Vol.97, No.SM8, pp. 1081–1098.

Silver, M.L. and Seed H.B. (1971b), "Volume changes in sands during cyclic loading", Proc. ASCE, Jour. Soil Mech. and Founds. Div., Vol.97, No.SM9, pp. 1171–1182.

Sivapalan, E. (1976), "The behaviour of plate anchors subjected to repeated loading", M. Eng. Thesis, University of Sheffield.

St. John, H.D., Randolph, M.F., McAnoy, R.P. and Gallagher, K,.A. (1983), "Design of piles for tethered platforms", Proc. ICE Conf. Developments in the Design and Construction of Offshore Structures, Publ. by Thomas Telford, pp. 61–72.

Steenfelt, J.S. (1982), "Scale effects on observations in particulate media", Euromech. Colloquium Quality of Mechanical Observations, pp. R1–R4.

Sutherland, H.B. (1965), "Model studies for shaft raising through cohesionless soil", Proc. 6th ICSMFE (Montreal), Vol.2, pp. 410–413.

Tagaya, K., Tanaka, A. and Aboshi, H. (1983), "Application of finite element method to pullout resistance of buried anchor", Proc. Japanese Society SMFE, Soils and Founds., Vol.23, pp. 91–104.

Tanimoto, K. and Nishi, M. (1970), "On resilience characteristics of some soils under repeated loading", Proc. Japanese Society SMFE, Soils and Founds, Vol.10, No.1, pp. 75–92.

Tavenas, F. and La Rochelle, P. (1972), "Accuracy of relative density measurements", Geotechnique, Vol.22, No.4, pp. 549–562.

Taylor, R.J., Jones, D. and Beard, R.M. (1975), "Handbook for uplift–resisting anchors," Naval Civil Engng. Lab., Port Hueneme, California, U.S.A. (153 p.).

Taylor, R.J. and Lee H.J. (1973), "Direct embedment anchor holding capacity", Technical Note N–1245, Naval Civil Engng. Lab., Port Hueneme, California, U.S.A. (34p).

Tetlow, J.H., Ellis, N., and Mitra, J.K. (1983), "The Hutton tension leg platform", Proc. ICE Conf. Developments in the Design and Construction of Offshore Structures, Publ. by Thomas Telford, pp. 137–150.

Timmerman, D.H. and Wu, T.H. (1969), "Behaviour of dry sands under cyclic loading", Proc. ASCE., Jour. Soil Mech. Founds. Div., Vol.95, No.SM4, pp. 1097–1112.

Trofimenkov, Y.G. and Mariupolskii, L.G. (1965), "Screw piles as foundations of supports and towers of transmission lines", Soil Mech. and Found. Engng., Vol.1, No.4, pp. 232–239. Translated from Osnovaniya, Fundamenty i Mekhanika Gruntov.

Trollope, D.H., Lee, I.K. and Morris, J. (1962), "Stresses and deformation in two layer pavement structures under slow repeated loading", Proc. Australian Road Research Board, Vol.1, No.2, pp.693–721.

True, D.G. and Link, H.F. (1979), "A large propellant embedment anchor for offshore moorings", Proc. 11th Offshore Technology Conf., Paper No. OTC 3668, pp. 2731–2736.

Tsangarides, S.N. (1978), "The behaviour of ground anchors in sand", Ph.D. Thesis, Queen Mary College, University of London.

Vermeer, P.A. and Sutjiadi, W. (1985), "The uplift resistance of shallow embedded anchors", Proc. 11th ICSMFE (San Francisco), Vol.3, pp. 1635–1638.

Vesic, A.S. (1971), "Breakout resistance of objects embedded in ocean bottom", Proc. ASCE, Jour. Soil Mech. and Founds. Div., Vol.97, No.SM9, pp. 1183–1205.

Vesic, A.S. (1972), "Expansion of cavities in infinite soil mass", Proc. ASCE, Jour. Soil Mech.and Founds. Div., Vol.98, No.SM3, pp.265–291.

Walker, B.P. and Whitaker, T. (1967), "An apparatus for forming uniform beds of sand for model foundation tests", Geotechnique, Vol.17, No.2, pp. 161–167.

Wang, T.C.W. (1986), "The behaviour of plate anchor groups in sand", M.Sc. Thesis, University of Glasgow.

Wang, M.C., Demars, K.R. and Nacci, V.A. (1978), "Applications of suction anchors in offshore technology", Proc. 10th Offshore Technology Conf. Paper No. OTC 3203, pp. 1311–1320.

Wilson, Q. and Sahota, B.S. (1980), "Pull–out parameters for buried suction anchors", Proc. 12th Offshore Technology Conf., Paper No. OTC 3816, pp. 205–216.

Wood, D.M. and Budhu, M. (1960), "The behaviour of Leighton Buzzard sand in cyclic simple shear tests", Proc. Int. Symp. Soils under Cyclic and Transient Loading (Swansea), pp. 9–21.

Yilmaz, M. (1971), "The behaviour of groups of anchors in sand", Ph.D. Thesis, University of Sheffield.

Youd, T.L. (1970), "Densification and shear of sand during vibration", Proc. ASCE, Jour. Soil Mech. and Founds, Div., Vol.96, No.SM3, pp. 863–880.

Youd, T.L. (1971), "Maximum density of sand by repeated straining in simple shear", Highway Research Record, No.374, pp. 1–6.

Youd, T.L. (1972), "Compaction of sands by repeated shear straining", Proc. ASCE, Jour. Soil Mech.and Founds Div., Vol.98, No.SM7, pp. 709–725.

Zakaria, I.B. (1986), "The effect on the uplift resistance of anchors of ground disturbance during placing", Ph.D Thesis, University of Glasgow.